SHORT NOTES ON ALASKA GEOLOGY 1995

Professional Report 117

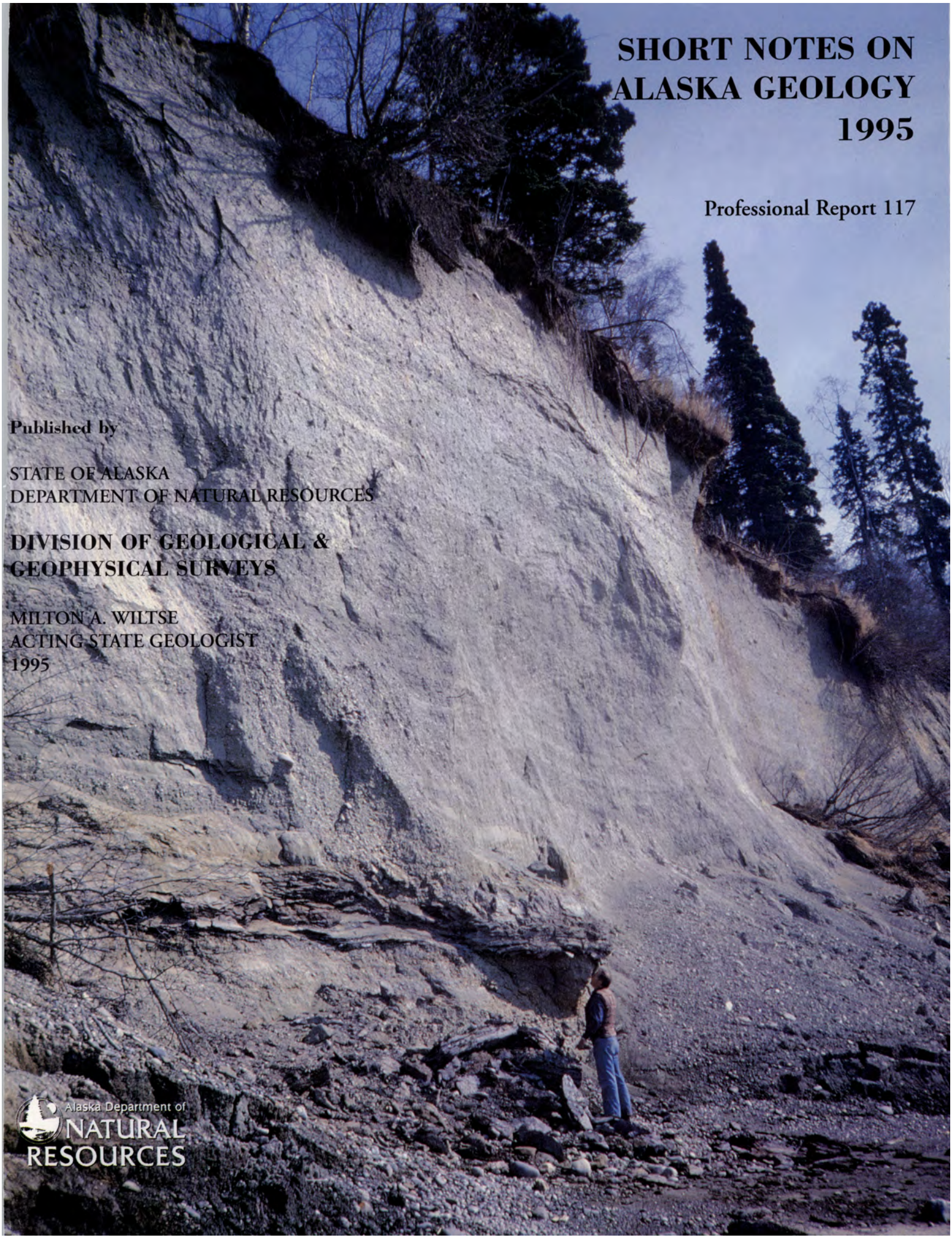

Published by

STATE OF ALASKA
DEPARTMENT OF NATURAL RESOURCES

DIVISION OF GEOLOGICAL & GEOPHYSICAL SURVEYS

MILTON A. WILTSE
ACTING STATE GEOLOGIST
1995

Alaska Department of NATURAL RESOURCES

SHORT NOTES ON ALASKA GEOLOGY 1995

Edited by Rodney A. Combellick and Fran Tannian
Cover design by Ann-Lillian C. Schell
Professional Report 117

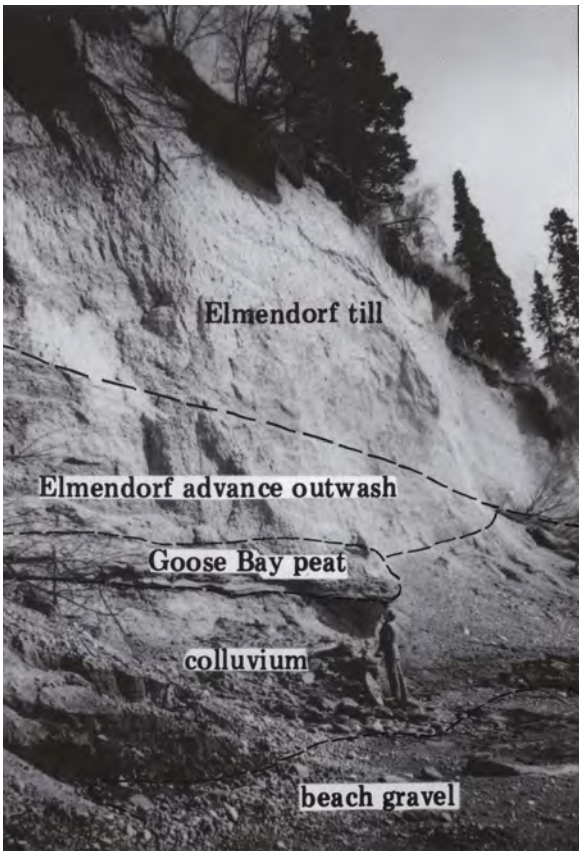

Front cover: *Exposure of till and outwash of the Elmendorf glacial advance at Goose Bay, west side of Knik Arm. (See paper by Reger and others, page 33.) Geologist Richard Reger examines Goose Bay peat of mid-Pleistocene age. Photograph by R.A. Combellick.*

Fairbanks, Alaska
1995

STATE OF ALASKA
Tony Knowles, *Governor*

DEPARTMENT OF
NATURAL RESOURCES
John T. Shively, *Commissioner*

DIVISION OF GEOLOGICAL &
GEOPHYSICAL SURVEYS
Milton A. Wiltse, *Acting*
State Geologist

Division of Geological & Geophysical Surveys publications may be inspected at the following locations. Address mail orders to the Fairbanks office.

Alaska Division of Geological &
Geophysical Surveys
Attn: Publications
794 University Avenue, Suite 200
Fairbanks, Alaska 99709-3645

Department of Natural Resources
Public Information Center
3601 C Street, Suite 200
Anchorage, Alaska 99510

This publication, released by the Division of Geological & Geophysical Surveys, was produced and printed in Anchorage, Alaska by A.T. Publishing & Printing, Inc., at a cost of $15 per copy. Publication is required by Alaska Statute 41, "to determine the potential of Alaskan land for production of metals, minerals, fuels, and geothermal resources; the location and supplies of groundwater and construction materials; the potential geologic hazards to buildings, roads, bridges, and other installations and structures; and shall conduct such other surveys and investigations as will advance knowledge of the geology of Alaska."

FOREWORD

The Alaska Division of Geological & Geophysical Surveys (DGGS) here presents *Short Notes on Alaska Geology 1995*, the ninth issue in this series. There are ten papers, two each in Quaternary geology, structural geology, stratigraphy-sedimentology, and paleontology, and one each in economic geology and geochemistry. Almost all geographic regions of the State are represented. Overall, they reflect the wide range of subjects and broad geographic distribution of current geologic research in Alaska.

I want to take this opportunity to recognize the contributions of Tom Smith and Dick Reger, veteran DGGS geologists retiring this year, for their long service with DGGS (14 years and 19 years, respectively) and contributions to Alaskan geology. Tom began his Alaskan work in 1966 as a geophysicist; I knew him best during his six years (1975–81) with the University of Alaska Fairbanks (UAF). Since 1981 Tom has served with DGGS–for the last four years as state geologist and director. Dick came to UAF in 1957 as an undergraduate student and has been in Alaska ever since, except for Ph.D. work and some teaching in Arizona. He has been with DGGS continuously since 1975. Together Tom and Dick possess an important part of what is known about the geology of Alaska as carried about in the brains of living geologists. Together they have more than 60 years of experience in Alaska and have published well over 150 articles, maps, and abstracts about Alaska geology.

They will, of course, also be missed as the fine and unique human individuals that they are. However, I want to reflect on the broader significance of the loss of so much knowledge and experience and implications for the status of geology in Alaska. For reasons I can't go into here, experience is more important in geology than in any other science, with the possible exception of biology. In most cases you can meet your needs in engineering or physics by hiring younger replacements. Often this is not the case in geology. Deep understanding of the proper scales of time and rates of processes requires years of field experience with a variety of rocks and sediments in many localities. In Alaska, those who have this experience represent a significant investment of time and money. They cannot be replaced except by a similar investment of time and money. My concern is not the occasional loss of geologists like Tom and Dick–this is inevitable–but failure to develop and maintain a continuing supply of geologists with decades of Alaskan experience. Their ranks are getting thin, perhaps dangerously so. Somewhere within the profession–DGGS, U.S. Geological Survey, University of Alaska, and industry–we must nurture a core of experience. The future of our state depends on it.

This brings me to my final point. These *Short Notes* are an important vehicle for the accumulation of Alaskan geological experience emphasized above. In particular, I hope that more younger geologists will contribute to future volumes and thereby be encouraged to stay in Alaska and become qualified replacements for the likes of Tom Smith and Dick Reger.

Don Triplehorn
Professor of Geology
University of Alaska Fairbanks

CONTENTS

Page

Radiocarbon age of probable Hayes tephra, Kenai Peninsula, Alaska
Rodney A. Combellick and DeAnne S. Pinney 1

Geochemistry of saline lakes of the northeastern Yukon Flats, eastcentral Alaska
Daniel B. Hawkins 11

Geometry and deformation of a duplex and its roof layer: Observations from the Echooka anticlinorium, northeastern Brooks Range, Alaska
Andrew J. Meigs and Teresa A. Imm 19

Late-Wisconsin events in the Upper Cook Inlet region, southcentral Alaska
Richard D. Reger, Rodney A. Combellick, and Julie Brigham-Grette 33

Stratigraphy and implications of a lakeside section, Glacial Lake, southwestern Kigluaik Mountains, Seward Peninsula, Alaska
Richard D. Reger and David M. Hopkins 47

Lithofacies, petrology, and petrophysics of the Kemik Sandstone (Lower Cretaceous), eastern Arctic Slope, Alaska
Rocky R. Reifenstuhl 53

A new species of the conodont *amydrotaxis* From the Early Devonian of southwestern Alaska
Norman M. Savage and Robert B. Blodgett 69

Early Devonian and Late Triassic conodonts from Annette and Hotspur Islands, southeastern Alaska
Norman M. Savage and George E. Gehrels 75

Mineralization and zoning of polymetallic veins in the Beaver Mountains volcano-plutonic complex, Iditarod Quadrangle, westcentral Alaska
David Szumigala 79

Possible thrust windows on the central Seward Peninsula, Alaska
Lorne E Young 97

Previous editions of *Short Notes on Alaska Geology* 115

RADIOCARBON AGE OF PROBABLE HAYES TEPHRA, KENAI PENINSULA, ALASKA

by
Rodney A. Combellick[1] and DeAnne S. Pinney[1]

INTRODUCTION

Hayes volcano in southcentral Alaska (fig. 1) produced as many as eight closely spaced tephra deposits about 3,650 ± 150 ^{14}C yr B.P. (3,730–4,150 cal yr B.P.) (Riehle, 1985; Riehle and others, 1990). These layers are the most widespread of all tephras in the Cook Inlet region and have been observed as far away as the lower Delta River area in central Alaska, more than 650 km northeast of the vent (Begét and others, 1991).

Hayes tephras have a bilobate distribution, one portion directed south and the other northeast of the vent (Riehle and others, 1990, fig. 3). Riehle determined the likely dispersal axes of individual tephra deposits by comparing glass and ilmenite compositions of distal layers with each of seven proximal layers, A–G, sampled about 50 km northeast of the vent. On the Kenai Peninsula, less than 100 km southeast of the vent, the apparent absence of tephras that can be positively correlated with the Hayes set indicates that tephrafall to the southeast was less extensive than to the south and northeast. Riehle sampled a tephra at Anchorage that correlates with the Hayes set in both mineralogy and glass chemistry (similarity coefficient of 0.96) but lacks bracketing ages. The mineralogy of a tephra he sampled near Kenai appears to correlate with the Hayes set but has a low similarity coefficient of 0.88 and lacks bracketing ages.

In this paper we describe the mineralogy, glass chemistry, and radiocarbon ages of tephra layers embedded in thick late-Holocene peat deposits along the Kasilof and Kenai River estuaries. We conclude that a 3-cm-thick tephra at each location strongly correlates with the Hayes set. Our data extend the apparent southeast limit of Hayes tephra deposits, show probable correlation with one of the seven proximal tephras, and provide additional age control for the eruption.

[1]Alaska Division of Geological & Geophysical Surveys, 794 University Avenue, Suite 200, Fairbanks, Alaska 99709-3645.

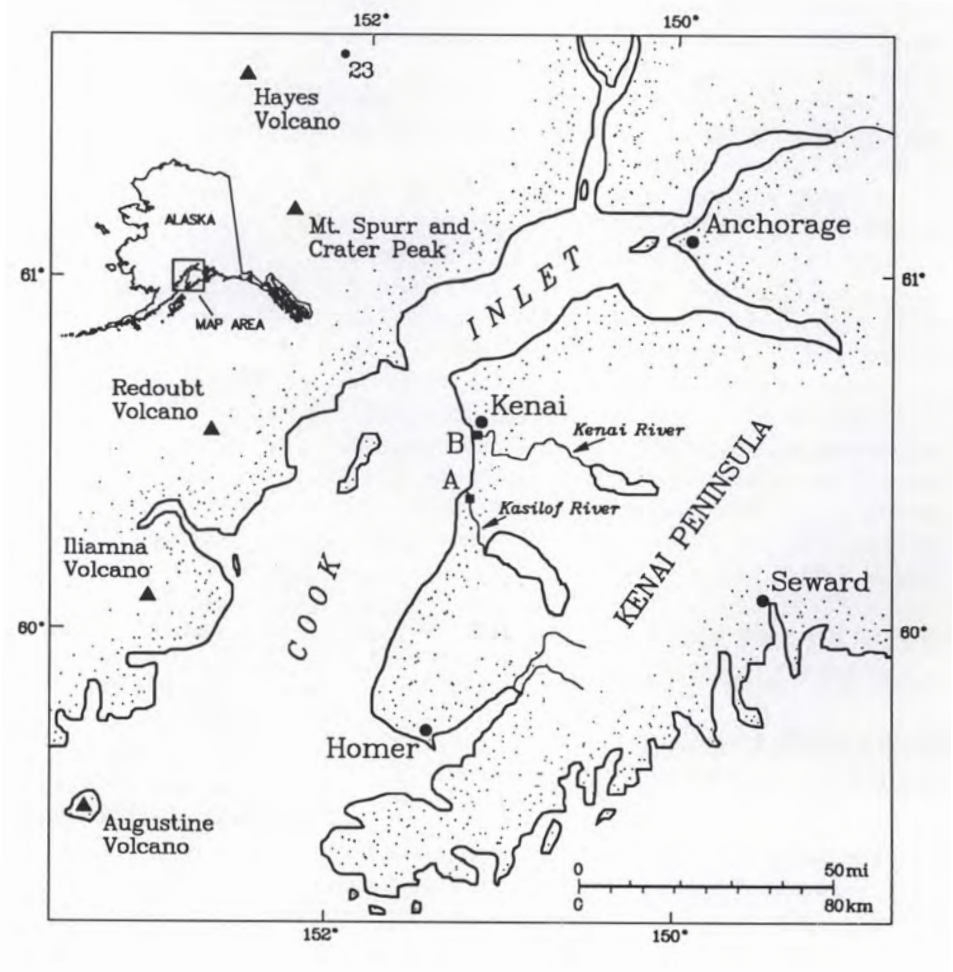

Figure 1. *Map of Cook Inlet region showing locations of Quaternary volcanoes (triangles) and study sites A (Kasilof River flats) and B (Kenai River flats). Site 23 is the location of proximal reference samples 23A-G of Riehle (1985).*

COOK INLET TEPHRAS

Spurr (Crater Peak), Redoubt, and Augustine volcanoes have erupted during historic time, blanketing much of the Cook Inlet region with tephra. Tephra deposits in the Cook Inlet region record numerous eruptions of Spurr and Redoubt volcanoes throughout Holocene time, as well as a series of six to eight eruptions at Hayes volcano about 3,650 ^{14}C yr B.P. (Riehle, 1985). Iliamna volcano has produced only steam or smoke emissions during historic time and no recognized tephras during Holocene time. Although tephra eruptions of Augustine volcano in 1883, 1935, 1963, and 1976 resulted in ashfalls in the region, older Holocene tephras in the Cook Inlet region have not been ascribed with certainty to Augustine.

Many Holocene tephra layers in surficial deposits of southcentral Alaska correlate with the Spurr, Redoubt, or Hayes reference tephras in mafic mineralogy and glass chemistry. Others correlate poorly with these reference tephras and have uncertain sources. They may have originated at Augustine, Iliamna, or more distant sources.

The mafic-phenocryst content clearly distinguishes Hayes reference samples from those of Spurr and Redoubt (Riehle, 1985, fig. 4). The 3,650-yr-old Hayes tephra set is characterized by amphibole-to-pyroxene ratios > 4 and trace biotite (Riehle and others, 1990). Tephras erupted from Spurr and Redoubt volcanoes contain far less amphibole and no biotite. Whole-rock analysis of a lapillus from a Hayes reference sample indicates dacitic composition with SiO_2 content of 64 percent (Riehle, 1985). Pumice lapilli from Spurr pyroclastic-flow deposits have SiO_2 contents of 61–62 percent, indicating high-silica andesite or low-silica dacite. Tephra erupted from the Crater Peak vent contains 55 percent SiO_2, indicating a composition of basaltic andesite. Whole-rock analysis of Redoubt eruptive products yields high-silica andesitic compositions (Till and others, 1993), and some glass separates are thought to indicate dacitic composition. Hayes glass compositions are calc-alkaline and can be distinguished from those of Spurr and Redoubt tephras on plots of SiO_2 versus FeO*/MgO and K_2O versus SiO_2 (Riehle, 1985, fig. 13).

TEPHRA LAYERS AT KASILOF AND KENAI RIVER FLATS

STRATIGRAPHY AND RADIOCARBON DATING

The Kasilof and Kenai River flats border estuaries near the mouths of these rivers (fig. 1, sites A and B) and are underlain by tidal silt and clay with peat interlayers of varying thicknesses. Deep boreholes show that the estuarine deposits are about 8 m thick and are underlain by sandy, gravely alluvium. Radiocarbon dating of basal peat overlying sand and gravel in a borehole at Kasilof River flats indicates that the estuarine deposits began accumulating about 12 ka ago (Combellick and Reger, 1994).

Extensive tidal-bank exposures along both estuaries show a thick peat layer with some clayey-silt interbeds extending from near the surface to about 2 m depth beneath the vegetated river flat (fig. 2). The peat consists of the remains of *Sphagnum* moss, sedge grasses, herbaceous plants, shrubs, and one to three layers of rooted tree stumps. Samples from the base of the peat layer yielded calibrated radiocarbon ages of 6–7 ka B.P., indicating when the estuary finished filling to about its present level and began to support tidal-marsh vegetation. Although estuaries farther northeast in upper Cook Inlet show evidence of repeated tectonic subsidence during the late Holocene, the Kenai-Kasilof area shows net tectonic stability during this period (Combellick, 1994).

Two prominent tephra layers about 3 cm thick (T1 and T2) are embedded in the thick peat at site A (figs. 2 and 3). A 3-cm-thick tephra layer (T1) is visible in the peat at site B as well as several thin tephras (<3 mm) that were not sampled. Radiocarbon dating of wood or bulk peat samples immediately above and below tephra T1 at sites A and B yields a weighted-average age of 3,530 ± 70 ^{14}C yr B.P. (3,690–3,880 cal yr B.P.). This age is consistent with the average age of the Hayes tephra set (table 1) and with the ages of one or more tephras from Spurr and Redoubt volcanoes. Bracketing ages for the lower tephra (T2) at site A indicate that T2 was deposited about 5–6 cal ka B.P. Several regional tephras originated from Spurr, Redoubt, and perhaps other sources during this period but there are no known Hayes tephras of this approximate age.

MINERALOGY

We performed petrographic analyses of the Kenai Peninsula tephra samples as the first step in determining whether they correlate with Hayes tephra. Mafic-mineral assemblages are frequently used in tephrochronology as an aid in correlation, particularly by using ratios of certain mafic mineral species (Riehle, 1985; Riehle and others, 1990; Begét and others, 1991). However, mafic mineralogy usually does not provide conclusive grounds for positive correlations. Magmas of similar composition from different sources are likely to contain similar phenocrysts, thereby limiting the value of phenocryst mineralogy as a sole means of correlation. Progressive downwind fractionation of phenocryst phases in an eruptive plume can substantially alter its apparent mineralogic characteristics. Additionally, contaminating grains from adjacent layers are common and may be impossible to distinguish from tephra-borne minerals, leading to erroneous results if included in mineral counts. This problem can be circumvented by counting only those mineral grains with attached glass, but this procedure may lead to the additional difficulty of locating

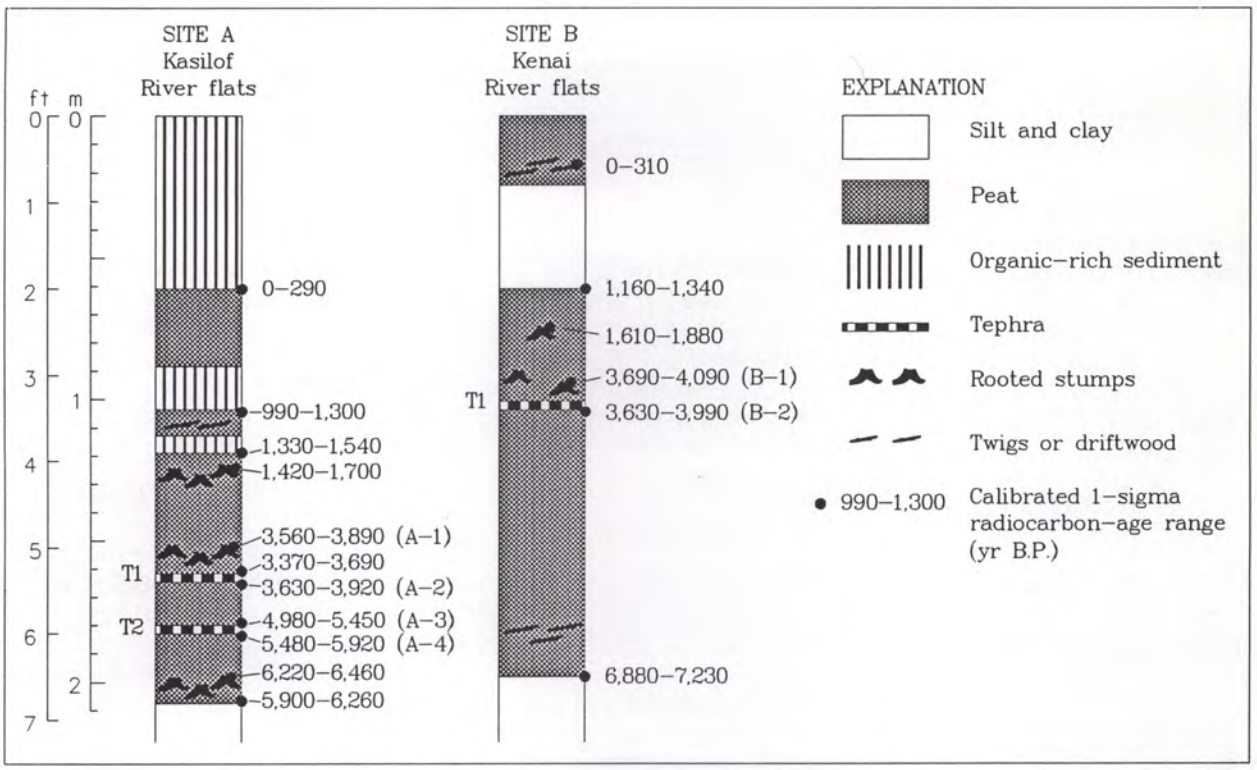

Figure 2. *Stratigraphic diagrams for tidal-bank exposures at Kasilof and Kenai River flats (fig. 1, sites A and B, respectively). See table 1 for radiocarbon ages bracketing tephras T1 and T2. (Modified from Combellick and Reger, 1994, figs. A8 and A11.)*

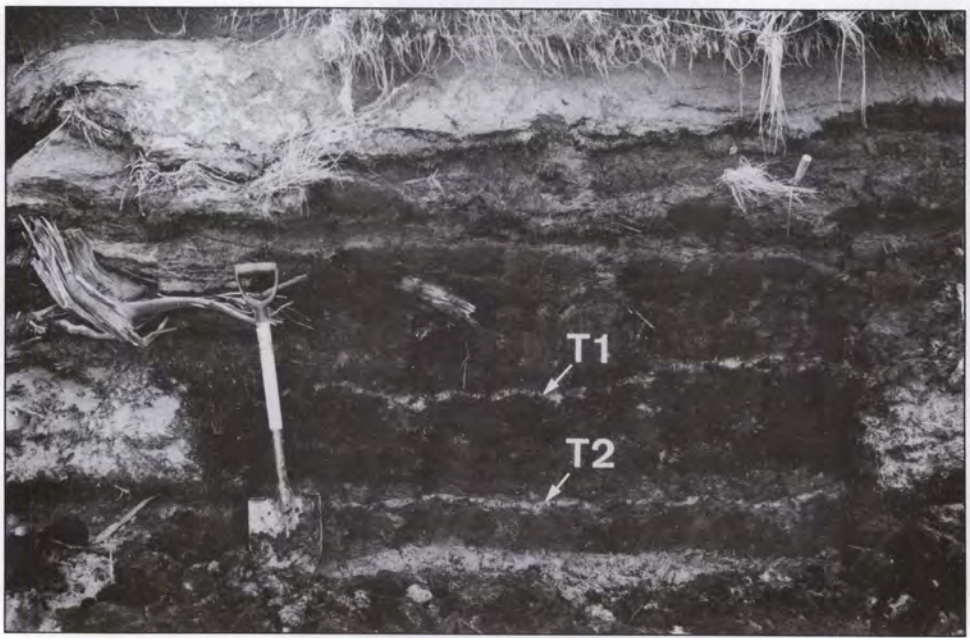

Figure 3. *Tidal-bank exposure along lower Kasilof River (site A), showing prominent tephras T1 and T2 embedded in peat of late-Holocene age. Tephra T1 correlates in age, mafic mineralogy, and glass chemistry with reference samples of the Hayes tephra set deposited 3,650 ± 150 ^{14}C yr B.P.*

Table 1. *Radiocarbon ages of peat and wood samples used to estimate ages of tephras* *[Age in ^{14}C yr B.P. is conventional radiocarbon age in years before A.D. 1950 with quoted laboratory counting error of one standard deviation. Calibrated ages are the one-sigma limits of age ranges based on tree-ring corrections of Pearson and Stuiver (1993) and are rounded to the nearest 10 yr. Calibrated ages incorporate an error multiplier of 2 to account for possible noncounting sources of laboratory error. Calibrations and weighted averaging were performed using a computer program by Stuiver and Reimer (1993). All ages include a correction for natural $^{13}C/^{12}C$ isotopic fractionation. For sample locations and stratigraphic positions, see figures 1 and 2, respectively]*

Site-sample	Beta Analytic number	Description	Age (^{14}C yr B.P.)	Calibrated age range (yr B.P.)
A-1	45204	Wood from a stump rooted 16 cm above tephra T1 (minimum age)[a]	3,470 ± 70	3,560–3,890
A-2	50332	3-cm-thick bulk peat in contact with overlying tephra T1 (maximum age)	3,510 ± 60	3,630–3,920
A-3	50333	3-cm-thick bulk peat in contact with underlying tephra T2 (minimum age)	4,550 ± 70	4,980–5,450
A-4	50334	3-cm-thick bulk peat in contact with overlying tephra T2 (maximum age)	4,970 ± 100	5,480–5,920
B-1	45210	4-cm-diameter branch of stump rooted 10 cm above tephra T1 (minimum age)	3,590 ± 70	3,690–4,090
B-2	50336	3-cm-thick bulk peat in contact with overlying tephra T1 (maximum age)	3,540 ± 70	3,630–3,990
T1 average	–	Weighted average of A-1, A-2, B-1, B-2[b]	3,530 ± 70	3,690–3,880
Hayes set	–	Average of numerous published samples (Riehle, 1985)	3,650 ± 150	3,730–4,150

[a]In view of a slight age reversal, we chose to use the age of this wood sample in preference to that of a bulk peat sample superjacent to tephra T1 at site A (see fig. 2). The rooted wood probably gives a more reliable age. If the peat age (3,310 ± 70 yr B.P.) is used, the weighted average age is 3,490 ± 70 radiocarbon yr B.P. (3,640-3,840 cal yr B.P.).

[b]Averaging all four samples above and below tephra T1 assumes contemporaneous deposition at sites A and B and that tephra accumulation was sufficiently brief that plant remains immediately above and below it are essentially identical in age.

sufficient grains for a meaningful count. Rare cases exist in which a single distinctive mineral is characteristic of a certain tephra layer, as are cummingtonite in Mount St. Helens tephra set Y (Westgate and Gorton, 1981) and rare biotite in tephras from Hayes volcano (Riehle, 1985; Riehle and others, 1990). Hayes vent tephras are also distinguished by amphibole-to-pyroxene ratios of ≥ 4:1 (Riehle and others, 1990).

The Kenai Peninsula tephra samples were cleaned and sieved, and petrographic examinations were carried out on grain mounts prepared from the -60 to +230-mesh fraction (0.250–0.063 mm) (table 2). Mafic phenocrysts were categorized as orthopyroxene (OPX), clinopyroxene (CPX), amphibole (AMP), and other minerals (Other). The mafic mineralogy of the three samples consisted exclusively of amphibole and pyroxene. No biotite was identified in any of the samples, with or without attached glass. This is troubling in light of the well-documented use of trace biotite as an indicator mineral of Hayes tephra (Riehle, 1985; Riehle and others, 1990; Begét and others, 1991). However, Riehle and others (1990) note that 2 percent of all Hayes tephra samples they have examined do not contain biotite. Although tephra deposits of Hayes volcano are widely dispersed to the south and northeast of the vent, it is possible that the Kenai Peninsula tephras discussed here were either deposited by a plume that did not contain biotite, or the biotite was removed by density fractionation during transport. Identifying more mineral grains might result in the recognition of biotite in one or more of these tephras, but this is unlikely because we identified a large number of grains (up to 692) to attain our results. In any event, the absence of biotite alone does not preclude a correlation with Hayes tephra.

Amphibole-to-pyroxene ratios for the Kenai Peninsula tephras are shown in table 2. Tephra A-T2 is distinctly different from the other tephras and is mineralogically dissimilar to Hayes tephra. Ratios for tephras A-T1 and B-T1 meet or closely approach the Hayes average of > 4:1. Although tephra A-T1 shows a slightly lower ratio than Hayes tephras studied by Riehle (1985), Begét and others (1991) reported correlative tephras with amphibole to pyroxene ratios as low as 1.5:1. Figure 4 shows the mineralogic data plotted on a ternary diagram using clinopyroxene, orthopyroxene, and amphibole as vertices. The diagram compares Holocene deposits that were erupted from Spurr, Redoubt, and Hayes volcanoes. Tephras A-T1 and B-T1 are similar to Hayes tephra and are distinctly dissimilar to Spurr and Redoubt tephras. Mineralogy of tephra A-T2 most closely resembles that of Redoubt.

Table 2. *Mafic-phenocryst mineralogy of Kenai Peninsula tephras* [*Numbers indicate grains indentified using a petrographic microscope. CPX: clinopyroxene; OPX: orthopyroxene; AMP: amphibole; PX: total pyroxene. For sample locations and stratigraphic positions, see figures 1 and 2, respectively*]

Location-sample	CPX	OPX	AMP	Other	Total	CPX/ OPX/AMP	AMP: PX
A-T1	18	66	271	0	355	5/19/76	3.2:1
A-T2	252	420	5	0	677	37/62/1	1:99
B-T1	31	96	565	0	692	4/14/82	4.5:1

GLASS COMPOSITION

Successful correlation of tephras requires that they possess distinguishing characteristics by which they may be identified as unique. The chemical composition of glass is one of the most reliable characteristics by which tephras can be compared. Sarna-Wojcicki (1976) and Sarna-Wojcicki and others (1979; 1981; 1984) showed that tephras that were erupted over periods as short as several tens to several hundreds of years could be successfully distinguished, even if erupted from the same source. This is possible because the composition of glass can be analyzed with a high degree of precision, silicic volcanic glass is usually homogeneous in a single eruption, and tephras erupted at different times from the same or different sources usually differ in chemical composition. Bulk glass analysis eliminates the problem of contamination due to reworking and mixing with detrital mineral grains but not the problem of detrital glass contamination, which can be pervasive in areas subject to repeated episodes of tephrafall because of proximity to volcanic source areas. Mineral, vapor, and fluid inclusions will also introduce error, as will coatings of weathering products on shard surfaces. Grain-discrete analysis by electron-microprobe of individual glass shards avoids most of these sources of error (Smith and Westgate, 1969).

We determined glass compositions of the Kenai Peninsula tephras using an automated nine-channel microprobe. The reported compositions in table 3 are averages of analyses of multiple glass shards. The values have been normalized to correct for hydration. We also determined chlorine contents but have omitted them because of their trace concentrations. Other workers rarely analyze for chlorine so it would be of little use in comparing with other data sets. Tephras A-T1 and B-T1 are very homogeneous and are highly similar in composition. Tephra A-T2 has two populations of glass composition that are different at one standard deviation. The less silicic population, A-T2(P2), strongly resembles the other two tephras, but the more silicic population, A-T2(P1), is quite different.

Also shown in table 3 are the chemical compositions of Hayes proximal and distal tephras reported by Riehle (1985) and Begét and others (1991). We omitted chlorine from the distal data of Begét and others (1991) and manganese from the proximal data of Riehle (1985). We then normalized the data for comparison with the Kenai Peninsula data. Tephras A-T1, B-T1, and A-T2(P2) overlap all the Hayes proximal samples and some of the Hayes distal samples at one standard deviation. Tephra population A-T2(P1) barely overlaps all the proximal

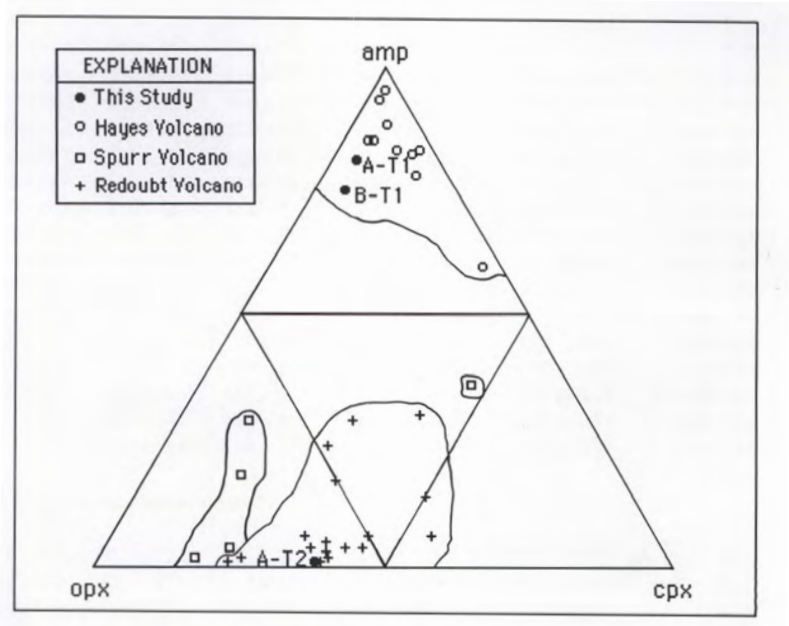

Figure 4. *Ternary diagram showing mafic-phenocryst mineralogy of tephra samples from Hayes, Spurr, and Redoubt volcanoes. (Data from Riehle, 1985; Begét and others, 1991; and this study.)*

tephra samples and overlaps none of the distal samples at one standard deviation.

Westgate and Gorton (1981) showed that tephras can be distinguished and correlated by plotting various oxide concentrations and identifying graphical fields characteristic of different tephras and source volcanoes. Riehle (1985) and Begét and others (1991) utilized this method to successfully differentiate between tephras erupted from Hayes volcano and those from other Cook Inlet volcanoes. Plots of SiO_2 against the ratio FeO*/MgO and K_2O against SiO_2 illustrate that tephras A-T1, B-T1 and A-T2(P2) fall well within the fields delimiting Hayes tephra (fig. 5). The same plots show that tephra population A-T2(P1) is distinctly different from most Hayes samples and, in fact, does not closely resemble any of the other Cook Inlet tephras plotted.

SIMILARITY COEFFICIENTS

The similarity coefficient (SC) developed by Borchardt and others (1972) to compare tephras analyzed by instrumental neutron activation is the average ratio of the major oxides with the lesser concentration always as the numerator. The result is a single parameter denoting

Table 3. *Glass compositions of Kenai Peninsula tephras and distal and proximal Hayes tephras* [*Major oxides in glass separates given in normalized weight percent. Total Fe reported as Fe_2O_3. N = total number of analyses. (-) Not known. Kenai Peninsula analyses carried out on the Washington State University Cameca MBX microprobe. Standards used were CCNM-211 (obsidian), K-411 (NBS glass for Mg, Ca) and KCl (CMTB-2 for Cl). Analytical conditions: 15kV, 13.5 nA, 8-µm beam, 10-sec counting time. Cl concentrations not reported. Data from Begét and others (1991) and Riehle (1985) normalized to 100 percent*]

Sample	SiO_2	Al_2O_3	Fe_2O_3	CaO	Na_2O	K_2O	MgO	TiO_2	Total	N
Probable Hayes tephra, Kenai Peninsula										
A-T1	75.29 ± 0.50	13.75 ± 0.26	1.73 ± 0.20	2.17 ± 0.21	3.84 ± 0.18	2.56 ± 0.13	0.45 ± 0.04	0.22 ± 0.05	100	17
B-T1	75.60 ± 0.61	13.51 ± 0.31	1.60 ± 0.32	2.17 ± 0.24	3.96 ± 0.30	2.53 ± 0.29	0.40 ± 0.10	0.23 ± 0.05	100	22
Tephra of unknown origin, Kenai Peninsula										
A-T2(P1)	77.34 ± 0.23	12.50 ± 0.17	1.40 ± 0.11	1.31 ± 0.07	4.06 ± 0.06	2.88 ± 0.06	0.27 ± 0.05	0.24 ± 0.07	100	15
A-T2(P2)	74.46 ± 0.63	13.89 ± 0.49	1.85 ± 0.44	2.21 ± 0.26	4.33 ± 0.19	2.49 ± 0.15	0.43 ± 0.15	0.35 ± 0.10	100	8
Hayes distal tephra (Begét and others, 1991)										
88-TL-CC	73.80 ± 0.35	14.68 ± 0.21	2.03 ± 0.18	2.29 ± 0.09	3.91 ± 0.12	2.55 ± 0.10	0.53 ± 0.05	0.22 ± 0.07	100	13
TL-3	74.08 ± 0.38	14.67 ± 0.16	1.87 ± 0.16	2.32 ± 0.10	3.78 ± 0.11	2.51 ± 0.07	0.53 ± 0.04	0.24 ± 0.04	100	13
TL-7	74.12 ± 0.47	14.61 ± 0.14	1.97 ± 0.22	2.26 ± 0.10	3.80 ± 0.17	2.47 ± 0.06	0.52 ± 0.10	0.25 ± 0.04	100	5
TL-8	74.06 ± 0.40	14.51 ± 0.33	1.99 ± 0.17	2.21 ± 0.27	3.82 ± 0.13	2.64 ± 0.45	0.50 ± 0.05	0.27 ± 0.07	100	15
TL-9	74.01 ± 0.57	14.64 ± 0.21	1.92 ± 0.20	2.31 ± 0.17	3.83 ± 0.11	2.54 ± 0.12	0.53 ± 0.07	0.22 ± 0.03	100	14
ATC-633	73.92 ± 0.36	14.55 ± 0.14	1.95 ± 0.21	2.24 ± 0.10	3.94 ± 0.08	2.63 ± 0.11	0.54 ± 0.03	0.23 ± 0.03	100	15
ATC-634	73.97 ± 0.36	14.59 ± 0.19	1.87 ± 0.14	2.24 ± 0.13	3.95 ± 0.13	2.62 ± 0.06	0.53 ± 0.05	0.23 ± 0.04	100	18
ATC-635	73.94 ± 0.58	14.66 ± 0.25	1.89 ± 0.19	2.24 ± 0.11	3.90 ± 0.15	2.59 ± 0.08	0.55 ± 0.05	0.23 ± 0.11	100	17
ATC-636	73.68 ± 0.50	14.71 ± 0.21	1.95 ± 0.17	2.32 ± 0.16	3.93 ± 0.11	2.62 ± 0.10	0.55 ± 0.05	0.24 ± 0.03	100	19
ATC-637	73.95 ± 0.53	14.60 ± 0.12	1.87 ± 0.21	2.26 ± 0.15	3.94 ± 0.10	2.60 ± 0.07	0.54 ± 0.07	0.24 ± 0.04	100	11
ATC-638(P1)	74.02 ± 0.33	14.51 ± 0.09	1.91 ± 0.07	2.26 ± 0.10	3.99 ± 0.07	2.58 ± 0.07	0.49 ± 0.06	0.24 ± 0.04	100	5
ATC-638(P2)	74.81 ± 0.22	14.27 ± 0.12	1.67 ± 0.13	2.02 ± 0.05	3.92 ± 0.15	2.61 ± 0.04	0.49 ± 0.03	0.21 ± 0.06	100	7
ATC-639	73.91 ± 0.34	14.70 ± 0.15	1.95 ± 0.11	2.24 ± 0.01	3.83 ± 0.08	2.57 ± 0.06	0.54 ± 0.04	0.25 ± 0.02	100	11
ATC-640	74.01 ± 0.47	14.55 ± 0.21	1.91 ± 0.15	2.26 ± 0.13	3.92 ± 0.13	2.58 ± 0.06	0.53 ± 0.04	0.24 ± 0.04	100	16
ATC-641	73.85 ± 0.39	14.70 ± 0.28	1.91 ± 0.16	2.26 ± 0.13	3.92 ± 0.17	2.61 ± 0.10	0.53 ± 0.07	0.22 ± 0.03	100	15
ATC-642(P1)	73.59 ± 0.22	14.74 ± 0.20	1.94 ± 0.12	2.36 ± 0.09	3.90 ± 0.10	2.61 ± 0.09	0.61 ± 0.14	0.24 ± 0.20	100	10
ATC-642(P2)	72.84 ± 0.43	14.98 ± 0.39	2.11 ± 0.26	2.44 ± 0.34	3.99 ± 0.12	2.73 ± 0.35	0.65 ± 0.14	0.26 ± 0.03	100	11
ATC-643	73.93 ± 0.35	14.64 ± 0.13	1.89 ± 0.13	2.26 ± 0.11	3.92 ± 0.12	2.59 ± 0.07	0.54 ± 0.04	0.23 ± 0.04	100	16
Hayes proximal tephra (Riehle, 1985)										
23-A	75.56 ± 1.5	13.86 ± 0.47	1.88 ± 0.24	2.23 ± 0.28	3.33 ± 0.30	2.45 ± 0.22	0.43 ± 0.02	0.27 ± 0.04	100	-
23-B	76.75 ± 5.3	13.09 ± 0.59	1.52 ± 0.11	1.71 ± 0.24	3.24 ± 0.21	2.98 ± 0.28	0.34 ± 0.07	0.36 ± 0.08	100	-
23-C	73.97 ± 3.5	14.88 ± 0.49	1.99 ± 0.17	2.30 ± 0.17	3.44 ± 0.20	2.65 ± 0.17	0.50 ± 0.05	0.27 ± 0.04	100	-
23-D	73.70 ± 1.6	15.08 ± 0.55	2.07 ± 0.14	2.42 ± 0.25	3.28 ± 0.12	2.60 ± 0.19	0.54 ± 0.04	0.31 ± 0.06	100	-
23-E	73.50 ± 3.1	14.97 ± 0.54	2.09 ± 0.22	2.48 ± 0.17	3.18 ± 0.25	2.89 ± 0.30	0.57 ± 0.02	0.32 ± 0.08	100	-
23-F	74.43 ± 4.6	14.89 ± 1.0	2.00 ± 0.34	2.33 ± 0.24	2.82 ± 0.27	2.71 ± 0.54	0.52 ± 0.06	0.31 ± 0.04	100	-
23-G	74.62 ± 3.8	14.84 ± 0.79	1.87 ± 0.36	2.03 ± 0.37	3.75 ± 0.34	2.17 ± 0.34	0.42 ± 0.09	0.31 ± 0.04	100	-

multivariate similarity, calculated using the simple equation:

$$d_{(A, B)} = (\sum_{i=1}^{n} Ri)/ n$$

where:

$d_{(A, B)} = d_{(B, A)}$ = SC for comparison between sample A and sample B
i = element number
$R_i = X_{iA}/X_{iB}$ if $X_{iB} > X_{iA}$
$R_i = X_{iB}/X_{iA}$ if $X_{iA} > X_{iB}$
X_{iA} = concentration of element i in sample A
X_{iB} = concentration of element i in sample B

The value of $d_{(A, B)}$ is a number between 0.00 and 1.00, with $d_{(A, B)} = 1.00$ denoting perfect similarity. Each sample in a data set may thus be compared with all other samples, and sample pairs having SCs approaching 1.00 may be considered correlative (Borchardt and others, 1972). In practice, Begét and others (1991) determined that SCs of 1.00 should not be expected, even for repeat analyses of the same sample, because the analytical precision of an electron microprobe may range from ± 0.5 to 5 percent.

Riehle (1985) made extensive use of SCs in his study of Cook Inlet tephras. He considered SCs greater than 0.95 indicative of samples from the same tephrafall, or of samples that were members of a tephra set with a high degree of similarity. Values of 0.93 or 0.94 were thought to represent samples comprising a tephra set or the same tephrafall where concentrations of one or more elements were unreliable. Similarity coefficients between 0.90 and 0.93 were considered to indicate samples of the same set but not the same tephrafall, provided that stratigraphy and mineralogy were in agreement. Riehle and others (1990) correlated distal samples with proximal Hayes deposits chiefly on the basis of SCs of at least 0.94 with one or more of the proximal samples. Begét and others (1991) accepted SCs greater than or equal to 0.94 as indicative of correlations between Hayes tephra samples.

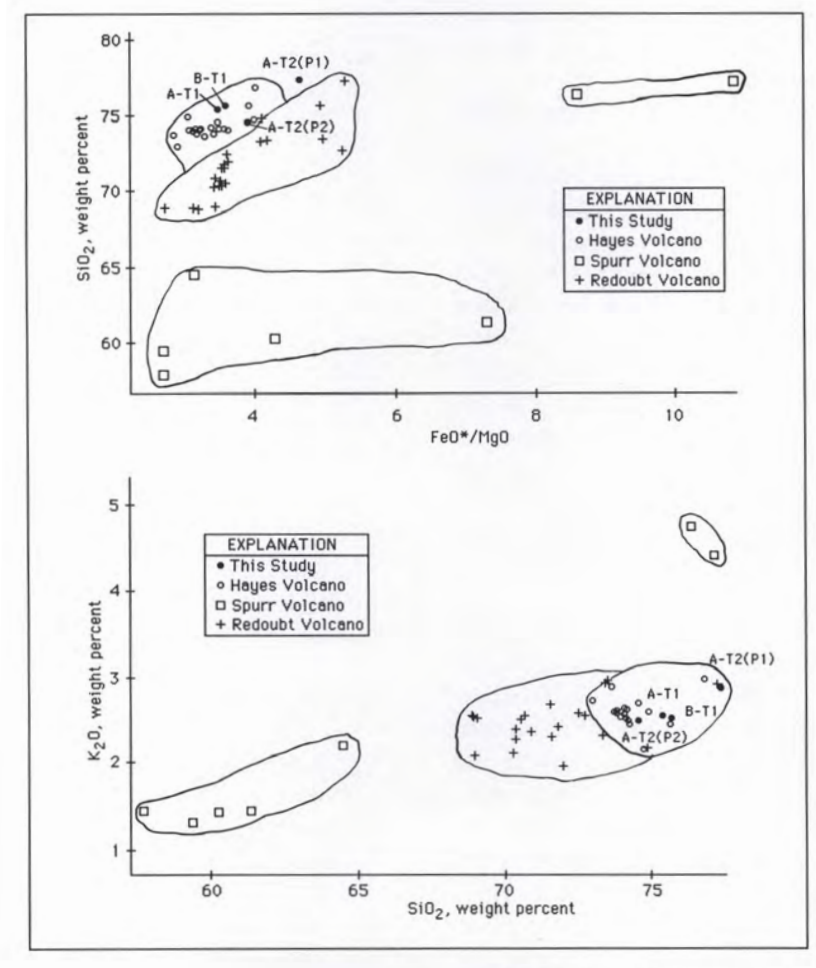

Figure 5. *Comparisons of plots of SiO_2 vs FeO*/MgO and K_2O vs SiO_2 in glass compositions of tephra samples from Hayes, Spurr, and Redoubt volcanoes (data from Riehle, 1985; Begét and others, 1991; and this study). Total iron expressed as FeO*.*

Table 4 shows SCs calculated between the Kenai Peninsula tephras and proximal and distal Hayes samples. Because analytical precision is poor for oxides of low concentration (Begét and others, 1991), and the resulting large variance can disproportionately affect the average ratio (Sarna-Wojcicki, 1976; Riehle, 1985; Riehle and others, 1990), the calculations do not include TiO_2. Tephras A-T1 and B-T1 are highly similar to each other (SC 0.97) and are probably correlative. Although population A-T2(P2) is also highly similar to these samples (SC 0.96, 0.95), factors discussed below preclude correlation with tephras A-T1 and B-T1. Tephra A-T1 is similar to most distal Hayes samples to which it is compared, with an average SC of 0.94. This sample is also most similar to proximal Hayes reference sample 23-A (SC 0.95). Tephra B-T1 is somewhat less similar to the distal Hayes samples, having an average SC of only 0.91, but it too is most similar to proximal Hayes sample 23-A (SC 0.94). Because of similarities in age, mineralogy, and chemistry, it seems highly likely that tephra layers A-T1 and B-T1 were deposited during the same eruption of Hayes volcano that deposited proximal sample 23-A.

Proximal sample 23-A was from tephra that erupted in an eastward-directed lobe with an axis just north of Anchorage (Riehle and others, 1990). If the Kenai tephra layers were deposited by this plume, as the data suggest, then either (1) they represent the southern margin of the plume, (2) the axis of this plume varied north and south of Anchorage during eruption, or (3) the axis of this lobe may be more southerly directed than previously suggested. The thickness of the Kenai ash layers (3 cm) contraindicates deposition at the plume edge. The data of Riehle (1985) and Riehle and others (1990) support a plume axis directed north of Anchorage at some time during the ash eruption. The most reasonable conclusion is that the plume axis shifted in response to changing wind direction during the eruption that deposited proximal sample 23-A and the Kenai ash layers.

Tephra population A-T2(P2) may appear to correlate with Hayes tephra, having an average SC of 0.93 with distal samples and SCs of 0.96 and 0.94 with proximal samples 23-A and 23-G. Because tephra A-T2 has been dated to about 5–6 ka B.P. (table 1) and is characterized by mineralogy distinctly different from that of Hayes tephra (fig. 4), it is highly unlikely that population A-T2(P2) correlates with the Hayes tephra set, which was erupted about 3,700 yr B.P. This similarity in chemical composition may reflect a similar source magma at another volcano, or perhaps it records a previously unrecognized 5–6 ka B.P. eruption at Hayes volcano. The other glass population, A-T2(P1), bears no resemblance to any of the Hayes samples (SC 0.74–0.88) and, in fact, does not resemble the composition of any other recorded Cook Inlet tephra.

Table 4. *Similarity coefficients of Kenai tephras*

Loc.-Sample:	A-T1	B-T1	A-T2(P1)	A-T2(P2)
Probable Hayes tephra, Kenai Peninsula				
A-T1	1.00	0.97	0.82	0.96
B-T1	0.97	1.00	0.84	0.95
Tephra of unknown origin, Kenai Peninsula				
A-T2(P1)	0.82	0.84	1.00	0.81
A-T2(P2)	0.96	0.95	0.81	1.00
Hayes distal tephra (Begét and others, 1991)				
88-TL-CC	0.93	0.91	0.78	0.93
TL-3	0.94	0.91	0.78	0.94
TL-7	0.94	0.91	0.77	0.94
TL-8	0.95	0.92	0.79	0.94
TL-9	0.94	0.91	0.78	0.93
ATC-633	0.94	0.91	0.79	0.93
ATC-634	0.94	0.92	0.79	0.94
ATC-635	0.94	0.92	0.78	0.93
ATC-636	0.93	0.91	0.78	0.92
ATC-637	0.94	0.92	0.79	0.94
ATC-638(P1)	0.95	0.93	0.79	0.95
ATC-638(P2)	0.96	0.94	0.82	0.93
ATC-639	0.94	0.91	0.78	0.93
ATC-640	0.94	0.92	0.79	0.94
ATC-641	0.94	0.92	0.79	0.94
ATC-642(P1)	0.92	0.89	0.77	0.91
ATC-642(P2)	0.88	0.86	0.76	0.88
ATC-643	0.94	0.92	0.79	0.94
Hayes proximal tephra (Riehle, 1985)				
23-A	0.95	0.94	0.79	0.96
23-B	0.87	0.89	0.88	0.84
23-C	0.92	0.90	0.77	0.92
23-D	0.90	0.87	0.74	0.89
23-E	0.87	0.84	0.75	0.86
23-F	0.89	0.86	0.75	0.89
23-G	0.93	0.92	0.79	0.94

We cannot determine whether tephra A-T2 is a single, bimodal ash or a combination of eruptive products from two separate volcanoes.

CONCLUSIONS

A prominent, 3-cm-thick tephra layer embedded in peat deposits along the lower Kasilof and Kenai Rivers shows strong similarity with the Hayes tephra set on the basis of mafic mineralogy, glass chemistry, and age. Although samples of the tephra lack biotite, which is a widely used indicator mineral of Hayes tephra, the mafic mineralogy otherwise correlates well with known Hayes tephras and is distinctly different from tephras originating at other sources. Lack of observed biotite may be a result of very low concentration, density fractionation during transport, or absence of biotite in the originating plume.

Tephra T1 was deposited by an east- to southeast-directed ash plume from Hayes volcano.

The weighted average age of peat and wood samples immediately above and below tephra T1 at sites A and B is 3,530 ± 70 ^{14}C yr B.P. (3,690–3,880 cal yr B.P.; table 1). This age is identical at ± 1 standard deviation to the average age of 3,650 ± 150 ^{14}C yr B.P. (3,730–4,150 cal yr B.P.) reported by Riehle (1985) for 11 radiocarbon ages throughout the region.

A second prominent tephra (T2) at site A was deposited about 5–6 cal ka B.P. Tephra T2 has two glass populations, one of which is similar to Hayes tephra. However, age and mafic mineralogy of tephra T2 are distinctly different from the Hayes set. Population T2(P2) may record a previously unrecognized 5–6-ka eruption of Hayes volcano or may be the product of another volcano with a similar source magma. Glass population T1(P1) does not resemble any samples of Hayes tephra or other recorded Cook Inlet tephras. We cannot determine the source of tephra T2 from the available data.

ACKNOWLEDGMENTS

The U.S. Geological Survey, Department of the Interior, partially supported this study under National Earthquake Hazards Reduction Program award 14-08-0001-G1949. We thank Richard Reger for his assistance in the field and in electron microprobe analysis of the tephra samples. We also thank microprobe technicians Scott Cornelius and Diane Johnson, Washington State University, for their assistance. Reger and James Riehle provided thoughtful review comments on the manuscript.

REFERENCES CITED

Begét, J.E., Reger, R.D., Pinney, D.S., Gillispie, Tom, and Campbell, Kathy, 1991, Correlation of the Holocene Jarvis Creek, Tangle Lakes, Cantwell, and Hayes tephras in south-central and central Alaska: Quaternay Research, v. 35, no. 2, p. 174-189.

Borchardt, G.A., Aruscavage, P.J., and Millard, H.T., Jr., 1972, Correlation of the Bishop Ash, a Pleistocene marker bed, using instrumental neutron activation analysis: Journal of Sedimentary Petrology, v. 42, no. 2, p. 301-306.

Combellick, R.A., 1994, Investigation of peat stratigraphy in tidal marshes along Cook Inlet, Alaska, to determine the frequency of 1964-style great earthquakes in the Anchorage region: Alaska Division of Geological & Geophysical Surveys Report of Investigations 94-7, 24 p.

Combellick, R.A., and Reger, R.D. 1994, Sedimentological and radiocarbon-age data for tidal marshes along eastern and upper Cook Inlet, Alaska: Alaska Division of Geological & Geophysical Surveys Report of Investigations 94-6, 60 p.

Pearson, G.W., and Stuiver, Minze, 1993, High-precision bidecadal calibration of the radiocarbon time scale 500-2500 BC: Radiocarbon, v. 35, p. 25-33.

Riehle, J.R., 1985, A reconnaissance of the major Holocene tephra deposits in the upper Cook Inlet region, Alaska: Journal of Volcanology and Geothermal Research, v. 26, p. 37-74.

Riehle, J.R., Bowers, P.M., and Ager, T.A., 1990, The Hayes tephra deposits, an upper Holocene marker horizon in south-central Alaska: Quaternary Research, v. 33, no. 3, p. 276-290.

Sarna-Wojcicki, A.M., 1976, Correlation of late Cenozoic tuffs in the central Coast Ranges of California by means of trace- and minor-element chemistry: U.S. Geological Survey Professional Paper 972, 30 p.

Sarna-Wojcicki, A.M., Bowman, H.W., and Russell, P.C., 1979, Chemical correlation of some late Cenozoic tuffs of northern and central California by neutron activation analysis of glass and comparison with x-ray fluorescence analysis: U.S. Geological Survey Professional Paper 1147, 15 p.

Sarna-Wojcicki, A.M., Meyer, C.E., Woodward, M.J., and Lamothe, P.J., 1981, Composition of air-fall ash erupted on May 18, May 25, June 12, July 22, and August 7, *in* Lipman, P.W., and Mullineaux, D.R., eds., The 1980 eruptions of Mount St. Helens, Washington: U.S. Geological Survey Professional Paper 1250, p. 667-681.

Sarna-Wojcicki, A.M., Bowman, H.R, Meyer, C.E., Russell, P.C., Woodward, M.J., McCoy, Gail, Rowe, J.J., Jr., Baedecker, P.A., Asaro, Frank, and Michael, Helen, 1984, Chemical analyses, correlations, and ages of upper Pliocene and Pleistocene ash layers of east-central and southern California: U.S. Geological Survey Professional Paper 1293, 40 p.

Smith, D.G.W., and Westgate, J.A., 1969, Electron probe technique for characterizing pyroclastic deposits: Earth and Planetary Science Letters, v. 5, p. 313-319.

Stuiver, Minze, and Reimer, P.J., 1993, Extended ^{14}C database and revised CALIB radiocarbon calibration program: Radiocarbon, v. 35, p. 215-230.

Till, A.B., Yount, M.E., and Riehle, J.R., 1993, Redoubt volcano, southern Alaska: A hazard assessment based on eruptive activity through 1968: U.S. Geological Survey Bulletin 1996, 19 p.

Westgate, J.A., and Gorton, M.P., 1981, Correlation techniques in tephra studies, *in* Self, S., and Sparks, R.S.J., eds., Tephra Studies: Dordrecht, Reidel, NATO Advanced Study Institute Series C, Mathematical and Physical Sciences, p. 73-94.

GEOCHEMISTRY OF SALINE LAKES OF THE NORTHEASTERN YUKON FLATS, EASTCENTRAL ALASKA

by
Daniel B. Hawkins[1]

ABSTRACT

Shallow alkaline (pH 9.3) brackish Mg-Na-$HC0_3$-C1 ponds rimmed with evaporite minerals such as trona ($Na_3(CO_3)(HCO_3)\cdot 2H_20$) occur in the Yukon Flats above the Arctic Circle in northeastern Alaska. These ponds form in an area of Alaska characterized by an extreme continental climate with about 15 cm of precipitation annually. The lakes and ponds are fed by ground water and surface water related to the major rivers of the area. Evaporite formation occurs because evaporation exceeds inflow. Fresh-water lakes and rivers are Ca-HCO_3 waters. In the rivers, 2m Ca^{+2} > then total alkalinity, and SO_4^{-2} is abundant relative to $C1^-$. In the fresh-water lakes 2m Ca^{+2} < total alkalinity, and SO_4^{-2} is almost absent. Reduction of sulfate accompanied by bicarbonate formation in the ground water produces a large excess of alkalinity over Ca^{+2}, resulting in depletion of Ca^{+2} through precipitation of calcite. Pond-water compositions have 2m Mg^{+2} < alkalinity, a condition that must produce trona and associated minerals on complete evaporation. It is unlikely that deposits of economic value result from such lakes of the region.

INTRODUCTION

Clautice and Mowatt (1982) described lakes in the Yukon Flats, eastcentral Alaska (fig. 1) that are alkaline (to pH 9.8) and rimmed with deposits of evaporite minerals such as trona ($NaHCO_3$-Na_2CO_3), nahcohlite ($NaHCO_3$), and dawsonite ($NaAlCO_3(OH)_2$). Clautice and Mowatt restricted their work to a study of the evaporite minerals and did not include water analyses. The present study focuses mainly on the chemistry of the waters. The geologic setting of the study area was summarized by Clautice and Mowatt and is not restated here.

Evaporite lakes such as those studied here are found elsewhere in the world, usually in hot arid regions like the inner basins of the western United States, the rift valleys of Africa, and similar regions of the Andes Mountains, Afghanistan, and China. Such lakes form in hydrologically closed basins where evaporation exceeds inflow. Furthermore, evaporite deposits can only form when a sufficient supply of solutes is available from the various inflow sources. These contradictory requirements are met in desert regions where high mountains provide a rain shadow for the basin floors and also act as a catchment area for precipitation. Saline lakes are the end result of a series of chemical interactions of water with bedrock and with previously deposited minerals in response to particular environmental conditions. The lakes are sensitive indicators of past and present climatic and tectonic conditions.

An extensive body of literature deals with saline lakes. Eugster and Hardie (1978), Eugster (1980), and Von Damm and Edmond (1984) reviewed the geochemistry of these lakes. More recently, in 1989 an International Consortium for Salt Lake Research (ICSLR) was established in 1989 and began publishing SALINET, a journal concerned with biology, conservation, hydrology, geology, chemistry, physics, and economic uses of inland salt lakes.

Evaporite lakes occur in both the Arctic and Antarctic. For example, Matsubaya and others (1979) and Keys and Williams (1981) reported marine evaporite lakes in Antarctica. Brine lakes originating from subpermafrost ground water are reported from Yakutia, (D.M. Hopkins, oral commun., 1994) an area climatically similar to the Yukon Flats. In Alaska, Slaughter and Hartzmann (1993) studied similar lakes with unusual hydrology and chemistry that resulted from the thawing of an open-system pingo: the brine lakes in Yakutia would probably be similar to these lakes. The lakes discussed in the present study, although probably influenced by permafrost, seem to form in the same way as other saline lakes of the world, that is, in situations where evaporation exceeds inflow. The climate of the upper Yukon Flats is that of a high-latitude desert. Annual precipitation is 25 cm and the area is characterized by extremes of temperature ranging from a maximum of 37.8°C to a minimum of -59.4°C (Hartman and Johnson, 1978, fig. 24).

The earliest report of the evaporite lakes north of Fort Yukon by Mertie and others (1929) described the presence of potassium salts in several lakes that did not freeze completely during winter. The evaporite lakes are well known to pilots of interior Alaska because of the white clouds of dust that blow up from the dry lake beds during windy days. Clautice and Mowatt (1982) noted that the various evaporite lakes are also visible on aerial, low-level, false-color IR photographs.

[1]University of Alaska, P.O. Box 755780, Fairbanks, Alaska 99775-5780.

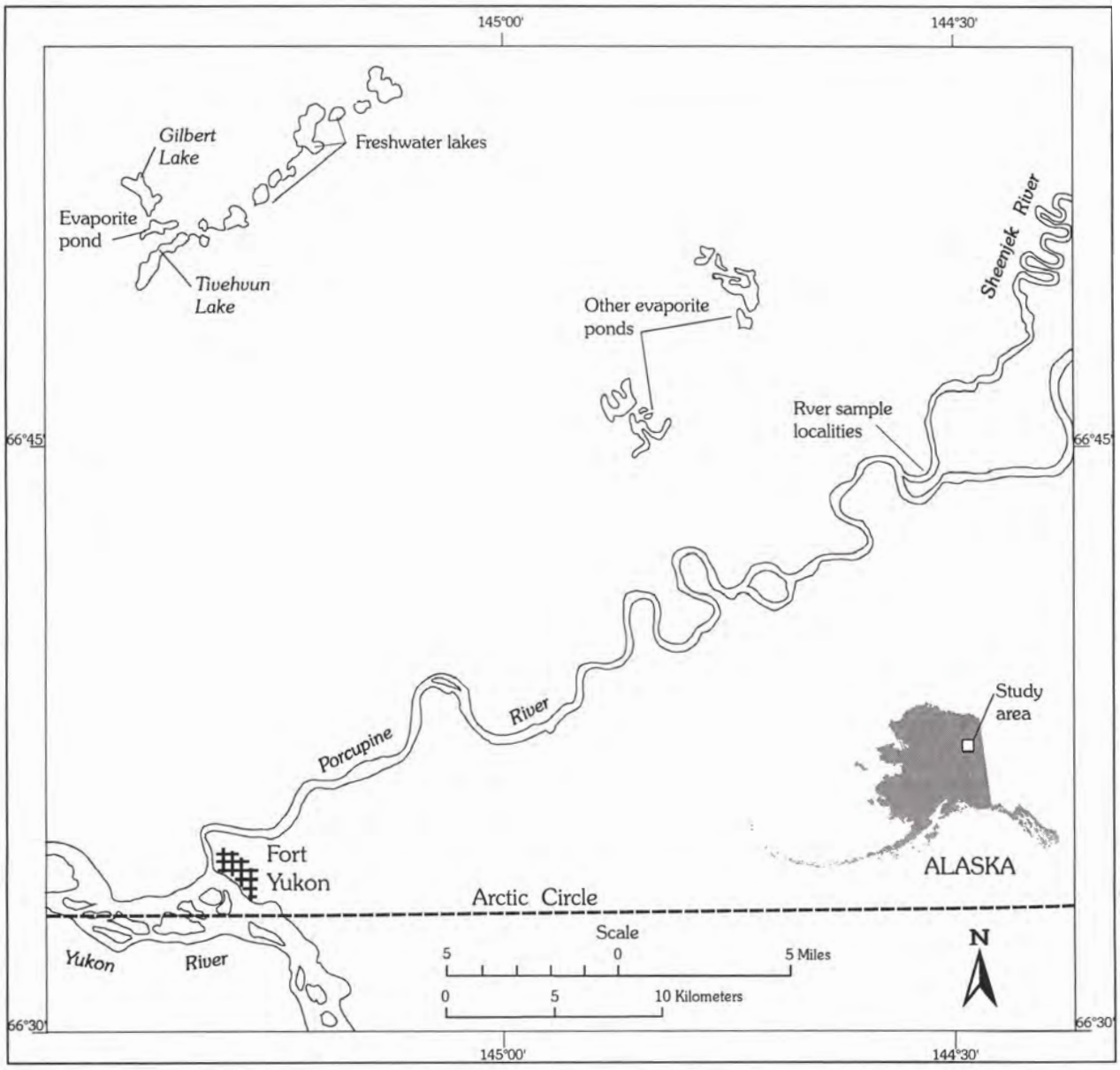

Figure 1. *Location map of the study area, evaporite pond, freshwater lakes, and river sample localities.*

It is not clear how large-scale tectonic features such as splays of the Kaltag–Porcupine and Tintina fault systems affect the distribution and hydrology of the lakes of the region. Evaporite lakes seem to be randomly distributed among nonevaporite lakes of the upper Yukon Flats. Many lakes, both fresh and saline, appear to be distributed in a roughly linear fashion that parallels the course of the Yukon River. Often, the lakes are old, cutoff meanders of the various rivers and streams of the region. Some of the lakes, for example, Tivehvun Lake (fig. 1), may be beaded-drainage lakes that were formed by a stream cross-cutting polygonal frozen ground. David Hopkins (oral commun., 1988) suggests that some of the lakes may also have formed by confinement behind natural levees, and, for the lakes near Stevens Village, from kettles in the glacial outwash. Deeper subpermafrost waters may contribute to the hydrology of the kettle lakes. As a result, these lakes may be chemically different from lakes influenced by surface water and shallow ground water. The evaporite lakes discussed here are those derived from such shallow waters.

The evaporite lakes of the Yukon Flats occur in a hydrologically and environmentally important area of Alaska. Because these saline lakes are sensitive to their environmental setting they provide information about the past and present hydrogeochemistry of this area that straddles the Arctic Circle, an area for which there is a paucity of such information.

My objectives in this study were to obtain data on the hydrogeochemistry of some saline lakes in the Yukon Flats; to determine possible geochemical pathways resulting in formation of evaporite minerals in such lakes; to evaluate the economic potential of evaporite deposits from such lakes.

METHODS

SAMPLING

Water samples were taken from evaporite lakes and from fresh water streams and lakes. Several lysimeters were placed on the wet margins of the evaporite ponds to obtain samples of soil water. Sampling followed the methods described by Jones, Eugster, and Rettig (1977), and Miller and Drever (1977), in which the water samples were collected and filtered through 0.45 micron filters. Those samples for cation analysis were acidified to pH 2 with nitric acid; those for anion analysis were not acidified. All samples were stored in acid-washed, deionized, water-rinsed polyethylene bottles. Temperature, pH, and conductivity were measured in the field using portable pH and conductivity meters.

Sediment samples were taken from the fresh-water lakes with a trip-activated grab sampler. Sediments and efflorescent crusts from the shallow evaporite ponds were collected with a trowell and stored in polyethylene bags. Several 30-cm-long core samples were taken during the placement of lysimeters.

ANALYTICAL METHODS

Alkalinity was determined on samples in the field by potentiometric titration with a standard acid solution. Alkalinity was redetermined in the laboratory by the same method. Water samples were analyzed for major ions by atomic absorption spectrometry and by ion chromatography. Sediment samples were analyzed by x-ray diffraction and optical microscopy.

RESULTS

Detailed results of the chemical analyses of the water samples, a description of the sediments, and the results of x-ray diffraction analyses are available from the author on request. A summary of the chemical analysis of the Porcupine and Sheenjek Rivers (combined), the fresh-water lakes (combined) and the evaporite lakes (combined) is shown in the bar graphs of figure 2. Important features of figure 2 are:

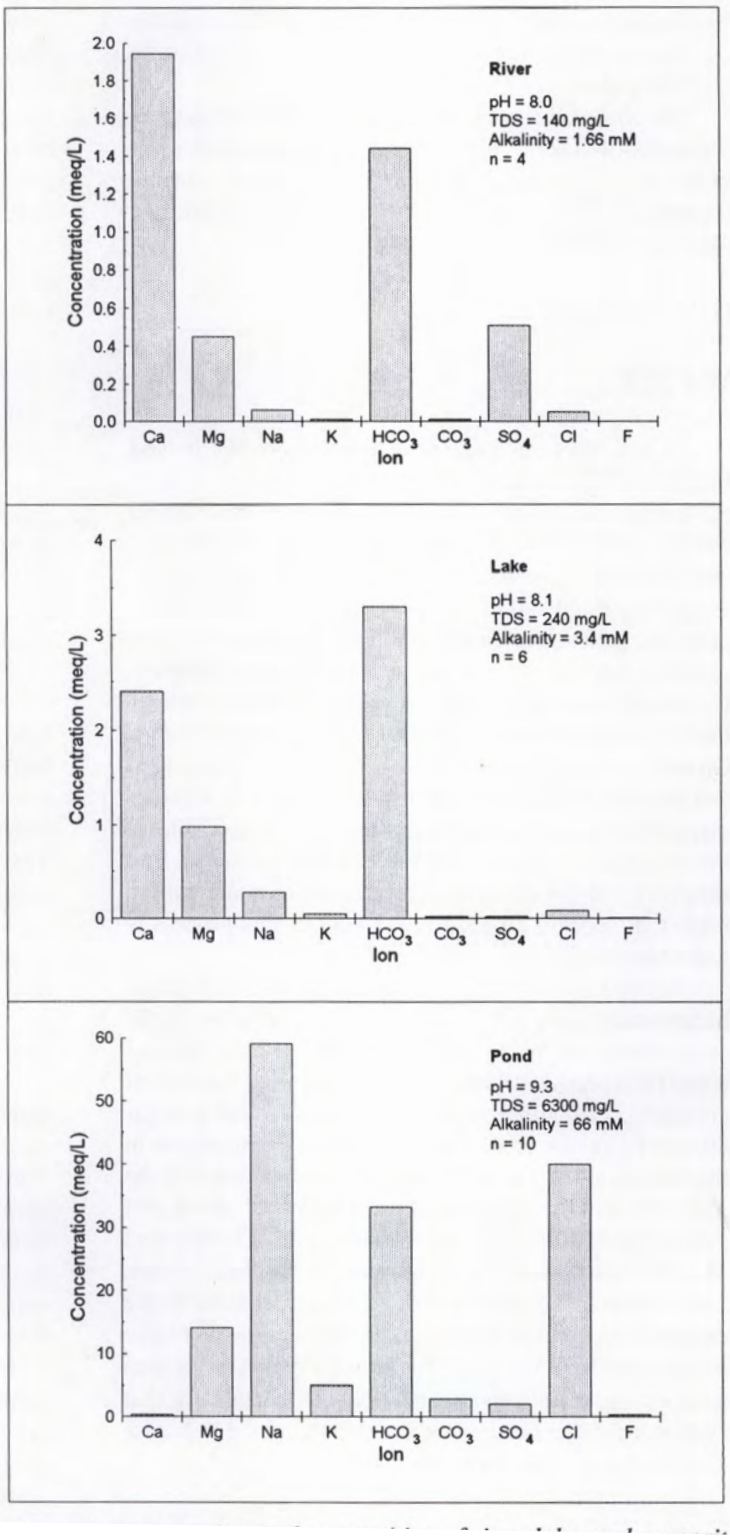

Figure 2. *Average chemical composition of river, lake, and evaporite pond waters. TDS = total dissolved solids.*

- In the river water, calcium exceeds bicarbonate; sulfate is a relatively major ion.
- In the lake water, alkalinity exceeds 2 m calcium, and sulfate concentration is very low.
- In the evaporite pond water, calcium is a minor constituent; alkalinity exceeds 2 m magnesium and the water is a sodium-magnesium-bicarbonate-chloride sulfate brine.

We observed that in the sediments from freshwater and evaporite lakes, calcite is a common phase in most samples, no gypsum is present, muscovite or illite is present in most of the evaporite pond samples, and we detected no trona or other evaporite minerals.

DISCUSSION

WATER

Figure 3, a flow diagram modified from Hardie and Eugster (1970) and Drever (1988), illustrates the chemical-divide concept and shows the various paths that natural waters can follow upon evaporation. Upon evaporation, water containing sodium, calcium, magnesium, bicarbonate, chloride and sulfate will precipitate calcite first. The particular path subsequently followed depends on whether calcium molarity exceeds twice the carbonate alkalinity. If calcium is in excess, the evaporation process follows Path II, if alkalinity is in excess, the process follows Path I. On further evaporation sepiolite[2] or dolomite[3] precipitate and the path subsequently followed depends on whether magnesium exceeds alkalinity. If not, the process follows Path III, the most common brine-evolution pathway. The result is a sodium-carbonate-bicarbonate-chloride-sulfate brine that deposits trona. An example of this process is Lake Magadi, Kenya.

In the river water, which is a calcium carbonate-bicarbonate water, calcium exceeds alkalinity (fig. 2). On evaporation, following precipitation of calcite, calcium could be expected to form gypsum. Keith Van Cleeve (oral commun., 1987) observed in soil evaporites the precipitation of gypsum from water of similar composition in the Tanana river. To emphasize, if the river water of the Yukon Flats were evaporated, trona may not result, but gypsum and, ultimately, halite could form. Clautice and Mowatt reported very little gypsum in the Yukon Flats. The absence of gypsum and the presence of trona in the evaporite lakes of the Yukon Flats, implies either that some source other than the major rivers and streams of the area is supplying the necessary chemical constituents, or that chemical changes occur in the river-water source and cause this water ultimately to produce trona.

Relative to the river water, the composition of the freshwater lakes (see fig. 2) shows an increase in concentration of the dissolved constituents. This increase probably results from dissolution of the minerals through which the ground water that feeds these lakes flowed. Most important, however, is the finding that the *alkalinity* of these waters exceeds calcium, and the sulfate concentration is very low. Because the alkalinity is now in excess, this water must precipitate calcite, and produce sodium-bicarbonate-chloride brines, such as those of the evaporite ponds graphed in figure 2, and produce trona on extreme evaporation.

Can the river-water composition be altered to yield the composition of the fresh-water lakes? The behavior of the sulfate suggests a plausible mechanism. As Drever (1988) has shown, loss of sulfate can be brought about by reduction of sulfate either inorganically or bacterially resulting in sulfide formation and *an increase in bicarbonate*. The following reaction from Drever (1988) shows this process:

$$8(SO_4)^{+2} + 2Fe_2O_3 + 14\,(C) + 7\,H_2O =$$
$$4\,FeS_2 + 14\,(HCO_3)^- + (CO_3)^{-2}$$

where (C) represents organic carbon and Fe_2O_3 is the reactive iron minerals in sediments with which the water is in contact. A similar reaction based upon bacterial reduction is given by Berner (1980) as follows:

$$2CH_2O + (SO_4)^{-2} = H_2S + 2(HCO_3)^-$$

These reactions result in conversion of sulfate to sulfide producing a stoichiometric equivalent of alkalinity. In the case of river water, reduction of sulfate from the observed 0.25 mM to the observed value of 0.025 mM in lake waters would produce 0.46 mM total alkalinity. This alkalinity, when combined with the measured alkalinity of the river water (1.66 mM), yields 2.12 mM alkalinity, a quantity twice the molar calcium concentration (2 x 0.97 mM) in the river water. Thus, through sulfate reduction, enough alkalinity can be generated to set the river water on the trona-producing path III (fig. 3).

The solid phase expected upon evaporation of the different waters can be seen in figure 4, a phase diagram modified from Hardie and Eugster (1970). Figure 4 illustrates that, if carbonate is removed from river water by precipitation of calcite, the water composition must move directly away from the carbonate-bicarbonate apex toward the sulfate field. Such waters would precipitate sulfate minerals such as mirabilite ($Na_2SO_4 \cdot 10H_2O$) and thenardite (Na_2SO_4) as well as trona. However, the fresh-water lakes and the evaporite ponds would precipitate trona, then trona and halite, with no sulfate minerals. Several features are clear: (1) If the fresh-water lakes are evaporated, they must ultimately yield trona. (2) River water can be converted to the "trona path" through sulfate reduction of this water during its residence as ground water feeding these lakes.

[2] ($H_6Mg_8Si_{12}O_{30}(OH)_{10}.6H_2O$)
[3] ($CaMg(CO_3)_2$)

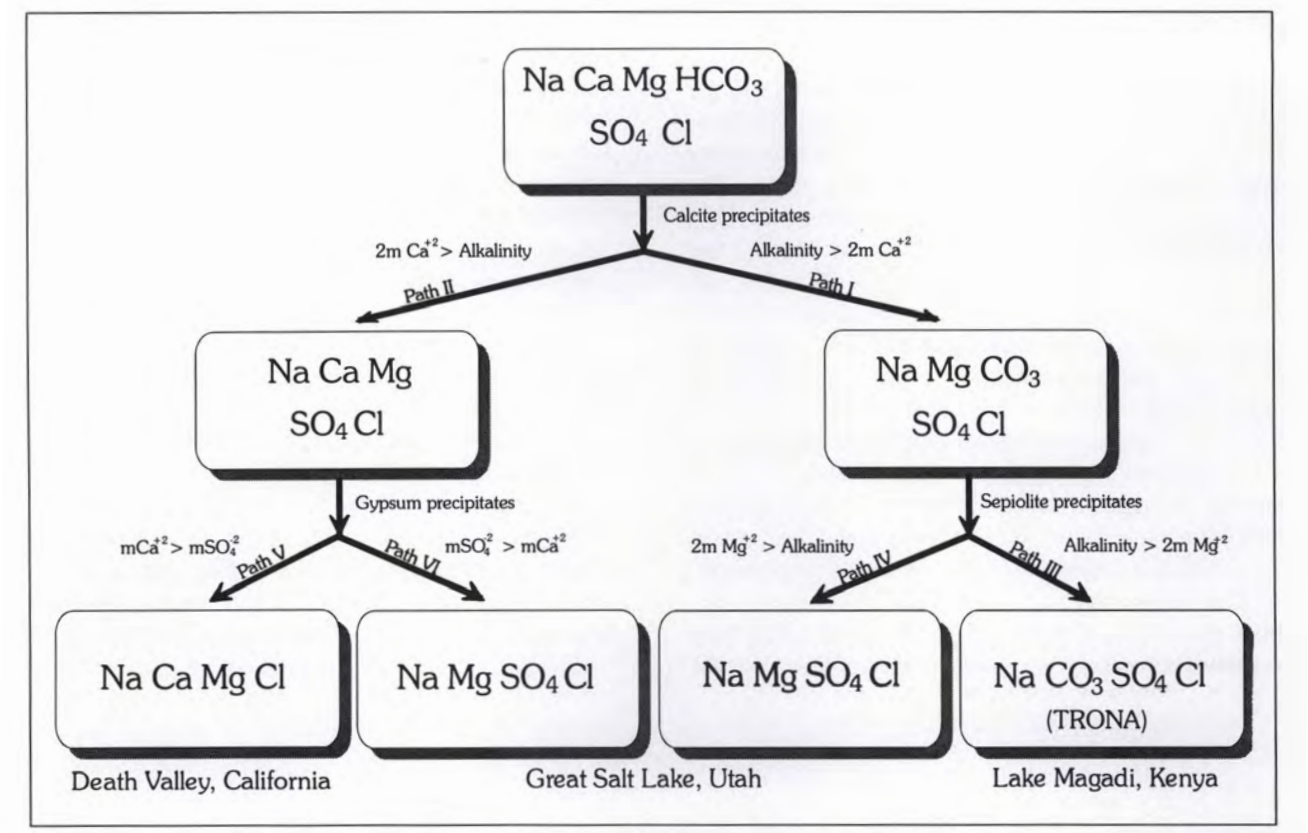

Figure 3. *Possible paths for the evaporation of waters. (Modified from Hardie and Eugster, 1970, and from Drever, 1988.)*

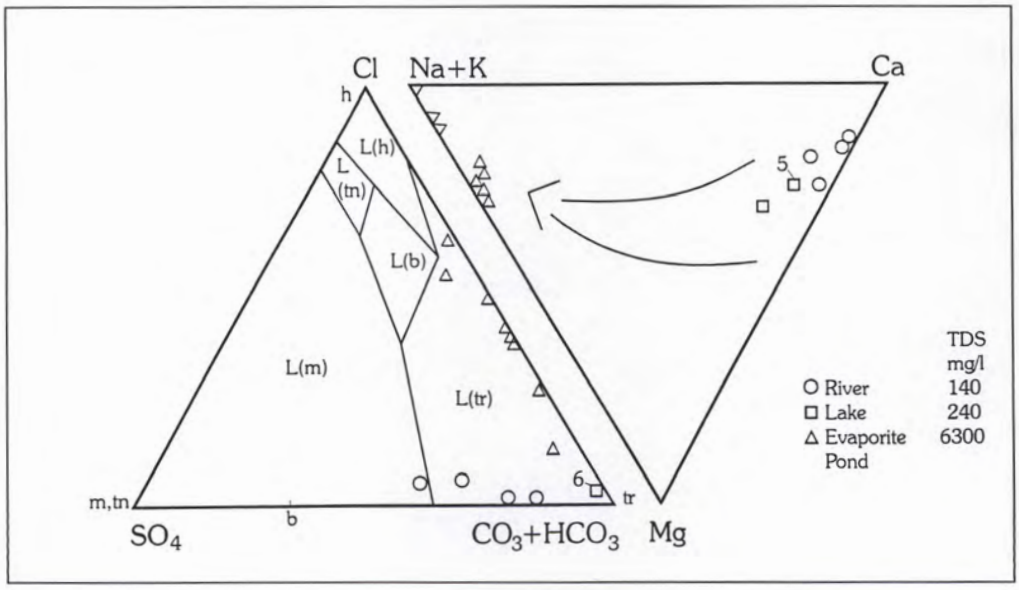

Figure 4. *Phase diagram for possible brine compositions for waters studied. (Modified from Hardie and Eugster, 1970.)*

SEDIMENTS

The lack of trona or other evaporite minerals in the sediments studied here is not surprising. Samples from the lake and pond bottom were in contact with water greatly undersaturated with respect to these phases. The evaporite ponds are subject to cycles of wetting and drying. Dried crusts from the evaporite ponds sampled had only recently dried, having undergone dissolution by rain in the days just previous to sampling. Thus, any evaporite minerals that might have been present were redissolved by the rain; there was insufficient time for significant buildup of the efflorescent crust of such minerals through prolonged evaporation of the residual water. Furthermore, as Clautice and Mowatt noted, in most cases, evaporite minerals were minor phases not readily detected by x-ray diffraction. Nonetheless, the chemistry of the pond waters is such that trona must result upon continued evaporation.

Calcite, as a major phase in the pond sediments, supports the chemical-divide mechanism invoked here because it is necessary for calcite to precipitate so that the pond waters can reach their observed composition. No sepiolite or dolomite were observed in this study. Clautice and Mowatt, however, reported abundant dolomite in many of their samples. Muscovite (probably 3T polytype) was a common and abundant constituent of the evaporite pond sediments studied here. It was especially abundant in the suspended fraction of the pond sediments. Minor chlorite usually was found with muscovite. Several samples were observed in which muscovite was accompanied by calcite, quartz and K(?)-feldspar.

Chlorite may partly control the magnesium concentration of the pond waters, but major control is probably maintained by precipitation of dolomite.

The origin of the muscovite is not clear. It could be detrital, or it could be authigenic as discussed for the Lake Shalla sediments by Van Damm and Edmond (1984). Muscovite and K-feldspar can exist stably in the waters of the evaporite ponds. This can be seen from figure 5, an ion-activity diagram modified from Garrels (1984). Here, it is seen that many water analyses plot within the muscovite stability field. The abundance of muscovite and chlorite

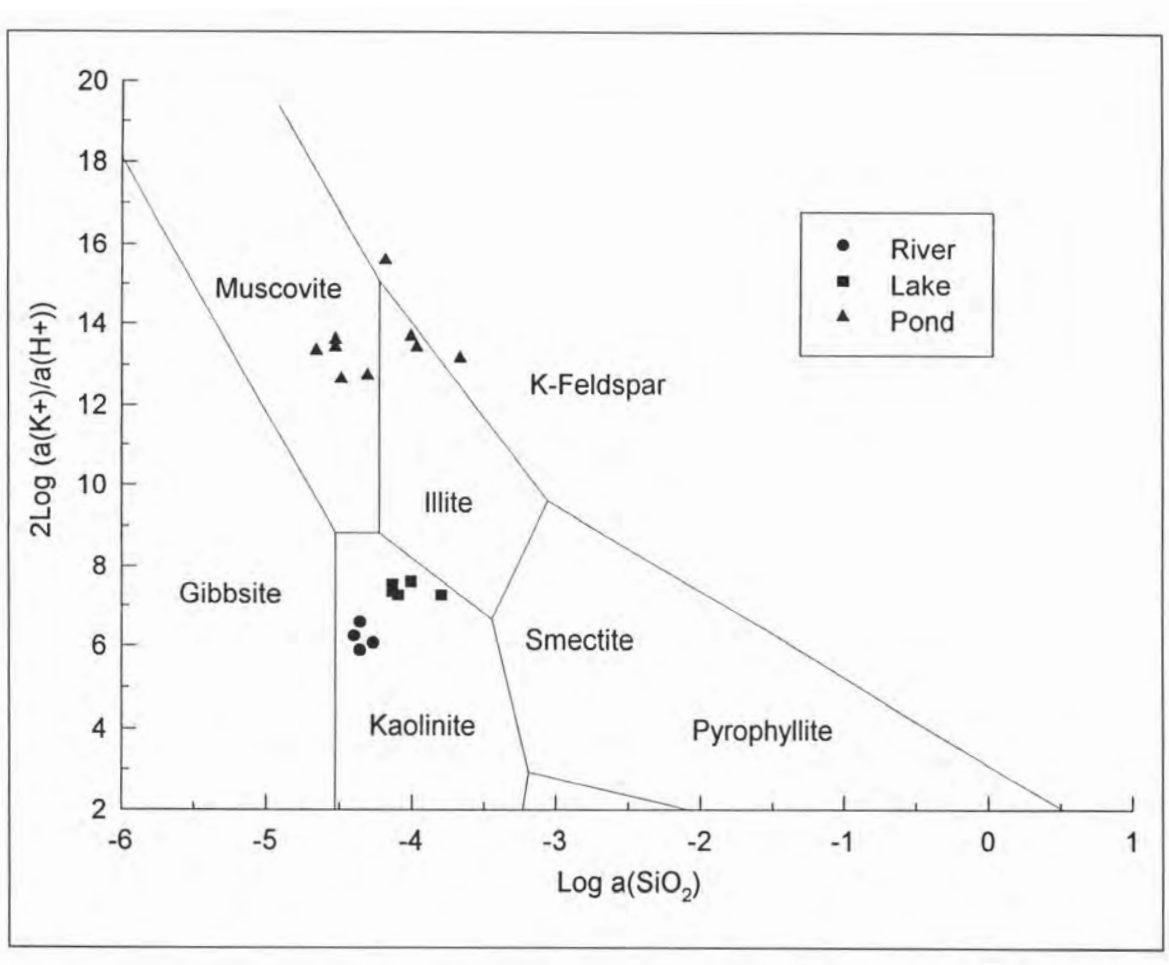

Figure 5. *Ion-activity diagram showing possible mineral phases with which the waters studied may be in equilibrium. (Modified from Garrels, 1984.)*

in the evaporite pond sediments, and their absence in the fresh-water lake sediments suggest that these phases and possibly K-feldspar as well, form authigenically in these evaporite ponds. If true, this is an important factor affecting the major-ion concentrations. As Von Damm and Edmond point out, formation of authigenic silicates should be evident in the O^{18} values of such minerals since they would have isotopic values related to those of the pond waters. Isotopic analyses of all the waters and sediments studied here would permit better understanding of the geochemistry of the lakes.

HYDROLOGIC MODEL

A possible hydrologic model for the evaporite ponds studied here is shown in figure 6. This model implies that the fresh-water lakes and the evaporite ponds are fed by ground water that is derived from the rivers and streams of the region. During periods of low flow in the rivers, the ground-water level drops below the base of the evaporite ponds. The ponds, because of their clayey bottoms, retain water and undergo cyclic wetting and drying , and this process yields trona, calcite, dolomite, muscovite and chlorite. The freshwater lakes are sufficiently deep to remain in contact with the ground-water table. Over time, these lakes may fill in with plant debris and sediment and become evaporite ponds. Evaporite-pond formation is therefore viewed as a dynamic process, driven by the meanderings of the rivers and streams and controlled by the arid climate of the region. Because of this postulated mode of origin, it is unlikely that economic deposits of trona are associated with such evaporite lakes.

ACKNOWLEDGMENTS

This research was done in 1983 and 1984, largely through the Water Research Center, University of Alaska Fairbanks, and was financed in part by a U.S. Department of Interior, Water Research and Development Act Grant. I thank M. McCrum for his assistance in sampling and for performing the water analyses discussed here. I also thank D.M. Hopkins and M. Edwards for their helpful comments on an earlier version of this paper, and D.M Hopkins and K.H. Clautice for their thoughtful reviews of this paper.

REFERENCES CITED

Berner, R.A., 1980, Early diagenesis, a theoretical approach: Princeton Series in Geochemistry, Princeton, New Jersey, Princeton University Press, 241 p.

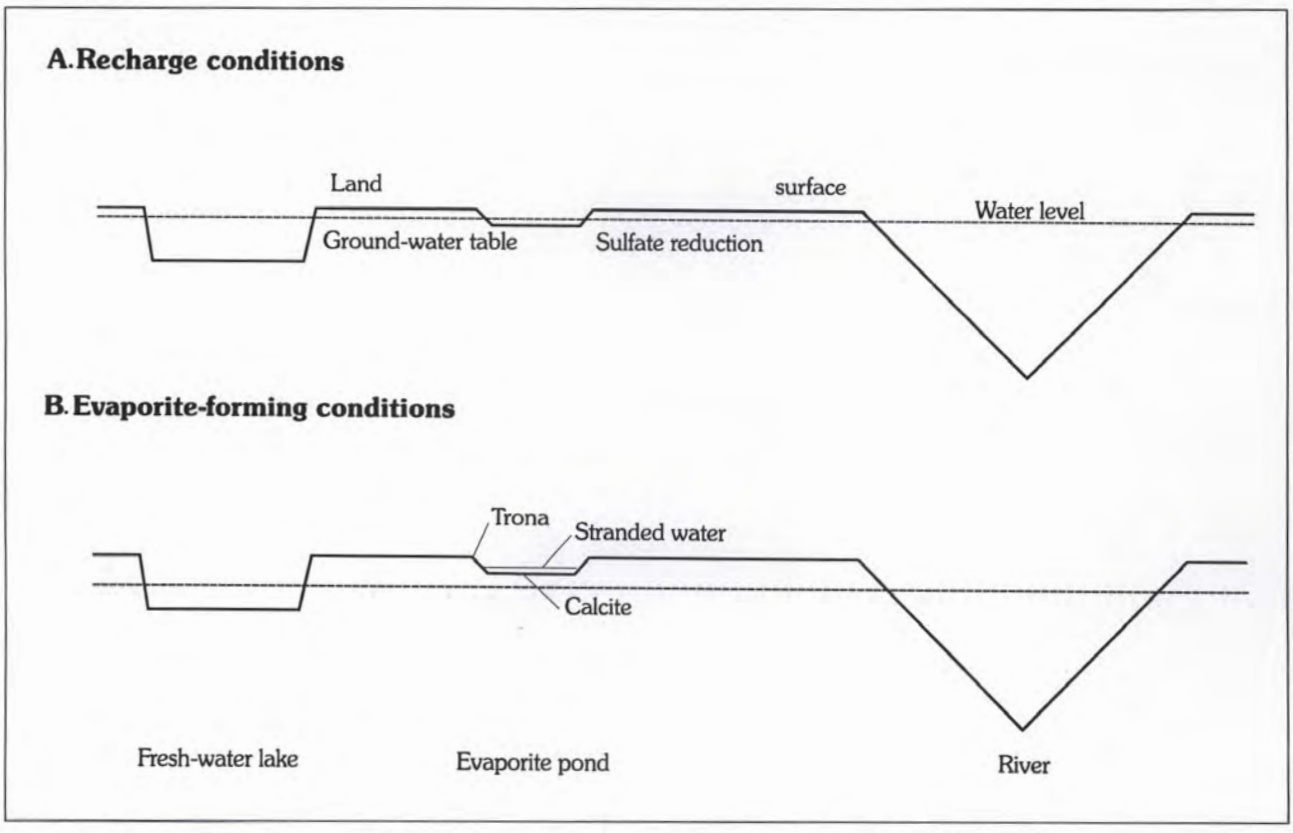

Figure 6. *Possible hydrologic model for the formation of some evaporite ponds of the Yukon Flats.*

Clautice, K.A., and Mowatt, T.C., 1982, Trona occurrences within the Yukon Flats Basin, Alaska : U.S. Bureau Mines Open-File Report 69-81.

Drever, J.A., 1988, The geochemistry of natural waters: Prentice Hall, 437 p.

Eugster, H.P., and Hardie, L.A., 1978, Saline lakes, *in* Lehrman, A., ed., Lakes, Chemistry, Geology, Physics: Springer-Verlag, New York, 363 p.

Eugster, H.P., 1980, Geochemistry of evaporitic lacustrine deposits: Annual Review of Earth Planetary Science, v. 8, p. 35-63.

Eugster, H.P., and Maglione, G., 1979 Brines and evaporites of the Lake Chad basin, Africa: Geochimical et Cosmochimica Acta, v. 43, p. 973-981.

Garrels, R.M., and Mackenzie. F.T., 1967, Origin of the chemical composition of some springs and lakes, *in* Equilibrium Concepts in Natural Water Systems: American Chemical Society, Advances in Chemistry, v. 67, p. 222-242.

Garrels, R.M., 1984, Montmorillonite/illite stability diagrams: Clays and Clay Minerals v. 32, p. 161-165.

Hardie, L.A., and Eugster, H.P., 1970, The evolution of closed-basin brines: Mineralogical Society of America, v. 3, p. 273-290.

Jones, B.F., Eugster, H.P., and Rettig, S.L., 1977, Hydrochemistry of the Lake Magadi Basin, Kenya: Geochimica et Cosmochimica Acta, v. 41, p. 53-72.

Keys, J.R., and Williams, K., 1981, Origin of crystalline, cold, desert salts in the McMurdo region, Antarctica: Geochimica et Cosmochimica Acta, v. 45, p. 2299 -2310.

Matsubaya, O., Sakai, H., Torii, T., Burton, V, and Knowles, K., 1979, Antarctic saline lakes-stable isotopic ratios, chemical compositions and evolution: Geochimica et Cosmochimica Acta, v. 43, p. 7-26.

Mertie, J.B., Jr., 1929, Preliminary report on the Sheenjek River district: U.S. Geological Survey Bulletin 797-C, p. 123.

Miller, W.R., and Drever, J.I., 1977, Chemical weathering and related controls on surface water chemistry in the Absaroka Mountains, Wyoming: Geochimical et Cosmochimica Acta, v. 41, p. 1693-1702.

Slaughter, C.W., and Hartzmann R.J., 1993, Hydrologic and water-quality characteristics of a degrading open-system pingo, *in* Sixth International Conference on Permafrost: Beijing, China.

Von Damm, K.L., and Edmond, J.M., 1984, Reverse weathering in the closed-basin lakes of the Ethiopian Rift: American Journal of Science, v. 284, p. 835-862.

GEOMETRY AND DEFORMATION OF A DUPLEX AND ITS ROOF LAYER: OBSERVATIONS FROM THE ECHOOKA ANTICLINORIUM, NORTHEASTERN BROOKS RANGE, ALASKA

by
Andrew J. Meigs[1] and Teresa A. Imm[2]

ABSTRACT

New mapping and a balanced cross section demonstrate that the Echooka anticlinorium is similar to other anticlinoria exposed throughout the fold-and-thrust belt in the northeastern Brooks Range. At the core of the Echooka anticlinorium, outcrops of the Kekiktuk Conglomerate and sub-Mississippian succession are interpreted to be the exposed top of a horse in the regionally extensive duplex that developed above the basal décollement of the thrust belt. The internal geometry of the duplex in the region of the Echooka anticlinorium is complex because horses also developed above a second, structurally high detachment in sub-Mississippian rocks. The roof thrust to the duplex occurs within the Mississippian Kayak Shale. At least six stratigraphic units in the roof layer acted as detachments during contraction. Tight to isoclinal folds developed between the Kayak Shale and a detachment in the mid-Lisburne Group (Mississippian-Pennsylvanian). Open kink folds formed above the mid-Lisburne detachment and below the Permian Echooka Formation. The Echooka Formation is folded into tight, short-wavelength folds below the Triassic Ivishak Formation. A spaced cleavage formed at a high angle to bedding in the Triassic Ivishak and Shublik Formations. Lower Cretaceous sandstones at the northwestern end on the anticlinorium are duplicated in a duplex thrust system between a floor thrust in the Kingak Shale and a roof thrust in overlying finer-grained clastic rocks. A balanced cross section indicates that 4.0 km of shortening occurred above the regional basal décollement, 4.5 km of shortening occurred above the structurally high sub-Mississippian detachment, and the roof layer shortened by 4.5 km. Because the local sense of displacement on the roof thrust is partly forward (~40 percent of the slip), it is not clear in the region of this transect whether the sense of displacement on the roof thrust is consistent with that expected for a passive-roof duplex.

INTRODUCTION

Beginning in the mid 1980s considerable attention was focused on the northeastern Brooks Range fold-and-thrust belt because of its proximity to the potentially oil-rich coastal plain of the Arctic National Wildlife Refuge. Detailed structural and stratigraphic studies were conducted in the mountainous region between the Canning River and the Canadian border (fig. 1A). These studies outlined the basic architecture of the thrust belt and delineated the region's structural style (Namson and Wallace, 1986; Wallace and Hanks, 1990; Wallace, 1993). An important conclusion of these studies was that the structural style in this part of the northeastern Brooks Range was clearly variable along strike from east to west (Wallace and Hanks, 1990). However, the structure in the region west of the Canning River remains relatively unknown (fig. 1A). We report here on a detailed study of structures from this region in an area between the Echooka and Ivishak Rivers (fig. 1B). Structures in the study area are generally similar to others in the northeastern Brooks Range but are unique in detail.

[1]Department of Earth Sciences, University of Southern California, Los Angeles, California 90087-0740.
[2]ASCG, 301 Arctic Slope Ave., Anchorage, Alaska 99518-3035.

REGIONAL GEOMETRY OF THE NORTHEASTERN BROOKS RANGE THRUST BELT

Regionally the northeastern Brooks Range thrust belt is interpreted to be a passive-roof duplex (Namson and Wallace, 1986; Vann and others, 1986; Mitra and Namson, 1989; Wallace and Hanks, 1990; Wallace, 1993). A duplex is a thrust system in which displacement is transferred from a structurally lower detachment (floor thrust) to a structurally higher upper detachment (roof thrust) along a series of imbricate thrusts (Boyer and Elliott, 1982). Structural packages of rock bounded by imbricate thrusts in a duplex are termed horses. Rocks above the roof thrust comprise the roof layer (Geiser, 1988). The roof thrust of a duplex can be at either the base of a previously emplaced thrust sheet (fig. 2A) or in an incompetent layer in an otherwise unduplicated stratigraphic sequence (fig. 2B). A passive-roof duplex refers to a duplex in which the roof thrust has a backthrust sense of displacement (Banks and Warburton, 1986). In order to be kinematically balanced, shortening in the duplex must be accommodated by shortening in the roof layer (Geiser, 1988). Although these terms are cumbersome at first, clearly defining them enables the description of northeastern Brooks Range structures using modern fold-and-thrust belt concepts.

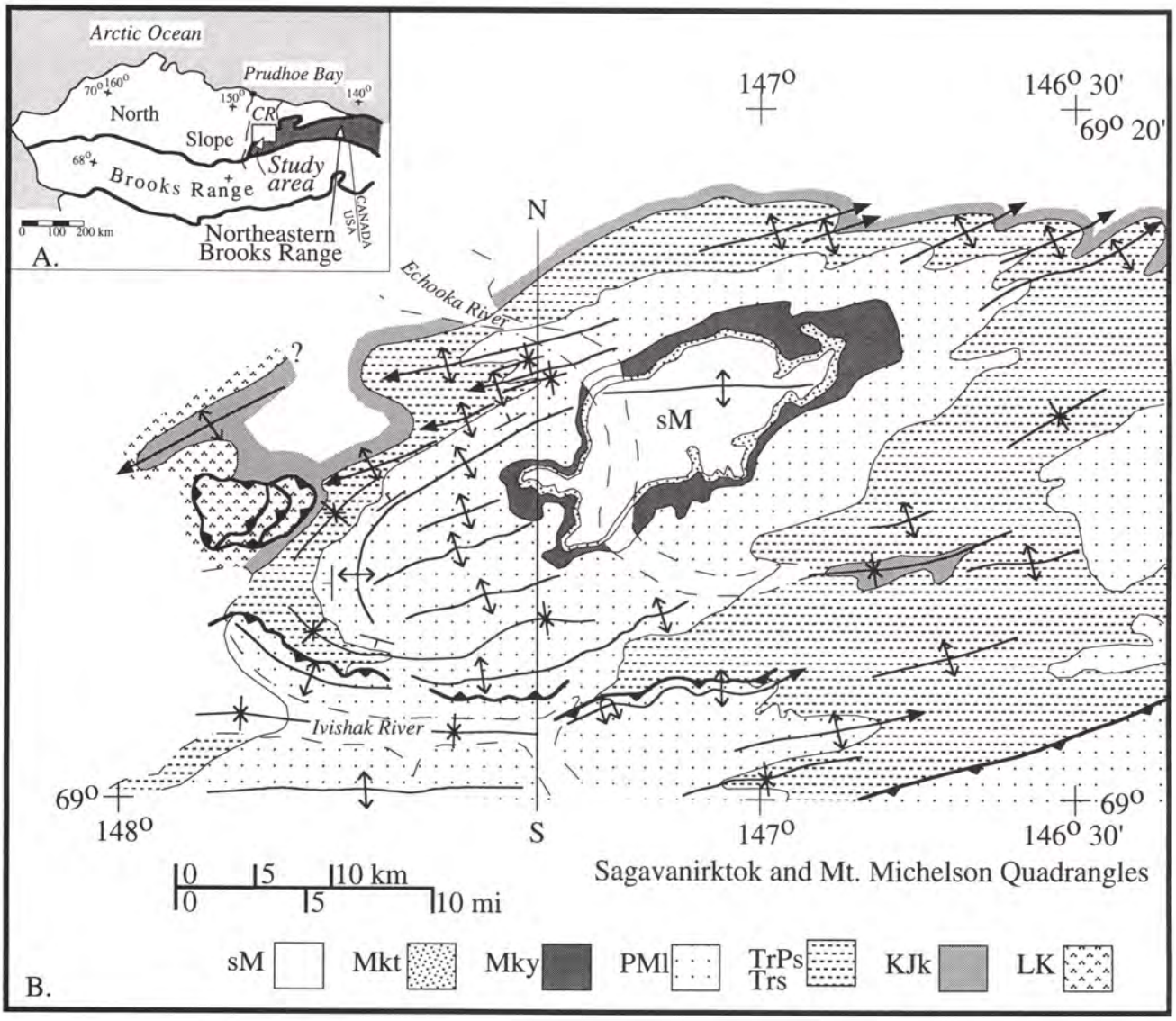

Figure 1. *(A) Location map of northeastern Brooks Range and study area in northern Alaska. CR = Canning River. (Modified from Wallace and Hanks, 1990.) (B) Geologic map of study area. Map units are: sM = sub-Mississippian undivided (s-M), Mkt = Kekiktuk Conglomerate, Mky = Kayak Shale, PMl = Lisburne Group, TrPs = Sadlerochit Group and Shublik Formation, KJk = Kingak Shale, LK = undifferentiated Lower Cretaceous clastic rocks. N-S is the line of cross section in figure 5A. See figure 3 for a generalized lithostratigraphic section. (Map compiled from personal field maps and unpublished Alaska Division of Geological & Geophysical Surveys maps.)*

A series of sub-Mississippian cored anticlinoria characterize the major structures of the northeastern Brooks Range. These anticlinoria are interpreted to comprise structural horses within a regional duplex thrust system (Namson and Wallace, 1986; Namson and Mitra, 1989; Wallace and Hanks, 1990; Wallace, 1993). Geometrically, the duplex formed by delamination of the pre-thrust stratigraphic succession (figs. 2B and 3). The floor thrust of the duplex is the regional basal décollement in the sub-Mississippian sequence and the roof thrust is in the Mississippian Kayak Shale (fig. 3). The remainder of the stratigraphic section above the Kayak Shale comprises the roof layer.

A passive-roof interpretation for the duplex is permitted by a key locality in the Sadlerochit Mountains northeast of the study area. At this location the northernmost horse of the duplex is exposed and the Kayak Shale is depositionally absent from the stratigraphic succession (Imm and Watts, 1987). Significant slip is not seen along the contact, which indicates that the roof layer is effectively pinned to the underlying horse (Wallace, 1993). Consequently, the roof layer has not translated forward (toward the foreland)

and must have a backthrust sense above horses exposed farther south.

DESCRIPTION OF THE ECHOOKA ANTICLINORIUM

A single major anticlinorium, cored by sub-Mississippian rocks, dominates the structure of the study area (fig. 1B), herein referred to as the Echooka anticlinorium. In this sense, the Echooka anticlinorium is typical of the structure across the northeastern Brooks Range (Wallace and Hanks, 1990; Wallace, 1993). At the core of the range a simple east-trending anticlinal fold is present in the Kekiktuk Conglomerate, although the Kayak Shale above it is intensely deformed and has a widely variable structural thickness (fig. 4A). Given this geometry, the Kekiktuk Conglomerate and the sub-Mississippian rocks below are interpreted to be a surface exposure of one of the horses in the regional duplex. Intense deformation of the Kayak Shale is interpreted to be a consequence of its role as the roof thrust for the duplex. Rocks above the Kayak Shale comprise the roof layer. The striking northeast map pattern of the anticlinorium is distracting; more important are the east-trending northern flank and northeast-trending northwestern flank (fig. 1B). We infer that these reflect the intersection of east-trending and northeast-trending segments of the footwall ramp above which the anticlinorium formed.

The roof layer is highly deformed because multiple stratigraphic units in it acted as structural detachments during deformation (fig. 3). Because of the presence of so many detachment horizons, the accommodation of slip is very disharmonic between different levels in the roof layer: Structures formed between any two detachments are geometrically distinct from those developed above or below the enveloping zones of decoupling. The remainder of this paper consists of (1) a systematic description of structural geometry at different levels within the roof layer, (2) an outline of the procedure used to construct a geological cross-section across the anticlinorium with emphasis on interpretation of the subsurface geometry, and (3) a calculation of shortening in both the duplex and roof layer from a restoration of the geological section.

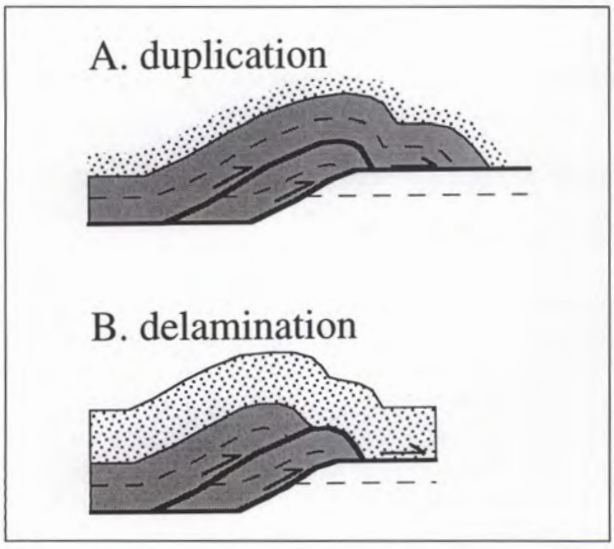

Figure 2. *Schematic diagram contrasting (A) duplication and (B) delamination modes of duplex formation.*

STRUCTURAL GEOMETRIES WITHIN THE ROOF LAYER

Mississippian and younger strata in the Echooka anticlinorium are typical of the stratigraphy observed in surface exposures throughout the northeastern Brooks Range and in the subsurface of the North Slope of Alaska (fig. 3) (Bird and Molenaar, 1987). A regionally extensive unconformity separates undifferentiated sub-Mississippian rocks from the Endicott Group, Lisburne Group, Sadlerochit Group, Shublik Formation, Kingak Shale, and a complex sequence of Lower Cretaceous and younger clastic rocks. Figure 3 illustrates the stratigraphic position of detachments within the study area. Detachments within the roof layer occur at approximately the same stratigraphic position in the Echooka anticlinorium as they do elsewhere in the northeastern Brooks Range (Wallace and Hanks, 1990; Wallace, 1993). The base of the section is the subsurface regional basal décollement. Exposures of different portions of the section are systematically distributed within the anticlinorium. Structures developed in sub-Mississippian rocks are exposed in the core of the Echooka anticlinorium; those involving the upper Sadlerochit Group and younger strata are exposed in structural lows around its periphery. Structures affecting the Lisburne and lower Sadlerochit Groups are exposed in the intervening mountainous region (figs. 1B and 3).

In the core of the Echooka anticlinorium, exposure of the roof layer is restricted to the Lisburne Group and lower part of the Sadlerochit Group (fig. 1B). Structures in the Lisburne Group exhibit two contrasting structural styles. Short-wavelength tight to isoclinal folds developed in the thin-bedded limestones between the Kayak Shale detachment and one within the Lisburne Group (fig. 4B). Above this mid-Lisburne detachment and superimposed on stratigraphically higher units, open box folds formed in the more massive limestones in the upper part of the Lisburne Group (fig. 4C). A detachment separating the top of the Lisburne Group from the base of the Sadlerochit Group is inferred because the Echooka Formation is folded by extremely tight small-wavelength folds (<20 m), which are clearly polyharmonic to box folds in the underlying Lisburne Group (fig. 4D). The Echooka Formation is in-

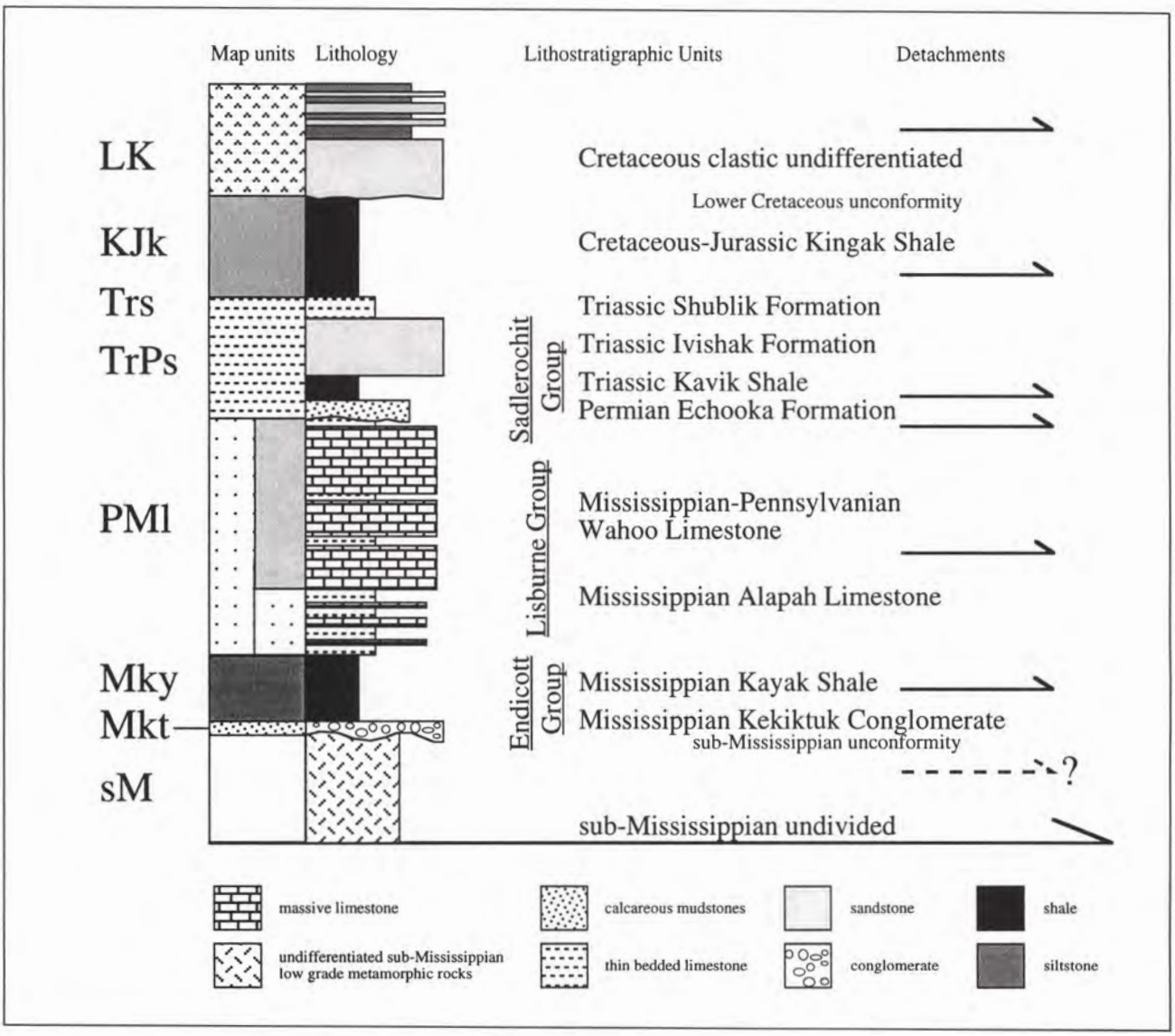

Figure 3. *Generalized stratigraphic section for the Echooka anticlinorium. Detachment horizons are indicated by arrows. Shading on the left corresponds to the shading of maps and cross-section units in figures 1 and 5.*

terpreted either to be bounded by detachments at its base and in the overlying Kavik Shale Member of the Ivishak Formation, or to be a zone of detachment because structures in the upper part of the Sadlerochit Group contrast in both style and wavelength to those of the Echooka Formation. Faults originating in the Lisburne Group locally cut both this detachment and folds formed above it (fig. 4D).

Along the northwestern flank of the anticlinorium adjacent to the range front, a distinctive suite of folds involving the upper part of the Lisburne and Sadlerochit Groups is exposed whose style strongly contrasts with structures exposed closer to the core. The most obvious is a suite of northeast-stepping enechelon anticlines cored by the upper part of the Lisburne Group (figs. 1B and 4E-G). Figure 4E beautifully illustrates the open nature of the folds. A prominent axial-planar cleavage (fig. 4F) is associated with these folds but is well-developed only in the Sadlerochit Group. An earlier-formed spaced cleavage which is oriented at a high angle (nearly 90°) to bedding (fig. 4G) is folded by these open folds and overprinted by the associated cleavage. We interpret this earlier cleavage to reflect a layer-parallel shortening event. Clearly, the cleavage is lithologically controlled (the spaced cleavage was observed only within the Sadlerochit Group), but its presence requires detachment within the Kavik Shale because a similar fabric is not observed in the underlying rocks. Imbrication of Lower Cretaceous clastic rocks above a detachment in the Kingak Shale is clearly demonstrated by repetition of the same strata in the Gilead Hills west of the range front (fig. 4H) (Pessel and others,

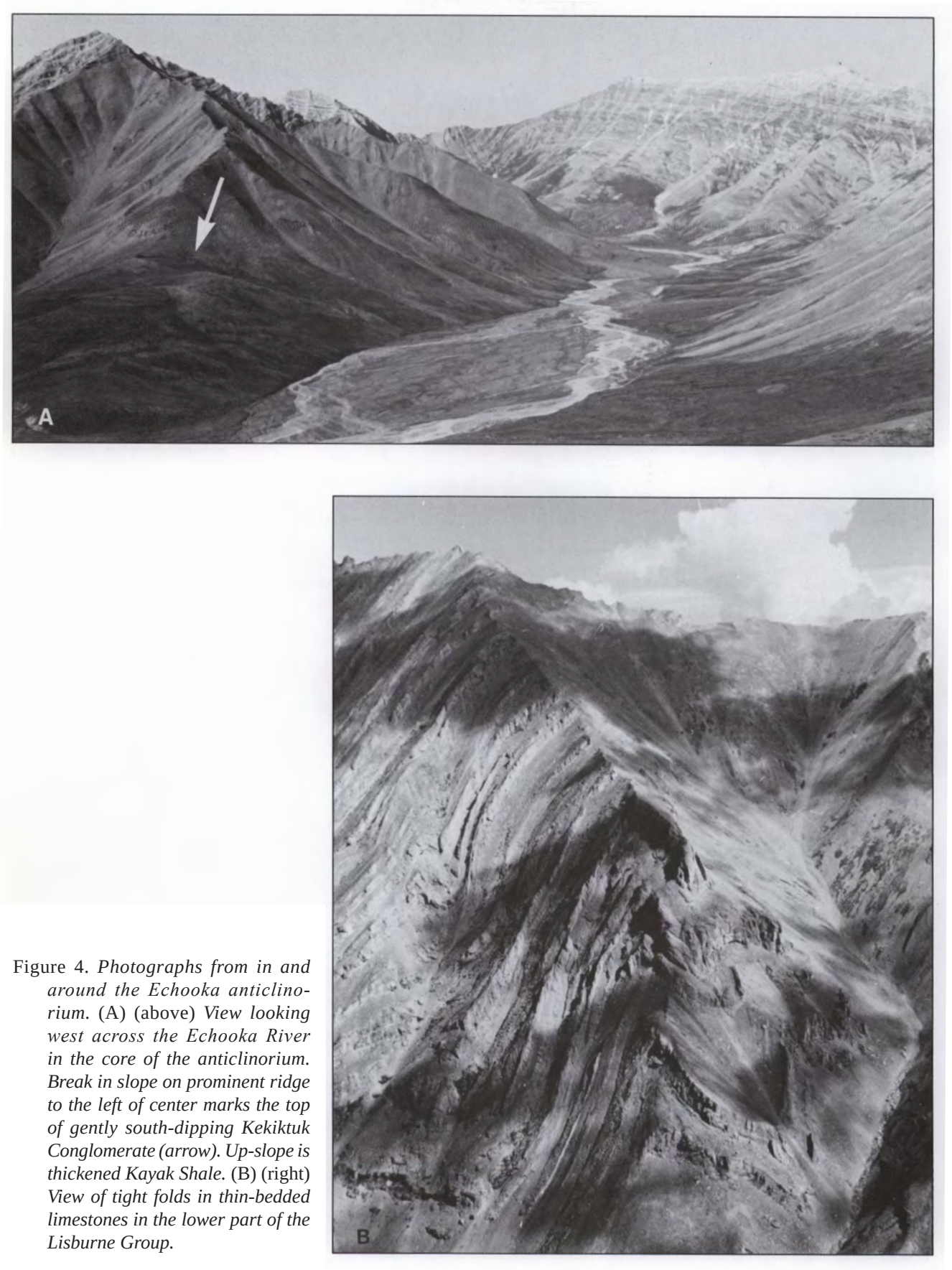

Figure 4. *Photographs from in and around the Echooka anticlinorium.* (A) (above) *View looking west across the Echooka River in the core of the anticlinorium. Break in slope on prominent ridge to the left of center marks the top of gently south-dipping Kekiktuk Conglomerate (arrow). Up-slope is thickened Kayak Shale.* (B) (right) *View of tight folds in thin-bedded limestones in the lower part of the Lisburne Group.*


C


D

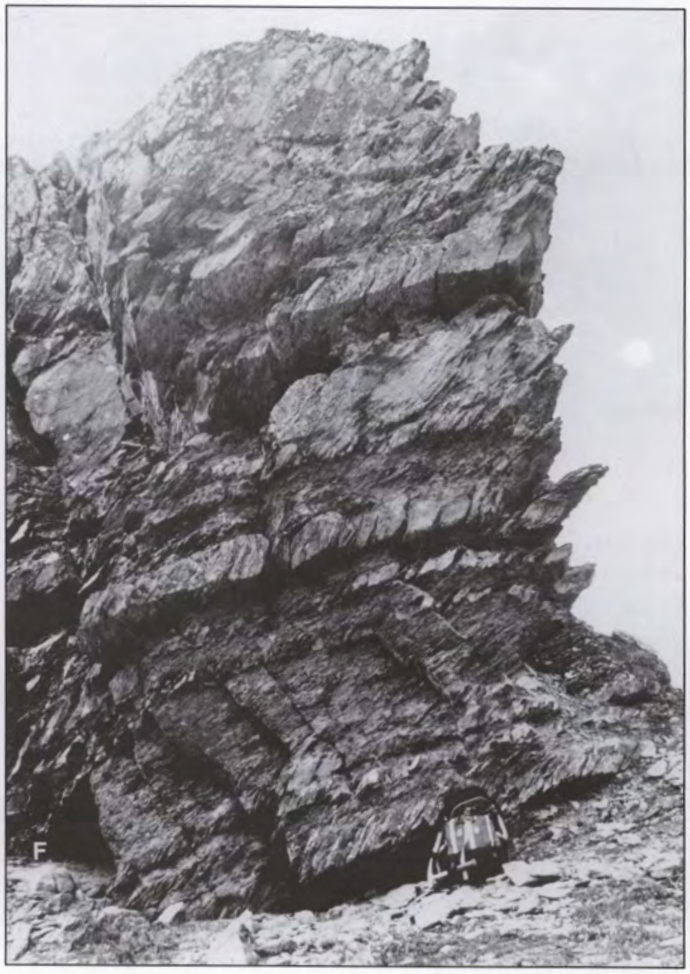

Figure 4 continued. (C) (top left) *Open box folds in the upper part of the Lisburne Group marked by beds seen on ridge at the skyline.* (D) (lower left) *Tight folding in the Echooka Formation (bullseye patterns) overthrust by gray limestones of the Lisburne Group.* (E) (above) *Open fold exposed at the range front near the Echooka River. Dark material mantling the fold is the Echooka Formation.* (F) (right) *Axial-planar cleavage (dipping to left) associated with folds*

Figure 4 continued. (G) (left) *Spaced cleavage formed at a high angle to bedding (parallel to scale). Cleavage in F overprints this earlier fabric.* (H) (below) *Duplicated Lower Cretaceous clastic rocks seen in distance. Each rib marks a thrust duplication of the section.*

1990). Because only a restricted part of the clastic succession is seen in the thrust slices, an upper detachment is suggested above relatively coarser strata at the base (fig. 3). These imbrications probably formed in a duplex whose floor thrust and roof thrust were the detachments in the Kingak Shale and Lower Cretaceous clastic rocks respectively. A similar structural style is observed in Jurassic and Lower Cretaceous rocks in the low-lying regions immediately north of the range front of the northeastern Brooks Range (Wallace and Hanks, 1990; Meigs, 1990). Direction of thrust vergence is difficult to determine from the map of the imbricates alone because they are preserved in a synclinal stack (fig. 1B).

CROSS-SECTION CONSTRUCTION AND RESTORATION

Balanced cross-sections are constructed to calculate shortening and to test the geometric viability of structural interpretations (Dahlstrom, 1969; Woodward and others, 1985). One of the fundamental obstacles in their construction is the interpretation of unexposed structure at depth in the absence of subsurface data (Woodward and others, 1985). In the northeastern Brooks Range, particularly within the study area, surface exposure of the roof layer is excellent, although horses comprising the regional duplex are only partially exposed. Because no subsurface information is available for the study area, extrapolation

of surface information from the roof layer to depth is required to characterize the geometry of subsurface structure. The objective of these extrapolations is to define specific characteristics of the duplex at depth: (1) the geometry of major horses, (2) the angle of their associated thrust ramps, and (3) the depth of the lower detachment, in this case the regional basal décollement.

From north to south three horses are inferred beneath the Echooka anticlinorium (fig. 5A). Outcrops of sub-Mississippian rocks comprising the duplex are limited and only the top of the northernmost horse is exposed (figs. 1B and 5A). Its geometry is inferred by the orientation of the Kekiktuk Conglomerate that defines an anticline in which the northern limb dips 40°-50° north and the southern limb dips gently to south. Given this geometry, a large fold related to an underlying footwall ramp in the duplex thrust system is inferred (anticline 1, fig. 5A). To the south, defining the geometry at depth is more problematic. There is no direct indication of the ramp angle in the surface data. Elsewhere in the northeastern Brooks Range, the southern limbs of the major anticlinoria are defined by moderately south-dipping homoclines (Wallace, 1993). It is from the dip of these limbs that the underlying ramp angle is inferred.

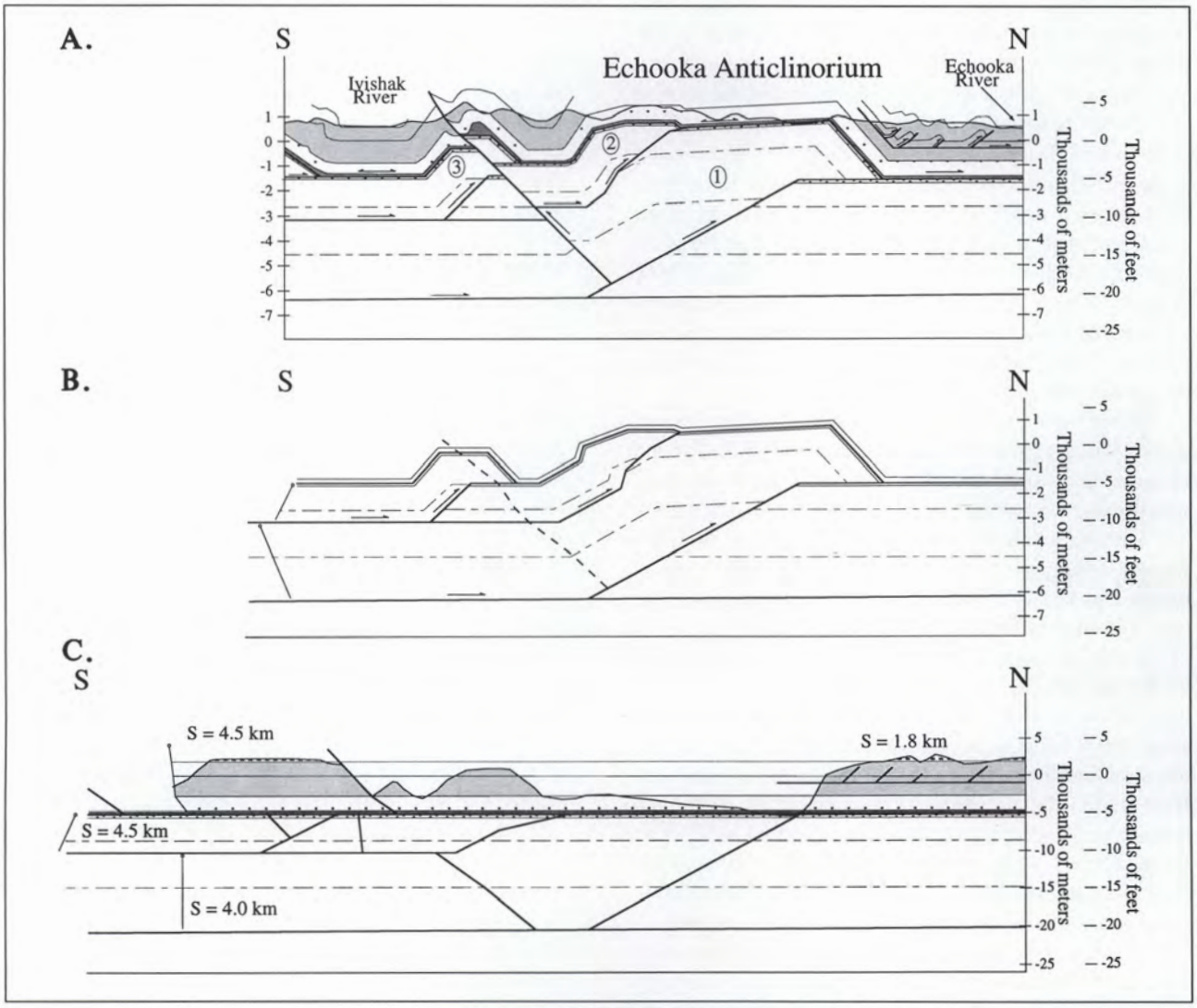

Figure 5. *Balanced cross section for the Echooka anticlinorium. Units as in figures 1B and 3. (A) Geologic cross section. Patterns distinguish the Alapah Formation (open dots) and Wahoo Limestone (shading) in the Lisburne Group to illustrate structure. Dashed lines in the sub-Mississippian sequence are for reference and have no geologic significance. Circled numbers refer to anticlines described in text. (B) Partial restoration of the duplex to show the inferred pre-backthrust geometry. (C) Complete restoration of the geologic cross section in A. S is shortening in kilometers. No vertical exaggeration.*

In contrast, the south flank of the Echooka anticlinorium consists of two anticlines separated by a syncline (anticlines 2 and 3, fig. 5A). From a purely geometric perspective, the point at which a ramp branches from a lower detachment is marked by a structural low in the overriding plate in some cases (Boyer and Elliott, 1983; Woodward and others, 1985). We infer that the point at which the ramp below the anticline branched from the regional basal décollement must occur at depth somewhere beneath the narrow syncline between anticlines 2 and 3 (fig. 5A). The point where the thrust ramp joins the roof thrust in the Kayak Shale is relatively straightforward to constrain by geometric construction. This point is where the roof thrust intersects the hinge of the hanging-wall anticline (Woodward and others, 1985). Projecting the Kayak Shale southward from its inferred horizontal orientation in the subsurface at the north end of the section to the hinge of anticline 1 marks the transition from thrust ramp to roof thrust (fig. 5A). Choosing a moderate ramp angle (~29°) and projecting it southward beneath the syncline gives a depth of detachment at about -6150 m, consistent with depths determined independently elsewhere in the northeastern Brooks Range (Meigs, 1990; Wallace, 1993). Detachment depth may be in error by ± 10 percent if the ramp angle is assumed constant whereas ramp angle may have errors of ± 15 percent if the detachment depth is held constant.

If the wavelength of a fold reflects the detachment depth (Mitra, 1992), anticlines 2 and 3 must have formed above a shallower detachment than anticline 1 (fig. 5A). Interpreting the subsurface in the regions of anticlines 2 and 3 is complicated by the fact that the projection of the Kayak Shale Lisburne Group contact is apparently structurally elevated at the bottom of the intervening syncline (fig. 5A). In structural lows on the north and south ends of the section (at the Ivishak and Echooka Rivers respectively) the inferred depth of this contact is greater than that in the core of the syncline. Uplift of this syncline suggests that a backthrust mapped on the southern edge of the anticlinorium (fig. 1B) may in fact have originated from within the sub-Mississippian sequence. Although there is no direct evidence that the roof thrust is offset by the backthrust, a partial restoration of deformation related only to the backthrust (fig. 5B) yields a plausible solution to the geometry of the pre-backthrust duplex. In particular, anticline 3 becomes a simple ramp anticline which can be used to infer the depth of its detachment. The ramp angle and the intersection of the ramp with the lower detachment (the basal décollement) and the upper detachment (roof thrust in the Kayak Shale) are determined by construction assuming the ramp angle is equal to the dip of the back limb (figs. 5A and B). This detachment depth is consistent with the wavelength of anticline 2 as well.

Shortening can be quantified for the roof layer and duplex by restoring the deformed-state sections to an undeformed state. All the restorations are line-length balanced. Thicknesses in the deformed and undeformed states are equal and no attempt was made to restore structurally thickened units. Consequently they represent minimum estimates of shortening (Woodward and others, 1985). Throughout the section the lower Lisburne Group is the most completely exposed of the roof layer units and serves as the key unit for the roof layer restoration. Approximately 4.5 km of shortening is recorded in the roof layer (fig. 5C). Shortening within the roof layer was accommodated in two regions: (1) in folds and related faults exposed to the north of the anticlinorium and (2) in folds and minor faults exposed across the top of the anticlinorium. Folds exposed on the north are not broken by faults at the surface (figs. 1B and 5A). Whether these folds are fault-propagation folds formed to accommodate displacement above a fault tip at depth (Mitra, 1990) or are truncated detachment folds is not clear from the surface data. Their geometry suggests that they formed above the mid-Lisburne detachment (fig. 3). Roughly 1.8 km of shortening is associated with these structures (fig. 5C). Shortening taken up by structures exposed across the top of the anticlinorium is approximately 2.7 km.

Total shortening within the duplex should be balanced by an equivalent amount of shortening in the roof layer (Mitra and Namson, 1989). If our interpretation is correct, the sub-Mississippian sequence is punctuated by two detachments; one is the regional basal décollement and the other occurs at a higher structural level. An artificial grid of markers was superimposed on the sub-Mississippian sequence to restore it because no physical markers, with the exception of the Kekiktuk Conglomerate, are exposed. Restoration of this grid indicates that 4.0–4.5 km of shortening was accommodated by structures above each detachment (fig. 5C). The restored lengths are different because the restoration of anticlines 2 and 3 includes shortening above the higher detachment *in addition to* piggyback translation above the basal décollement from shortening associated with the formation of anticline 1 (figs. 5A and C). If this interpretation is correct, the length discrepancy must be compensated out of the line of section to the south. Shortening on the late-stage backthrust is small (0.8 km) and must be accompanied by an equivalent amount of displacement from a heterogeneous shear (compare the inclinations of the pin lines in figure 5).

DISCUSSION

A roof layer responds to slip transfer from the duplex by a combination of translation and thickening (fig. 6). Thickening, via folding, thrust faulting, or penetrative deformation, is ultimately the mechanism by which

shortening in the duplex is compensated in the roof layer (Dunne and Ferrill, 1988; Geiser, 1988). It is important to recognize, however, that the roof layer is detached from and consequently may translate semi-independently of underlying horses. If the displacement of the roof layer is defined using the subjacent horse as a reference frame, roof layer translation occurs in two end-member modes. A simple graphical model consisting of a single horse and its superjacent roof contrasts various roof responses (fig. 6). When the underlying roof layer and horse are coupled (fig. 6B), the roof layer on the foreland side of the horse is detached and displaced forward. Alternatively, hindward translation of the roof occurs when the underlying horse is emplaced as a wedge along the upper detachment (fig. 6C). In this case roof material on the foreland side of the tip of the horse is structurally coupled to material below the roof thrust and the roof thrust has a backthrust sense of displacement. This is a "passive-roof" duplex geometry (Banks and Warburton, 1986). Naturally, some combination of these senses of translation is possible as well (fig. 6D).

Quantifying the extent to which a roof layer has translated forward or hindward depends on the existence of a piercing point across the roof thrust. Although such data exists in the Sadlerochit Mountains farther to the northeast (Wallace, 1993), no unique tie can be demonstrated between the roof layer and the duplex across the Echooka anticlinorium. If we assume for the sake of argument that the roof layer has not been significantly translated with respect to the duplex, we can infer that about 40 percent of the shortening in the roof layer resulted from forward slip on the roof thrust. Geometrically this scenario is most similar to figure 6D. Forward slip on the roof thrust suggests that the regional duplex may not be an ideal passive-roof duplex (fig. 6C) along this transect. A longer section, including the subsurface to the north in particular, is necessary to test this hypothesis. Clearly the presence of the Kayak Shale in this northernmost exposed horse enabled slip to occur between the roof layer and the duplex.

Deformational style within the roof layer was strongly influenced by the high proportion of incompetent units in the stratigraphic succession (fig. 3). At least six discrete detachments were established across the roof layer because numerous thin bedded and relatively incompetent units were present. Folding is polyharmonic across the anticlinorium; the geometry of deformation between any two pairs of detachments is strongly disharmonic and folding that affected structurally lower units is commonly superposed on higher units (fig. 5). These folding styles are controlled by the pre-deformational character of the stratigraphic succession. It is interesting to speculate that the folds and related faults north of the anticlinorium (figs. 1B and 5A) formed above the mid-Lisburne detachment which marks the top of a diffuse zone of thickening by folding.

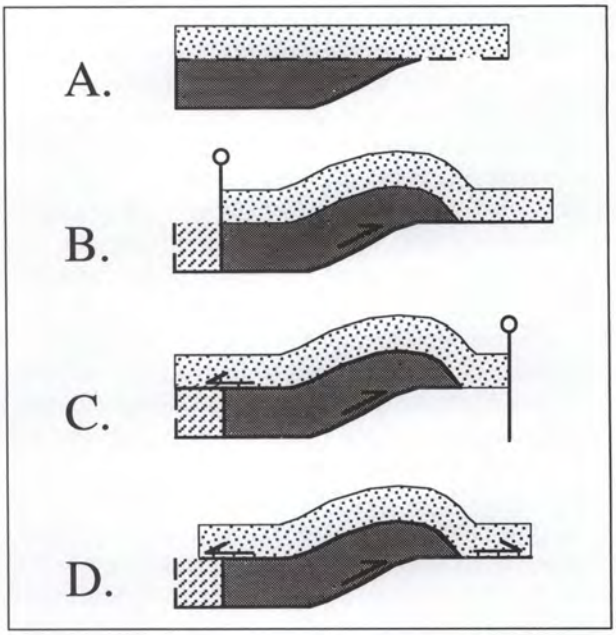

Figure 6. *Simple graphical models illustrating possible roof responses to horse emplacement in a duplex. (A) Pre-emplacement configuration with future horse indicated by dark shading and the roof by stippling. (B) Forward translation, roof pinned to the horse on hindward side. (C) Hindward translation, roof pinned on forward side of the horse. (D) Combined (B) and (C), roof detached from the horse. For a more complete discussion see Dunne and Ferrill (1988) or Geiser (1988).*

As such, it is tempting to think of the entire package of rocks, including the Kayak Shale and lower portion of the Lisburne Group as comprising the roof thrust zone of the duplex. Regardless, a diverse range of structures in the roof accommodated slip transferred from the duplex.

CONCLUSIONS

Structural geometry of the Echooka anticlinorium is compatible with the regional structural style of the northeastern Brooks Range. Sub-Mississippian rocks (and the Kekiktuk Conglomerate) are interpreted to comprise horses of a regional duplex thrust system. The roof thrust for this duplex was localized in the Kayak Shale. Rocks in the roof layer accommodated displacement on the roof thrust predominantly by folding, although very disharmonically between different levels. Structurally, the Echooka anticlinorium is the northernmost exposed horse in the duplex for this transect. Because the section only includes one major structure it is unclear whether the regional sense of displacement on the roof thrust is backward indicating the duplex has a passive-roof geometry.

Folds north of the anticlinorium suggest that part of the displacement on the roof thrust was forward. The presence of the Kayak Shale distinguishes this horse from the one exposed at an equivalent structural position to the northeast in the Sadlerochit Mountains where the duplex is clearly a passive-roof duplex. In the absence of subsurface data to the north, it is not possible to convincingly argue for or against a passive-roof duplex interpretation for this transect.

At least six detachments formed in incompetent units in the roof layer, as denoted by arrows in figure 3. A distinct structural style developed in rocks between pairs of detachments: (a) tight to isoclinal folds formed between the Kayak Shale and the Mid-Lisburne Group; (b) open folds formed between the Mid-Lisburne Group and the basal Echooka Formation; (c) tight folds (<20 m wavelength) formed between the basal Echooka Formation and the Kavik Shale Member of the Ivishak Formation; (d) pressure solution cleavage formed between the Kavik Shale and the Kingak Shale; (e) thrust imbrications formed between the Kingak Shale and the Lower Cretaceous shales.

Complex deformational patterns are observed in the roof layer. For example faults originating from the Lisburne Group cut folds in the Echooka Formation. The pressure solution cleavage in rocks above the Kavik Shale detachment is folded around folds involving the upper Lisburne Group and younger units. Horse emplacement in the subsurface duplex superimposed folds on a deformed roof layer. Some combination of the detachments probably were active at the same time. In addition, it seems likely that slip along the roof thrust accumulated from the subjacent horse and slip transferred from horses emplaced farther south off the line of section.

Deformation in the sub-Mississippian is complex and includes structures formed above both the regional basal décollement and a second, structurally higher detachment. Structures formed above these two detachments have fundamentally different wavelengths.

Late-stage (with respect to the formation of the anticlinorium) formation of a backthrust is inferred to have cut the roof thrust. Other late-stage faults in the northeastern Brooks Range, although generally forethrusts, have similar displacements and cut the roof thrust in some cases (Wallace and Hanks, 1990; Meigs, 1990). The implied heterogeneous shear associated with this backthrust may have resulted from translation of a heterogeneous hanging-wall through the basal décollement-thrust ramp transition.

Shortening within the duplex includes 4.0 km above the regional basal décollement and 4.5 km above the structurally high detachment with the sub-Mississippian sequence. This represents about 16 percent shortening across this section. Roof layer shortening is 4.5 km and includes 1.8 km accommodated by folds north of the range front.

ACKNOWLEDGMENTS

This study was conducted in conjunction with a regional mapping program in the northeastern Brooks Range by the Alaska Division of Geological & Geophysical Surveys (DGGS). DGGS provided logistical support for the field work. The interpretations benefited from lively discussions with Gil Mull, Rocky Reifenstuhl, Mark Robinson, and Gar Pessel. Reviews by Gil Mull, Rich Beck, and Julio Friedmann greatly improved the manuscript. Wes Wallace provided an extensive review which, substantially improved the focus of and interpretations in the manuscript. However, the authors are solely responsible for the observations, interpretations, and conclusions.

REFERENCES CITED

Banks, C.J., and Warburton, J., 1986, "Passive-roof" duplex geometry in the frontal structures of the Kirthar and Sulaiman mountain belts, Pakistan: Journal of Structural Geology, v. 8, p. 229-237.

Bird, K.J., and Molenaar, C.M., 1987, Stratigraphy, in Bird, K.J. and Magoon, L.B. eds., Petroleum geology of the northern part of the Arctic National Wildlife Refuge, northern Alaska: U.S. Geological Survey Bulletin 1778, p. 37-60.

Boyer, S.E., and Elliott, D., 1982, Thrust systems: American Association of Petroleum Geologists Bulletin, v. 66, p. 1196-1230.

Dahlstrom, C.D.A., 1969, Balanced cross sections: Canadian Journal of Earth Sciences, v. 6, p. 743-757.

Dunne, W.M., and Ferrill, D., 1988, Blind thrust systems: Geology, v. 16, p. 33-36.

Geiser, P.A., 1988, The role of kinematics in the construction and analysis of geological cross sections in deformed terranes, in Mitra, G., and Wojtal, S., eds., Geometries and Mechanisms of Thrusting with Special Reference to the Appalachians: Boulder, Geological Society of America, p. 47-76.

Imm, T.A., and Watts, K.F., 1987, Changes in structural styles due to depositional pinch-out of the Mississippian Kayak Shale between the Sadlerochit and Shublik Mountains, northeast Brooks Range, Alaska: Geological Society of America Abstracts with Programs, v. 19, p. 390.

Meigs, A.J., 1990, Structural Geometry and Sequence in the Eastern Sadlerochit Mountains, Northeastern Brooks Range, Alaska [Master's thesis]: University of Alaska, 220 p.

Mitra, S., 1990, Fault-propagation folds: Geometry, kinematic evolution, and hydrocarbon traps: American Association of Petroleum Geologists Bulletin, v. 74, p. 921-945.

_____1992, Balanced structural interpretations in fold and thrust belts; *in*, Mitra, S. and Fisher, G.W., eds., Structural Geology of Fold and Thrust Belts: Baltimore, Johns Hopkins University Press, p. 53-80.

Mitra, S., and Namson, J.S., 1989, Equal area balancing: American Journal of Science, v. 289, p. 563-599.

Namson, J.S., and Wallace, W.K., 1986, A structural transect across the northeastern Brooks Range, Alaska: Geological Society of America Abstracts with Programs, v. 18, p. 163.

Pessel, G. H., Robinson, M. S., Clough, J. M., Reifenstuhl, R. R., Ryherd, T. J., Myers, M. D., and Mull, C. G., 1990, Preliminary geologic map of the Gilead Creek area, Sagavinirktok A-2 Quadrangle, Arctic Foothills, Alaska: Alaska Division of Geological & Geophysical Surveys Public-Data File 90-18, 7 p., 1 sheet, scale 1:63,360.

Vann, I.R., Graham, R.H. and Hayward, A.B., 1986, The structure of mountain fronts: Journal of Structural Geology, v. 8, p. 215-227.

Wallace, W.K., 1993, Detachment folds and a passive-roof duplex *in* Solie, D.N., and Tannian, Fran, eds., Short Notes on Alaskan Geology, 1993, Alaska Division of Geological & Geophysical Surveys Professional Report 113, p. 81-99.

Wallace, W.K., and Hanks, C.L., 1990, Structural provinces of the northeastern Brooks Range, Arctic National Wildlife Refuge, Alaska: American Association of Petroleum Geologists Bulletin, v. 74, p. 1100-1118.

Woodward, N.B., Boyer, S.E. and Suppe, J., 1985, An outline of Balanced cross-sections: Knoxville, University of Tennessee, 175 p.

LATE-WISCONSIN EVENTS IN THE UPPER COOK INLET REGION, SOUTHCENTRAL ALASKA

by
Richard D. Reger,[1] Rodney A. Combellick,[1] and Julie Brigham-Grette[2]

ABSTRACT

New evidence and reconsideration of previously published evidence for late-Wisconsin events in the upper Cook Inlet region support the conclusions of Schmoll and others (1972) against criticism by Williams (1986). Nine new radiocarbon dates strongly confirm the late-Wisconsinan age of the Bootlegger Cove Formation. We document Elmendorf-age glacial advances in Knik Arm, Turnagain Arm, and elsewhere in southcentral Alaska as evidence that the Elmendorf advance was of regional significance and not a local aberration.

INTRODUCTION

Shoreline bluffs along Knik Arm and Turnagain Arm in upper Cook Inlet (fig. 1) expose well-preserved evidence of glacial and marine events late in the Naptowne glaciation.[3] This complex record has been studied by many workers during the past 45 years, commonly with conflicting interpretations. The purpose of this article is to present new evidence related to these controversies.

HISTORY OF INVESTIGATIONS

The late-Pleistocene stratigraphic framework in the Anchorage area has been understood since the pioneering work by Miller and Dobrovolny, although the ages of various units have been controversial. They (1959, p. 35) first defined the Bootlegger Cove clay[4] as the silty clay that underlies most of the lowland in the vicinity of Anchorage and is conspicuously exposed in the bluffs along Knik Arm (fig. 1). They recognized that this formation overlies and interfingers with relatively coarse-grained glaciodeltaic deposits in southwest Anchorage (fig. 2). Dominant dip directions, decreasing grain size toward the east and southeast, and the presence of clastic coal convinced Miller and Dobrovolny (1959, p. 31) that the glaciodeltaic complexes in the Point Woronzof-Point Campbell area and on nearby Fire Island are related to glacial ice that entered the Anchorage lowland from the west or northwest. Clearly, they are, at least in part, the same age as the interfingering Bootlegger Cove Formation (BCF).

Till and outwash of the late-Naptowne Elmendorf advance overlie BCF in the Anchorage area (fig. 2). Miller and Dobrovolny (1959, p. 48) found local, 0.5- to 0.6-m-thick oxidation zones in the uppermost BCF beneath outwash alluvium of the Elmendorf advance. They interpreted these zones as part of a weathering profile and, because of the thickness of the zones, concluded that a significant amount of time passed between BCF deposition and formation of the Elmendorf moraine. At that time they believed that the Elmendorf moraine marked the maximum extent of the Naptowne glaciation in the Anchorage area. They (1959, p. 84–86) attributed the glaciodeltaic complex and BCF to the late Knik glaciation, and they assigned an early Wisconsinan age to them. However, Cederstrom and others (1964) contended that Miller and Dobrovolny (1959) misinterpreted the temporal significance of permeable zones of groundwater staining between BCF and deposits of the Elmendorf advance in the Anchorage area. Cederstrom and his colleagues (1964, p. 41) argued that the BCF is not much older than the Elmendorf moraine.

The environment of deposition of the BCF has also been the subject of some debate. Miller and Dobrovolny (1959, p. 44–45) acknowledged the presence of marine fossils in colluvium derived from BCF exposures but believed that the dominant evidence, including numerous dropstones and large erratics and varvelike laminations in some facies, supported a model of glaciolacustrine deposition. However, Schmidt (1963) discovered marine mollusks, foraminifera, and ostracodes in place in BCF and proposed that the environment of deposition was at least in part marine. Most other workers agreed that BCF was deposited in conditions of variable salinity, ranging from lacustrine to marine, with variations in glacier proximity (Karlstrom, 1964; Cederstrom and others, 1964; Trainer and Waller, 1965; Hansen, 1965). In 1967, Hopkins reported foraminifera and marine ostracodes throughout BCF and fairly abundant marine mollusks in the middle of

[1]Alaska Division of Geological & Geophysical Surveys, 794 University Avenue, Suite 200, Fairbanks, Alaska 99709-3645.
[2]Department of Geology and Geography, Box 35820, University of Massachusetts at Amherst, Amherst, Massachusetts 01003-5820.
[3]Named by Karlstrom (1953, 1964) for a series of moraines in the vicinity of Sterling, then called Naptowne, in eastcentral Kenai lowland.
[4]Renamed Bootlegger Cove Formation by Updike and others (1982) because clay is not the dominant grain size in most of the unit. For clarity, in this report we use the term "Bootlegger Cove Formation" even if the original references cited used the term "Bootlegger Cove clay."

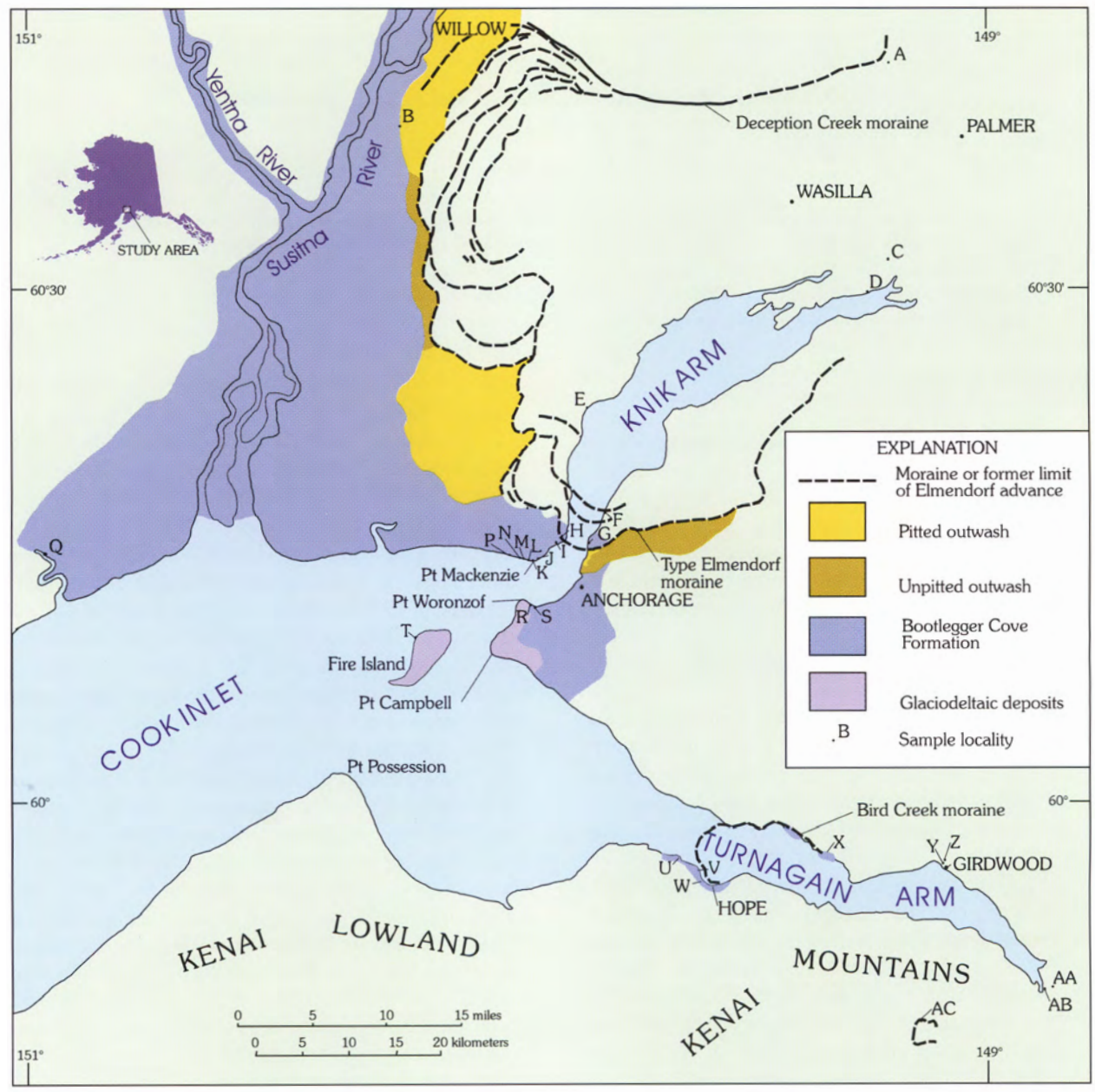

Figure 1. *Map showing sample localities and associated geologic units in the upper Cook Inlet region. (Modified slightly from Reger and Updike, 1983, sheet 1.)*

the formation. He attributed the BCF to a marine invasion of upper Cook Inlet, which he named the Woronzofian transgression. The foraminifera indicate normal salinities during deposition of the lower BCF and low salinities during deposition of the upper BCF. Hopkins (1967, p. 82–83) recognized that isostatic and tectonic changes significantly affected the Woronzofian transgression in the Anchorage area.

Thus, BCF has been variously attributed to (1) the late Knik glaciation (Miller and Dobrovolny, 1959), (2) the late Knik and early Naptowne glaciations (Karlstrom, 1964; Trainer and Waller, 1965), and (3) a mid-Naptowne interstadial transgression (Hopkins, 1967). Karlstrom first attempted an absolute date of marine shells from the BCF and obtained a ^{230}Th age of 33,000–48,000 yr. In a key paper, Schmoll and others (1972) presented the results of radiocarbon analyses of four collections of marine shells from the upper BCF at three localities in the Anchorage area (fig. 1, localities H, J, and S) and uranium-series analyses of collections from two localities (fig. 1, localities J and S). The most reliable results indicate that the four shell samples range in age from 13,690 ± 400 to 14,900 ± 350 ^{14}C yr B.P. and average 14,160 ± 400 ^{14}C yr B.P. For the first time, the radiocarbon data provided solid evidence (1) that shell-bearing diamictons from separate exposures in the Anchorage area are close to the same age and

(2) that, at its type locality, the Woronzofian transgression was a late-glacial submergence event (Hopkins, 1973).

After 1972, geologic mapping and additional radiocarbon dates helped clarify the late Wisconsin glacial history of the upper Cook Inlet region (Kachadoorian and others, 1977; Schmoll and Yehle, 1983, 1986; Reger and Updike, 1983; Ulery and Updike, 1983; Bartsch-Winkler and Schmoll, 1984; Schmoll and others, 1984; Updike and Ulery, 1986). The known distribution of BCF in the upper Cook Inlet region has been extended northwest as far as 60 km inland from Cook Inlet, west to lower Beluga River, and east into Turnagain Arm (fig. 1).

Recently, our work along Knik Arm and Turnagain Arm and elsewhere in the Cook Inlet region has concentrated on late Pleistocene and Holocene deposits and histories (Combellick, 1991, 1993, 1994; Combellick and Reger, 1994; Reger and Pinney, in press). These studies both confirm and challenge previous interpretations and provide important data on late Naptowne–Holocene events in the vicinities of Knik Arm and Turnagain Arm.

KNIK ARM EVIDENCE

The stratigraphy that we have seen is consistent with a model of deglaciation of the Anchorage area just prior to the Elmendorf glacial advance (Reger and Updike, 1983). Glaciodeltaic deposits in the southwest Anchorage–Fire Island area (figs. 1 and 2) formed when the pre-Elmendorf glacier stagnated and melted, discharging debris-laden streams into upper Cook Inlet, where deltaic deposits interfinger with BCF, the upper part of which is dated as old as 14,900 ± 350 ^{14}C yr B.P. (fig. 1 and table 1, loc. S). The presence of numerous dropstones, some block sized, especially in the lower BCF (Miller and Dobrovolny, 1959) is evidence that a calving glacier fronted in the same waters just prior to 14,900 ^{14}C yr B.P. The mass of the pre-Elmendorf glacier that occupied the Anchorage lowland depressed the land at least 86 m. This minimum depression is based on the difference between the highest level of BCF there and the worldwide sea-level curve about 14,000 ^{14}C yr B.P. (Reger and Pinney, in press) and implies that the pre-Elmendorf glacier was at least 258 m thick in the Anchorage lowland.[5]

Previously unpublished atomic-mass-spectrometer (AMS) dates for five collections of marine mollusk shells and barnacle plates from BCF just beyond the limit of the Elmendorf advance on the west side of Knik Arm support previous dating of the shell-rich zone of the BCF by Schmoll and others (1972) (fig. 1 and table 1, locs. I, K, M, N, and P). An AMS date of 13,470 ± 120 ^{14}C yr B.P. (table 1, loc. N) provides the youngest known age for the BCF in the type area.

[5]Based on the assumption that local bedrock and sediments with a density of 2.7 gm/cm^3 or greater are displaced downward at least 86 m by glacial ice with a density of 0.9 gm/cm^3. The upper Cook Inlet area in the vicinities of Knik Arm and Turnagain Arm has been tectonically lowered at rates of 0.13 to 0.3 cm/yr for at least 2,000 to 4,000 yr (Combellick, 1991, 1994). The long-term effect is to decrease the apparent maximum elevation of the BCF there, also decreasing the apparent isostatic depression. For this reason, and because former sea level was at least as high as the present highest exposure of BCF, our estimate is a minimum value.

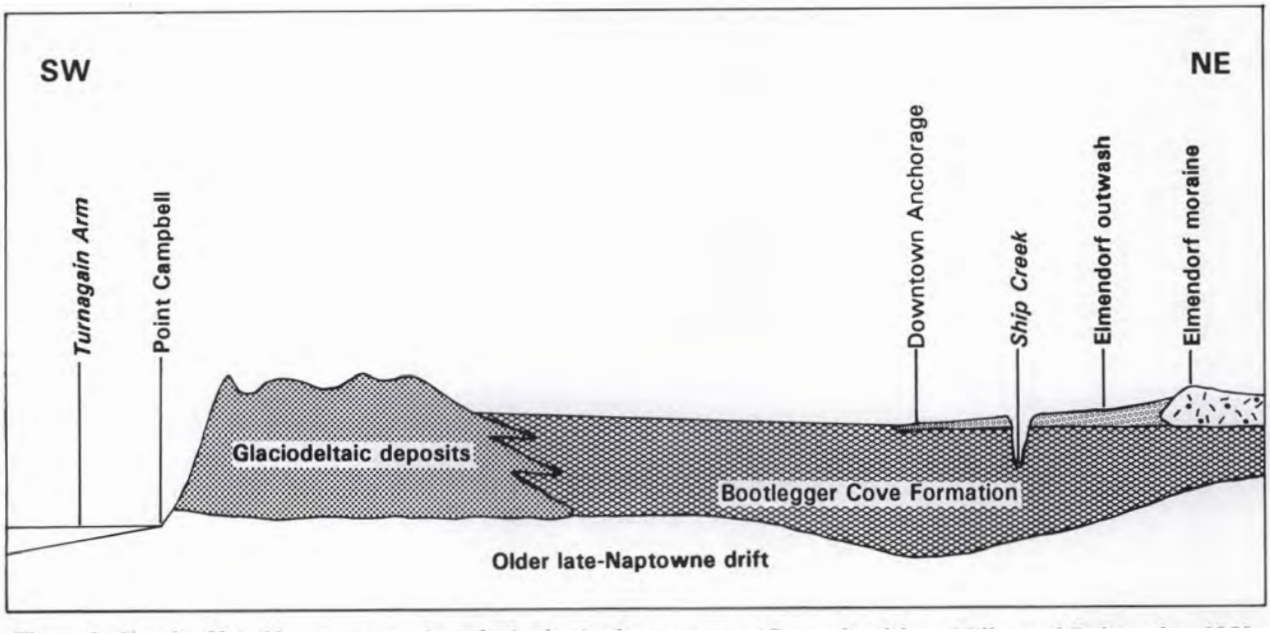

Figure 2. *Sketch of late Naptowne stratigraphy in the Anchorage area. (Generalized from Miller and Dobrovolny, 1959; Hansen, 1965; Schmoll and others, 1972; Schmoll and Barnwell, 1984; Updike and Ulery, 1986; and Yehle and others, 1991.)*

Table 1. *Radiocarbon and calibrated ages and significance of selected organic samples in the upper Cook Inlet region*

Sample[a] locality	Material and stratigraphic context	Chronological significance	Radiocarbon age[b] (^{14}C yr B.P.)	Calibrated mean age and 1σ range[c] (cal yr B.P.)	Source
A	Silty peat with scattered wood fragments from base of 0.9-m-thick layer underlying 1.2-m-thick silty alluvial-fan sand and overlying gravelly sand deposited in ice-marginal bedrock channel	Minimum age for thinning of Elmendorf-age glacier blocking mouth of Little Susitna River canyon north of Palmer	9,155 ± 215 (GX-5019)	10,040 9,650-10,860	Reger and Updike (1983, loc. C)
B	Organic silt 0.1 to 0.2 m below top of 1.0-m-thick silty and sandy peat underlying 0.6-m-thick woody sphagnum peat and overlying 0.4-m-thick organic silt on top of sandy gravel at base of scarp cut into pitted outwash of Elmendorf age during estuarine transgression	Minimum age for outwash from Elmendorf-age moraine to east and cutting of scarp by glacio-estuarine waters in which BCF[d] deposited in Red Shirt Lake area	10,720 ± 460 (GX-6041)	12,650 10,990-13,580	Reger and Updike (1983, loc. I)
C	Organic silt from depth of 7.7 m in estuarine deposits	Minimum age for recession of Elmendorf-age glacier from upper Knik Arm	11,400 ± 720[e] (GX-15241)	13,310 11,050-15,180	Combellick (1990, 1991, borehole KA6)
D	Organic silt from depth of 8.5 m in estuarine fjord filling	Minimum age for recession of Elmendorf-age glacier from upper Knik Arm	8,850 ± 120[fg] (GX-15229)	9,880 9,520-10,030	Combellick (1990, 1991, borehole KA1)
E	Organic silt from depth of 3.8 m in estuarine deposits	Minimum age for recession of Elmendorf-age glacier from Goose Bay area, middle Knik Arm	9,255 ± 420[g] (GX-15294)	10,210, 10,260, 10,280 9,400-11,670	Combellick (1990, 1991, borehole KA4B)
F	Peat from base of paludal deposit overlying postglacial alluvium	Minimum age for recession of glacier from type Elmendorf moraine in lower Knik Arm	9,760 ± 350 (W-2936)	10,970 10,010-12,380	Yehle and others (1990, loc. 3)
G	Basal organic swamp deposits overlying till of type Elmendorf moraine	Minimum age for recession of glacier from type Elmendorf moraine in lower Knik Arm	12,350 ± 350 (W-2589)	14,440 13,580-15,520	Yehle and others (1990, 1991, loc. 4)
H	Peat from beneath colluvium overlying till of type Elmendorf moraine	Minimum age for Elmendorf advance in lower Knik Arm	11,690 ± 300 (W-2375)	13,630 13,000-14,370	Schmoll and others (1972, loc. F), Spiker and others (1977, p. 346)

H	Mollusk shells from macrofossil-rich zone in BCF	Dates middle or upper sublittoral glacioestuarine environment in which BCF deposited in lower Knik Arm	13,750 ± 500 (W-2389)	15,960 14,430-17,200	Schmoll and others (1972, loc. D), Spiker and others (1977, p. 346)
I	Hiatella arctica shells from 6 m below top of BCF and 0.3 m above pre-Elmendorf diamicton	Dates BCF in lower Knik Arm and minimum age for recession of pre-Elmendorf glacier from lower Knik Arm	14,300 ± 140[fg] (AA-2226)	16,670 16,310-17,020	This study
J	Mollusk shells from macrofossil-rich zone of BCF	Dates middle or upper sublittoral glacioestuarine environment in which BCF deposited in Point MacKenzie area	14,300 ± 350 (W-2367)	16,670 15,740-17,490	Schmoll and others (1972, loc. C), Spiker and others, 1977, p. 346)
K	*Balanus* plates from 1- to 2-cm-thick medium-coarse sand layers interbedded with clayey silt in upper BCF overlain by up to 5 m of fan-delta sand	Dates upper BCF at Point MacKenzie	14,100 ± 90[fg] (GX-19989)	16,420 16,170-16,670	This study
L	Organic silt from beneath 1.8-m-thick peat overlying 3-m-thick fan-delta sand above BCF	Minimum age for recession of pre-Elmendorf glacier and emergence from glacioestuarine waters in which BCF deposited at mouth of Knik Arm	12,250 ± 140 (BETA-5580)	14,300 13,940-14,720	Reger and Updike (1983, p. 202)
M	*Mya truncata* shells from dropstone-rich diamicton 3 m below top of BCF	Dates upper BCF west of Point MacKenzie	14,078 214[fg] (GX-20128)	16,390 15,810-16,930	This study
N	*Mya truncata* shells from silty clay facies of BCF 1 m above contact with ice-stagnation deposits of pre-Elmendorf age	Dates BCF at mouth of Knik Arm	13,470 ± 120[fg] (AA-2227)	15,550 15,140-15,920	This study
P	*Mya truncata* shells from interbedded medium sand and silt layers up to 20 cm thick 6 m below top of BCF	Dates upper BCF west of Point MacKenzie	13,994 ± 90[fg] (GX-20127)	16,290 16,030-16,530	This study

[a]See figure 1 for locations of sample sites.
[b]Based on Libby half-life for radiocarbon (5,570 yr) and referenced to A.D. 1950.
[c]Rounded to nearest 10 yr. Combines standard deviation in radiocarbon age and a conservative laboratory error multiplier of 2 to compensate for possible unreported laboratory errors (Stuiver and Pearson, 1986).
[d]BCF = Bootlegger Cove Formation.
[e]Because disseminated organic material, which could include very fine-grained detrital coal, was dated, this age could be spuriously old.
[f]Atomic-mass-spectrometer date.
[g]Sample corrected for natural isotopic fractionation based on ^{13}C content.

Table 1. *Radiocarbon and calibrated ages and significance of selected organic samples in the upper Cook Inlet region—Continued*

Sample[a] locality	Material and stratigraphic context	Chronological significance	Radiocarbon age[b] (^{14}C yr B.P.)	Calibrated mean age and 1σ range[c] (cal yr B.P.)	Source
Q	Shells in glacioestuarine silt and clay of BCF	Dates BCF in lower Beluga River area	14,350 ± 200 (W-4292)	16,730 16,220-17,210	Schmoll and Yehle (1983, loc. B; 1986, loc. B5), Schmoll and others (1984, loc. B5)
R	Peat from base of 2.4-m-thick bed overlying 3 m of sand that overlies 1.8 to 3 m of BCF	Minimum age for emergence from glacioestuarine waters in which BCF deposited in Point Woronzof area	11,600 ± 300 (W-540)	13,530 12,920-14,250	Rubin and Alexander (1960, p. 165), Miller and Dobrovolny (1959, p. 68, pl. 9), Schmoll and others (1972, loc. E)
S	Mollusk shells from macrofossil-rich zone of BCF	Dates middle or upper sublittoral glacioestuarine environment in which BCF deposited in Point Woronzof area	13,690 ± 400 (W-2151)	15,870 14,620-16,900	Sullivan and others (1970, p. 333), Schmoll and others (1972, loc. A)
S	Mollusk shells from macrofossil-rich zone of BCF	Dates middle or upper sublittoral glacioestuarine environment in which BCF deposited in Point Woronzof area	14,900 ± 350 (W-2369)	17,370 16,540-18,130	Schmoll and others (1972, loc. B), Spiker and others (1977, p. 346)
T	Peat from base of 1.8-m-thick bed overlying BCF	Minimum age for emergence from glacioestuarine waters in which BCF deposited in Fire Island area	11,450 ± 150 (BETA-5581)	13,360 13,060-13,710	Reger and Updike (1983, p. 202)
U	*Macoma balthica* shells from 3-m-thick, dropstone-rich, thin-bedded sand in upper BCF overlain by 3 m of colluvium	Dates upper BCF just beyond Elmendorf maxium west of Hope in Turnagain Arm	13,718 ± 160[fg] (GX-20129)	15,910 15,420-16,350	This study
V	*Hiatella arctica* and *Macoma balthica* shells from colluvium derived from BCF	Dates BCF and nearby Elmendorf-equivalent advance in Hope area	14,160 ± 140[fg] (GX-16529)	16,500 16,130-16,850	This study

W	*Hiatella arctica* shells from colluvium derived from BCF	Dates BCF and nearby Elmendorf-equivalent advance in Hope area	14,200 ± 100[fg] (GX-17133)	16,550 16,280-16,810	This study
X	Mollusk shells from colluvial bedrock rubble incorporating reworked BCF	Dates BCF and maximum age for Elmendorf-equivalent advance in upper Turnagain Arm	13,900 ± 400 (W-2919)	16,160 14,940-17,150	Schmoll and Yehle (1983, loc. A; 1986, loc. B4), Bartsch-Winkler and Schmoll (1984)
X	*Macoma balthica* shells from BCF incorporated into till of Elmendorf-age advance	Dates BCF and maximum age for Elmendorf-equivalent advance in upper Turnagain Arm	14,290 ± 140[fg] (GX-16524)	16,660 16,300-17,000	This study
Y	Organic silt from depth of 16.8 m in estuarine deposits	Minimum age for recession of Elmendorf-age glacier from Girdwood area	10,375 ± 310 (GX-15215)	12,260 10,970-12,920	Combellick (1990, 1991, borehole TA1)
Z	Compressed wood and peat from beneath diamicton and estuarine silt and clay and overlying bedded deltaic gravel	Minimum age for recession of Elmendorf-age glacier from Girdwood area and deposition of BCF in upper Turnagain Arm	10,180 ± 350 (W-2302)	11,920 10,480-12,810	Bartsch-Winkler and Schmoll (1984)
AA	Wood fragments from laminated silt near depth of 93 m in estuarine deposits	Minimum age for recession of Elmendorf-age glacier from head of Turnagain Arm	8,230 ± 100 (—)	9,210 8,960-9,440	Bartsch-Winkler and others (1983), Bartsch-Winkler and Schmoll (1984)
AB	Organic silt from depth of 15.4 m in estuarine deposits	Minimum age for recession of Elmendorf-age glacier from head of Turnagain Arm	10,730 ± 525 (GX-15224)	12,660 10,940-13,740	Combellick (1990, 1991, borehole TA8)
AC	Peat from depth of 1.8 m in organic sediments ponded behind outer end moraine	Minimum age for readvance of glaciers from Tincan Creek and Lyons Creek valleys after recession of Elmendorf-age glacier from upper Turnagain Arm	9,850 ± 390 (GX-10649)	11,000 10,020-12,560	This study

[a]See figure 1 for locations of sample sites.
[b]Based on Libby half-life for radiocarbon (5,570 yr) and referenced to A.D. 1950.
[c]Rounded to nearest 10 yr. Combines standard deviation in radiocarbon age and a conservative laboratory error multiplier of 2 to compensate for possible unreported laboratory errors (Stuiver and Pearson, 1986).
[d]BCF = Bootlegger Cove Formation.
[e]Because disseminated organic material, which could include very fine-grained detrital coal, was dated, this age could be spuriously old.
[f]Atomic-mass-spectrometer date.
[g]Sample corrected for natural isotopic fractionation based on ^{13}C content.

Northwest of Point MacKenzie is a large outwash fan that is genetically related to the type Elmendorf moraine, which Schmoll and others (1972) bracketed between 11,690 ± 300 ^{14}C yr B.P. (table 1, loc. H) and 13,750 ± 400 ^{14}C yr B.P. (table 1, loc. S) (fig. 1). This fan is unmodified and clearly postdates the Woronzofian transgression. However, scarps that truncate early Elmendorf outwash and end moraines related to the Deception Creek moraine near Willow were cut west of Wasilla during the Woronzofian transgression (fig. 1, loc. B). These physiographic relations are evidence that the Woronzofian transgression at least in part postdates the early phase of the Elmendorf advance. The main erosion scarp there is older than a basal peat, which dates 10,720 ± 460 ^{14}C yr B.P. (table 1, loc. B).

Radiocarbon dating of basal freshwater peats that overlie BCF provides minimum ages for isostatic rebound of the Anchorage lowland from beneath estuarine waters in which BCF was deposited. These dates range from 11,450 ± 150 ^{14}C yr B.P. (table 1, loc. T) to 12,350 ± 350 ^{14}C yr B.P. (table 1, loc. G). We speculate that land emergence began generally just after culmination of the Elmendorf glacial advance, which in Knik Arm probably occurred about 13,500 ^{14}C yr B.P. in response to the interaction of eustatic, isostatic, and tectonic conditions (fig. 3).

Not long after the culmination of the Elmendorf advance, the expanded glacier system from lower Matanuska and Knik valleys developed a negative budget. The final phase of the Naptowne glaciation is characterized by ice stagnation and retreat, widespread meltwater activity, and rapid downcutting by streams (Reger and Updike, 1983). Radiocarbon dates of organic sediments from deep boreholes in paludal and estuarine deposits provide minimum ages for deglaciation of Knik Arm (fig. 1, locs. C, D, E, and F). A generalized time-distance curve, tentatively based on available physiographic and stratigraphic evidence, indicates that by 11,400 ^{14}C yr B.P. the Elmendorf glacier had retreated at least 47 km from the terminal moraine just north of Anchorage (fig. 3). However, the northeastern end of this curve is based on a single radiocarbon date of organic silt in estuarine deposits, and we are suspicious that this date is spuriously old because of possible contamination by very fine-grained detrital coal (table 1, loc. C). Pitting of low terraces of the Matanuska River near Palmer is evidence that stagnant glacial ice, probably from Knik Glacier, existed there until quite late, perhaps into the early Holocene (Reger and Updike, 1983, p. 230). A date of 9,155 ± 215 ^{14}C yr B.P. (table 1, loc. A) for basal peat in an ice-marginal channel at the mouth of the upper canyon of Little Susitna River provides a minimum age for deglaciation there (fig. 1 and table 1, loc. A).

TURNAGAIN ARM EVIDENCE

Kachadoorian and others (1977) described a complex stratigraphy along the southern shore of Turnagain Arm in the vicinity of Hope that resulted from a late-Wisconsin glacial advance westward down the shallow fjord. During this episodic advance, the glacier overrode its own outwash as well as associated deltaic and marine sediments. According to their model (p. B50), the advance terminated about 2 km west of Hope, where the upper limit of the massive terminal moraine stands at a modern elevation of 83 m. Although they did not mention the presence of marine fossils in the oldest exposed sediments and provided no radiocarbon ages, the authors correlated the basal deposits with the BCF.

In 1982, in discontinuous exposures through the dense alder vegetation for about 5 km along the southern shore of Turnagain Arm west of Hope, we observed a fine-grained, undeformed diamicton that contains marine shells, many unbroken, and is locally rich in cobbles and boulders, especially in the upper part of the unit (fig. 1, locs. U, V, and W). We did not find the thick morainal diamicton that Kachadoorian and others (1977, p. B49) reported overlies outwash, deltaic deposits and the BCF there, but exposures were very limited in extent. We measured the top of the fossiliferous unit at between 3 and 12 m above the high-tide line. AMS ages for marine mollusk shells in the undeformed diamicton west of Hope are 13,718 ± 160 ^{14}C yr B.P. (table 1, loc. U), 14,160 ± 140 ^{14}C yr B.P. (table 1, loc. V), and 14,200 ± 100 ^{14}C yr B.P. (table 1, loc. W). These ages confirm correlation of this fossiliferous deposit with type BCF in the Anchorage area by Kachadoorian and others (1977, p. B49).

During our traverse, we noted that there is a contrast in the degree of deformation of BCF east and west of Hope. About 1 km east of Hope, shells in the clay-rich BCF diamicton are rare and severely crushed. Farther east we could not find fossils in the BCF. Our impression was that the deformation is pervasive and widespread throughout the unit there, which argues against local deformation by grounding ice bergs. In contrast, the BCF west of Hope is undeformed. We propose that the glacier that advanced westward down Turnagain Arm during deposition of the upper BCF was grounded at least during low tides as far west as Hope. The undeformed nature of the BCF and the presence of unbroken marine-mollusk shells west of Hope are evidence that floating, not grounded ice was the source of the large clasts in the upper BCF there. We suggest that the BCF accumulated in glacioestuarine waters there as a result of (1) the rainout of material from turbid sediment plumes related to efflux jets emerging from beneath the nearby glacier and (2) dropstone deposition from the floating terminal zone of the tidewater glacier, an ice shelf, or

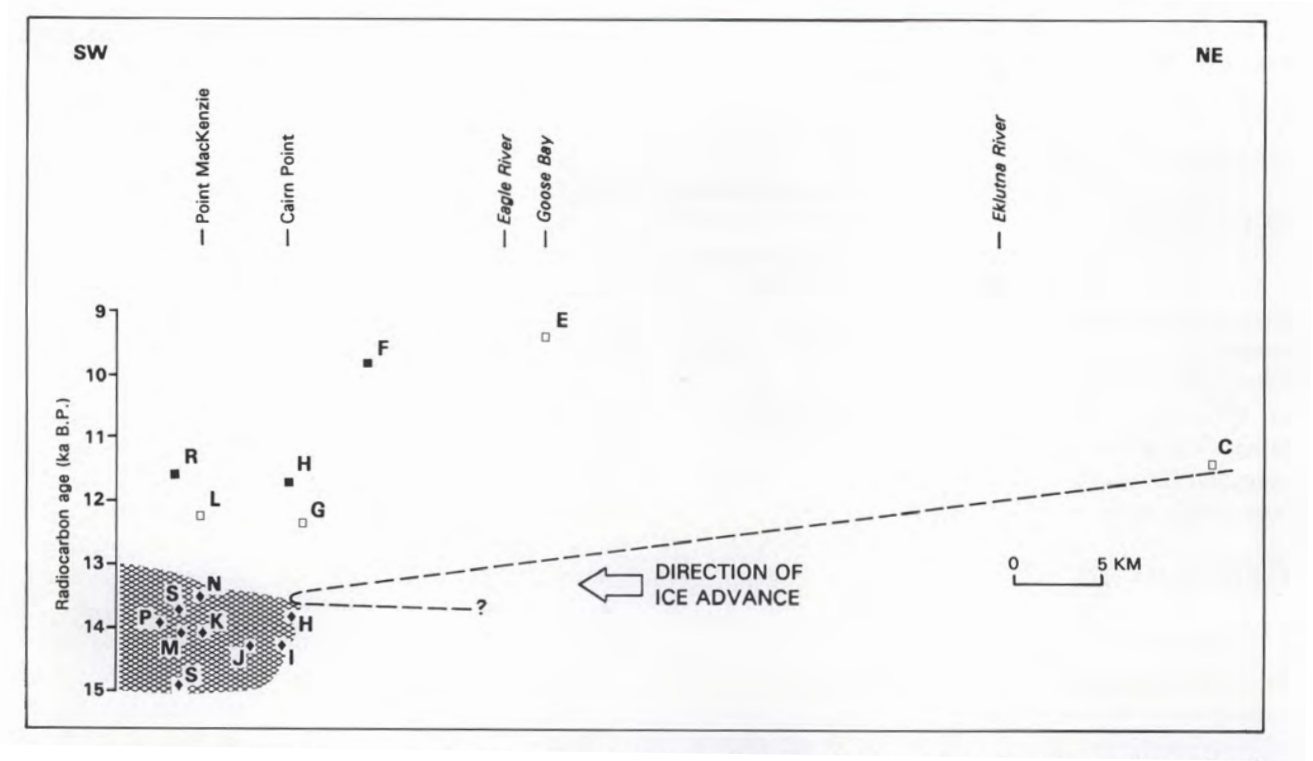

Figure 3. *Tentative time-distance curve for Elmendorf advance in Knik Arm. Letters refer to locations in figure 1 and table 1. Symbols:* □ *= organic silt,* ■ *= peat,* ♦ *= shell, BCF = Bootlegger Cove Formation.*

from debris-laden, melting ice bergs (Eyles and McCabe, 1989). We correlate the terminal position at Hope with the Bird Creek moraine, which is reported to overlie BCF on the northern shore of Turnagain Arm (Bartsch-Winkler and Schmoll, 1984; Schmoll and others, 1984, fig. 7; and Schmoll and Yehle, 1986, fig. 5), and with the type Elmendorf moraine (fig. 1).

In 1982, we also revisited the shell-bearing diamicton at Mile 99.5 Seward Highway, where Dobrovolny and Schmoll discovered and dated crushed marine shells at 13,900 ± 400 ^{14}C yr B.P. (table 1, loc X). The highway-cut exposure there was about 15 m above the high-tide line before subsequent highway realignment destroyed it. Dobrovolny and Schmoll interpreted the exposure to be colluvial bedrock rubble that incorporated reworked BCF (Schmoll and Yehle, 1986, p. 205). We suggest that the Mile 99.5 exposure can also be interpreted as BCF that was overridden by a glacier that advanced westward into estuarine waters of Turnagain Arm. The shells could have been preserved there in the lee of the bedrock shoulder, although perhaps badly broken as we found them, if the overriding glacier was partially floating. Our collection of severely fragmented *Macoma balthica* shells from that locality has an AMS age of 14,290 ± 140 ^{14}C yr B.P. (table 1, loc X). The weighted average age of our collection and that of Dobrovolny and Schmoll is 14,245 ± 270 ^{14}C yr B.P., which is essentially the same age as shells preserved in BCF near Hope, 8 km to the west (fig. 1).

Their interpretation of the Mile 99.5 exposure and a tenuously extrapolated age of about 14,000 ^{14}C yr B.P. for basal sediments in the thick fjord fill at the head of Turnagain Arm (Bartsch-Winkler and others, 1983) (fig. 1, loc. AA) convinced Bartsch-Winkler and Schmoll (1984) and Schmoll and Yehle (1986) that Turnagain Arm was free of glacial ice about 14,000 ^{14}C yr B.P. However, we question the estimate of about 14,000 ^{14}C yr B.P. for the age of basal sediments in the >303-m-thick fill at the head of Turnagain Arm. Their estimate is based on an assumed sedimentation rate that was derived from four radiocarbon samples, the oldest of which is 8,230 ± 100 ^{14}C yr B.P. (table 1, loc AA) at a depth of only 93 m in the thick fill (Bartsch-Winkler and others, 1983, fig. 11). In our opinion, the actual sedimentation rate probably varied considerably, especially between depths of 90 m and the base of the thick fjord fill in that part of the section deposited in late glacial time, when sedimentation rates were undoubtedly much higher than Holocene rates. Our skepticism is reinforced by the presence of a clay and rock unit, which is probably till, at a depth of 210–225 m in the 305-m water well at that location (Bartsch-Winkler and others, 1983, fig. 10).

A simplified and tentative time-distance curve (fig. 4) reflects our belief that the Elmendorf advance in Turnagain Arm terminated about 14,000 ^{14}C yr B.P in shallow estuarine waters at Hope. West of Hope, diamictons of this age probably accumulated in glacioestuarine conditions. Undoubtedly, waxing and waning of the trunk glacier in

Turnagain Arm were interrupted by minor still-stands and even reversals. The stratigraphy preserved along the southern shore of Turnagain Arm just east of Hope records these events (Kachadoorian and others, 1977). By 10,730 ± 525 ^{14}C yr B.P. (table 1, loc. AB), ice had retreated at least 44 km up Turnagain Arm. A date of 10,180 ± 350 ^{14}C yr B.P. (table 1, loc. Z) is a minimum age for a post-Elmendorf delta at a present elevation of about 12 m in the Girdwood area. Peat in organic sediments ponded against a small terminal moraine in Turnagain Pass (Combellick, 1984) dates 9,850 ± 390 ^{14}C yr B.P. (table 1, loc. AC). The age of the peat demonstrates that glaciers had retreated nearly to the heads of tributary valleys in the nearby Kenai Mountains and then readvanced just before the end of the Naptowne glaciation (fig. 4).

OTHER EVIDENCE

Reger and Updike (1983) proposed that simultaneous expansion of glaciers from lower Matanuska and Knik valleys resulted in the Elmendorf advance. Williams (1986) dated a basal peaty silt overlying till in a depression filling <0.2 km from the terminus of Matanuska Glacier at the head of Matanuska valley about 73 km east-northeast of Palmer. Samples of the organic silt date 13,100 ± 60 ^{14}C yr B.P. (USGS-2175) and 12,210 ± 210 ^{14}C yr B.P. (BETA-11174), which provides a local minimum limiting age for the late Naptowne retreat of Matanuska Glacier. These dates encouraged Williams (1986, p. 87) to question dating of the type Elmendorf moraine at Anchorage and to challenge interpretations of stratigraphic relations between BCF and deposits of the Elmendorf advance (Schmoll and others, 1972; Reger and Updike, 1983; Schmoll and Yehle, 1986). Evidence presented in this report reaffirms the previous interpretations. We emphasize that Matanuska Glacier was not the only source of ice in lower Matanuska valley. Several large tributary glaciers entered middle Matanuska valley from the Talkeetna Mountains to the north. Although the floor of upper Matanuska valley is deeply scoured bedrock and no obvious ice limits have been identified during casual observations, ice-stagnation and associated glaciofluvial deposits related to former glaciers in the middle and lower valley are mentioned in guidebooks of the area (Reger and Updike, 1983; Clardy and others, 1984). We further contend that radiocarbon dates from Kenai Peninsula, Chugach Mountains, St. Elias Mountains, and southeastern Alaska, which Williams (1986) cited as evidence against our dating and

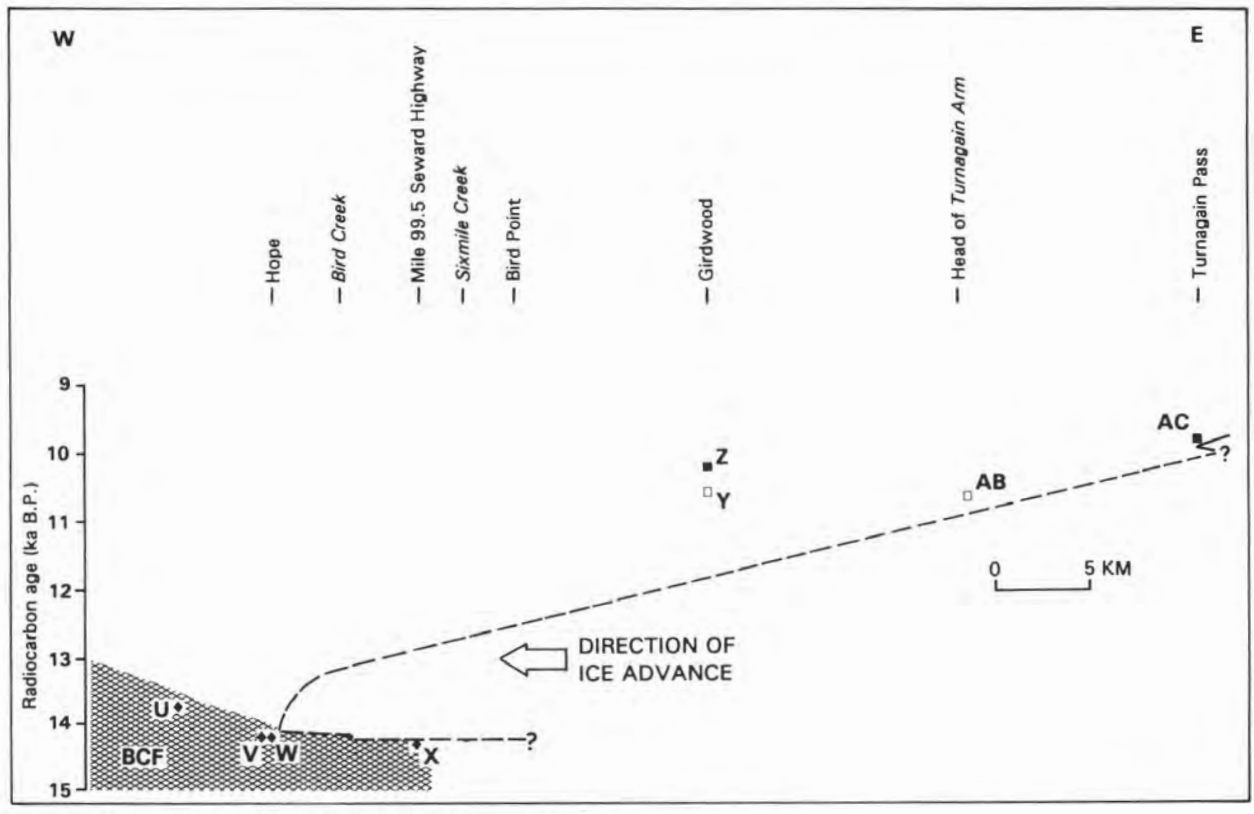

Figure 4. *Tentative time-distance curve for Elmendorf advance in Turnagain Arm. Letters refer to locations in figure 1 and table 1. Symbols:* □ *= organic silt,* ■ *= peat,* ♦ *= shell, BCF = Bootlegger Cove Formation.*

interpretation of the late-Naptowne record in the Anchorage area, actually relate to pre-Elmendorf deposits and events. This is certainly the case at Hidden Lake in the eastcentral Kenai lowland, where the lake basin was deglaciated at the end of the pre-Elmendorf Skilak stade of the late Naptowne glaciation (Reger and Pinney, in press).

Evidence in the upper Cook Inlet region demonstrates that the Elmendorf advance in the Anchorage area was not an isolated late Naptowne event as suggested by Williams (1986). After considering physiographic and stratigraphic evidence, Reger and Pinney (in press) attribute range-front ice limits in many valleys in the western Kenai Mountains to the Elmendorf advance. In the Valdez area, Wilber and others (1991) found physiographic and stratigraphic evidence that Port Valdez became ice free at the end of the Skilak stade. They correlated a subsequent glacial advance that built moraines at the mouths of tributary valleys with the Elmendorf advance. Reger (1991) published a minimum age of 11,820 ± 560 ^{14}C yr B.P. (GX-10,789) for the readvance of ice out of the valley of Allison Creek on the southern shore of Port Valdez and correlated that event with the Elmendorf advance in upper Cook Inlet.

CALIBRATION OF RADIOCARBON DATES

To this point in this paper we have not complicated our presentation by introducing calibrated radiocarbon dates. However, past variations in radiocarbon content of the atmospheric and marine reservoirs introduced significant errors in the radiocarbon time scale. Available calibration programs, although not yet perfected, at least partly correct these errors as far back as 18,760 ^{14}C yr B.P. (21,950 cal yr B.P.) (Stuiver and Reimer, 1993). For terrestrial samples, detailed calibrations are based on changes in the radiocarbon contents of dendrochronologically-dated tree rings; for marine shells in the time range of our study, corrections are based on uranium-thorium and radiocarbon dating of corals.

Clearly, if we are to keep the sequence of late Naptowne events in upper Cook Inlet in proper perspective, we need to consider the effects of calibration on radiocarbon ages related to these events. In table 1 we list both radiocarbon and calibrated dates and relate them to significant events in upper Cook Inlet. We ignore small potential errors that are due to local variations in the ^{14}C content of the estuarine waters of Cook Inlet. And we do not compensate for possible errors up to 400 ^{14}C yr due to comparison of 11 dates that are corrected for fractionation, based on their ^{13}C contents, with 20 dates that are not corrected for fractionation.

When we compare mean ages, the main effect of converting radiocarbon ages to calibrated (calendar) ages is to extend back in time the Holocene and late Naptowne events in upper Cook Inlet. According to the calibrated time scale provided by CALIB 3.0 (Stuiver and Reimer, 1993), the oldest dated event, deposition of the shell-rich zone in the type area of the BCF, occurred between 15,140 and 18,130 cal yr B.P. (at 1σ) (table 1, locs. N and S). Interfingering relations between the glaciodeltaic complex and BCF indicate that stagnant ice existed in the south Anchorage–Fire Island area at the same time. The type Elmendorf moraine was built between 13,000 and 17,200 cal yr B.P. (at 1σ) (table 1, loc. H). In Turnagain Arm, shell-bearing BCF was deposited between 14,940 and 17,000 cal yr B.P. (at 1σ) (table 1, locs. U, V, W, and X), and the Elmendorf advance down Turnagain Arm culminated shortly after. The land surface in the Anchorage area rebounded out of Cook Inlet waters before freshwater peats began accumulating there between 13,060 and 15,520 cal yr B.P. (at 1σ) (table 1, locs. T and G). The latest Naptowne advance in Turnagain Pass ended between 10,020 and 12,560 cal yr B.P. (at 1σ) (table 1, loc. AC).

CONCLUSIONS

Recently acquired evidence reaffirms previous dating of the upper BCF in the Anchorage area and supports previous interpretations of the stratigraphy and history by Schmoll and others (1972), Reger and Updike (1983), and Schmoll and Yehle (1983). The BCF was deposited during and after deposition of a glaciodeltaic complex in the south Anchorage–Fire Island area and just before the height of the type Elmendorf advance about 13,500 ^{14}C yr B.P. (roughly 16,200 cal yr B.P.). We concur with previous correlations of shell-bearing glacioestuarine deposits in Turnagain Arm with the type BCF (Schmoll and Yehle, 1983, 1986; Schmoll and others, 1984). However, we believe there is strong evidence for an Elmendorf-equivalent advance in Turnagain Arm that culminated in shallow estuarine waters at Hope about 14,000 ^{14}C yr B.P. (about 16,270 cal yr B.P.). By about 9,850 ^{14}C yr B.P. (11,000 cal yr B.P.) tributary glaciers in Turnagain Arm had receded nearly to the heads of source valleys and then readvanced slightly. Comparison with late Naptowne events elsewhere in southcentral Alaska indicates that the Elmendorf advance was regionally significant and not a local aberration as suggested by Williams (1986).

ACKNOWLEDGMENTS

We greatly appreciate preparation of figure 1 by Alfred G. Sturmann (DGGS). Excellent assistance was provided in the field by DeAnne S. Pinney, Milton A. Wiltse, Alfred G. Sturmann, Cheri L. Daniels, and Sven Lagerberg. Fossil identifications were confirmed by Nora R. Foster,

Curator for Invertebrate Collections, University of Alaska (Fairbanks) Museum. Thoughtful reviews by Thomas D. Hamilton (USGS) and Jeffrey T. Kline (DGGS) helped clarify this paper. Radiocarbon ages were determined by University of Arizona (AA), Beta Analytic (BETA), Geochron Laboraties (GX), and United States Geological Survey (W) (table 1).

REFERENCES CITED

Bartsch-Winkler, Susan, Ovenshine, A.T., and Kachadoorian, Reuben, 1983, Holocene history of the estuarine area surrounding Portage, Alaska, as recorded in a 93 m core: Canadian Journal of Earth Sciences, v. 20, no. 5, p. 802-820.

Bartsch-Winkler, Susan, and Schmoll, H.R., 1984, Guide to late Pleistocene and Holocene deposits of Turnagain Arm: Anchorage, Alaska Geological Society guidebook, 70 p.

Cederstrom, D.J., Trainer, F.W., and Waller, R.M., 1964, Geology and ground-water resources of the Anchorage area, Alaska: U.S. Geological Survey Water-Supply Paper 1773, 108 p., 2 pls., 2 map sheets, scale 1:63,360.

Clardy, B.I., Hanley, P.T., Hawley, C.C., and LaBelle, J.C., 1984, Guide to the bedrock and glacial geology of the Glenn Highway, Anchorage to the Matanuska Glacier and the Matanuska coal mining district: Anchorage, Alaska Geological Society, 63 p., 2 sheets, scale 1:96,000.

Combellick, R.A., 1984, Surficial-geologic map of the Seward D-6 Quadrangle, Alaska: Alaska Division of Geological & Geophysical Surveys Report of Investigations 84-15, 1 sheet, scale 1:63,360.

_____1991, Paleoseismicity of the Cook Inlet region, Alaska: Evidence from peat stratigraphy in Turnagain and Knik Arms: Alaska Division of Geological & Geophysical Surveys Professional Report 112, 52 p.

_____1993, The penultimate great earthquake in southcentral Alaska: Evidence from a buried forest near Girdwood, Alaska, *in* Solie, D.N., and Tannian, Fran, eds., Short Notes on Alaskan Geology 1993: Alaska Division of Geological & Geophysical Surveys Professional Report 113, p. 7-15.

_____1994, Investigation of peat stratigraphy in tidal marshes along Cook Inlet, Alaska, to determine the frequency of 1964-style great earthquakes in the Anchorage region: Alaska Division of Geological & Geophysical Surveys Report of Investigations 94-7, 24 p.

Combellick, R.A., and Reger, R.D., 1994, Sedimentological and radiocarbon-age data for tidal marshes along eastern and upper Cook Inlet, Alaska: Alaska Division of Geological & Geophysical Surveys Report of Investigations 94-6, 60 p.

Eyles, Nicholas, and McCabe, A.M., 1989, The late Devensian (<22,000 BP) Irish Sea basin: The sedimentary record of a collapsed ice sheet margin: Quaternary Science Reviews, v. 8, p. 307-351.

Hansen, W.R., 1965, Effects of the earthquake of March 27, 1964, at Anchorage, Alaska: U.S. Geological Survey Professional Paper 542-A, 68 p., 2 sheets, scales 1:480 and 1:2400.

Hopkins, D.M., 1967, Quaternary marine transgressions in Alaska, *in* Hopkins, D.M., ed., The Bering Land Bridge, Stanford, Stanford University Press, p. 47-90.

_____1973, Sea level history in Beringia during the past 250,000 years: Quaternary Research, v. 3, no. 4, p. 520-540.

Kachadoorian, Reuben, Ovenshine, A.T., and Bartsch-Winkler, Susan, 1977, Late Wisconsin history of the south shore of Turnagain Arm, Alaska, *in* Blean, K.M., ed., The United States Geological Survey in Alaska: Accomplishments during 1976: U.S. Geological Survey Circular 751-B, p. B49-B50.

Karlstom, T.N.V., 1953, Upper Cook Inlet region, *in* Péwé, T.L., and others, Multiple glaciation in Alaska: A progress report: U.S. Geological Survey Circular 289, 13 p., 1 sheet, scale 1:3,115,400.

_____1964, Quaternary geology of the Kenai Lowland and glacial history of the Cook Inlet region, Alaska: U.S. Geological Survey Professional Paper 443, 69 p., 2 pls., 5 map sheets, scales 1:63,360, 1:250,000, 1:1,594,490, and 1:5,000,000.

Miller, R.D., and Dobrovolny, Ernest, 1959, Surficial geology of Anchorage and vicinity, Alaska: U.S. Geological Survey Bulletin 1093, 128 p., 1 sheet, scale 1:63,360.

Reger, R.D., 1991, Deglaciation of the Allison–Sawmill Creeks area, southern shore of Port Valdez, Alaska, *in* Reger, R.D., ed., Short Notes on Alaskan Geology 1991: Alaska Division of Geological & Geophysical Surveys Professional Report 111, p. 55-61.

Reger, R.D., and Updike, R.G., 1983, Upper Cook Inlet region and the Matanuska Valley, *in* Péwé, T.L., and Reger, R.D., eds., Guidebook to permafrost and Quaternary geology along the Richardson and Glenn Highways between Fairbanks and Anchorage, Alaska: Alaska Division of Geological & Geophysical Surveys Guidebook 1, p. 185-263, 1 sheet, scale 1:250,000.

Reger, R.D., and Pinney, D.S., in press, Late Wisconsin glaciation of the Cook Inlet region with emphasis on Kenai lowland and implications for early peopling, *in* Davis, N.Y., and Davis, W.E., eds., The Anthropology of Cook Inlet: Proceedings from a Symposium: Alaska Anthropological Association Conference, 20th annual meeting, Anchorage, April 8–10, 1993, Cook Inlet Historical Society.

Rubin, Meyer, and Alexander, Corrine, 1960, U.S. Geological Survey radiocarbon dates V: American Journal of Science Radiocarbon Supplement, v. 2, p. 129-185.

Schmidt, R.A.M., 1963, Pleistocene marine microfauna in the Bootlegger Cove Clay, Anchorage, Alaska: Science, v. 141, no. 3578, p. 350-351.

Schmoll, H.R., and Barnwell, W.W., 1984, East-west geologic cross section along the DeBarr Line, Anchorage, Alaska: U.S Geological Survey Open-File Report 84-791, 10 p.

Schmoll, H.R., Szabo, B.J., Rubin, Meyer, and Dobrovolny, Ernest, 1972, Radiometric dating of marine shells from the Bootlegger Cove Clay, Anchorage, Alaska: Geological Society of America Bulletin, v. 83, no. 4, p. 1107-1114.

Schmoll, H.R., and Yehle, L.A., 1983, Glaciation in the upper Cook Inlet basin: A preliminary reexamination based on geologic mapping in progress, *in* Thorson, R.M., and Hamilton, T.D., eds., Glaciation in Alaska: Extended abstracts from a workshop: University of Alaska Museum Occasional Paper 2, p. 75-100.

_____1986, Pleistocene glaciation of the upper Cook Inlet basin, *in* Hamilton, T.D., Reed, K.M., and Thorson, R.M., eds., Glaciation in Alaska–the geologic record: Anchorage, Alaska Geological Society, p. 193-218.

Schmoll, H.R., Yehle, L.A., Gardner, C.A., and Odum, J.K., 1984, Guide to surficial geology and glacial stratigraphy in the upper Cook Inlet basin: Anchorage, Alaska Geological Society guidebook, 89 p.

Spiker, Elliott, Kelley, Lea, Oman, Charles, and Rubin, Meyer, 1977, U.S. Geological Survey radiocarbon dates XII: Radiocarbon, v. 19, no. 2, p. 332-353.

Sullivan, B.M., Spiker, Elliott, and Rubin, Meyer, 1970, U.S. Geological Survey radiocarbon dates XI: Radiocarbon, v. 12, no. 1, p. 319-334.

Stuiver, Minze, and Pearson, G.W., 1986, High-precision calibration of the radiocarbon time scale, AD 1950-500 BC, *in* Stuiver, Minze, and Kra, Renee, eds., Proceedings of the 12th International Radiocarbon Conference, Trondheim, 1985: Radiocarbon, v. 28, no. 2B, p. 805-838.

Stuiver, Minze, and Reimer, P.J., 1993, Extended ^{14}C data base and revised CALIB 3.0 ^{14}C age calibration program: Radiocarbon, v. 35, no. 1, p. 215-230.

Trainer, F.W., and Waller, R.M., 1965, Subsurface stratigraphy of glacial drift at Anchorage, Alaska, *in* Geological Survey Research 1965: U.S. Geological Survey Professional Paper 525-D, p. 167-174.

Ulery, C.A., and Updike, R.G., 1983, Subsurface structure of the cohesive facies of the Bootlegger Cove Formation, southwest Anchorage, Alaska: Alaska Division of Geological & Geophysical Surveys Professional Report 84, 5 p., 3 sheets, scale 1:15,840.

Updike, R.G., Cole, D.A., Jr., and Ulery, Cathy, 1982, Shear moduli and damping ratios for the Bootlegger Cove Formation as determined by resonant-column testing, *in* Short Notes on Alaskan Geology 1981: Alaska Division of Geological & Geophysical Surveys Geologic Report 73, p. 7-12.

Updike, R.G., and Ulery, C.A., 1986, Engineering-geology map of southwest Anchorage, Alaska: Alaska Division of Geological & Geophysical Surveys Professional Report 89, 1 sheet, scale 1:15,840.

Wilber, S.C., Molinari, M.P., and Burke, R.M., 1991, Late Wisconsin and Holocene glacial history of Port Valdez, Alaska (abs.): Geological Society of America Abstracts with Programs, v. 23, no. 5, p. A62.

Williams, J.R., 1986, New radiocarbon dates from the Matanuska Glacier bog section, *in* Bartsch-Winkler, Susan, and Reed, K.R., eds., Geologic studies in Alaska by the U.S. Geological Survey during 1985: U.S. Geological Survey Circular 978, p. 85-88.

Yehle, L.A., Schmoll, H.R., and Dobrovolny, Ernest, 1990, Geologic map of the Anchorage B-8SE and part of the Anchorage B-8NE quadrangles, Alaska: U.S. Geological Survey Open-File Report 90-238, 37 p., 1 sheet, scale 1:25,000.

_____1991, Geologic map of the Anchorage B-8SW quadrangle, Alaska: U.S. Geological Survey Open-File Report 91-143, 30 p., 1 sheet, scale 1:25,000.

STRATIGRAPHY AND IMPLICATIONS OF A LAKESIDE SECTION, GLACIAL LAKE, SOUTHWESTERN KIGLUAIK MOUNTAINS, SEWARD PENINSULA, ALASKA

by

Richard D. Reger[1] and David M. Hopkins[2]

ABSTRACT

A 3.6-m-high, fresh, wavecut bluff on the western shore of Glacial Lake in the southwestern Seward Peninsula exposed drift of the Salmon Lake glaciation overlain by lacustrine, paludal, and eolian deposits. Three radiocarbon dates of organic material from two beds in the section provide evidence for the age of sediments overlying the drift. However, the radiocarbon evidence is suspicious because (1) the lower bed dates several thousand years younger than the upper bed, and (2) standard errors are large for the two dates of the upper bed. Nonetheless, the dates overlap or nearly overlap at two standard errors. These dates support previous contentions by others that the Salmon Lake glaciation is at least as old as the early Wisconsin.

INTRODUCTION

In the summer of 1993, evidence of the age of late Pleistocene glaciation in the southwestern Kigluaik Mountains (fig. 1) was documented during geologic mapping in the Nome mining district. The purpose of this article is to report and discuss this evidence.

GEOLOGIC SETTING

The Kigluaik Mountains are an uplifted fault block of crystalline igneous and metamorphic rocks that is located about 30 km north of Nome in the southwestern Seward Peninsula. Glacial Lake occupies a glacier-scoured, south-trending valley in the southwestern Kigluaik Mountains (fig. 1). The walls of this valley bear well-developed colluvial features, including lobate rock glaciers and debris fans of Holocene and late Pleistocene age (Kaufman and others, 1989). In the vicinity of Glacial Lake, the glacial deposits are discontinuously notched by former lake shorelines at heights of 4.5 and 14 m above the present lake level of 119 m (fig. 1).

HISTORY OF GLACIATION

During middle and late Pleistocene cold periods, the Kigluaik Mountains supported several generations of glaciers. Ice of the Nome River glaciation radiated outward from the Kigluaik Mountains during a particularly extensive middle-Pleistocene advance and coalesced with local ice from cirques and small ice caps in uplands to the south. This glacier complex flowed as far south as several kilometers beyond the northern shore of Norton Sound (Hopkins and others, 1960; Kaufman and Hopkins, 1989; Kaufman and others, 1991) and initially dispersed much of the gold that eventually formed many of the younger placers in the Nome district (Collier and others, 1908; Moffit, 1913; Nelson and Hopkins, 1972; Kaufman and Hopkins, 1989). Drift of this age is extensively modified by slope processes so that primary microrelief features are rarely preserved.

The subsequent Stewart River glaciation spread out of the southern Kigluaik Mountains as far as 10 km beyond the mountain front. Ice from Kigluaik sources blocked and flowed up tributary valleys in the northern uplands south of the Kigluaik Mountains and joined with local ice from small, north-facing cirques (Bundtzen and others, 1994). The Stewart River glaciation is thought to predate the last interglaciation (Kaufman and Hopkins, 1986; Kaufman and others, 1988). Morphologies of moraines of this age are typically moderately modified by postglacial processes (Kaufman and others, 1988; Kaufman and Calkin, 1988).

Slightly modified drift of the Salmon Lake glaciation forms lobate moraines that reach beyond the front of the southern Kigluaik Mountains nearly to the terminal moraine of the Stewart River glaciation (Kaufman and others, 1989). Several recessional moraines document retreat of ice of this age south of Glacial Lake (fig. 1). Hopkins and others (1983) published two infinite radiocarbon dates (>33,000 yr. B.P. [I-7,710] and >40,000 yr B.P [I-7,709]) for fine-grained, possibly allochthonous organic detritus in lacustrine clay overlying drift of the Salmon Lake glaciation from the same locality 19.2 km northwest of the Glacial Lake section in the valley of Canyon Creek. These dates and the morphologies of the moraines are evidence that the Salmon Lake glaciation is at least as old as early Wisconsin (Kaufman and Hopkins, 1986).

[1]Alaska Division of Geological & Geophysical Surveys,794 University Avenue, Suite 200, Fairbanks, Alaska 99709-3645.
[2]Alaska Quaternary Center, University of Alaska, Fairbanks, Alaska 99775.

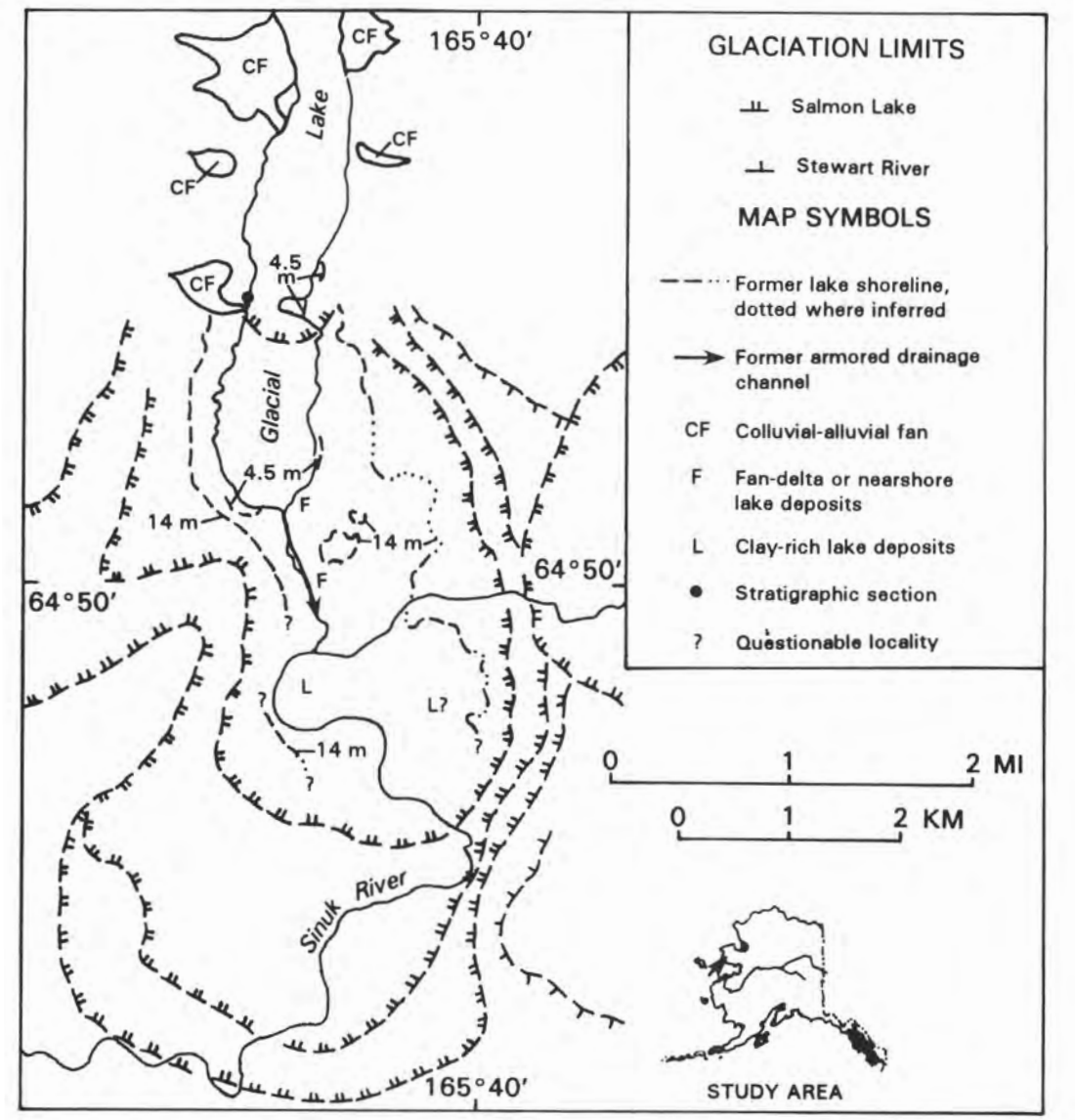

Figure 1. *Landforms in the vicinity of lower Glacial Lake, southwestern Kigluaik Mountains, relative to the lakeside stratigraphic section shown in figure 2.*

Sharp-crested, well-preserved moraines of the Mount Osborn glaciation are limited to tributary valleys in the higher mountains of the Seward Peninsula. Fresh morphologies of Mount Osborn drift, cirques, and valley walls and a radiocarbon age of 11,530 ± 450 yr B.P. (I-15,041) for peat[3] in a valley glaciated during Mount Osborn time demonstrate that this glaciation is probably late Wisconsin in age (Kaufman and others, 1988).

Today, only three small glaciers exist in steep-walled, north-facing cirques between 600 and 830 m elevation in the northcentral Kigluaik Mountains (Kaufman and others, 1989).

[3]Later described as fine-grained organic detritus from a depth of 1.3 m in lacustrine deposits that postdate retreat of ice of Mount Osborne age (Kaufman and others, 1989).

LAKESIDE SECTION

During a helicopter reconnaissance on July 11, 1993, we initially examined a fresh exposure of sediments that contain organic materials and overlie glacial deposits along the western shore of Glacial Lake. The drift at that site is part of a recessional moraine that is clearly visible even beneath the adjacent waters of Glacial Lake (fig. 1), and the surface of the moraine in the vicinity of the fresh exposure exhibits considerable evidence of active instability due to the melting of ground ice. Close examination of the 3.6-m-high exposure revealed that lacustrine, paludal, and eolian deposits overlie a sandy and bouldery drift of the Salmon Lake glaciation (fig. 2). The section is located near the toe of a complex colluvial-alluvial fan that was

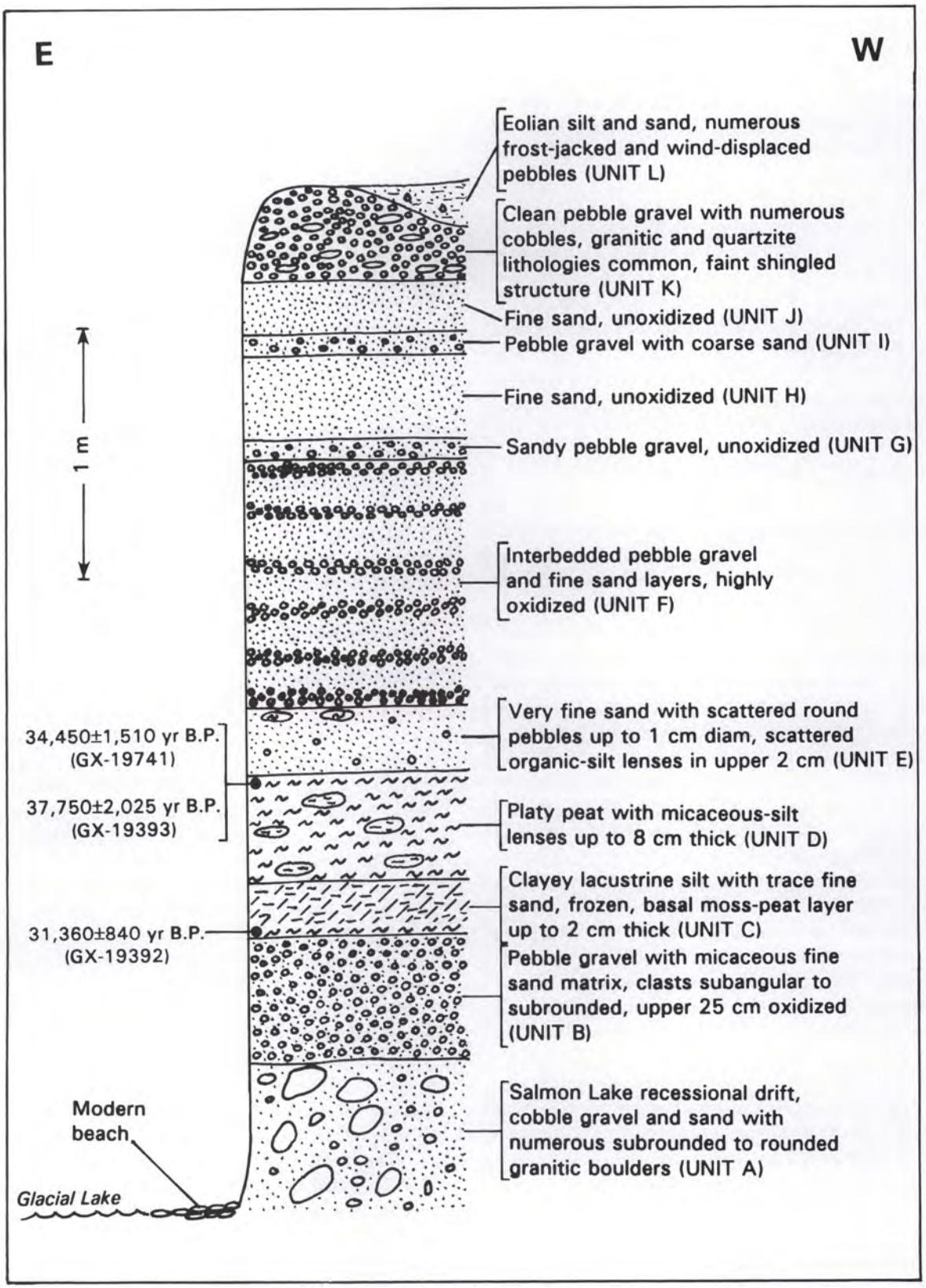

Figure 2. *Stratigraphic section in recessional moraine of Salmon Lake glaciation, western shore of Glacial Lake, Nome D-2 Quadrangle. Lake level about 119 m on July 11, 1993.*

built by a stream draining a small nearby cirque of probable Salmon Lake age.

A 338.6-gm sample of fine-grained silty moss was recovered from a 1-cm-thick layer at the base of a 20-cm-thick clayey lacustrine silt (fig. 2, unit C) that overlies till and associated ice-stagnation gravel of the Salmon Lake recessional moraine (fig. 2, units A and B). A total of 561.4 gm of peat and silt was collected from the upper part of a 45-cm-thick platy peat with micaceous silt lenses (fig. 2, unit D) that overlies unit C. Subsequent radiocarbon analysis of these organic samples indicates that the basal part of unit C dates 31,360 ± 840 yr B.P. (GX-19392) and the upper part of unit D dates 34,450 ± 1,510 yr B.P. (GX-19741) and 37,750 ± 2,025 yr B.P. (GX-19393) (fig. 2). All three ages are corrected for natural isotopic fractionation based on the carbon-13 contents of the samples.

INTERPRETATION OF SECTION

The sediments preserved in the lakeside section document a local history of deglaciation and subsequent deposition. Ablation till and associated glaciofluvial gravel at the base of the wavecut bluff (fig. 2, units A and B) were deposited as a consequence of ice stagnation and melting after the culmination of the Salmon Lake glaciation and during construction of the third recessional moraine behind the terminal moraine (fig. 1). Although oxidation of the upper 25 cm of unit B may by evidence of a truncated weathering profile associated with an unconformity between the glaciofluvial gravel and the overlying lake deposit (unit C), it most likely resulted from the movement of iron-bearing groundwater through the permeable gravel.

We interpret unit C to represent a former lake environment. The waters of this lake must have been shallow enough for moss to grow on the bottom. Unit D, a platy peat, must represent paludal or shallow, lake-marginal conditions. Clearly, water levels were lower at this location when unit D accumulated than during deposition of unit C. We believe that units E through K document nearshore lake conditions during which there was significant influx of clastic sediments from the nearby landscape. Scattered round pebbles in unit E probably represent dropstones, perhaps indicating that a calving glacier terminus fronted in ancestral Glacial Lake north of this section. The faint shingling of unit K probably is evidence that a polymictic beach gravel formed at this site late in the history of the lake. If so, at one time waters of the former lake must have stood about 3 m higher than today. Another possibility is that the gravel was transported to this site across the nearby colluvial-alluvial fan (fig. 1), but the local physiography does not support this mechanism.

Clearly, the top layer in the section (unit L) was deposited by winds sweeping silt, sand, and pebbles from nearby exposures. Frost-jacked pebbles in this sandy loess are evidence of subsequent seasonal frost action.

DISCUSSION

The lacustrine sequence in our section probably relates to the 4.5-m shoreline and not the 14-m shoreline. The top of the section is 3.6 m above the present level of Glacial Lake, so the lake deposits in the section were below the level of the 4.5-m lake. The 4.5-m shoreline notches the third recessional moraine (fig. 1) and so is younger than the moraine, as is the lake sequence in our section.

Distribution of the 14-m shoreline is consistent with impoundment of a much larger ancestral Glacial Lake by the second recessional moraine of the Salmon Lake glaciation, which is notched by that shoreline (fig. 1). Clean, medium to coarse fan-delta or nearshore lacustrine sand exposed in the bluff at the outlet of the modern lake dips 22° west and is overlain by anomalous concentrations of polymictic boulders and blocks up to 2 m in diameter in a matrix of sand. The upper surface of the sand is higher than 4.5 m above Glacial Lake and the bases of the largest granitic blocks are more than 3.5 m above the modern lake. We interpret these boulder nests as dropstone concentrations dumped into the former lake by the tipping of debris-laden, melting icebergs. Clearly, the former lake was higher than 4.5 m above Glacial Lake and a calving glacier fronted in the lake when the boulder nests were built. Concurrently, lacustrine clay was deposited in the 14-m lake about 2 km south of the modern outlet of Glacial Lake, where hundreds of carbonate-cemented, discoid concretions litter the ground surface.

The present underfit stream outlet of Glacial Lake (fig. 1) obviously postdates the 14-m lake. The former drainage channel is up to 50 m wide, stands as a terrace about 1 m above the modern lake level, and is armored with boulders (as is the present stream). The armoring is probably evidence that the outlet stream cut down through the glacial deposits essentially in its present location, perhaps during and after the existence of the 4.5-m lake. The known distribution of the 4.5-m shoreline is consistent with this interpretation. No other drainageway related to the 4.5-m shoreline was observed.

The radiocarbon date of 31,360 ± 840 yr B.P. (GX-19392) for the base of unit C provides a minimum age for the Salmon Lake glaciation in the Glacial Lake area (fig. 1). The discrete moss layer from which the sample was collected is undoubtedly authochthonous. However, an explanation is required of the fact that this stratigraphically lowest date in the section is several thousand years younger than the two dates of the overlying bed (unit D). At two sigma, which incorporates 95 percent of the counting variability during the radiocarbon analyses, sample GX-19741

(34,450 ± 1,510 yr B.P.) actually overlaps with samples GX-19392 and GX-19393 (37,750 ± 2,025 yr B.P.). At two sigma, the youngest sample (GX-19392) is within 700 yr of overlapping with the oldest sample (GX-19393). If one assumes (1) that units C and D were deposited within the maximum range of time indicated by the three radiocarbon dates, and (2) that these overlapping or near-overlapping ages accurately reflect the statistical (Poisson) variation of the counts about the true ages of units C and D, their weighted average composite age is 32,748 ± 690 radiocarbon yr B.P. according to the CALIB program (Stuiver and others, 1986), and there is a 95 percent likelihood that the true age is between 31,370 and 34,130 radiocarbon yr B.P.

There are several possible sources of error for the radiocarbon analyses. Sample size is a concern, particularly for the upper part of unit D, which contained significant silt. The sigma values for the two analyses of the upper sample are large, although not unreasonable for dates this close to the 42,000-yr limit of the instrument used for these analyses (H.W. Krueger, written commun., 1994), indicating that both samples of the upper part of unit D, although each weighed more than 200 gm, provided a small amount of datable carbon. In contrast, the sigma value of 840 radiocarbon yr for the age of the basal sample is small for a sample with a mean age of 31,360 radiocarbon yr, indicating that sample size is adequate and that the counting variation is small.

Several possible sources of contamination can be eliminated or minimized as factors. First, this is a permafrost environment, and the deposits have probably been frozen most of the time. Second, the exposure was fresh, and we dug into obviously fresh and undisturbed (in-situ) sediment before we collected the samples. We saw no evidence for contamination by the roots of modern vegetation or for mixing of sediments in any of the samples. Third, postsampling contamination is unlikely. All three samples were carefully wrapped in clean aluminum foil when they were collected, they were thoroughly dried in a standard drying oven and repacked in aluminum foil immediately upon our return from the field soon after they were collected, and they were quickly submitted for analysis. Sample contamination in the radiocarbon laboratory is extremely unlikely.

The most likely cause of dating error is incorporation of dead carbon into the mosses that grew in lake waters containing dead carbon. Samples of living moss (*Drepanocladus* sp.) from Glacial Lake and from a stream entering the northern end of Glacial Lake contain about 15 percent dead carbon. Possible sources of dead carbon in lake waters include carbonate rocks (marbles, skarns, calcareous schists) or graphitic rocks (schists, and native graphitic carbon) in the vicinity of Glacial Lake (Moffit, 1913; Hummel, 1962; Sainsbury and others, 1972; and Robinson and Stevens, 1984). Assuming that the fossil aquatic moss in the samples from the lakeside section also grew in equilibrium with shallow lake waters containing 15 percent dead carbon (which may not be a valid assumption), the initially reported dates would be 2,360 ± 360 to 4,220 ± 235 radiocarbon yr too old (H.W. Krueger, written commun., 1994). The corrected age for the base of unit C in these circumstances would be 27,140 ± 605 yr. B.P. (GX-19392), and the corrected ages for the upper part of unit D would be 32,090 ± 1,150 yr. B.P. (GX-19741) and 33,600 ± 1,250 yr B.P. (GX-19393).

CONCLUSIONS

Radiocarbon evidence from the lakeside section provides an uncorrected minimum age of 31,360 ± 840 yr B.P. and a possible corrected minimum age of 27,140 ± 605 yr B.P. for the underlying drift of the Salmon Lake glaciation. Although the reliability of the radiocarbon results from the Glacial Lake section is suspicious, the three ages reported here support prior contentions (Hopkins and others, 1983; Kaufman and Hopkins, 1986; Kaufman and others, 1988) that the Salmon Lake glaciation is at least as old as early Wisconsin. The radiocarbon dates also provide a maximum age for lowering of the waters of the former lake to the present level, probably by incision of the outlet through glacial deposits that impound Glacial Lake to the south (fig. 1).

ACKNOWLEDGMENTS

We thank DeAnne S. Pinney for her very competent assistance in the field, laboratory, and office. Radiocarbon analyses were conducted at DGGS expense by Geochron Laboratories Division of Krueger Enterprises, Inc. We appreciate Hal Krueger's quick responses and advice concerning the ages of the organic samples. This report was thoughtfully reviewed by James E. Begét (University of Alaska Fairbanks) and Jeffrey T. Kline (DGGS), and it was greatly improved by their input. Using the CALIB program, Rod Combellick kindly provided weighted averages for the radiocarbon dates.

REFERENCES CITED

Bundtzen, T.K., Reger, R.D., Laird, G.M., Pinney, D.S., Clautice, K.H., Liss, S.A., and Cruse, G.R., 1994, Preliminary geologic map of the Nome mining district: Alaska Division of Geological & Geophysical Surveys Public-Data File 94-39, 2 sheets, scale 1:63,360.

Collier, A.J., Hess, F.L., Smith, P.S., and Brooks, A.H., 1908, The gold placers of parts of Seward Peninsula, Alaska, including the Nome, Council, Kougarok, Port Clarence, and Goodhope precincts: U.S. Geological Survey Bulletin 328, 343 p.

Hopkins, D.M., MacNeil, F.S., and Leopold, E.B., 1960, The coastal plain at Nome, Alaska: A late Cenozoic type section for the Bering Strait region, *in* Sorgenfrei, Theodor, Report of the Twenty-first Session, International Geological Congress, Part 4, p. 46-57.

Hopkins, D.M., Pratt, Richard, Nelson, R.E., and Powell, C.L., II, 1983, Glacial sequence, southwestern Seward Peninsula, *in* Glaciation in Alaska: Extended abstracts from a workshop: Fairbanks, University of Alaska Museum Occasional Paper 2, p. 45-50.

Hummel, C.H., 1962, Preliminary geologic map of the Nome C-1 quadrangle, Seward Peninsula, Alaska: U.S. Geological Survey Mineral Investigations Field Studies Map MF-247, 1 sheet, scale 1:63,360.

Kaufman, D.S., and Calkin, P.E., 1988, Morphometric analysis of Pleistocene glacial deposits in the Kigluaik Mountains, northwestern Alaska, U.S.A.: Arctic and Alpine Research, v. 20, no. 3, p. 273-284.

Kaufman, D.S., Calkin, P.E., Whitford, W.B., Przybyl, B.J., Hopkins, D.M., Peck, B.J., and Nelson, R.E., 1989, Surficial geologic map of the Kigluaik Mountains area, Seward Peninsula, Alaska: U.S. Geological Survey Miscellaneous Field Studies Map MF-2074, 1 sheet, scale 1:63,360.

Kaufman, D.S., Hopkins, D.M., and Calkin, P.E., 1988, Glacial geologic history of the Salmon Lake area, Seward Peninsula, *in* Galloway, J.P., and Hamilton, T.D., eds., Geologic studies in Alaska by the U.S. Geological Survey during 1987: U.S. Geological Survey Circular 1016, p. 91-94.

Kaufman, D.S., and Hopkins, D.M., 1986, Glacial history of the Seward Peninsula, *in* Hamilton, T.D., Reed, K.M., and Thorson, R.M., eds., Glaciation in Alaska—the geologic record: Anchorage, Alaska Geological Society, p. 51-78.

Kaufman, D.S., and Hopkins, D.M., 1989, Late Cenozoic geologic controls on placer-gold distribution in the Nome nearshore area, *in* Dover, J.H., and Galloway, J.P., eds., Geologic studies in Alaska by the U.S. Geological Survey, 1988: U.S. Geological Survey Bulletin 1903, p. 26-45.

Kaufman, D.S., Walter, R.C., Brigham-Grette, Julie, and Hopkins, D.M., 1991, Middle Pleistocene age of the Nome River glaciation, northwestern Alaska: Quaternary Research, v. 36, no. 3, p. 277-293.

Moffit, F.H., 1913, Geology of the Nome and Grand Central quadrangles, Alaska: U.S. Geological Survey Bulletin 533, 140 p.

Nelson, C.H., and Hopkins, D.M., 1972, Sedimentary processes and distribution of particulate gold in the northern Bering Sea: U.S. Geological Survey Professional Paper 689, 27 p.

Robinson, M.S., and Stevens, D.L., 1984, Geologic map of the Seward Peninsula, Alaska: Alaska Division of Geological & Geophysical Surveys Special Report 34, 1 sheet, scale 1:500,000.

Sainsbury, C.L., Hummel, C.L., and Hudson, Travis, 1972, Reconnaissance geologic map of the Nome quadrangle, Alaska: U.S. Geological Survey Open-File Report 543, 28 p., 1 sheet, scale 1:250,000.

Stuiver, Minze, and Reimer, P.J., 1986, A computer program for radiocarbon age calibration: Radiocarbon, v. 28, no. 2B, p. 1022-1030.

LITHOFACIES, PETROLOGY, AND PETROPHYSICS OF THE KEMIK SANDSTONE (LOWER CRETACEOUS), EASTERN ARCTIC SLOPE, ALASKA

by
Rocky R. Reifenstuhl[1]

ABSTRACT

Regional distribution of Kemik Sandstone, equivalent sands, and the pebble shale unit and their relationship to the mid-Neocomian unconformity suggest that these rocks were derived from the north and deposited over the rifted margin of the Arctic Alaska plate. Outcrop mapping and measured sections of the Kemik on the Canning and the Echooka Rivers indicate coarsening-up, thickening-up sandstone successions. Depositional environments include upper shoreface, barrier island with tidal-channel fill, subaerial with local paleosol, and offshore shelf. Petrographic data indicate a recycled orogenic or quartzose recycled provenance. From west to east in the subsurface, local sources are indicated by the significant increase in chert and carbonate clasts. Petrophysical analyses indicate porosity up to 11 percent but very low permeability. The Kemik is dated as Hauterivian to Barremian (Early Cretaceous) based on paleontology of foraminifera, palynology, and macrofossils.

INTRODUCTION

The Kemik Sandstone is predominantly a very fine to fine-grained, clean, quartzose sandstone. In the subsurface the Kemik or equivalent sand bodies are potential reservoirs. It is both overlain and underlain by black shale with a high content of organic material. Because of its possible reservoir potential and close association with hydrocarbon source beds, it is considered a major objective for hydrocarbon exploration in the subsurface of the northern Arctic National Wildlife Refuge (ANWR) and adjacent areas.

This report focuses on the Kemik Sandstone (Lower Cretaceous) in the Canning River–Sagavanirktok River area, eastern North Slope, and Brooks Range foothills, Alaska (fig. 1). Analytical data reported here include analyses of petrographic point counts, paleontology, porosity, permeability, grain density, vitrinite reflectance, and thermal alteration index (TAI) on outcrop samples collected in this study. In addition petrographic analysis was carried out on subsurface core samples on file at the State of Alaska Geologic Materials Center (GMC) 1985, 1990. Subsurface correlations and facies are analyzed by using core samples and by interpreting well induction logs and American Stratigraphic Company (AMSTRAT) logs from the drill holes: Echooka, Susie 1, Fin Creek, Kemik 1, and Kavik 1. Alaska Division of Geological & Geophysical Surveys geologists mapped the geology between the Canning and Echooka Rivers at 1:63,360 scale. Two Kemik stratigraphic sections, Canning River (56 m) and Echooka River (59 m), provide detailed stratigraphic control.

The Kemik overlies the Lower Cretaceous unconformity (LCU) of mid-Neocomian age (fig. 2). The LCU truncates progressively older rocks to the north. To the southwest the LCU becomes a correlative conformity. Well data from the Bush well to the Aurora-1 well show that the Kemik Sandstone overlies a variety of rock units. Subsurface correlations and Kemik Sandstone petrography from the Bush well to the Aurora-1 well support these differences in sub-unconformity lithology.

Post-depositional structures in the Kemik include open-, tight-, overturned- folds, and thrust-fault imbrications. Imbricate thrust-fault repetitions of the Kemik are interpreted from logs of the Canning River Unit A-1 well and the Kemik-1 well (40 km west; Bird and others, 1987) and at Marsh Creek (Meigs, 1986).

LOCATION AND DISTRIBUTION

The Kemik crops out in the area from the eastern Sadlerochit and Shublik Mountains to the Canning River (Mull, 1987, Knock, 1987; Robinson and others, 1989) and in scattered rubble ridges and stream cuts from the Canning River 56 km southwest to the Echooka River. The Kemik is present in a number of wells on the east-central North Slope as far as 110 km west of the Canning River. The Kemik correlates with several discontinuous sandstone bodies, including the Put River Sandstone in the Prudhoe Bay oil field, the upper part of the Kuparuk River Formation in the Kuparuk oil field, the Cape Halkett sandstone in the National Petroleum Reserve Alaska, and a reported hydrocarbon-productive sandstone and conglomerate interval in the subsurface of the Point Thomson area west of the Arctic National Wildlife Refuge (ANWR) (Gautier, 1987). Aurora-1 well, east of Kaktovik, contains 70 m of coarsening- and thickening-upward sandstone and shale

[1]Alaska Division of Geological & Geophysical Surveys, 794 University Avenue, Suite 200, Fairbanks, Alaska, 99709-3645.

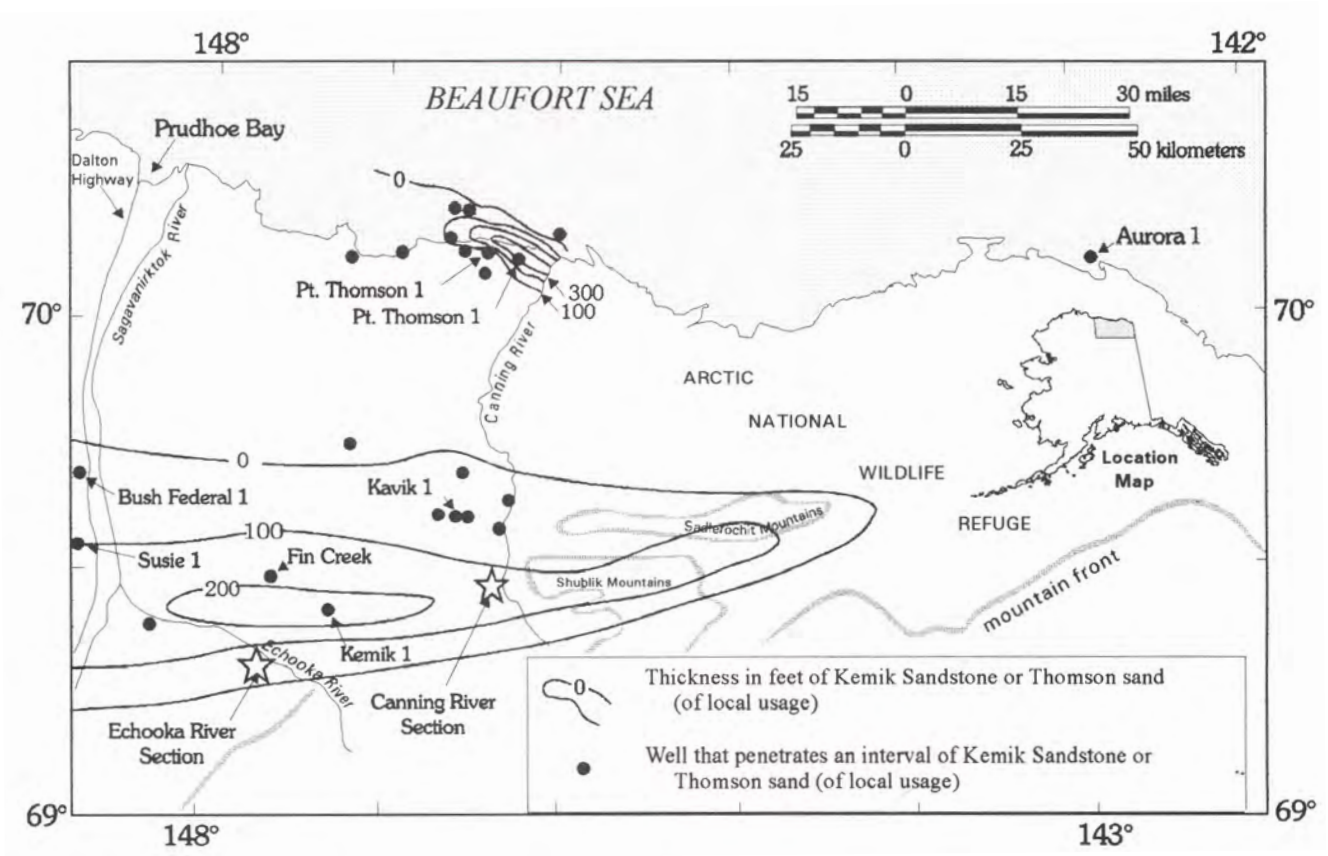

Figure 1. *Location map of eastern Arctic Slope and northeastern Brooks Range, Alaska, showing Kemik Sandstone isopachs and well locations. (Isopachs and map modified from Bird and others 1987.)*

that is post-LCU (Banet, 1992, calls this sandstone the Tapkaurak sand). Regionally, in northeast Alaska where sandstone is absent above the unconformity, the pebble shale unit lies directly on the unconformity.

PREVIOUS INVESTIGATIONS

Rocks now known as the Kemik Sandstone were originally mapped by Leffingwell (1919) as a part of a unit known as the Ignek Formation (abandoned name) in the Sadlerochit Mountains area and as the Kemik member of the Okpikruak Formation by Keller and others (1961). Detterman and others (1975) redefined the Kemik as a member of the Kongakut Formation. In order to clarify stratigraphic relationships and simplify the nomenclature of the North Slope and northeastern Brooks Range, Mull (1987) raised the Kemik Sandstone to formation status with two members. Knock (1987) carried out a detailed study of Kemik facies and depositional environments in Ignek Valley, between the Sadlerochit and Shublik Mountains, and on the north side of the Sadlerochit Mountains.

STRATIGRAPHY OF KEMIK AND ADJACENT FORMATIONS

In the northern part of the outcrop belt, the Kemik Sandstone conformably and unconformably overlies the Lower Cretaceous to Jurassic Kingak Shale and, locally, older rocks (fig. 2). However, southwest on the Echooka River the Kemik lies with apparent conformity above the Kingak Shale. The regional relationships suggest that the unconformity dies out to the south. The underlying Kingak Shale is over 300 m thick in many areas (Molenaar, 1983).

The Kemik is overlain by the pebble shale unit which consists of laminated, highly organic, black shale, which contains zones with scattered matrix-supported chert and quartzite pebbles and cobbles. The top of the pebble shale unit also contains thin bentonite beds and a zone of high radioactivity informally known as the gamma ray zone; these beds are as young as Albian. The pebble shale unit is widely recognized both in the subsurface and in surface exposures of the North Slope. It was originally described by Collins and Robinson (1967) in the subsurface of the Barrow area, 275 km northwest of ANWR. It is not well exposed on the surface, but in most places in the subsurface its thickness is remarkably uniform, ranging from 61 to

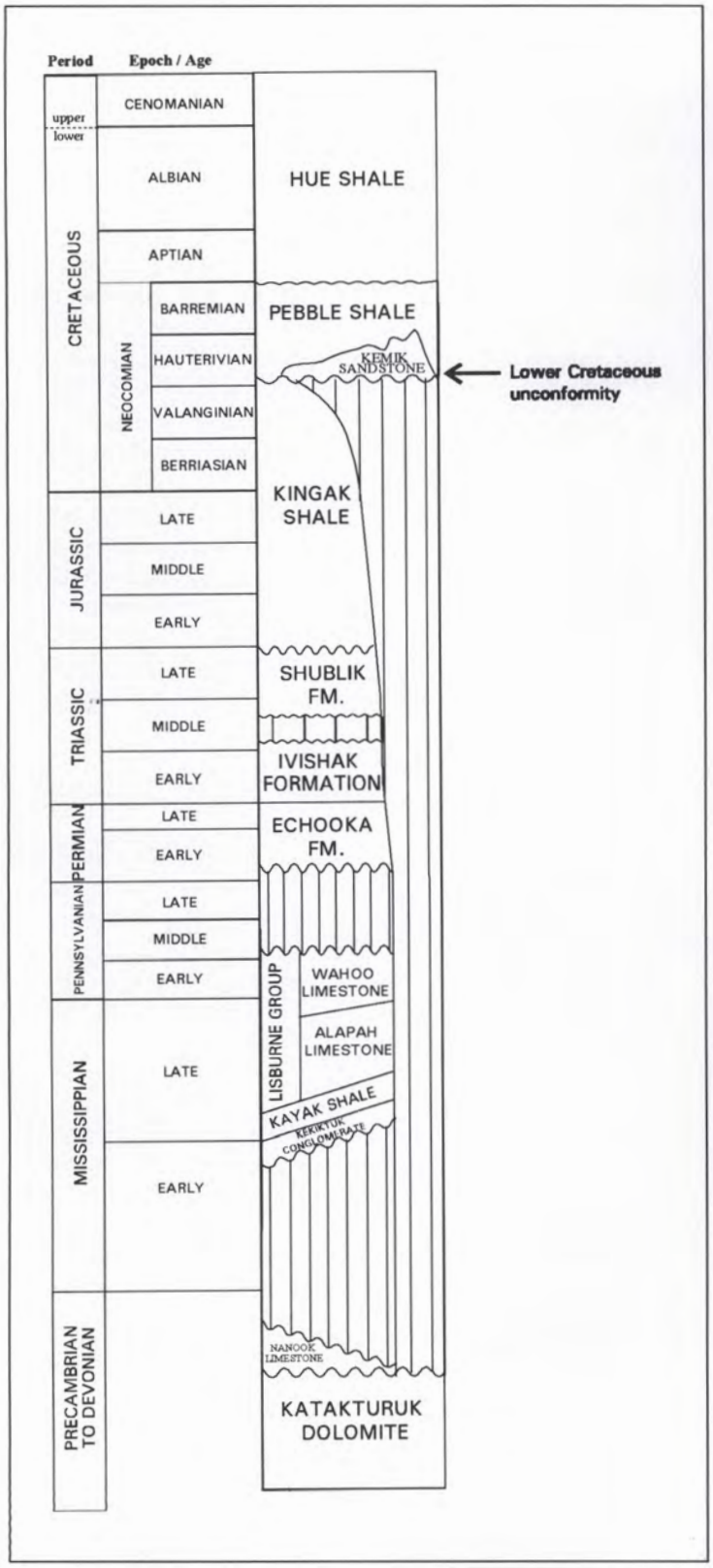

Figure 2. *Generalized stratigraphic sections, eastern North Slope and Brooks Range, Alaska.*

92 m (Molenaar, 1983; Mull, 1985). The contact of the Kemik Sandstone with the overlying pebble shale unit is sharp but conformable, although Detterman and others (1975) suggest an unconformity at which the Kemik is locally truncated.

The Kemik Sandstone and pebble shale unit were deposited at a significant time in the stratigraphic evolution of northern Alaska, during which a long-standing, relatively stable platform area to the north ceased to dominate deposition. This pattern was abruptly truncated and transgressed by marine deposits. This abrupt change in sedimentation has been interpreted as the result of rifting of the Arctic Alaska plate (Grantz and May, 1982).

The Kemik Sandstone is Hauterivian (Early Cretaceous) age based on the ammonite *Simbirskites* sp. collected from the Kemik on the Echooka River (J.H Callomon, written commun. to C.G. Mull, 1986). Molenaar (1983) also reported a probable *Simbirskites* sp. from the Echooka River locality, and Detterman and others (1975) reported *Simbirskites* sp. from their Kemik Sandstone Member type locality of the Kongakut Formation at Bathtub Ridge. Early Cretaceous ammonites, belemnites, and bivalves were recovered at the Echooka River Kemik measured section (W.P. Elder, written commun., 1993). A Hauterivian to Barremian microfauna has been recovered from shales interbedded with the Kemik and from the overlying pebble shale unit (M.B. Mickey, written commun., 1992, 1993; Mull, 1987; Vandergon, 1986, Knock, 1986). Pelecypods appear at many Kemik outcrop localities, and *Ditrupa* are locally present.

MEASURED-SECTION LITHOFACIES

Nine lithofacies of the Kemik Sandstone have been delineated in two measured sections and in study of other outcrops. Measured thickness of Kemik Sandstone is 56 m on the Canning River (Reifenstuhl and Myers, 1992) (fig. 3) and 59 m on the Echooka River (Reifenstuhl, 1994). All nine of the lithofacies of this report would be included in the "crossbedded sandstone facies" of Mull (1985).

In outcrop the Kemik Sandstone typically comprises more than 90 percent sandstone, 5 percent silty sandstone and siltstone, and less than 3 percent pebbly sandstone or conglomerate. The sandstone is commonly medium-gray to light-gray, moderately to well sorted, subangular

to subrounded, commonly glauconitic (average <1.2 percent), very fine to coarse grained quartzose sandstone. Sedimentary structures include: cross-, planar-, tabular-, and hummocky-cross-bedding, and ripple-lamination. Bioturbation is common; locally obliterating all sedimentary structures. Beds are laterally continuous across the outcrop and only rarely channelized (for example Erosive-base sandstone lithofacies). Individual lithofacies units typically thicken- and coarsen-up, and range from 6 m to 20 m thick (thickness listed below is for Canning River section). In the study area, generally, the Kemik is a coarsening-up and shoaling-upward succession (overlain by the transgressive pebble shale unit).

KEMIK SANDSTONE LITHOFACIES, CANNING RIVER TO ECHOOKA RIVER

Nine Kemik lithofacies are recognized in the study. The following list proceeds from base to top:

1. Basal conglomerate
2. Hummocky-cross stratified sandstone
3. Vertically burrowed, massive sandstone
4. Planar-laminated sandstone with pebble lags
5. Erosive-base sandstone
6. Paleosol
7. Bioturbated sandstone
8. Planar-bedded and ripple-laminated sandstone
9. Planar-bedded and tabular cross-bedded sandstone

1. BASAL CONGLOMERATE

A basal conglomerate is the lowermost lithofacies of the Kemik Sandstone in the area from the Canning River to Echooka River. It is not present in the Echooka River area where the Kemik conformably overlies Kingak Shale. The basal conglomerate ranges from a few centimeters to 50 cm thick and consists of well sorted to bimodal, matrix- to grain-supported, black chert- and quartz-pebble (0.5 –1 cm) conglomerate. The matrix is very fine- to fine-grained, locally glauconitic quartoze sandstone. The contact with the underlying Kingak Shale where well exposed is sharp and planar (fig. 3).

I interpret the basal conglomerate as a reworked transgressive lag deposit lying directly on the regional unconformity above the Kingak Shale. The lag deposit rests on a Type 1 (Posamentier and others, 1988) unconformity at the Shaviovik River locality, where root casts suggest subaerial exposure. Bioturbated and hummocky cross stratified sandstone gradationally overlies the basal conglomerate.

2. HUMMOCKY CROSS-STRATIFIED SANDSTONE

The hummocky cross-stratified (HCS) sandstone lithofacies is about 6 m thick and consists of very fine- to fine-grained sandstone with low angle and gently undulating cross-stratification. This facies locally includes rock that is bioturbated up to about 50 percent. The cross-bed sets are irregular and convex-up. The wavelength averages about 1 m with surface relief of up to 5 cm. The base of HCS beds may be erosive with up to 15 cm of relief, and silty-shale rip-up zones are common. Interbedded with the HCS sandstone are lesser ripple-laminated, cross-laminated, and bioturbated zones. The bioturbation is mostly horizontal, with lesser subvertical burrows. HCS sandstone beds average about 0.5 m thick and are commonly overlain by silty sandstone and cross-bedded sandstone.

I interpret the HCS sandstone as a shallow marine shelf that was reworked and deposited by storm waves. Water depth for HCS was in the 10–40 m range (Harms, 1975). The erosional base recorded maximum storm intensity, cross-stratification characterized the waning phase, and bioturbation occurred during the inter-storm periods of recolonization and reworking by organisms.

3. VERTICALLY BURROWED, MASSIVE SANDSTONE

The vertically burrowed, massive sandstone lithofacies occurs as resistant, apparently structureless, light-gray and orange-brown weathering, well sorted, very fine-grained sandstone, up to 6 m thick. Large vertical burrows are abundant and range up to 1 cm in diameter and up to 40 cm long. Burrows include *Skolithos* and *Arenicolites* and are characteristic of the *Skolithos* ichnofacies (Pemberton and others, 1992). Locally the upper part of the burrow is truncated by the overlying sand bed. This lithofacies is less argillaceous, lighter gray, and more massive-weathering than other lithofacies.

I interpret the massive, vertically burrowed sandstone lithofacies as deposition in a moderate-to high-average energy environment near or above fair-weather wave base. An upper shoreface depositional environment is suggested by sedimentary structures and *Skolithos* ichnofacies.

4. PLANAR-LAMINATED SANDSTONE WITH PEBBLE LAGS

The planar-laminated sandstone lithofacies comprises about 6 m of planar-laminated, very fine-grained sandstone with local pebble lags. It also contains lesser ripple-laminated, tabular-crossbedded sandstone, and minor sandstone with large-diameter vertical burrows. The lag deposits are typically 0.5 to 4 cm thick, and clasts include quartz, black chert, and conspicuous white-leached tripolitic chert.

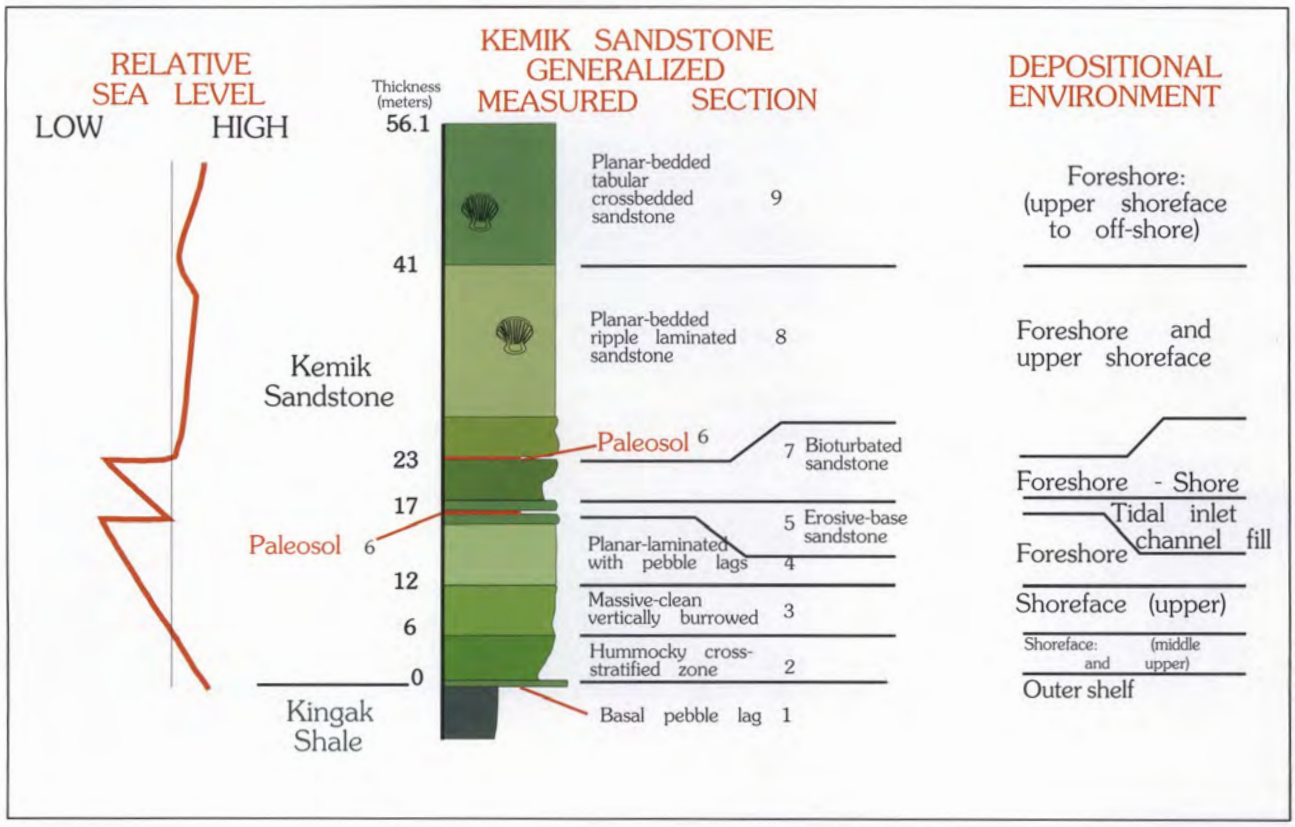

Figure 3. *Generalized stratigraphic section of Kemik Sandstone, Canning River, northeastern Alaska. From left to right: Relative sea-level curve based on depositional environments; generalized measured section with lithofacies (see text for lithofacies descriptions); depositional environments of lithofacies. Bivalve outlines in the section indicate fossil-collection locality.*

I interpret the planar-laminated sandstone lithofacies as deposition in a foreshore to upper shoreface environment. The parallel laminated and rippled sandstones are traction-load deposits produced by the waning current flow. Reworking of the bed tops produced ripple-laminated sands.

5. EROSIVE-BASE SANDSTONE

The erosive-base sandstone is up to 3 m thick but crops out only rarely. It comprises a variety of sandstone, siltstone, argillite, and clay-rich rocks, and a paleosol (described in the section below). The sandstone is medium gray, very fine to fine grained, locally organic rich and includes rippled, convolute-laminated, and lesser planar-laminated structures. Pebble lags with erosional bases and unidirectional sets of two-dimensional current ripples are also present. Convolute-laminated sandstone beds are up to 20 cm thick.

I interpret this lithofacies as a record of a drop in relative sea level or a shallow-water environment. The concave-up morphology of the erosive basal sandstone is interpreted as a tidal channel-fill succession, and the variety of sedimentary structures record migrating channel bars.

6. PALEOSOL

Paleosols are visible along the Canning and Shaviovik Rivers. The paleosols in the Canning River measured section were initially recognized by M.D. Myers in 1991, and are a significant paleoenvironmental lithofacies. One of the two paleosols in the Canning River measured section is at 27 m and consists of a 20-cm-thick section of argillaceous siltstone overlying a thin, highly organic-rich silty clay that grades downward into 2 cm of mottled brown-black, organic-rich silty clay, and this overlies 5 cm of brown uncemented clay. This upper paleosol appears at the base of the planar-bedded ripple laminated sandstone lithofacies. The lower paleosol appears at 17.5 m in the erosive-base sandstone lithofacies in the Canning River section. It consists of an uppermost 3 mm of highly organic-rich clay above 9 cm of mottled, mixed brown and black organic-rich clay and silt, above 3 cm of brown uncemented clay, which is underlain by 8 cm of argillite.

The paleosol in the Shaviovik River section is at the base of the Kemik Sandstone, and lies unconformably on Kingak shale. This well-exposed section includes common, well-defined root casts, organic material; bimodal, rounded quartz pebble lag deposits; red-brown weathering horizons; glauconite-bearing, fine and medium-grained sandstone; 0.5 m of black silty shale; and rare 4-cm-diameter pelecypods. The underlying 30 m of Kingak Shale is a coarsening- and thickening-upward succession.

I interpret the paleosol lithofacies as a record of a shoaling-upward sandstone and pebble-lag environment, with subaerial exposure, rooted plant colonization, subaerial weathering and erosion, yielding a Type 1 unconformity (Posamentier and others, 1988) at a sea level lowstand.

7. BIOTURBATED SANDSTONE

The bioturbated sandstone lithofacies is about 4 m thick and is characterized by abundant bioturbation and burrows that destroy most of the primary sedimentary structures. The facies is typified by dark-gray, reddish-brown and orange-brown-weathering, very fine- to fine-grained sandstone in beds ranging from 20 to 50 cm thick. Sedimentary structures include parallel lamination, minor trough cross-bedding, and rare current ripples. Sandstone of this facies is most commonly massive or appears structureless due to extensive bioturbation. Vertical burrows of the *Skolithos* ichnofacies are common, and include *Skolithos, Dioplocraterion, Arenicolites,* and *Ophiomorpha*.

I interpret this facies as deposition under moderate to high energy conditions near or above fair-weather wave base. An upper shoreface depositional environment is suggested by sedimentary structures and *Skolithos* ichnofacies.

8. PLANAR-BEDDED AND RIPPLE-LAMINATED SANDSTONE

The planar-bedded, ripple-laminated sandstone lithofacies is about 18 m thick and comprises medium-gray, well-sorted, fine-grained and very fine grained, planar-bedded and ripple-laminated sandstone with rare thin pebble layers. Typically the basal planar bed grades up into ripple-laminated sandstone. The current ripples are unidirectional, in 1–2-cm-thick bed sets. Bedding averages about 0.6 m thick. The uppermost part of the sandstone beds are ripple laminated but internal ripple laminations, if present, are obscured. The basal planar sedimentary structures sharply overlie rippled-top sandstone beds. In the Canning River section an 8-cm-thick very dark gray, clay-rich paleosol zone crops out at the base of this lithofacies.

I interpret the planar-bedded and ripple-laminated sandstone lithofacies as a record of deposition above a fair-weather wave base in a foreshore to upper shore face environment of fluctuating energy and sediment conditions. Storm currents produced rapid deposition as the energy level decreased. The parallel bedding and ripple laminations were deposited as traction load. Subsequent currents may have reworked the bed tops. The paleosol at the base of this lithofacies records subaerial exposure.

9. PLANAR-BEDDED AND TABULAR CROSS-BEDDED SANDSTONE

The planar and tabular cross-bedded lithofacies is about 15 m thick and comprises medium-gray, thick-bedded (0.5–1.0 m) very well sorted, very fine to fine-grained sandstone. Individual bed sets typically have sharply defined bases that truncate the underlying beds. Locally, bed bases are marked by pebble layers that range from lags only one pebble thick to pebble-conglomerate beds as thick as 2 cm. These conglomerate zones typically fine upward into sandstone characterized either by planar laminations or small- to large-scale low-angle cross-lamination. Isolated matrix-supported pebbles are present in many beds. Convolute bedding is rare. These rocks weather to a conchoidally fractured rubble.

I interpret the planar-bedded, tabular cross-bedded sandstone lithofacies as recording deposition above fair-weather wave base in a foreshore to upper shore face environment by traction currents. Migrating sand waves formed tabular sets of cross beds. Offshore bar environments also produce planar and tabular cross-bedded sandstone and are an alternative interpretation.

SUMMARY OF SEDIMENTARY STRUCTURES AND DEPOSITIONAL ENVIRONMENTS

A sharply defined erosional base, typically with a basal conglomerate, overlies a regional Lower Cretaceous unconformity (Canning River and Shaviovik River areas) (fig. 3) that becomes conformable southward in the Echooka Point area. Lithofacies generally coarsen upward. The pebble shale unit overlies the Kemik with a sharp contact that records a rapid marine transgression for which the pebble shale unit may be an effective time line. Individual beds in the Kemik have sharply defined bases that truncate the underlying beds; thin conglomerate layers form the base of many beds, and matrix-supported pebbles are common. The base of the Kemik typically includes the *Cruziana* and *Skolithos* ichnofacies; the top

of the unit contains only the *Skolithos* ichnofacies. Internal bedding structures low in the section commonly have been obliterated by bioturbation, but higher in the section, planar lamination and low-angle cross-lamination are more commonly preserved. Bioturbation is locally pervasive and includes the trace fossils *Skolithos, Dioplocraterion, Arenicolites,* and *Ophiomorpha,* of the *Skolithos* ichnofacies, typically a high-energy, sandy shoreface and foreshore environment. *Thalassinoides, Condrites,* and *Rosellia,* of the *Cruziana* ichnofacies commonly occur in poorly-sorted, unconsolidated substrates of moderate energy. This ichnofacies is typically subtidal, below fair-weather wave base, but above storm wave-base.

I interpret the Kemik Sandstone in the Canning River to Echooka River area to represent deposition in foreshore, upper shoreface, and tidal inlet environments of a barrier island complex (fig. 4). Shaly and mud-rich rocks of the lagoon and marsh crop out to the east and northeast in the Sadlerochit and Shublik Mountains of ANWR and are mapped as the burrowed pebbly siltstone lithofacies by Mull (1987) and Knock (1987). In the Canning River to Echooka River area all nine of the lithofacies of this study would be part of the laminated, cross-bedded sandstone facies or Ignek Valley Member of Mull (1987).

The cross-bedded sandstone lithofacies of this study consists of a generally shallowing- and coarsening-upward succession that records a transition from inner shelf to shoreface and beach environments (figs. 3B and 4). The more intensely burrowed sandstone of the cross-bedded sandstone lithofacies represents repetitive cycles of storm-dominated deposition below the fair weather wave base. Laminated and cross-bedded intervals represent deposition in shallower shoreface to beach environments of the barrier island complex.

PETROGRAPHY

Petrographic study of more than 100 thin sections of the Kemik Sandstone and correlative rocks (Reifenstuhl, 1993) indicates that the cross-bedded sandstone lithofacies Kemik of Mull (1987) is predominantly medium-gray, very fine to fine-grained, with lesser medium- and minor coarse-grained, moderately to well sorted, subangular to subrounded quartzose sandstone (sublitharenite to litharenite of Folk, 1968). It is composed of 75–80 percent quartz, 15–20 percent rock fragments, and less than 5 percent feldspar (fig. 5). The quartz is dominantly monocrystalline, with minor amounts of stretched metaquartz and vein quartz (table 1). Chert is the dominant rock fragment and is black and leached-white tripolitic-weathered, with lesser shale, siltstone, limestone, dolomite, and siliceous sandstone. Glauconite, muscovite, sericite, collophane, zircon, and tourmaline are minor constituents. Silica cementation is extensive as quartz overgrowths. Pebbly sandstone and conglomerate are locally important, and clasts consist dominantly of quartz and gray to black chert. The Point Thomson sand is dominantly dolomite-clast conglomerate and is from the Point Thomson wells northwest of the Canning River delta.

Detrital modal analyses were made on 17 thin sections of the Kemik Sandstone from drill holes, and 19 from thin sections from surface exposures. Table 1 summarizes these data.

Additional thin sections were examined for texture, mineralogy, alteration, and diagenetic history. Three hundred points were counted on 24 stained thin sections in the predominantly very fine grained sandstone, from outcrop and well samples and 100 points were counted on 12 stained thin sections. Thin sections were stained for calcite (alizarin red) and ankerite (potassium ferricyanide), and some were impregnated with blue epoxy resin for porosity.

PROVENANCE

Framework grains of the Kemik in the Canning and Echooka River area exposures and subsurface samples suggest a mature sedimentary provenance with a minor metamorphic source contribution. Protolith interpretations are based on sandstone and conglomerate petrography and regional stratigraphic constraints, and include sandstone (Sadlerochit Group(?); Permian to Triassic), Conglomerate (Kekiktuk? Lower Mississippian), and other lower Paleozoic rocks that contributed quartz, lithics (including micaceous quartzite), and minor feldspar. Some chert clasts in the Kemik are similar to chert of the Lisburne Limestone Group (Mississippian to Pennsylvanian). This is based only on chert color and texture. One granitic clast was observed in outcrop sample 91RR76A and one locality included biotite. Basal Point Thomson well samples are predominantly conglomerate comprising dolomite clasts, apparently from the underlying Katakturuk(?) Dolomite (Precambrian). Local sources for the Kemik are indicated by significant differences in framework-grain abundance (figs. 5 and 6), as seen in the increase of chert and carbonate from southwest to northeast, in the progression from Bush to Echooka to Point Thomson wells. Also, the absence of Kemik Sandstone in some of the wells drilled between Point Thomson and Kavik supports a local source for the Kemik.

Compositional differences are shown on the triangular plot of quartz (+ chert)-lithics-feldspar (fig. 5), and a graph of chert/chert + lithics versus total quartz (fig. 6). Modal clast analyses indicate a progressive quartz decrease and lithic (predominantly chert and carbonate) increase from Bush Federal 1 southeast to Echooka 1 to Point Thomson on the northeast (fig. 6).

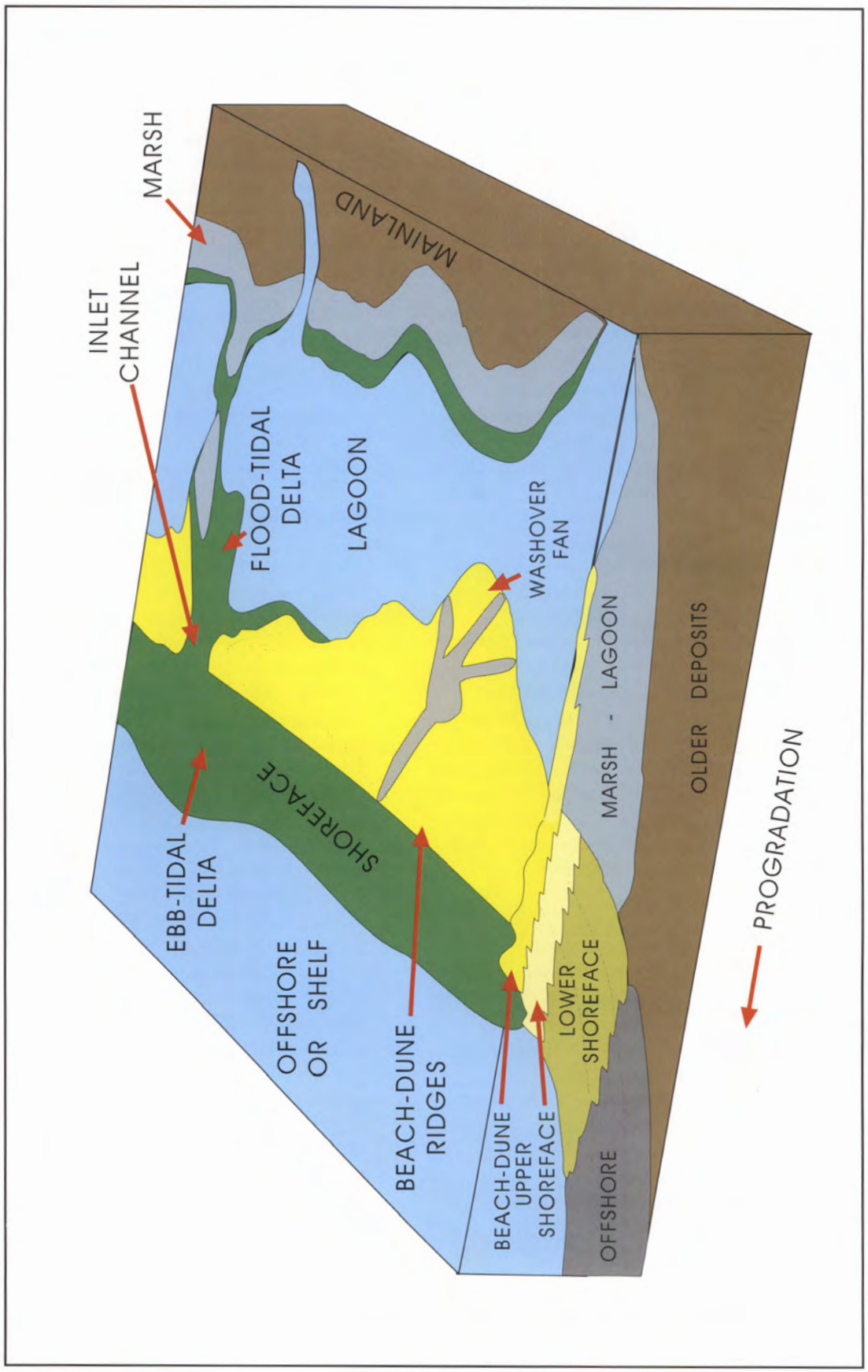

Figure 4. *Generalized environments of depositional and facies of a barrier-island lagoon system.*

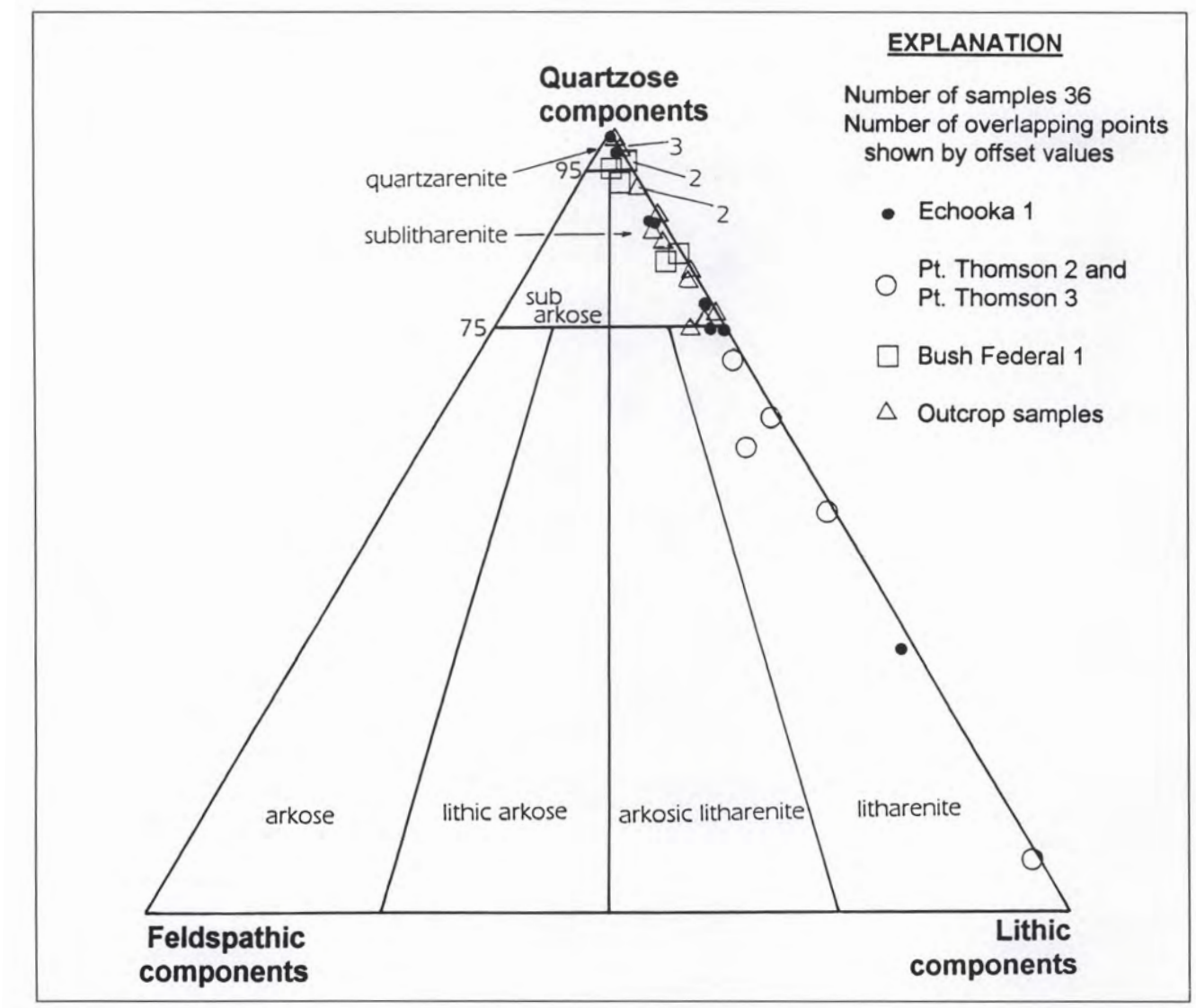

Figure 5. *Quartz-feldspar-lithic triangular plot of petrography of samples of Kemik and equivalent sandstones from outcrops and wells. Quartzose components include chert. Point counts per thin section is 100 or 300 (see table 1 for petrographic details). Classification is from Folk (1968). Petrography shows a general increase in lithic components from south to north. The outcrop belt and Bush Federal-1 well samples are predominantly quartzarenite and sublitharenite. The Echooka-1 well sandstones are sublitharenite and litharenites. The Point Thomson well samples are very lithic rich, indicating their local source.*

PHYSICAL PROPERTIES

More than 60 samples, predominantly outcrop samples, were analyzed for porosity, permeability, grain density vitrinite reflectance (Ro), or thermal alteration index (TAI) (Reifenstuhl, 1993). Additional subsurface physical data were compiled from data reports from the Alaska Geologic Materials Center and from published well reports (table 2).

RESERVOIR PROPERTIES

Reservoir properties analyzed in this study of the Kemik Sandstone include porosity, permeability, and grain density. Porosity is the measure of the percentage of total rock volume that is pore space; and does not indicate whether the pores are connected. Permeability, measured in millidarcys (mD), is the measure of how easily fluids pass through a rock. Grain density is used in conjunction with dry, bulk-rock density to also express porosity (North,

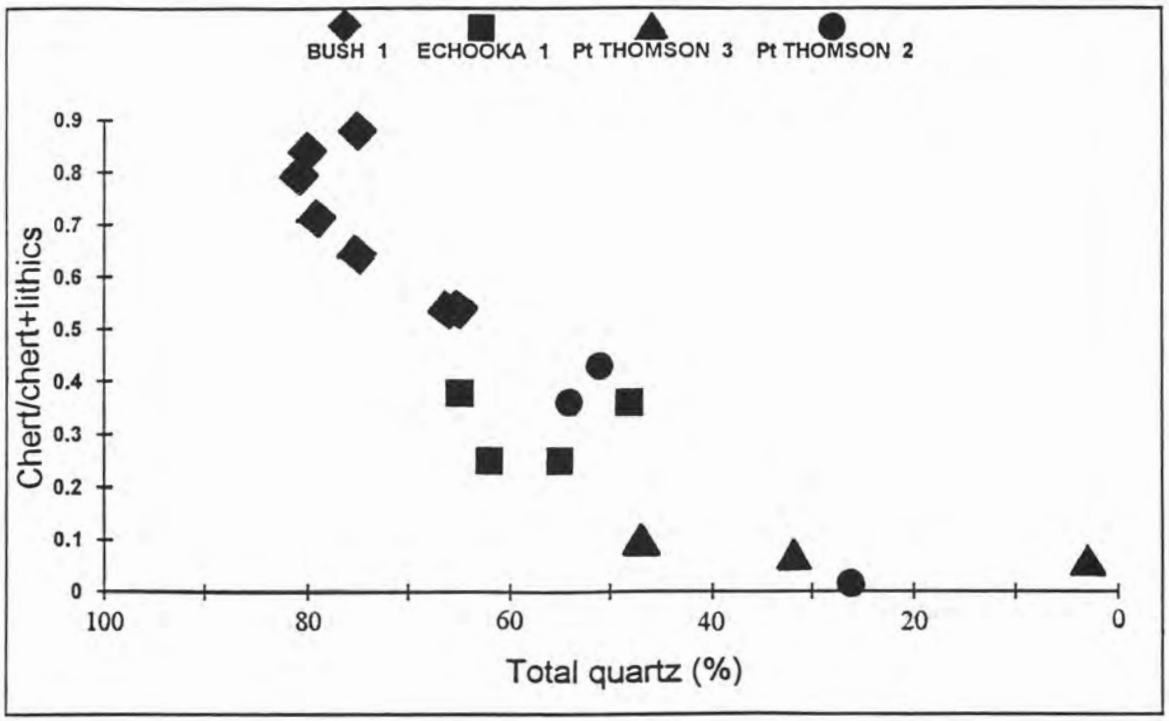

Figure 6. *Graph of chert/chert + lithics versus total quartz from point-count data from well samples. Data show significant decrease in quartz from west to east. Lithic grains also increase from west to east. See table 1 for point-count data, and figure 1 for well locations.*

1985), which can indicate effects of cementation agents, reflects clast variations, and is used to calibrate density logs.

POROSITY

Porosity values for all Kemik samples range from 0.8 to 14.1 percent and average 5.3 percent. The maximum porosity of 14.1 percent is an outcrop sample of pebbly sandstone just above the LCU. Subsurface samples range from 3.9 percent in the Echooka well to 8.4 percent in the Point Thomson-2 well, and average 6.2 percent. Comparing the average porosity of the 43 surface samples (5.3 percent) to the average porosity of the 5 subsurface samples (6.2 percent) shows a 17 percent higher subsurface porosity.

PERMEABILITY

Permeability was reported on 17 Kemik rock samples (Reifenstuhl, 1993) as routine air permeability in millidarcys (mD) and insitu Klinkenberg Permeability (mD). Insitu Klinkenberg permeability values range from 0.00012 to 0.0157 mD. One anomalously fractured sample yielded 0.271 mD and is not considered representative. Four subsurface permeability samples from the Echooka well range from 0.00253 to 0.00020 mD.

GRAIN DENSITY

Grain-density values range from 2.57 to 3.05 g/cm^3 and cluster in two populations, the principal cluster (74 percent of the total population) at 2.64 g/cm^3 and a smaller cluster (26 percent) at 2.90 g/cm^3 (Reifenstuhl, 1993). There is no apparent correlation between grain density and porosity. Six samples yield grain-density values 10 percent greater than the average for the cluster of 17 samples. All six of these high-density samples are outcrop samples of medium-grained sandstone to pebble conglomerate from within 1 m of the basal Kemik (LCU). These coarse-grained clastic rocks represent lag-type deposits that presumably have been substantially reworked and sorted during sea-level lowstands.

DISCUSSION OF RESERVOIR PROPERTIES

On the basis of these reported data (porosity, permeability and grain density) the Kemik Sandstone surface samples suggest the following: The porosity values average 5.3 percent for surface samples and 6.2 percent for the subsurface and are in the "poor" range of reservoir quality of North (1985), with only one fractured surface sample within North's "fair" qualitative evaluation. Permeability values range from 0.00012 to 0.0157 mD. These are in the "poor to fair" range (North, 1985) for reservoir quality. Grain-density values show no correlation with increased or

Table 1. *Kemik Sandstone and correlative sandstone: point count data*

Sample number	Total grain count	Qm	Qpe	Qpf	Kspar	Plagioclase	Chert	Phyllite	Cherty argillite	Sandstone	Shale	Carbonate	Glauconite	White mica	Heavy minerals: ZrTrRtGt	Detrital, other	Mtx arg	Mtx undiff	Porosity	Silica porefill	Carbonate porefill	Clay porefill	Other porefill
BUSH 11150	100	47	18	--	2	--	19	1	6	--	--	4	--	2	--	--	--	--	7	--	13	1	--
BUSH 11160	100	50	25	--	--	--	16	--	1	--	--	3	4	1	--	--	--	--	1	--	8	--	--
BUSH 11170	100	72	8	--	--	--	17	--	--	--	--	--	--	2	1	--	--	--	7	1	--	2	--
BUSH 11180	100	47	18	--	2	2	19	--	--	--	--	8	1	3	--	--	--	1	8	--	10	1	3
BUSH 11190	100	57	18	--	--	--	22	--	--	1	--	1	--	1	--	--	--	--	8	--	--	--	--
BUSH 11200	100	61	18	--	--	2	15	--	--	--	--	--	1	3	--	--	--	--	4	1	--	--	--
BUSH 11220	100	58	23	--	--	2	15	--	--	--	--	--	--	2	--	1	1	2	8	2	--	--	1
PtTh3-13904	100	3	--	--	--	--	5	--	--	--	--	92	--	--	--	--	--	--	--	--	4	--	--
PtTh3-13833	100	35	11	1	--	--	5	--	--	--	--	47	--	1	--	--	3	5	5	--	4	--	--
PtTh3-13742	100	3	28	1	--	--	4	5	--	30	5	24	--	--	--	--	--	--	5	1	1	--	--
PtTh2-13060	100	38	15	2	--	1	16	18	2	--	10	2	--	6	--	--	13	4	--	--	--	--	--
PtTh2-13101	100	37	13	1	--	5	19	5	3	--	1	9	2	5	--	1	3	2	--	1	3	2	4
PtTh2-13124	300	45	21	1	--	5	2	114	--	15	1	50	--	--	3	1	10	--	--	--	31	--	--
Echka 12797	300	121	5	1	--	4	27	45	--	11	--	6	2	--	4	7	3	--	--	34	1	21	--
Echka 12833	300	156	8	1	--	3	33	22	--	11	1	2	--	11	4	2	--	--	1	26	2	23	--
Echka 12874	300	115	4	--	--	2	18	19	--	5	--	5	2	3	7	13	93	--	--	4	--	--	5
Echka 12860	300	104	9	--	--	1	44	43	--	13	7	--	1	1	2	10	15	--	--	28	1	12	7
91RR68A	300	160	6	1	--	--	26	1	--	1	--	--	2	--	6	5	--	--	1	44	31	1	15
91RR68B	300	151	14	2	--	--	57	1	--	6	1	--	--	--	1	3	--	--	7	36	--	2	16
91RR68C	300	95	5	--	--	--	20	2	--	3	1	--	--	--	4	4	--	--	2	37	20	2	20
91RR68D	300	126	--	1	--	1	28	--	--	--	--	--	4	--	--	7	--	--	--	43	39	2	40
91RR71A	300	137	3	1	--	--	53	19	--	6	--	--	1	--	--	8	--	--	3	58	1	2	7
91RR73A	300	115	6	--	--	--	36	2	--	1	1	--	--	--	--	2	--	--	2	9	117	--	1
91RR73B	300	157	4	--	--	3	13	2	--	--	5	--	--	2	2	13	--	--	--	56	6	8	28
91RR76A	300	65	5	--	--	--	3	--	--	1	12	3	--	--	--	5	--	--	1	1	170	1	1
91RR76B	300	165	8	--	--	--	23	2	--	--	--	--	1	--	--	--	--	--	30	69	--	1	--
91RR76C	300	62	17	--	--	2	10	1		--	16	--	--	--	--	14	--	--	1	5	145	3	1
91RR78A	300	127	7	--	--	1	47	8	--	4	--	--	5	--	--	7	--	--	9	59	--	6	20
91RR80A	300	125	11	--	--	--	42	21	--	6	2	--	2	--	--	5	--	--	7	66	--	10	3
91RR81B	300	46	3	--	--	--	14	1	--	--	--	--	--	--	--	1	--	--	--	21	12	1	12
91RR81C	300	91	5	--	--	--	22	1	--	6	--	--	3	--	--	4	--	--	4	3	141	5	14
91RR84-00	300	118	12	--	--	--	30	3	--	--	10	--	5	5	2	7	--	--	--	--	3	88	6
91RR84-19	300	116	7	--	--	2	42	31	--	9	2	3	3	--	2	8	--	--	--	31	2	23	17
91RR86A	300	105	9	--	--	3	36	28	--	7	4	10	3	--	5	9	--	--	--	10	4	57	6
91RR92	300	110	6	--	--	--	30	4	--	1	--	--	1	--	1	11	--	--	--	--	134	--	1
91RR90C	300	144	4	--	--	2	12	--	--	--	8	--	--	1	5	15	--	--	1	53	12	18	24

Qm = monocrystalline quartz; Qpe = polycrystalline quartz - equigranular; Qpf = polycrystalline quartz - foliated; Kspar = alkali feldspar; Sandstone includes micaceous quartzite; Heavy minerals: ZrTrRtGt = zircon, tourmaline, rutile, garnet; Detrital, other includes rare biotite (6 counts in 91RR71A) and granitic clast (1 grain in 91RR76c); Mtx arg = argillaceous/pseudomatrix; Mtx undiff = matrix undifferentiated; Silica porefill includes quartz overgrowths; Carbonate porefill includes siderite; Clay porefill includes glauconitic clay; Other porefill includes deadoil.
BUSH = Bush Federal 1, and five digit number is well depth in feet; PtTh3 = Pt Thomson 3; Echka = Echooka 1; 91RR- — = outcrop samples.
- - = Not found.

Table 2. *Kemik Sandstone and correlative sandstone: subsurface data*

Well and operator	Kemik or correlative interval (ft)	TOC%[a]	Temperature maximum °C	Porosity % and permeability (mD)	Vitrinite reflectance (Ro)	Density (g/cm^3)	Thin sections [sample interval (number of samples)] Core in ft	Thin sections [sample interval (number of samples)] Ditch in ft	Clasts: Q:F:L[b]	Comments
Kemik #1[c] BP	3,583–3,780 4,445–4,650 (repeat)	1.51 0.5 - 2.0[d] 1.04	454 470	- -	- -	- -	(0)	4,400–16,050 (89)	- -	Moderate intergranular pores and overgrowths; minor chlorite; microporous chert and phosphate. Pyrolysis: mature; G.P = 1,000-3,000; P.I. = 0.1-0.3; H.I. = 50-400; O.I. = <400[d].
Kavik #1[c] ARCO	3,463–3,490	1.0 - 4.0	465	- -	- -	- -	(0)	(0)	- -	Maturity = mature; G.P. = <4,000; P.I. = 0.2-0.9.
Fin Creek[c,d] McCullock	10,375–10,535	2.17 1 - 2[d] 1.37	463	- -	- -	- -	(0)	4,150–15,020 (22)	- -	S1 = 0.26; S2 = 0.28; S3 = 0.81; Marginal maturity. Coaly kerogen. G.P. = 1,000-10,000; P.I. = 0.1-0.3; H.I. = <100; O.I. = 100-200.
Suzie #1 Atlantic Richfield	12,990–13,080	- -	- -	- -	- -	- -	(0)	13,020–13,060 (1)	- -	- -
Echooka [c,e,f] Mobil Oil	12,736–12,925	2.04 1.79	434	6.3 / 0.00123[g] 7.4 / 0.00084 4.8 / 0.00020 3.9 / 0.00253	- -	2.64[g] 2.65 2.70 2.66	12,787–12,875 (10)	(0)	- -	Moderate quartz, chlorite, illite; minor plagioclase, dolomite, pyrite. S1 = 0.38; S2 = 0.64; S3 = 0.69; (at 12,787 ft-12,875 ft). Coaly kerogen.
Nora Federal #1 Atlantic Richfield	12,460–12,560	2.23	468		1.6 (estimated) GMC report 25	- -	(0)	12,460–12,550 (7)	- -	oil = 27% Saturates; S1 = 0.35 26% Aromatics; S2 = 0.25 47% Polars; S3 = 0.74
Bush Federal[e] Home Oil	11,147–11,210	3.13 at 11,150 ft	455		1.25 (estimated) GMC report 168 1.20 GMC report 25	- -	(0)	11,150–11,350 (10)	- -	S1 = 0.75; S2 = 0.99; S3 = 1.33. Woody kerogen. Seven thin sections point counted for this study.
Pt. Thompson #2[e,f] Exxon	13,013–13,116 Thompson sand	0.07 - 7.0 0.6 - 2.3	- -	8.4 / - - at 13,124 ft[g]	0.6 at 11,500 ft 0.5 at 8,000 ft 0.4 at 3,500 ft	2.92[g]	10,750–13,157 (50) 12,837–12,995 (10)	13,060–13,140 (2)	55:1:44 at 13,060 ft 55:1:44 51:5:44	Intergranular porosity destroyed. Mica and schist grain deformation. 248 barrels/day, 21° API at 11,750 ft.
Pt. Thompson #3[e] Exxon	13,056 –13,931 Thompson sand	0.5 - 5.0 1.0 - 7.0	- -	5-25% typically at high end	- -	- -	13,159–14,008 (49) 13,673–13,788 (8)	(0)	32:0:68 at 13,742 ft 47:0:53 at 13,833 ft 3:0:97 at 13,904 ft 47:0:53 at 13,833 ft 32:0:68 at 13,742 ft	Three thin sections point counted for this study. Pyrolosis: immature; G.P. approx. 1,000. P.I. = 0.1-0.4; H.I. = 30-300.
Aurora #1 OCS-Y-0943[d]	16,443–16,620 Tapkaurak sand	1.0 -2.0; 5.0 at 15,750 ft	472 at 16,400 ft	- -	1.4 at 16,500 ft 1.6 at 16,700 ft 1.8 at 16,800 ft	2.38	(0)	14,680–16,630 (14)	85:5:10	Minor gas show at 18,200 ft. Amorphous kerogen[h]. Minor glauconite[i], TAI = 3.2, 3.8, 3.4, 3.6. Kemik-Kalubik-Kuparuk equivalent. Pyrolisis: G.P. = 900; P.I. = 0.1-0.3; H.I. = 50; O.I. = <50.

[a]TOC = Total organic carbon.
[b]Q = quartz: monocrstalline and polycrystalline; F = feldspar; L = lithic clasts + chert.
[c]AMSTRAT log available at DGGS.
[d]Banet, 1993.
[e]Thin sections.
[f]Petrophysical analyses of Kemik Sandstone core from this study.
[g]Analyses: Geocore, A. Byrnes, 1993.
[h]Banet, 1992.
[i]Mowatt and others, 1992.

decreased porosity. It is not known what cementing agent is responsible for the higher grain densities that range from 2.64 to 2.90 g/cm^3.

ORGANIC GEOCHEMISTRY

Organic, geochemical analyses consisted of thermal alteration index (TAI) and vitrinite reflectance (Ro) on 15 samples.

THERMAL ALTERATION INDEX (TAI)

TAI analysis value on one Kemik outcrop sample is 2.7. Kemik correlative sands from the Aurora-1 well, east of the Canning River, yield values of 3.2, 3.8, 3.4, and 3.6 (Banet, 1992; table 2). TAI values for 11 Kingak Shale surface samples (Reifenstuhl, 1991a; 1991b) range from 2.5 to 3.8 (average 3.4). One pebble-shale outcrop TAI value is 3.0.

VITRINITE REFLECTANCE (Ro)

Ro values are from subsurface Kemik and correlative samples and range from the low of 0.6 percent in Point Thomson-2 well (State of Alaska Geologic Materials Center [GMC], 1984), to 1.25 and 1.20 percent in the Bush well (State of Alaska GMC, 1990), to 1.6 percent in Nora (State of Alaska GMC, 1984), and 1.4, 1.6 and 1.8 percent in Aurora-1 to the east of the Canning River (Banet, 1990).

TOTAL ORGANIC CARBON (TOC)

TOC values are subsurface data from the State of Alaska GMC (1984). Some of the analyses are from the Kemik Sandstone and some are from adjacent formations (table 2). The TOC ranges from 0.5 percent in the Kemik-1 well to 7.0 percent in the Point Thomson-2 and -3 wells. An approximate average for the wells of table 2 is 2.2 percent.

DISCUSSION OF ORGANIC GEOCHEMISTRY

The TAI and Ro values for Kemik and correlative rocks indicate a wide range in the petroleum-generation zones. This is in part a result of depth of burial and accompanying thermal influences. In the Point Thomson 2 well, Ro values are at the top of the peak oil generation window (North, 1985 p. 66). The Bush well Ro data lie below the oil generation window. The Nora well Ro data lie within the gas generation window. To the east of the Canning River, the Aurora well TAI data (Banet, 1992; table 2) are in the lower part of the gas window, with one TAI value in the post-mature region. The TOC well data (table 2) indicate a locally fair to excellent (North, 1985) source-rock quality, whereas the typical TOC analysis of 2.3 percent is in the "very good" range of North (1985). Locally and regionally the overlying organic-rich pebble shale unit and underlying Kingak Shale both have hydrocarbon source-rock potential (Banet, 1990).

RESERVOIR POTENTIAL

Kemik framework grains consist dominantly of stable grains of quartz and chert with little matrix. However, silica cementation is common in outcrop samples. Although the permeability analyses of the outcrop samples suggest only poor to fair (North, 1985) reservoir potential, surface Kemik values are consistently less than subsurface Kemik values due to surface weathering effects. Porosity values are mostly in the poor (North, 1985) range for the Kemik. However, in the Point Thomson wells the porosity is in the good and very good range. Organic geochemistry data indicate that Kemik Sandstone and correlative sandstone are within the oil-generation window in some wells (Point Thompson, Echooka) and in the gas-generation window (Bush, Aurora).

Jamison and others (1980) report that the Put River Sandstone in the Prudhoe Bay field, which is approximately correlative with the Kemik, has porosity values averaging 12 percent and measured permeability of 10–404 mD. In addition, the Kuparuk River Formation, the upper part of which is probably correlative with the Kemik, is oil productive in the Kuparuk River oil field (Masterson and Paris, 1987).

SUMMARY AND CONCLUSIONS

The Kemik Sandstone is up to 59 m thick and consists of very fine to fine-grained quartzose sandstone interpreted to have been deposited in a shallow shelf setting as a barrier-island complex and a back-barrier lagoon. The barrier-island complex can be traced along a linear northeast trend for over 130 km from the Sadlerochit Mountains on the east to the Echooka River on the west (Mull, 1987). Paleosols, developed locally within the Kemik, suggest a sea-level lowstand and Type 1 unconformity (Posamentier and others, 1988). The Kemik is early Hauterivian in age and overlies a regional mid-Neocomian unconformity that, in outcrop, truncates rocks as old as Early Triassic. This unconformity is present in the subsurface throughout northern Alaska, and in the Point Thomson area it truncates rocks as old as Precambrian (Katakturuk Dolomite(?)). Regional relationships suggest that the unconformity and truncation in northern Alaska developed during the early stages of rifting and continental breakup of the Arctic Alaska plate (Grantz and May, 1982; May and Grantz, 1983; Mull, 1982; Mull, 1987). The Kemik and other coeval but separate sandstone intervals were derived from and deposited on the margins of uplifted blocks along the extensional margin.

Deposition of the barrier island complex was followed by rapid submergence of the coastline and deposition of the overlying transgressive pebble shale unit of Hauterivian–Barremian age.

The Kemik may have reservoir potential in the subsurface and is a potential objective for hydrocarbon exploration in northeastern Alaska.

ACKNOWLEDGMENTS

Geologists who collaborated on this field project include C.G. Mull, Alaska Division of Geological & Geophysical Surveys (DGGS); M.D. Myers and T.J. Ryherd of the Alaska Division of Oil and Gas; G.H. Pessel, University of Alaska Fairbanks; M.S. Robinson, DGGS, and John Decker, ARCO Alaska. Identification of megafossils by W.P. Elder, USGS; of microfauna and microflora by Michael B. Mickey and Hideyo Haga, Micropaleo Consultants, Inc. Petrophysics by Alan P. Byrnes of Geocore. I thank C.G. Mull and John Decker for critical reviews of an earlier version of this paper.

REFERENCES CITED

Banet, A.C., Jr., 1990, Petroleum Geology and Geochemistry of the Arctic National Wildlife Refuge 1002 Area: U.S. Bureau of Land Management Alaska Technical Report 12, 26 p., 6 sheets, various scales.

_____1992, Log Analysis of Aurora 890-#1, OCS-Y-0943 Well, Offshore of the Arctic National Wildlife Refuge 1002 Area, Northeast Alaska: U.S. Bureau of Land Management Alaska Technical Report 15, 37 p., 2 sheets, scale 1:12,000.

Bird, K.J., Griscom, S.B., Bartsch-Winkler, Susan, and Giovannetti, D.M., 1987, Petroleum reservoir rocks, *in* Bird, K.J. and Magoon, L.B., eds., Petroleum geology of the northern part of the Arctic National Wildlife Refuge, northeastern Alaska: U.S. Geological Survey Bulletin 1778, 329 p., 4 sheets.

Collins, F.R., and Robinson, F.M., 1967, Subsurface stratigraphic, structural and economic geology, northern Alaska (NPR-4 and adjacent areas): U.S. Geological Survey [Inv. Naval Petroleum Reserve No. 4 and adjacent areas] Open-File report, 252 p.

Detterman, R.L., Reiser, H.N., Brosgé, W.P., and Dutro, J.T., Jr., 1975, Post-carboniferous stratigraphy, northeastern Alaska: U.S. Geological Survey Professional Paper 886, 46 p.

Dixon, James, 1982, Jurassic and Lower Cretaceous subsurface stratigraphy of the Mackenzie Delta–Tuktoyaktuk Peninsula, N.W.T.: Geological Survey of Canada Bulletin 349, 52 p.

Folk, R.L., 1968, Petrology of Sedimentary Rocks: Austin Hemphill Publishing Company, Texas, 182 p.

Gautier, D.L., 1987, Petrology of Cretaceous and Tertiary reservoir sandstones in the Point Thomson area, *in* Bird, K.J. and Magoon, L.B., eds., Petroleum geology of the northern part of the Arctic National Wildlife Refuge, northeastern Alaska: U.S. Geological Survey Bulletin 1778, p 117-122.

Grantz, Arthur, and May, S.D., 1982, Rifting history and structural development of the continental margin north of Alaska, *in* Watkins, J.S., and Drake, C.L., eds., Studies in continental margin geology: American Association of Petroleum Geologists Memoir 34, p. 77-100.

Harms, J.C., 1975, Stratification and sequence in prograding shoreline deposits: Society of Economic Paleontologists and Mineralogist Short Course 2, p. 81-102.

Jamison, H.C., Brockett, L.K., McIntosh, R.A., 1980, Prudhoe Bay - A ten year perspective, *in* Halbouty, M.T., ed., Giant fields of the last decade: American Association of Petroleum Geologists Memoir 30, p. 289-314.

Keller, A.S., Morris, R.H., and Detterman, R.L., 1961, Geology of the Shaviovik and Sagavanirktok Rivers region, Alaska: U.S. Geological Survey Professional Paper 303 D, p. 169-219.

Knock, D.G., 1986, Compilation of megafossils of Mesozoic and Cenozoic units, Arctic National Wildlife Refuge, northeastern Alaska: Alaska Division of Geological & Geophysical Surveys Public-Data File 86-1f, 40 p.

_____1987, Lithofacies, depositional setting, and petrography of the Kemik Sandstone, Arctic National Wildlife Refuge (ANWR), northeastern Alaska: University of Alaska Fairbanks Unpublished Master of Science Thesis, 135 p., 7 sheets, scale 1:100.

Leffingwell, E. de K., 1919, The Canning River region, northern Alaska: U.S. Geological Survey Professional Paper 109, 251 p.

Masterson, W.D., and Paris, C.E., 1987, Depositional history and reservoir description of the Kuparuk River Formation, North Slope, Alaska, *in* Tailleur, I.L., and Weimer, Paul, eds., Alaskan North Slope Geology: Bakersfield, Pacific Section of Society of Economic Paleontologists and Mineralogists and the Alaska Geological Society, v. 50, p 95-107.

May, S.D., and Grantz, Arthur, 1983, Origin of the Canada Basin as inferred from the seismic geology of offshore northern Alaska: Journal of the Alaska Geological Society, v. 2, p. 9-15.

Meigs, A.J., 1986, Structural evolution of the eastern Sadlerochit Mountains, northeastern Brooks Range, Alaska: A preliminary report based on the summer 1986 field season, North Slope, Alaska: Alaska Division of Geological & Geophysical Surveys Public-Data File 86-86f, 8 p, 1 sheet, scale 1;25,000.

Molenaar, C.M., 1983, Depositional relations of Cretaceous and lower Tertiary rocks, northeastern Alaska: American Association of Petroleum Geologists Bulletin, v. 67, p. 1066-1080.

Mowatt, T.C., Banet, A.C., Jr., and Reeder, J.W., 1992, Petrographic analyses of selected horizons, Aurora 089 No.1 OCS-Y-0943 well, offshore northeast Alaska: U.S. Bureau of Land Management-Alaska Open-File Report 42, 48 p., 2 sheets, scale 1 inch = 1,000 feet.

Mull, C.G., 1987, Kemik Formation, Arctic National Wildlife Refuge, northeastern Alaska, *in* Tailleur, I.L., and Weimer, Paul, eds., Alaskan North Slope Geology: Bakersfield, Pacific Section of Society of Economic Paleontologists and Mineralogists, and the Alaska Geological Society, v. 50, p. 405-431.

_____1982, The tectonic evolution and structural style of the Brooks Range, Alaska: An illustrated summary, *in* Powers, R.B., ed., Geological studies of the Cordilleran thrust belt: Denver, Rocky Mountain Association of Geologists, v. 1, p. 1-45.

_____1985, Cretaceous tectonics, depositional cycles and the Nanushuk Group, Brooks Range and Arctic Slope, Alaska, *in* Huffman, A.D., ed., Geology of the Nanushuk Group and related rocks, North Slope, Alaska: U.S. Geological Survey Bulletin 1614, p. 7-36.

North, F.K., 1985, Petroleum geology: Boston, Unwin Hyman, Inc., 631 p.

Pemberton, S.G., Frey, R.W., Ranger, M.J., and MacEachern, J.A., 1992, The conceptual framework of ichnology, *in* Pemberton, S.G., ed., Applications of Ichnology to Petroleum Exploration: A core workshop: Society for Sedimentary Geology, SEPM Core Workshop No. 17, p. 1-32.

Posamentier, H.W., Jervey, M.T. and Vail, P.R., 1988, Eustatic controls on clastic deposition I - Conceptual framework, *in* Wilgus, C.K., Hastings, B.S., Kendall, C.G.St.C., Posamentier, H.W., Ross, C.A., and Van Wagoner, J.C., eds., Sea-level changes: an integrated approach: Society of Economic Paleontologists and Mineralogists Special Publication 42, p. 109-124.

Reifenstuhl, R.R., 1990, Vitrinite reflectance data for some early Tertiary through Jurassic outcrop samples, northeastern Alaska: Alaska Division of Geological & Geophysical Surveys Public-Data File 90-5, 3 p.

_____1991b, Biostratigraphic report of 12 Cretaceous to Jurassic age outcrop samples from the Sagavanirtok, Mt. Michelson, and Chandler Lake Quadrangles, North Slope, Alaska: Alaska Division of Geological & Geophysical Surveys Public-Data File 91-21d, 10 p.

Reifenstuhl, R.R., 1991a, Paleontology data from 29 outcrop samples of Late Cretaceous to Jurassic age, Sagavanirktok Quadrangle, northeastern Brooks Range, Alaska: Alaska Division of Geological & Geophysical Surveys Public-Data File 91-21b, 11 p., 1 sheet, scale 1:250,000.

_____1993, Kemik Sandstone, petrology, physical properties, and facies of 40 outcrop and subsurface samples, Canning River, northeast North Slope Alaska: Alaska Division of Geological & Geophysical Surveys, U.S. Minerals Management Service Contract Report #14-35-0001-30643, 63 p., 2 sheets.

_____1994, Kemik Sandstone, depositional environment, facies, petrology, and petrophysics, northeast North Slope Alaska (abs.): Geological Society of America Abstracts with programs, v. 26, no. 2, p. 83.

Reifenstuhl, R.R., and Myers, M.D., 1992, Kemik Sandstone: An environment of deposition interpretation from a Canning River section, North Slope, Alaska (abs.): International Conference on Arctic Margins, Abstracts, p. 51.

Robinson, M.S., Decker, John, Clough, J.G., Reifenstuhl, R.R., Bakke, Arne, Dillon, J.T., Combellick, R.A. and Rawlinson, S.E., 1989, Geology of the Sadlerochit and Shublik Mountains, Arctic National Wildlife Refuge, northeastern Alaska, Alaska Division of Geological & Geophysical Surveys, Professional Report 100, 1 sheet, scale 1:63,360.

State of Alaska Geologic Materials Center, 1984, Report 25, Various Oil Companies, Geochemical Analysis (total organic carbon, Rock - Eval pyrolysis, kerogen type, vitrinite reflectance): Alaska Division of Geological & Geophysical Surveys, 580 p.

_____1990, Report 168, The Home Oil Company, vitrinite reflectance data of cuttings (5390-14,850)-Bush Federal No. 1 Well, Alaska Division of Geological & Geophysical Surveys, 14 p.

Vandergon, M.A., 1986, Microfossil compilation of Mesozoic and Cenozoic units, Arctic National Wildlife Refuge, northeastern Alaska: Alaska Division of Geological & Geophysical Surveys Public-Data File 86-1g, 74 p.

A NEW SPECIES OF THE CONODONT *AMYDROTAXIS* FROM THE EARLY DEVONIAN OF SOUTHWESTERN ALASKA

by
Norman M. Savage[1] and Robert B. Blodgett[2]

INTRODUCTION

During the summer of 1993 the authors worked with geologists from the Alaska Division of Geological & Geophysical Surveys in several areas of southwestern Alaska and had the benefit of helicopter and other support that permitted the collection of numerous paleontologic samples. Some of these samples have yielded conodonts and other fossils. Two of the samples that yielded conodonts are from Hill 2001 in the Lime Hills D-5 Quadrangle (figs. 1A–C) and are of interest because the specimens, although few in number, appear to represent the full apparatus of the youngest known species of the genus *Amydrotaxis*.

[1] University of Oregon, Eugene, Oregon 97403.
[2] U. S. Geological Survey, 970 National Center, Reston, Virginia 22092.

OCCURRENCE AND AGE OF COLLECTIONS

The conodonts described here are from an unnamed lithologic unit consisting of Emsian-age (late Early Devonian) limestone exposed as scattered, isolated exposures in the SE¼SW¼ sec. 15, T. 20 N., R. 29 W. (Seward Meridian) of the Lime Hills D-5 Quadrangle. No detailed geologic map has yet been issued for this part of the Lime Hills D-5 Quadrangle. The strata have been strongly folded and hence no precise measurement has been made of their total thickness, but they are estimated to be no less than 50 m thick. Various types of lithologies are present, vary-

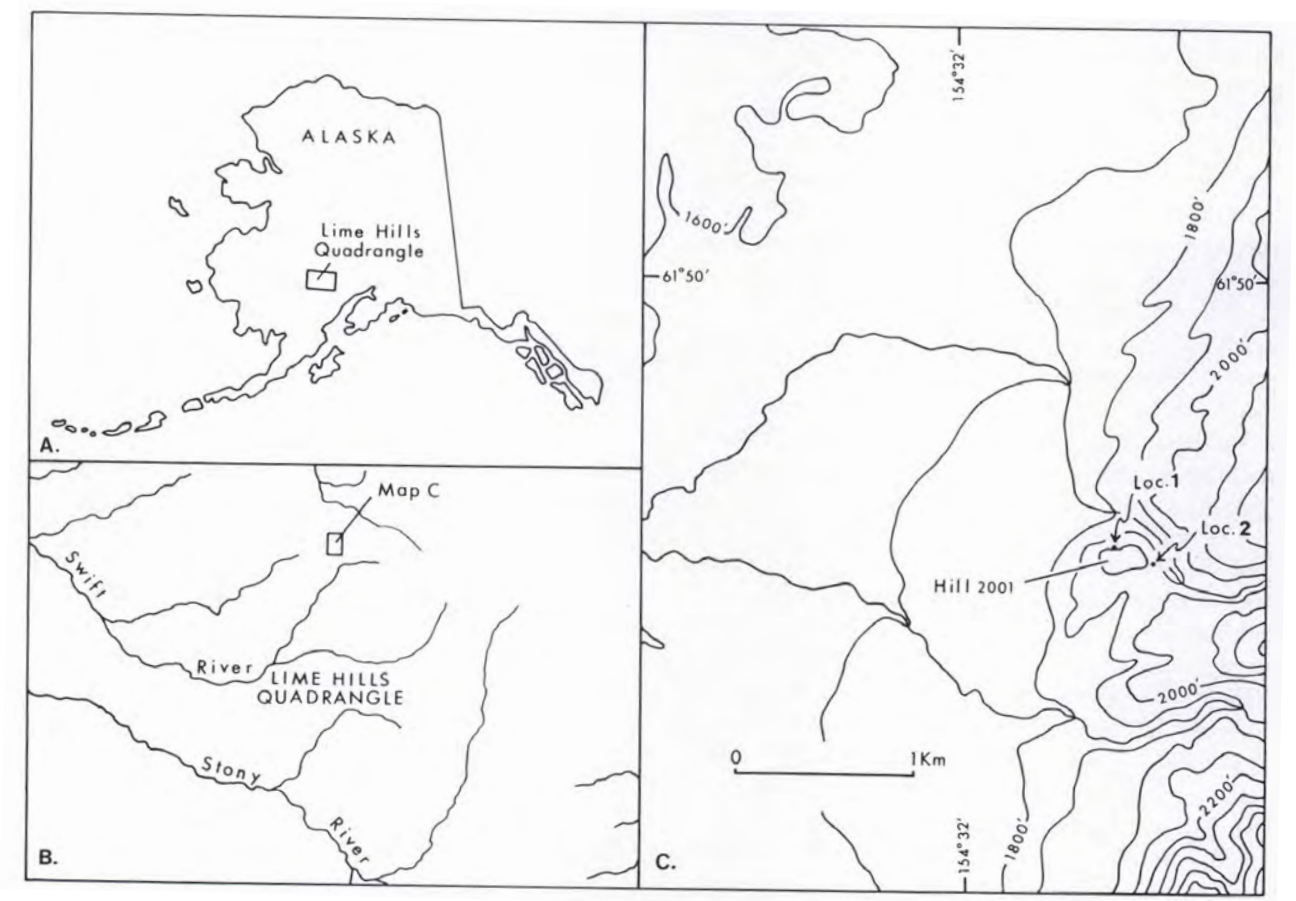

Figure 1. *Maps showing (A) Alaska and the position of the Lime Hills Quadrangle; (B) Lime Hills Quadrangle and the location of the sample area; (C) sample area in the D-15 15-minute quadrangle and the sites of localities 1 and 2.*

ing from lime mudstone to lime grainstone. The latter is composed of encrinite with abundant two-holed crinoid ossicles. The strata are typically medium to dark gray on fresh surfaces. Brachiopods, corals, the stick-like stromatoporoid *Amphipora* and large ostracodes are common. This unit locally forms the base of the Mystic sequence (Blodgett and Gilbert, 1992; Gilbert and Bundtzen, 1984), which overlies the Cambrian to Lower Devonian deep-water Dillinger sequence. The two localities from which the conodont-bearing samples were collected are described below.

Locality 1(93ABd42) (fig. 1C) is a small limestone exposure, approximately 5 m thick, on the north-facing slope just below the ridge crest and summit of Hill 2001, situated at lat 61°49'10"N., long 154°31'01"W. The rock is a dark-gray lime mudstone to wackestone and appears to be a continuous sequence of beds. Megafossils consist mostly of dendroid tabulate corals, stromatoporoids, and two-holed crinoid columnals. The conodont sample was taken from the middle of the outcrop in an argillaceous limestone that bears frequent athyrid brachiopods.

Locality 2 (93ABd44) (fig. 1C) is talus rubble at the base of a massive cliff at the southeast slope of Hill 2001. The cliff is composed of strata that dip steeply to the northeast. The talus appears to be derived from the exposure which is no more than 7 m thick. Locality 2 is in sec. 15, T. 20N., R. 29 W., Lime Hills D-5 Quadrangle. It is 250 m north of the border separating sections 15 and 22, and is on the border separating the SW¼ from the SE¼ sec. 15 at lat 61°49'08"N., long 154°30'46"W. Although the sample was collected from talus, the thickness of the unit, the lithologies, and the megafossils, including the two-holed crinoid columnals, are similar to those at locality 1. The cliff is exposed intermittently between the two localities, so there is good reason to consider that the two samples come from horizons within the same 5–7-m-thick unit.

The new species *Amydrotaxis murphyi*, described below, is represented by only a few specimens of the constituent elements, but is sufficiently distinctive and stratigraphically higher than other species that formal naming seems warranted. Its occurrence with *Polygnathus serotinus*, a conodont that is characteristic of the late Emsian *serotinus* Zone, and with megafossils considered to be of late Emsian to early Eifelian age, places it well above the early Lochkovian to late Pragian species of *Amydrotaxis* previously described from Devonian deposits. This small conodont fauna is therefore of interest to Alaskan bio-stratigraphers in that *Polygnathus serotinus* establishes the age of this horizon, and is of interest to conodont workers in greatly extending the range of *Amydrotaxis* and indicating the morphologic characteristics of this late form of the genus.

SYSTEMATIC PALEONTOLOGY

In this paper the multi-element notation and suprageneric classification used are those of Sweet (1988).

Family SPATHOGNATHODONTIDAE Hass, 1959
Genus AMYDROTAXIS Klapper and Murphy, 1980

Type species.—Amydrotaxis johnsoni Klapper, 1969.

Discussion

Seven species of Amydrotaxis have been described previously and appear to be particularly characteristic of the early Lower Devonian of western and northern North America and eastern Australia. The genus seems to have a seximembrate apparatus. The Pa element is carminate and typically has one or more high anterior denticles. The platform is usually asymmetrical and restricted to the posterior half of the unit, with one lobe often prominent and extending at a right angle of even slightly anterior of the axis of the blade. The Pb element is angulate, has a prominent reclined main cusp, a few smaller anterior denticles and just one or two much lower posterior denticles. The M element is digyrate and often has a slightly reclined main cusp with several closely placed denticles on the anterior process and about two on the posterior process. The Sa element is alate to palmate with three or four fused denticles situated symmetrically either side of a flattened main cusp. The Sb element is bipennate and generally has a large laterally compressed main cusp and subequal anterior and posterior processes, each bearing laterally compressed posteriorly reclined fused denticles. The Sc element is typically digyrate and curved, with a high reclined main cusp, two or three slender anterior denticles successively increasing in height toward the main cusp, and two or three posterior denticles that tend to increase in height toward the posterior tip of the element. It is the apparatus as a whole that characterizes *Amydrotaxis*, for in some cases the Pa element viewed in isolation might be confused with the Pa element of *Ozarkodina* or *Pandorinellina*. However, the Pa elements of the known species of the genus differ from each other sufficiently to be distinctive.

AMYDROTAXIS MURPHYI n. sp.
Figures 2.1–17

Material

A total of 20 specimens from locality 1, comprising 8 Pa elements, 3 Pb elements, 2 M elements, 4 Sa elements, 1 Sb element, and 2 Sc elements; and a total of 4 specimens from locality 2 comprising 3 Pa elements and 1 Sa element. Figured Pa element USNM 481676 from locality 1 is the holotype.

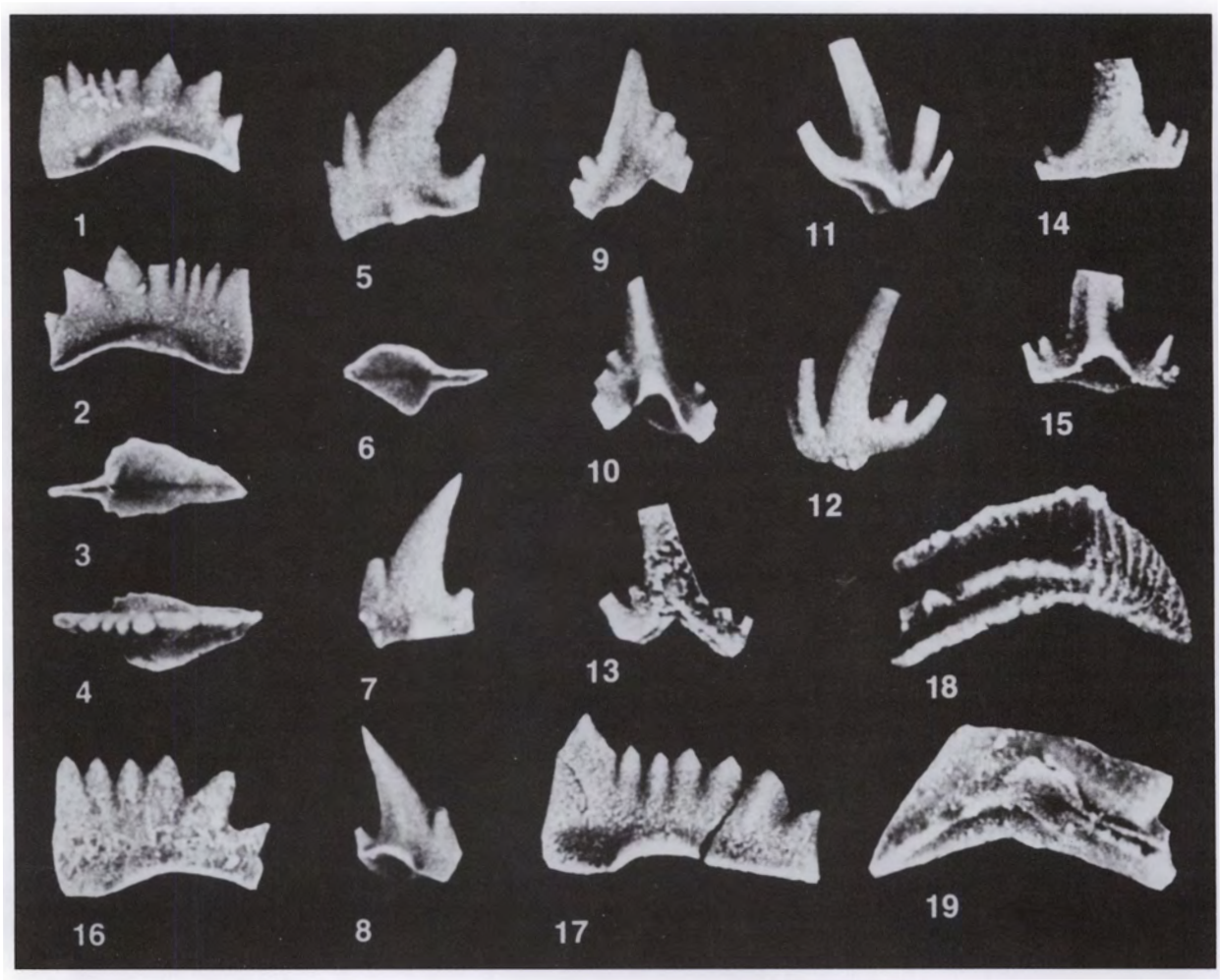

Figure 2. *(1-17)* Amydrotaxis murphyi *n. sp., (1-4) lateral, lower, and upper views of Pa element USNM 481676 (holotype) from locality 1; (5-6) lateral and lower views of Pb element USNM 481677 from locality 1; (7-8) lateral and lower-lateral views of Pb element USNM 481678 from locality 1; (9-10) inner and outer views of M element USNM 481679 from locality 1; (11-12) inner and outer views of Sc element USNM 481680 from locality 1; (13) inner view of Sb element USNM 481681 from locality 1; (14-15) anterior and posterior views of Sa element USNM 481682 from locality 1; (16) lateral view of Pa element USNM 481683 from locality 1; (17) lateral view of Pa element USNM 481684 from locality 2. (18-19)* Polygnathus serotinus *Telford, 1975. (18) upper view of broken Pa element USNM 481685 from locality 2, showing the platform margins, deep adcarinal trough, position of the carina, and shape of the geniculate tongue; (19) lower view of the same specimen showing the distinctive inverted basal cavity and projecting outer lip of the basal pit. All figures x 50.*

Diagnosis

A species of *Amydrotaxis* with a Pa element that is short for the genus and has three large posterior denticles that are progressively reclined. The platform lobes are flared from about one third the unit length and taper to the posterior tip.

Description

The Pa element is short and bears six to eight denticles. The anterior denticle is large and erect and is succeeded by two or three smaller denticles and then three denticles that are stout and progressively reclined. Viewed from above, the blade is straight and the platform lobes are asymmetrically flared from about one third the unit length and taper to the posterior tip. In lateral view the margin of the basal cavity is concave downward.

The Pb element has a large reclined cusp, with one or two small anterior denticles and a single small reclined posterior denticle. The basal margin is asymmetrically flared, with the narrower but more laterally pronounced flare on the outer margin.

The M element has a prominent cusp with two small anterior denticles and three posterior denticles on a short

posterior process. The basal cavity is widest under the cusp, most expanded inward, and tapers posteriorly.

The Sa element is known from only two specimens. The figured one is better preserved but has relatively short lateral processes, each bearing only two small denticles. The main cusp is large and has carinate lateral edges. A symmetrical basal cavity tapers laterally. The unfigured specimen is more palmate and has three larger denticles on the lateral processes.

The Sb element is known only from a single broken specimen. It appears to be somewhat intermediate between the M and the Sc elements, with a high, reclined main cusp, an anterior process bearing two well-separated denticles, and a rather shorter posterior process bearing two denticles, of which the posterior one is the larger. The basal cavity is narrow but extends up the inside of the main cusp.

The Sc element is markedly curved, with the inward curvature of the anterior process greater than that of the posterior process. A high main cusp is reclined both inward and backward, a short anterior process bears two slender denticles, with the anterior one the shorter, and a rather longer posterior process has two reclined denticles of which the posterior one is the longer and more reclined. The basal cavity is long, widest below the main cusp, and tapers posteriorly.

Discussion

Amydrotaxis murphyi differs from the other species in having an unusually short Pa element that has large reclined posterior denticles. In its relatively symmetrical, posteriorly tapering outline, the platform of the new species, when viewed from above, differs considerably from the platforms of *A. sexidentata* Murphy and Matti, 1983, *A. praejohnsoni* Murphy and Springer, 1989, *A. johnsoni* (Klapper, 1969), *A.* sp. n. of Savage 1984, and *A. druceana* (Pickett, 1980). Each of these species has a platform that is variable but usually highly asymmetrical, with one platform lobe projecting laterally from a point about half the unit length. The only other known species of *Amydrotaxis* with a platform similar to that of the Alaska species is *A. corniculans* Mawson, 1986, from eastern Australia, but the Pa element of that species differs from *A. murphyi* in length and lateral profile, as discussed above. *A. chattertoni* Uyeno, 1990, from the Canadian Arctic Archipelago, has a Pa element that differs from the Alaska species in possessing very high, stout, anterior and posterior cusps, and a platform that is relatively symmetrical and reminiscent of that of *Ozarkodina*.

It is premature to compare the other elements of *A. murphyi* with homologous elements of the other species of the genus because the collection is so small and the elements thus too poorly known to be confident of their typical form. This is particularly the case with the Sb, Sc, and M elements, which are represented by only one or two specimens, and hardly better with the Sa and Pb elements. The element described above as the Sa element may instead be the M element, and that described as the M element may be an unusually asymmetrical Sa element. Only the Pa element is represented by enough specimens to give some idea of its range of form, and even this element is inadequately represented and hardly worth formal description were it not for the stratigraphic interest of this occurrence.

The earliest known species of *Amydrotaxis* are *A. sexidentata* Murphy and Matti, 1983, from the early Lochkovian of Nevada (Murphy and Matti, 1983) and eastern Canadian Cordillera (Uyeno, 1991), and *A. chattertoni* from the early Lochkovian of the Canadian Arctic Archipelago (Uyeno, 1990). The next occurrences stratigraphically appear to be *A. corniculans* Mawson, 1986, from the early to late Lochkovian of eastern Australia (Mawson, 1986), *A. praejohnsoni* Murphy and Springer, 1989, from *delta* Zone beds of early to middle Lochkovian age in Nevada, east-central Alaska, eastern Australia, and Yukon Territory, Canada (Klapper, 1969; Lane and Ormiston, 1979; Murphy and Matti, 1983; Mawson, 1986; Murphy and Springer, 1989; Wilson, 1989). *A. johnsoni* (Klapper, 1969) occurs in the *delta* and *pesavis* Zones in Yukon Territory (Klapper, 1969) and Nevada (Murphi and Matti, 1983) but is not known in eastern Australia. The very poorly known species *Amydrotaxis* n. sp. of Savage (1984), from a small exposure on Jones Island, northwest Washington (Savage, 1984), occurs with *Ozarkodina remscheidensis* (Ziegler, 1960) and is thus of poorly constrained Early Devonian age. *A. druceana* (Pickett, 1980) is from the mid Lochkovian of central New South Wales in eastern Australia. Mawson and others (1992) show in their table 6 the occurrence of a few elements of *Amydrotaxis* sp. that they conclude, from the associated conodonts, to be of latest Pragian age.

The occurrence of *Amydrotaxis murphyi* in the late Emsian of Alaska makes the absence of a record of *Amydrotaxis* in beds of the early to middle Emsian age all the more interesting. Although the number of specimens comprising the present collection are insufficient for adequate description, they clearly represent the genus *Amydrotaxis*, and may be all the specimens we are going to get unless a further helicopter visit to the locality becomes possible.

Etymology

Named in honor of M. A. Murphy in recognition of his contributions to the study of Silurian and Devonian conodonts.

Genus POLYGNATHUS Hinde, 1879

Type species.—Polygnathus dubius Hinde, 1879

POLYGNATHUS SEROTINUS Telford, 1975

Figure 2.18–19

Discussion

Only two broken Pa elements of the species from locality 2 can be identified with confidence, although there are two other broken Pa elements and one M element. No specimens have been recovered from locality 1.

ACKNOWLEDGMENTS

We thank the Alaska Division of Geological & Geophysical Surveys for helicopter and other support. Funds from the National Science Foundation Award EAR-9312954 were used to process the samples. Barbara Savage separated and picked the conodonts. M.A. Murphy and T.T. Uyeno kindly read the submitted manuscript and made valuable suggestions.

REFERENCES CITED

Blodgett, R.B., and Gilbert, W.G., 1992, Upper Devonian shallow-water siliciclastic strata and associated fauna and flora, Lime Hills D-4 quadrangle, southwest Alaska *in* Bradley, D.C., and Dusel-Bacon, C., eds., Geologic studies in Alaska by the United States Geological Survey, 1991: U.S. Geological Survey Bulletin 2041, p. 106-115.

Gilbert, W.G., and Bundtzen, T.K., 1984, Stratigraphic relationships between the Dillinger and Mystic terranes, western Alaska Range, Alaska: Geological Society of America Abstracts with Programs, v. 16, no. 5, p. 286.

Hass, W.H., 1959, Conodonts from the Chappel Limestone of Texas: U.S. Geological Survey Professional Paper 295-J, p. 365-369.

Hinde, G.J., 1879, On conodonts from the Chazy and Cincinnati Group of the Cambro-Silurian, and from the Hamilton and Genesee-Shale of the Devonian, in Canada and the United States: Quarterly Journal of the Geological Society of London, v. 35, p. 351-369.

Klapper, G., 1969, Lower Devonian conodont sequence, Royal Creek, Yukon Territory, and Devon Island, Canada (with a section on Devon Island stratigraphy by A.R. Ormiston): Journal of Paleontology, v. 43, no. 1 , p. 1-27.

Klapper, G., and Murphy, M.A., 1980, Conodont zonal species from the *delta* and *pesavis* Zones (Lower Devonian) in central Nevada: Neues Jahrbuch für Geologie und Paläontologie, Monatshefte, Hefte 8, p. 490-504.

Lane, H.R., and Ormiston, A.R., 1979, Siluro-Devonian biostratigraphy of the Salmontrout River area, east-central Alaska: Geologica et Palaeontologica, v. 13, p. 39-96.

Mawson, R., 1986, Early Devonian (Lochkovian) conodont faunas from Windellama, New South Wales: Geologica et Palaeontologica, v. 20, p. 39-71.

Mawson, R., Talent, J.A., Brock, G.A., and Engelbretsen, M.J., 1992, Conodont data in relationship to sequences about the Pragian-Emsian boundary (Early Devonian) in southeastern Australia: Proceedings of the Royal Society of Victoria, v. 104, part 1, p. 23-56.

Murphy, M.A., and Matti, J.C., 1983, Lower Devonian conodonts (*hesperius-kindlei* Zones), central Nevada. University of California Publications, Geological Sciences, Berkeley, v. 123, 83 p.

Murphy, M.A., and Springer, K.B., 1989, Morphometric study of the platform elements of *Amydrotaxis praejohnsoni* n. sp. (Lower Devonian, Conodonts, Nevada): Journal of Paleontology, v. 63, p. 349-355.

Pickett, J., 1980, Conodont assemblages from the Cobar Supergroup (Early Devonian), New South Wales: Alcheringa, v. 4, no. 1 , p. 67-88.

Savage, N.M., 1984, Devonian conodonts from Jones Island, northwest Washington: Canadian Journal of Earth Sciences, v. 21, no. 11, p. 1339-1343.

Sweet, W.C., 1988, The Conodonta: morphology, taxonomy, paleoecology, and evolutionary history of a long-extinct animal phylum: Oxford Monographs on Geology and Geophysics, No. 10, Oxford, Oxford University Press, 212 p.

Telford, P.G., 1975, Lower and Middle Devonian conodonts from the Broken River Embayment, north Queensland, Australia: Special Papers in Palaeontology, London, v. 15, 96 p.

Uyeno, T.T., 1990, Biostratigraphy and conodont faunas of Upper Ordovician through Middle Devonian rocks, Eastern Arctic Archipelago: Geological Survey of Canada Bulletin 401, p. 1-210.

_____1991, Pre-Famennian Devonian conodont biostratigraphy of selected intervals in the eastern Canadian Cordillera, *in* Orchard, M.J., and McCracken, A.D., eds., Ordovician to Triassic conodont paleontology of the Canadian Cordillera: Geological Survey of Canada Bulletin 417, p. 129-161.

Wilson, G.A., 1989, Documentation of conodont assemblages across the Lochkovian-Pragian (Early Devonian) boundary at Wellington, central New South Wales, Australia: Courier Forschungsinstitut Senckenberg, no. 117, p. 117-171.

Ziegler, W., 1960, Conodenten aus dem Rheinischen Unterdevon (Gedinnium) des Remscheider Sattels (Rheinisches Schiefergebirge). Paläontologische Zeitschrift, v. 34, p. 169-201.

EARLY DEVONIAN AND LATE TRIASSIC CONODONTS FROM ANNETTE AND HOTSPUR ISLANDS, SOUTHEASTERN ALASKA

by
Norman M. Savage[1] and George E. Gehrels[2]

INTRODUCTION

Numerous spot samples were collected from Annette Island and adjacent small islands, southeastern Alaska, as part of a more widespread program of geologic and conodont studies in the region. Although most of the samples contained no conodonts, three yielded small faunules that are of interest in constraining the age of deposition and indicating the thermal maturation history of the two areas.

The two units for which the new information is presented include the Karheen Formation and the Hyd Group. Rocks of the Karheen Formation occur on southern Annette Island and adjacent regions of Hotspur Island (fig. 1), and are also found on several other islands in the southern part of southeastern Alaska (Eberlein and others, 1983; Gehrels and Berg, 1992). In the study area the Karheen Formation consists of a basal conglomerate that rests on various Ordovician-Silurian meta-igneous rocks and an overlying section of fine- to coarse-grained marine clastic strata interbedded with thin limestone layers and thick olistostromes. These strata become tuffaceous upsection and grade into an overlying sequence of unnamed mafic volcanic flows and breccia. The distribution and stratigraphy of the Karheen Formation in the Annette-Hotspur area are described by Gehrels and others, (1987).

The Hyd Group on Annette Island consists of limestone, fine- to coarse-grained clastic strata, conglomerate, rhyolite, and basalt (Berg, 1972) that are characteristic of Triassic strata in much of southeastern Alaska (Gehrels and Berg, 1992). The age of some lithic components in the group has been controversial: Berg (1972, 1982) and Berg and Cruz (1982) reported that clastic strata and limestone in the upper part of the section were not known to be Late Triassic in age, but Berg (1972, 1973) noted that felsic volcanic rocks and clastic strata low in the section were probably middle and late(?) Paleozoic in age. Gehrels and others (1987) reported a U-Pb age of 225 ± 3 Ma on rhyolite from nearby Gravina Island (~10 km northwest of Annette Island) which suggested (but did not prove) that the rhyolite on Annette Island was also Triassic in age. The distribution and stratigraphy of the Hyd Group on Annette Island are described by Gehrels and others (1987).

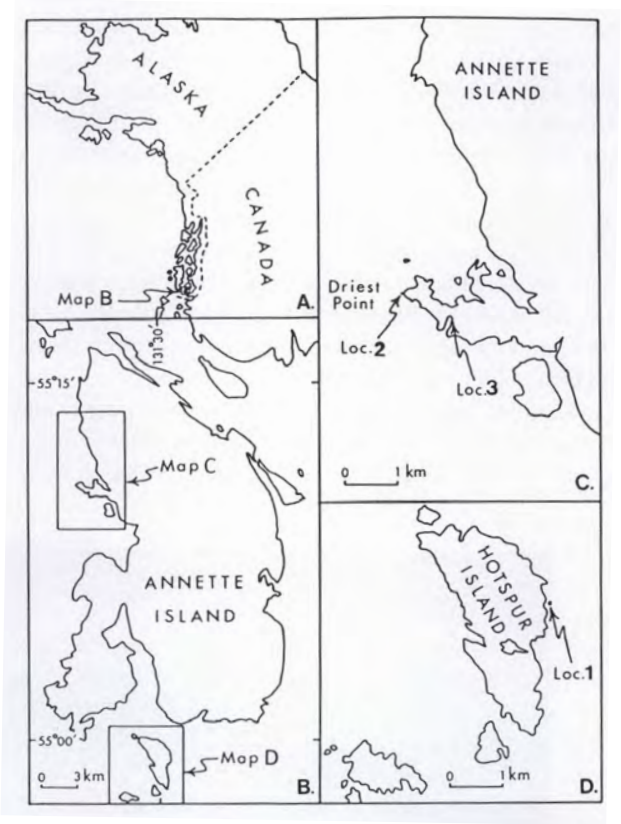

Figure 1. *Location map of Annette and Hotspur Islands, southeastern Alaska, with insets showing localities 1-3.*

CONODONT DETERMINATIONS AND AGES

A sample from locality 1 (lat 54°59'14"N., long 131°29'50"W.) yielded Early Devonian conodonts. The locality is on a small island, about 10 m wide, which is situated approximately 40 m to the east of Hotspur Island and just south of Annette Island (figs. lA, B, and D). The sample, which weighed approximately 400 g, yielded 36 conodonts, comprising *Pandorinellina exigua philipi* (Klapper, 1969) and *Eognathodus sulcatus sulcatus* Philip, 1965 (fig. 2). These indicate a middle Early Devonian (*sulcatus* zone) age. The conodonts all exhibit a Color Alteration Index of 5.0, using the indices of Epstein, and others (1977). This suggests considerable thermal alteration equivalent to prolonged temperatures of about 300°C.

[1] University of Oregon, Eugene, Oregon 97403.
[2] University of Arizona, Tucson, Arizona 85721.

The sample was collected from a 10 cm x 5.3 cm x 5 cm gray limestone block in an olistostrome that occurs near the base of the Karheen Formation (Gehrels and others, 1987). Adjacent strata consist of interbedded dark-gray to tan mudstone, siltstone, sandstone, and minor limestone. The olistoliths in the olistostrome generally include gray limestone, tan limestone, and tan sandstone and siltstone set in a matrix of chaotic, unbedded dark-brown to dark-gray mudstone and sandstone. Many of the blocks in the olistostrome show evidence of soft-sediment deformation, indicating they were incorporated into the olistostrome prior to lithification. However, such evidence is not present for the block that was sampled. Berg (1972) suggested that the strata are of Middle Devonian age but could be as old as latest Silurian. As the olistostrome must have formed after the deposition of the limestone block, it is now clear from our data that the olistostrome and overlying strata can be no older than middle Early Devonian.

Samples from localities 2 and 3 on the western side of Annette Island have each yielded Late Triassic conodonts. Locality 2 (lat 55°10’37"N., long 13l°36’16"W.), is at the western tip of Driest Point (figs. lA–C). The sample was taken from a 50-cm-thick layer of light-gray, fossiliferous, moderately recrystallized limestone in a sequence of interbedded light-gray limestone and dark-gray mudstone that occurs near the base of the Hyd Group (Gehrels and others, 1987). The 400 g sample yielded 45 conodonts that include 18 indeterminate fragments and 27 specimens of *Epigondolella abneptis* (Huckriede, 1958). These appear to fit well within *E. abneptis* ssp. B of Orchard, 1983, characterized by well developed posterior platform nodes (fig. 3). According to Orchard’s zonal subdivision, the presence of this subspecies indicates the *E. abneptis* ssp. B zone encompassing the upper half of the Lower Norian (Orchard, 1983, fig. 1). This age is perhaps slightly older than the Norian and Late Norian megafossil-based age calls reported by Berg and Cruz (1982) for a nearby sequence of siltstone, limestone, and slate.

Locality 3 (lat 55°10’19"N., long 13l°35’24"W.) is in a small inlet 1.1 km southeast of locality 1 (figs. lA–C).

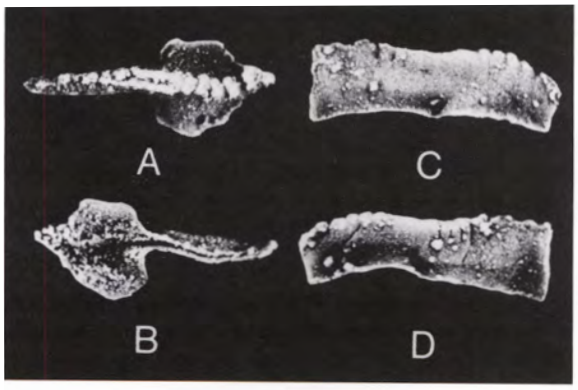

Figure 2. Eognathodus sulcatus sulcatus *Philip, 1965: (A-D) upper, lower, and lateral views of Pa element USNM 331767 from locality 1, Hotspur Island. All figures x 32.*

Figure 3. Epigondolella abneptis *(Huckriede, 1958): (A-C) lateral, upper, and lower views of Pa element USNM 331768; (D-F) lateral, upper, and lower views of Pa element USNM 331769; (G-I) lateral, upper, and lower views of Pa element USNM 331770; all from locality 2, Annette Island. All figures x 40.*

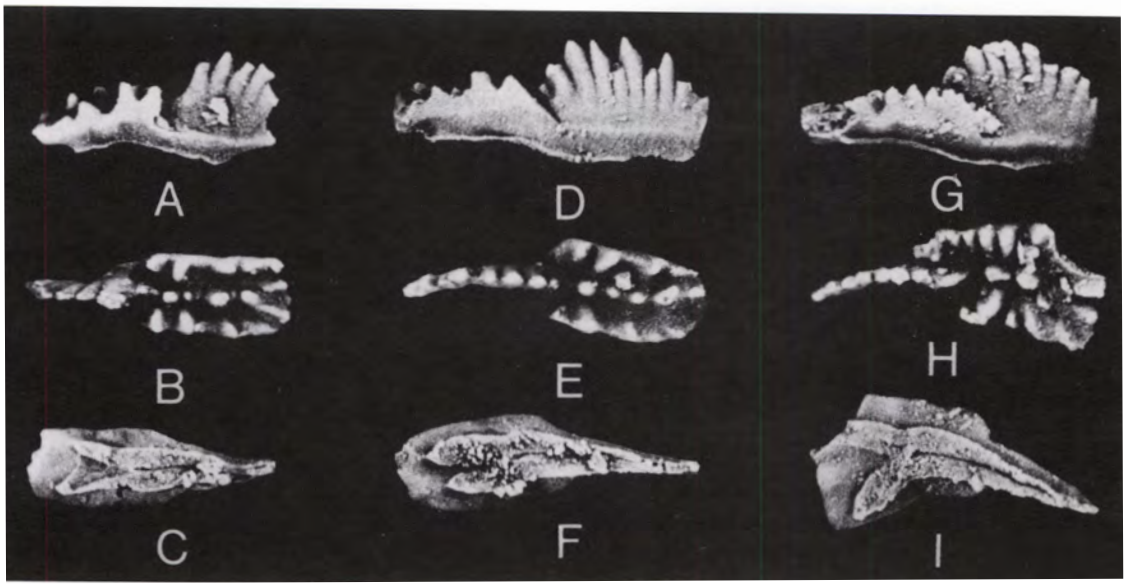

The sample weighed about 400 g and was collected from a discontinuous 20-cm-thick limestone layer in a sequence of interbedded silicic tuff, green volcaniclastic sandstone, and discontinuous limestone near the base of the Hyd Group (Gehrels and others, 1987). Only three specimens were recovered and these comprise one indeterminate specimen and two specimens of *Epigondolella primitia* Mosher, 1970 (fig. 4). This species is known from the uppermost Carnian and the lowest quarter of the Lower Norian (Orchard, 1983, fig. 1) and demonstrates that the felsic volcanic rocks and associated clastic strata on Annette Island are middle Late Triassic in age.

THERMAL-MATURATION EVIDENCE

The color of the conodonts from both Triassic localities is the same as for the Early Devonian conodonts and accordingly also records temperatures of approximately 300°C. This thermal alteration of Devonian and Triassic conodonts may have been produced by a post-Triassic sedimentary accumulation of 9 km (assuming an average geothermal gradient), or by a similar thickness of tectonic overburden, or by interaction with hot fluids during a regional late Mesozoic or early Cenozoic hydrothermal event (Gehrels and Taylor, 1984).

ACKNOWLEDGMENTS

Robert Blodgett and Thomas Bundtzen kindly read the submitted manuscript and made valuable suggestions.

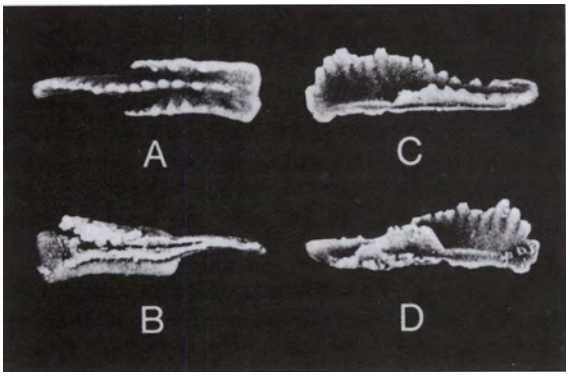

Figure 4. Epigondolella primitia *Mosher, 1970: (A-D) upper, lower, and lateral views of Pa element USNM 331771 from locality 3, Annette Island. All figures x 32.*

REFERENCES CITED

Berg, H.C., 1972, Geologic map of Annette Island, Alaska: U.S. Geological Survey Miscellaneous Geologic Investigations Series Map I-684, 8 p., scale 1:63,360.

_____1973, Geology of Gravina Island, Alaska: U.S. Geological Survey Bulletin 1373, 41 p.

_____1982, The Alaska Mineral Resource Assessment Program: Guide to information about the geology and mineral resources of the Ketchikan and Prince Rupert quadrangles, southeastern Alaska: U.S. Geological Survey Circular 855, 24 p.

Berg, H.C., and Cruz, E.L., 1982, Map and table describing fossil collections and related samples in the Ketchikan and Prince Rupert quadrangles, southeastern Alaska. U.S. Geological Survey Open-File Report 82-1088, 27 p.

Eberlein, G.D., Churkin, M. Jr., Carter, C., Berg, H.C., and Ovenshine, A.T., 1983, Geology of the Craig quadrangle, Alaska: U.S. Geological Survey Open-File Report 83-91, 28 p.

Epstein, A.G., Epstein, J.B., and Harris, L.D., 1977, Conodont color alteration - an index to organic metamorphism: U.S. Geological Survey Professional Paper 995, 27 p.

Gehrels, G.E., and Berg, H.C., 1992, Geologic map of southeastern Alaska: U.S. Geological Survey Miscellaneous Investigations Series Map I-1867, scale 1:600,000.

Gehrels, G.E., and Taylor, H.P., 1984, Fossil hydrothermal systems in the Ketchikan area, southeastern Alaska: *in* Coonrad, W.L., and Elliott R.L., eds., The United States Geological Survey in Alaska: Accomplishments during 1981: U.S. Geological Survey Circular 868, p. 134-136.

Gehrels, G.E., Saleeby, J.B., and Berg, H.C., 1987, Geology of Annette, Gravina, and Duke Islands, southeastern Alaska: Canadian Journal of Earth Sciences, v. 24, p. 866-881.

Huckriede, R., 1958, Die conodonten der mediterranen Trias und ihr stratigraphischer Wert: Paläontologische Zeitschrift, v. 32, no. 3/4, p. 141-175.

Klapper, G., 1969, Lower Devonian conodont sequence, Royal Creek, Yukon Territory, and Devon Island, Canada, with a section on Devon Island stratigraphy by A. R. Ormiston: Journal of Paleontology, v. 43, no. 1, p. 1-27.

Mosher, L.C., 1970, New conodont species as Triassic guide fossils: Journal of Paleontology, v. 44, no. 4, p. 737-742.

Orchard, M.J., 1983, *Epigondolella* populations and their phylogeny and zonation in the Upper Triassic: Fossils and Strata, no. 15, p. 177-192.

Philip, G.M., 1965, Lower Devonian conodonts from the Tyers area, Gippsland, Victoria: Proceedings of the Royal Society of Victoria, v. 79, part 1, p. 95-117.

MINERALIZATION AND ZONING OF POLYMETALLIC VEINS IN THE BEAVER MOUNTAINS VOLCANO-PLUTONIC COMPLEX, IDITAROD QUADRANGLE, WESTCENTRAL ALASKA

by
David Szumigala[1]

ABSTRACT

The Beaver Mountains contain a Late Cretaceous-early Tertiary volcano-plutonic complex consisting of dominantly andesitic volcanic rocks and quartz-monzonitic plutonic rocks. Plutonic rocks have contact-metamorphosed nearby volcanic rocks and Cretaceous Kuskokwim Group sedimentary rocks. The igneous rock units are comagmatic, and all units have been weakly to intensely altered by hydrothermal fluids.

The Beaver Mountains may be the source of placer gold located in and mined from the Innoko mining district. Quartz and quartz-tourmaline veins are ubiquitous throughout the igneous rocks. The Beaver Mountains contain many areas with mineralized veins, stockworks, and breccias that have anomalously high Au, Ag, Cu, Pb, and As contents. The most significant lode prospects are found in a five-square-mile area informally known as the South Quartz zone. Gold mineralization is associated with silicification and quartz veining of basaltic andesite and monzonite porphyry. Mineralization is related to at least four spatially distinct structural zones with trends similar to the Iditarod-Nixon Fork fault. This relation suggests that the regional stress regime was important in the localization of the mineralization, and possibly in the localization of the volcano-plutonic complex.

Vein minerals exhibit a concentric zoning pattern from a central core of axinite or axinite-chalcopyrite, to a chalcopyrite zone, to an incomplete outer zone of arsenopyrite. The primary zoning pattern of the vein minerals is evidence of a large hydrothermal system. An isolated area of cinnabar-rich veins and breccias may represent a separate, younger system or, less likely, the outermost zone of the large Cu-Fe-As system.

Characteristics of polymetallic vein mineralization in the Beaver Mountains are similar to those of peripheral veins associated with porphyry copper deposits. However, porphyry-style alteration and mineralization have not been found in the Beaver Mountains. This study reveals that there is potential for plutonic-hydrothermal systems in the Kuskokwim Mountains and that these systems may contain significant gold.

INTRODUCTION

The Beaver Mountains are a rugged mountainous area with some of the greatest relief and highest elevations in the Kuskokwim region of western-southwestern Alaska (fig. 1). As a result of multiple periods of alpine glaciation (Bundtzen, 1981), the Beaver Mountains contain some of the best exposures of plutonic and volcanic rocks in the Kuskokwim Mountains. However, outcrops are generally restricted to precipitous, inaccessible cirque walls, whereas ridges contain boulder-size rubble.

The Beaver Mountains are the headwaters of several large creeks of the Innoko mining district, a major placer gold district that has produced approximately 600,000 ounces of gold since 1906 (Bundtzen and others, 1985, Nokleberg and others, 1987). Ganes Creek, in particular, has produced a significant portion of the total placer gold production from the Innoko mining district. It is probable that lode gold sources were from the Beaver Mountains and that possible gold sources (both lode and placer) still exist in the Beaver Mountains.

The purpose of this study is to describe the extent and style of mineralization associated with one of the large intrusive bodies constituting part of the Kuskokwim Mountains volcano-plutonic belt. Exploration in the Beaver Mountains for potential mineralization has been very limited. Examination of the alteration styles and types of mineralization should reveal the potential for a porphyry-type ore deposit or economic lode gold mineralization.

Leveille and others (1988) and Newberry and others (1988) have shown in other mineralized regions of Alaska that gold favorable plutons can be recognized by moderate to high alkalinity and low oxidation state, similar to results obtained by Mutschler and others (1985) for plutons in the North American Cordillera. Preliminary work by the author in westcentral Alaska indicated that many of the plutons in the Kuskokwim Mountains magmatic belt, including plutonic rocks from the Beaver Mountains, are gold favorable by those criteria (Szumigala, 1993). Examination of mineralization in the Beaver Mountains would help to determine whether the discrimination scheme used by Leveille and others (1988) and Newberry and others (1988) is applicable to the Beaver Mountains and plutonic rocks in the rest of the Kuskokwim region.

Field investigations (geologic mapping and sampling)

[1]2071 East Worchester Drive, Salt Lake City, Utah 84121-3826.

were largely limited to ridgeline traverses during geologic mapping and chemical sampling to cover the maximum area during reconnaissance. Significantly mineralized areas, as determined by geochemical results from initial traverses, were generally retraversed and many more geochemical samples were collected. Some color anomalies present in cirque walls were investigated, but many more remain to be sampled.

GEOLOGY

The Kuskokwim Mountains volcano-plutonic belt constitute one of four Late Cretaceous to early Tertiary volcano-plutonic belts that crop out across wide areas of southern, western, and central Alaska (Hudson, 1979; Wallace and Engłebretson, 1984; Moll-Stalcup, 1990). The Beaver Mountains are a composite igneous complex consisting of dominantly intermediate-composition volcanic and plutonic rocks covering approximately 250 km^2 in the northern Iditarod Quadrangle of westcentral Alaska (fig. 2). The generalized geologic map of this study differs in some areas from the map by Bundtzen and Laird (1982) in the relative amounts of basalt and andesite, and location and extent of a tuff unit.

The southern Beaver Mountains contain fairly equal amounts of volcanic and plutonic rocks, whereas the northern Beaver Mountains are mostly plutonic rocks with hornfelsed Kuskokwim Group argillite and (sub) lithic sandstone around the outer margins of the igneous rocks. Volcanic rocks are mostly andesitic in composition, but rock units range from dacite to basalt. Mafic volcanic rocks constitute more than 90 percent of the volcanic rocks that overlie and flank plutonic rocks of the central Beaver Mountains. The volcanic rocks are part of the Beaver Mountains volcanic field (Miller and Bundtzen, 1994), which extends approximately 50 km southward from the Beaver Mountains. Potassium-argon age dates from the Beaver Mountains volcanic field range from 76 Ma (base) to 58 Ma (top) (Miller and Bundtzen, 1988).

Most of the volcanic rocks are porphyritic, with phenocrysts of plagioclase, orthoclase, and occasionally pyroxene. The mafic volcanic rocks have been divided into andesite (Kvm), or basaltic andesite/basalt (Kvb) on figure 2. These field distinctions have largely been made on the basis of color, and in reality these rocks may belong to the same volcanic unit with differences in degree of alteration, degree of weathering, or other factors. Some of the mafic volcanic rocks appear to have been contact metamorphosed by the plutonic rocks. Other volcanic rocks that are volumetrically much have been less abundant than the above units (fig. 2) include dacite (Kvi), felsic volcanic rocks (Kvf-rhyolite or latite), andesitic lapilli tuff (Kvt), and volcanic dikes of trachytic composition. Many of the volcanic units are probably fairly thin and underlain by plutonic rocks. Where bedding is discernible, the units are flat to gently dipping. All volcanic exposures on Crater Mountain (southeast Beaver Mountains) dip approximately 50° to the southeast (Bundtzen and Laird, 1982) and away from the center of the plutonic masses, implying uplift and disturbance by emplacement of the plutonic bodies.

Plutonic rocks were classified in the field as monzonite or syenite. However, there are no differences in whole-rock chemistry (both major-oxide and trace element) between these mapped rock types, therefore, syenite and monzonite will be referred to as monzonite 1 and monzonite 2, respectively (table 1). Almost all plutonic chemical data plot in the quartz monzonite field on figure 3. Overall, monzonite 1 is slightly more abundant than monzonite 2. Monzonite 1 units are white to light gray, with sparse, altered, mafic minerals; while monzonite 2 units are light to moderate gray with a salt-and-pepper appearance. It is possible that differences in appearance are simply weathering and alteration phenomena.

The Beaver Mountains plutonic rocks are metaluminous to slightly peraluminous, alkaline to subalkaline, and alkalic or alkali-calcic (Szumigala, 1993). The only published age of a plutonic rock from the Beaver Mountains is a K-Ar date of 70 Ma (Bundtzen and Laird, 1982). Plutonic rock types (field classification), in order of decreasing abundance, include monzonite, syenite, monzodiorite, and quartz syenite. Most plutonic rocks are porphyritic, with phenocrysts of plagioclase, orthoclase, augite, and biotite. All plutonic rocks in the Beaver Mountains contain biotite phenocrysts, and biotite is generally finer grained than the rest of the phenocrysts in any rock. Large areas of monzonite 2 are porphyry dominated by feldspar phenocrysts. None of the plutonic rocks contain recognizable xenoliths.

All monzonite 1 is more altered than nearby monzonite 2, but in almost all cases there are no crosscutting or structural relationships. Most contacts between the plutonic units appear to be gradational, and in places there are gradations in grain size within plutonic bodies (toward finer grain size) as the volcanic contact is approached. Some of these areas are shown in figure 2 as border phases. Fine-grained plutonic border phases are also present along contacts with metasedimentary rocks.

Figure 1. *Location map for the Beaver Mountains study area. Sample numbers are the same as those listed in tables 1 and 2. The South Quartz zone and the Syenite Porphyry prospect insets refer to areas discussed in text. Map area is located in the Iditarod D-2 and D-3 Quadrangles and the topographic features shown on this figure are taken from USGS topographic maps for these quadrangles.*

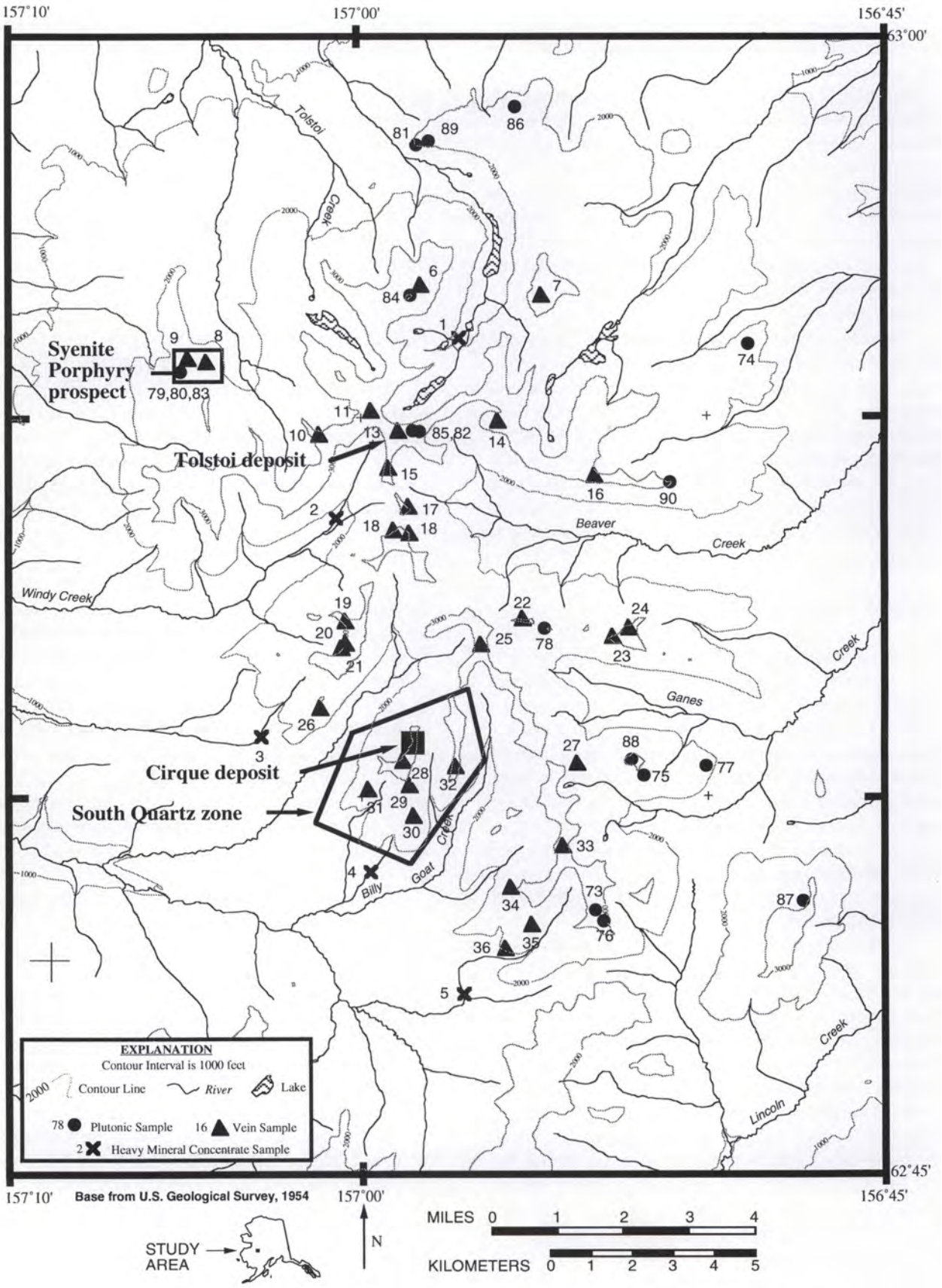
157°10'
157°00'
156°45'
63°00'
62°45'
Tolstoi Creek
Beaver Creek
Windy Creek
Ganes Creek
Goat Creek
Billy Creek
Lincoln Creek
Syenite Porphyry prospect
79,80,83
Tolstoi deposit
Cirque deposit
South Quartz zone
EXPLANATION
Contour Interval is 1000 feet
Contour Line
River
Lake
Plutonic Sample
Vein Sample
Heavy Mineral Concentrate Sample
Base from U.S. Geological Survey, 1954
STUDY AREA
N
MILES 0 1 2 3 4
KILOMETERS 0 1 2 3 4 5

The plutonic rocks are younger than most of the overlying volcanic rocks and in numerous areas have metamorphosed the volcanic rocks. The only cross-cutting age relationship seen between plutonic units is on the western side of the Beaver Mountains (at the Syenite Porphyry prospect, fig. 1), where monzonite 1 is cut by numerous monzonite-2 dikes. Aplite and monzonite-2 dikes in the area have trends of N. 65° E. and occur as thin (<1–15 cm wide), closely spaced (6–10 dikes per meter across width) dikelets. Monzonite 1 is older than monzonite 2 because of the crosscutting relationship and the consistently more altered appearance of monzonite 1 versus monzonite 2.

Several prominent faults can be traced for several kilometers along strike. A major northeast-trending, high-angle fault forms the northern topographic boundary of the Beaver Mountains (Bundtzen and Laird, 1982). Fault traces range from orientations of N. 10° E. to N. 70° E. The faults generally cut igneous units, but there is no discernible offsets of units. Slickensides are locally abundant. The faults appear to act as channels for late hydrothermal fluids in several areas discussed in more detail in the next section.

MINERALIZATION

The mineral potential of the Beaver Mountains is largely unknown, except for several prospects mentioned in Bundtzen and Laird (1982) and Nokleberg and others (1987). Geochemical results from more than 600 rock-chip samples collected during the present study from the Beaver Mountains reveal that mineralization is much more extensive than indicated by previous work. Most geologic and mineralogical relationships discussed below were determined by observations of rubble crop and float, with little true outcrop (especially of veins) in the prospect area, as veins usually have a negative topographic expression.

No known placer mining has occurred in the immediate area of the Beaver Mountains, which may be due to the Beaver Mountains' ruggedness and relative isolation from historic trade routes. Bundtzen and others (1987) reported gold in pan-concentrate samples from tills in the Beaver Mountains. Significant gold anomalies occur in samples from a number of streams along the immediate flanks of the Beaver Mountains. Gold anomalies in stream sediment samples from the Beaver Mountains correlate well with anomalous concentrations of Ag, Sb, As, Cu, Pb, Zn, Sn, or W in stream-sediment or heavy-mineral concentrate samples (BMEC unpub. data, 1990 company report; Hopkins and others, 1991).

Hornfelsed Kuskokwim Group sedimentary rocks, mainly found on a half-dozen rounded knobs to the north of the main body of the Beaver Mountains (fig. 2), appear to lack significant mineralization. Quartz veining is rare and sporadic. Several areas of hornfels contain trace amounts of fine-grained pyrite or pyrrhotite, which commonly weather to iron-stained rubble and outcrops that weather orange and red-brown. These sulfides are likely of sedimentary origin and unrelated to hydrothermal mineralization. Most rock samples from quartz-veined or pyritiferous hornfels do not have anomalous Au or Ag contents or other anomalous geochemical signatures. Geochemical data suggest that potential mineral prospects are confined to igneous units of the immediate uplands of the Beaver Mountains.

WALL-ROCK ALTERATION

In general, most igneous rocks in the study area are weakly to intensely altered, but the primary igneous textures have not been destroyed. The plutonic-rock matrix is more strongly altered than the phenocrysts, resulting in a greenish cast to the most altered rocks. Feldspar phenocrysts in all studied samples are slightly to extremely altered to sericite or kaolinitic clay. Plagioclase phenocrysts were more altered than coexisting orthoclase. Clinopyroxene and biotite are replaced by fine-grained mixtures dominated by chlorite and shreddy amphibole. The alteration style is phyllic (compare, Guilbert and Park, 1986, p. 183) with dominance of fine-grained white mica, chlorite and amphibole. Cobaltinitrite staining of vein-alteration halos shows the presence of K-rich micas and clay minerals resulting from sericitic alteration, rather than secondary K-feldspar potassic alteration. Plutonic rocks are locally bleached and replaced by a mixture of quartz and tourmaline for up to several meters adjacent to quartz veins. Intense quartz and tourmaline replacement of plutonic rocks is not accompanied by significant addition of mica minerals.

Large areas of igneous rock contain sparse tourmaline clots or rosettes. Intense tourmalinization is limited to narrow zones less than 30 m wide (generally less than 6 m wide), and consists of yellow, completely argillized clots of igneous rock surrounded by black, interlocking crystals and veins of fine- to coarse-grained tourmaline with minor quartz. Tourmalinized rock is usually cut by quartz stringers and is moderately iron stained. Supergene manganese oxides may be intermixed with tourmaline.

Small breccia zones are common in the southern Beaver Mountains. The breccias are generally white to yellow, argillized igneous clasts supported in a black fine-grained tourmaline (and manganese oxides?) matrix. A small percentage of these breccias are mineralized and contain chalcopyrite. The largest exposed breccia is a 12 x 60 m rubblecrop. Many breccia bodies appear tabular in plan view. Some of the breccia bodies are cut by later quartz-tourmaline veins.

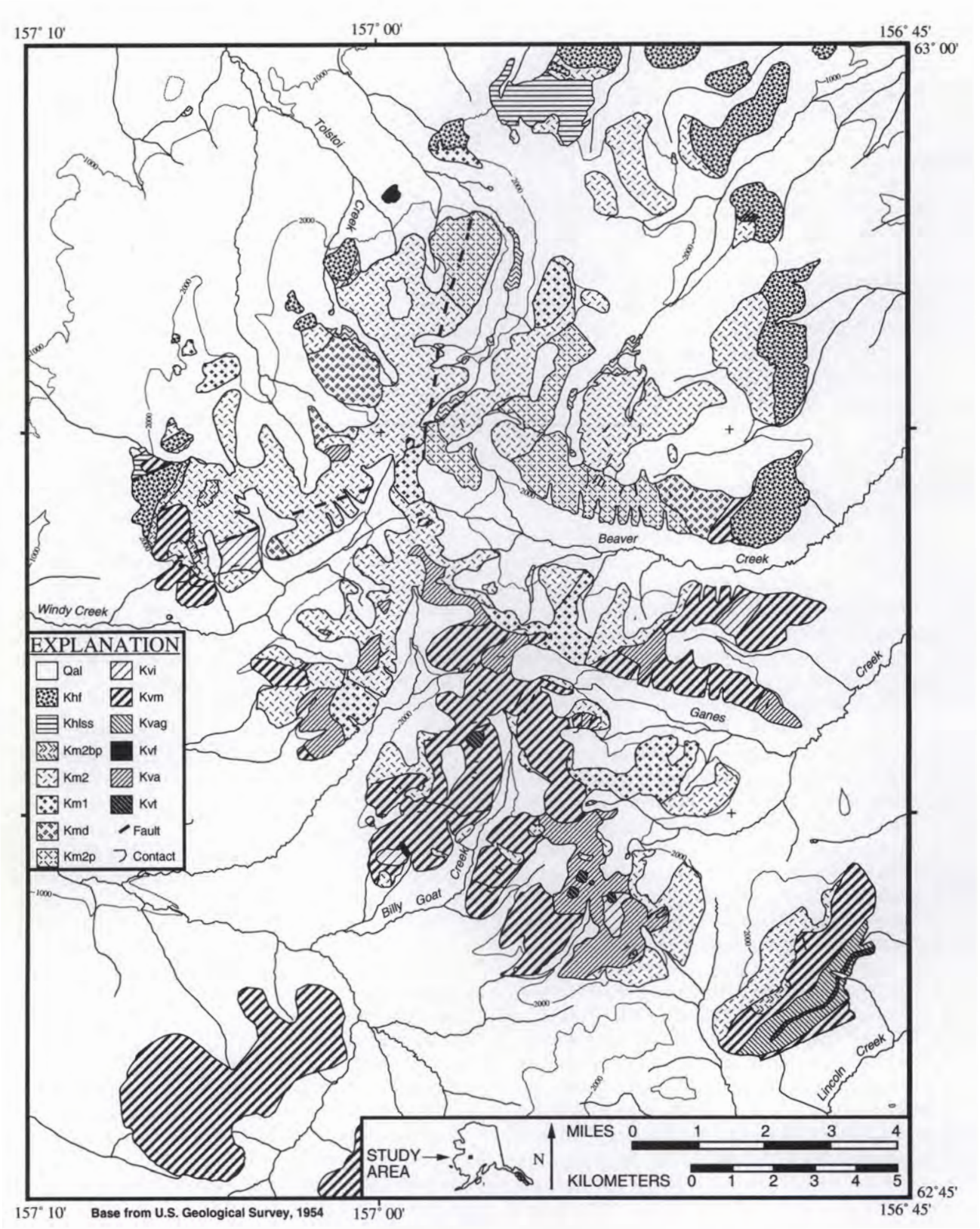

Figure 2. *Beaver Mountains geologic map. Figure outline is the same as that for figure 1. Topographic reference for features on this map are given in figure 1. Some of the geology, particularly the contacts of the various rock units with Qal, are modified from Bundtzen and Laird (1982).*

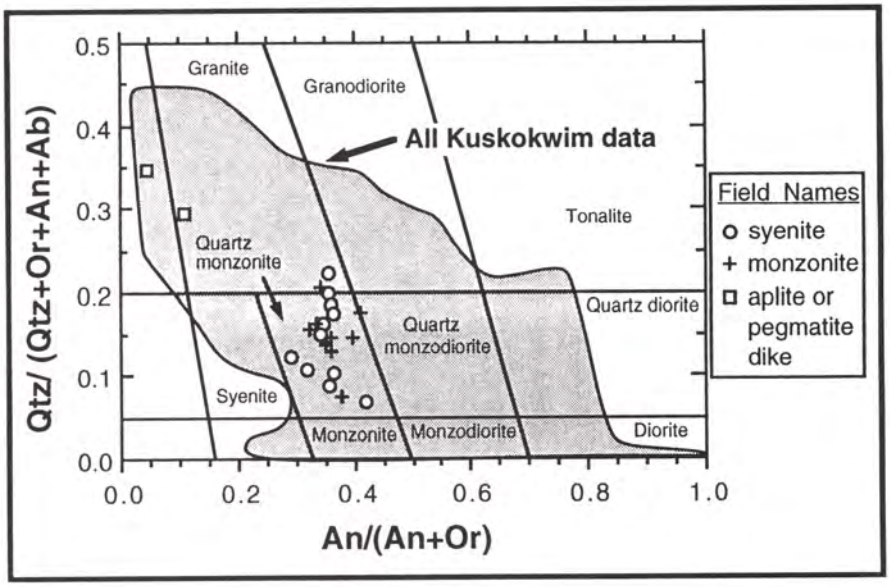

Figure 3. *Compositional plot for Beaver Mountain plutonic rocks. Qtz = quartz, An = anorthite, Or = orthoclase, Ab = albite. Shaded area indicates compositional range for plutonic rocks from the Kuskokwim region (Szumigala, 1993). Beaver Mountains plutonic data given in table 1. (Modified from Streckeisen and LeMaitre, 1979.)*

VEINS

Veining is abundant throughout most of the Beaver Mountains and occurs in most rock units. Every ridge traversed contains vein float or rubblecrop. Veins in the Beaver Mountains generally trend northeast with steep southeast or vertical dips. The dominant trend is N. 50° E. to N. 70° E., which is roughly parallel to the trend of the Iditarod-Nixon Fork fault, the major regional structure in the Iditarod Quadrangle (Miller and Bundtzen, 1988; Bundtzen and others, 1988). Veins locally crosscut one another. Regional uniformity of vein orientations, without regard to rock type, indicates that vein development and orientation are controlled by the regional stress regime rather than local stresses related to magmatic activity. Vein orientations at the Sulfide Cirque Prospect/Tolstoi deposit and the Syenite Porphyry prospect (fig. 1) mimic local joint attitudes in the surrounding igneous rocks.

In general, most veins have similar mineral assemblages including a combination of quartz, tourmaline, axinite, carbonates, and sulfides. Quartz-tourmaline veins are the most common type. Gangue minerals have massive to coarsely crystalline textures. Sulfides present in veins, and less commonly in tourmaline-quartz breccias, include chalcopyrite, arsenopyrite, pyrite, galena, and lesser amounts of tennantite and sphalerite. Some veins contain up to 30-cm-wide masses of fine-grained sulfides. Massive sulfides consist dominantly of arsenopyrite, with minor inclusions of chalcopyrite, galena, and pyrite. Sulfide minerals exhibit a concentric zoning pattern in the Beaver Mountains (fig. 4), as discussed in the next section.

Vein abundances vary from one vein per 30 m up to 6-10 veinlets (<1 cm wide) per meter over 30 m intervals. Veins have vuggy, white quartz centers usually with open spaces partially filled by euhedral or drusy quartz crystals. The vein margins consist of black, fine-grained to massive tourmaline. Some veins have a distinct banded structure, with tourmaline and quartz composing rhythmically alternating bands. Axinite, when present, is almost always moderately to coarsely crystalline, and is paragenetically later than tourmaline and possibly contemporaneous with quartz. When sulfides are visible in hand samples, they are commonly restricted to the center of veins and are usually accompanied by abundant gossaneous, orange to red iron oxides.

Lilac to violet-gray axinite is generally present in narrow veinlets with quartz and occasionally with tourmaline. Veinlets are found in plutonic and volcanic rocks in the central Beaver Mountains. Axinite-dominant veins or axinite-altered rocks do not contain sulfides and are not anomalous in gold or other metals. Axinite also occurs as clots and appears to selectively replace feldspar phenocrysts in igneous rocks, especially quartz-trachytic and trachytic-volcanic dikes. Igneous rocks with phenocryst-like axinite clots also commonly contain axinite veinlets. It does not appear that this is primary (igneous) axinite, as has been suggested for similar occurrences to the southwest in the Russian Mountains (Hietanen and Erd, 1978).

Quartz-tourmaline veins and veinlets are ubiquitous throughout the Beaver Mountains. Prospects commonly consist of a series of veins, or less commonly breccias, with quartz and tourmaline ± axinite gangue and sulfides, including chalcopyrite, arsenopyrite, galena, sphalerite, and minor tennantite. Generally, anomalous gold values are only found in quartz-tourmaline veins that contain sulfides or abundant iron oxides. Veins and breccias are usually localized in fault zones or in igneous breccias in cupolas of the Beaver Mountains stock (Bundtzen and Gilbert,

Table 1. *Major oxides, CIPW norms, and trace-element analyses of selected plutonic rocks from the Beaver Mountains*[a]

Map no.	73	74	75	76	77	78	79	80	81	82	83	84	85	86	87	89	90
Sample no.	90ZBM1008	90ZBM1009	90ZBM1010	90ZBM1011	90ZBM1012	90ZBM1014	90ZBM1016	90ZBM1017	90ZBM1018	90ZBM1021	90ZBM1024	90ZBM1025	90ZBM1027	90ZBM1028	90ZBM1029	90ZBM9561	90ZBM9644
Field name	monzonite 1	monzonite 2	monzonite 1	tourmaline monzonite 2	monzonite 2	porphyry monzonite 1	monzonite 1	mafic monzonite 1	monzonite 1	monzonite 1 porph	aplite dike	porphyry monzonite 2	monzonite 2	monzonite 2	monzonite 2	pegmatite	monzonite 2
Rock type	TKqm	TKqm	TKqm	tourmaline TKqm	TKqm	TKg	TKqm	TKqm	TKqm	TKqm	TKg	TKqm	TKg	TKqm	TKqm	TKag	TKqm
SiO_2	59.80	59.70	61.80	73.81	61.40	64.00	62.60	57.70	58.70	62.97	71.85	61.01	63.20	59.70	58.90	74.74	61.50
TiO_2	0.58	1.01	0.73	0.85	0.72	0.63	0.52	0.90	0.95	0.62	0.28	0.72	0.60	0.89	0.86	0.18	0.75
Al_2O_3	13.77	15.70	15.90	14.31	15.00	14.80	19.10	15.90	16.10	16.06	14.10	15.94	14.60	15.40	16.50	12.75	15.70
Fe_2O_3	1.20	1.39	1.41	3.52	1.68	1.47	1.19	2.06	0.65	0.69	0.92	1.72	0.44	1.28	0.97	0.96	1.48
FeO	3.10	3.85	3.30	total	3.00	3.40	1.05	3.35	4.65	3.47	1.67	3.60	3.20	4.35	4.20	1.54	3.15
MnO	0.10	0.11	0.11	0.10	0.90	0.10	0.40	0.11	0.11	0.60	0.40	0.12	0.80	0.11	0.11	0.30	0.90
MgO	3.31	2.76	2.61	3.12	3.19	2.85	0.98	3.78	3.08	3.01	0.48	3.56	2.88	3.62	3.31	0.17	3.16
CaO	4.34	4.37	3.85	0.84	4.25	3.60	3.84	4.70	4.40	3.17	0.98	3.27	3.51	5.00	4.96	0.37	3.89
Na_2O	2.52	2.82	2.71	0.70	3.06	2.67	3.42	2.66	3.16	3.16	2.88	2.82	2.96	2.58	3.40	2.56	3.11
K_2O	4.24	4.88	5.10	0.47	4.70	4.55	5.32	4.95	4.80	4.31	6.27	4.77	4.40	4.46	4.54	6.52	4.75
P_2O_5	0.35	0.47	0.23	0.23	0.37	0.30	0.41	0.31	0.39	0.22	0.60	0.28	0.48	0.45	0.35	0.10	0.19
LOI[b]	**4.36**	1.22	1.49	**2.00**	1.19	1.08	1.01	**2.54**	0.81	1.30	0.10	1.40	1.36	0.73	0.78	-0.10	1.65
Total	97.67	98.28	99.24	99.86	98.65	99.45	99.48	98.96	97.80	99.04	99.63	99.21	97.71	98.57	98.88	99.73	99.42
CIPW Norm (+)																	
Quartz	16.15	11.39	13.88	63.57	12.87	18.55	13.96	8.28	7.03	15.57	27.72	13.20	17.35	11.45	5.99	33.12	12.10
Corundum	0.00	0.00	0.00	11.94	0.00	0.00	1.74	0.00	0.00	0.98	0.94	0.88	0.00	0.00	0.00	0.83	0.00
Orthoclase	26.85	29.71	30.83	2.84	28.50	27.33	31.93	30.34	29.24	26.06	37.23	28.82	26.99	26.94	27.35	38.59	28.71
Albite	22.85	24.58	23.46	6.06	26.57	22.97	29.39	23.34	27.57	27.36	24.48	24.39	25.99	22.31	29.32	21.70	26.91
Anorthite	14.72	16.25	16.53	2.73	13.66	15.21	16.63	17.45	16.05	14.62	4.49	14.71	14.07	17.65	16.67	1.77	15.19
Nepheline	0.00	0.00	0.00	0.00	0.00	0.00	0.00	0.00	0.00	0.00	0.00	0.00	0.00	0.00	0.00	0.00	0.00
Diopside	4.77	2.39	1.20	0.00	4.42	0.78	0.00	3.71	3.15	0.00	0.00	0.00	0.61	3.83	4.97	0.00	2.65
Hypersthene	10.74	10.51	10.05	7.95	9.21	11.08	2.64	11.27	13.20	12.67	3.13	13.38	11.99	13.14	11.78	2.22	10.34
Olivine	0.00	0.00	0.00	0.00	0.00	0.00	0.00	0.00	0.00	0.00	0.00	0.00	0.00	0.00	0.00	0.00	0.00
Magnetite	1.86	2.08	2.09	0.98	2.50	2.17	1.75	3.10	0.97	1.02	1.34	2.55	0.66	1.90	1.43	1.39	2.19
Ilmenite	1.18	1.98	1.42	1.65	1.40	1.22	1.00	1.77	1.86	1.20	0.53	1.40	1.18	1.73	1.66	0.34	1.46
Apatite	0.82	1.06	0.51	1.73	0.83	0.67	0.91	0.70	0.88	0.49	0.13	0.63	1.09	1.00	0.78	0.20	0.42
Hematite	0.00	0.00	0.00	0.51	0.00	0.00	0.00	0.00	0.00	0.00	0.00	0.00	0.00	0.00	0.00	0.00	0.00
D.I.	65.86	65.69	68.17	72.48	67.94	68.85	75.27	61.95	63.84	68.98	89.43	66.41	70.33	60.70	62.66	93.41	67.72
Trace Element Analyses[c]																	
Ba, ppm	1300	1600	1700		1400	1300	2500	1800	1600	1638	445	1859	1300	1700	1700	113	1300
Nb, ppm	19	20	15	23	21	22	14	16	23	21	29	20	16	26	20	20	19
Y, ppm	18	23	20	9	19	21	11	15	19	15	7	18	17	22	20	18	21
Zr, ppm	189	254	283	179	243	249	58	114	229	212	213	253	210	185	222	229	245
Sr, ppm	447	516	515	254	422	410	740	524	509	512	140	464	446	559	552	46	438
Rb, ppm	231	254	232	na	252	255	259	192	261	na	na	na	216	238	231	na	269

[a]Samples analyzed by Bondar-Clegg & Co. Ltd..,Vancouver, B.C., Canada, except underlined values analyzed by ACME Analytical Co. Vancouver, B.C., Canada. Bondar-Clegg Co. analyses done by borate fusion extraction followed by ICP. All FeO analyses done by the titrametric method.
[b]Boldface LOI values are higher than generally accepted.
[c]Trace Element Analyses are by XRF method.
LOI = Loss on ignition.
D.I. = Differentiation index.
na = Not analyzed.

1983). Some of the best gold mineralization associated with quartz-tourmaline veining occurs at contacts between rock units, especially at volcanic-plutonic contacts.

SULFIDE ZONING PATTERNS

There is a clear concentric zoning pattern of vein minerals in the Beaver Mountains, as displayed in figure 4. Quartz and tourmaline are present throughout the area. A zone of axinite veining is located near the center of the mineral zoning pattern and occupies about 25 km^2. Chalcopyrite is present in the same area and extends beyond the axinite zone over a 70 km^2 oval-shaped area. The arsenopyrite zone begins at the outer periphery of the chalcopyrite zone and occupies the zone farthest from the center. The arsenopyrite zone is not a complete concentric doughnut: it is present as two parts. The largest area is on the western side of the system and a smaller zone is on the southern side. The two arsenopyrite zones occupy a total area of about 27 km^2. Pyrite is a minor constituent in most veins, especially in veins with massive sulfide pods, where it is present as minor disseminations. The low abundance of other minerals, such as galena, sphalerite, or ankerite inhibit determination of other possible zoning patterns.

Most rock samples analyzed from the Beaver Mountains do not contain anomalous mercury. Samples with the highest Hg values (table 2) are from the Syenite Porphyry prospect on the northwestern margin of the Beaver Mountains (fig. 1). Mineralization at this prospect area consists of chalcedonic quartz veins, smoky and amethyst quartz veins, some possible cinnabar-rich sinter, and cinnabar + quartz cemented breccia with moderate Au values. Iron oxides are present with fine-grained cinnabar, and plutonic rock breccia clasts have been completely argillized. Tourmaline has not been found at the Syenite Porphyry prospect. Samples with the highest gold values contain iron staining, gossaneous earths and boxworks (samples 90Z9541 and 90Z9542, table 2).

Cinnabar mineralization at the Syenite Porphyry prospect implies a shallow structural level of emplacement, distal to mineralization position, or a late-stage mineralizing event. This area of cinnabar-quartz sinter on the northwestern side of the Beaver Mountains may be related to a second, younger, hydrothermal system. If so, the Hg-(Au)-rich system is much smaller than the B-Cu-Pb-Zn-Fe-(Au)-(Ag) system. The lack of a concentric zoning pattern (that is, no other known mercury-rich areas peripheral to the core of the Beaver Mountains) and lack of tourmaline (ubiquitous throughout the rest of the Beaver Mountains) indicate that it is less likely that the cinnabar-rich area is part of the larger B-Cu-Pb-Zn-Fe-(Au)-(Ag) system.

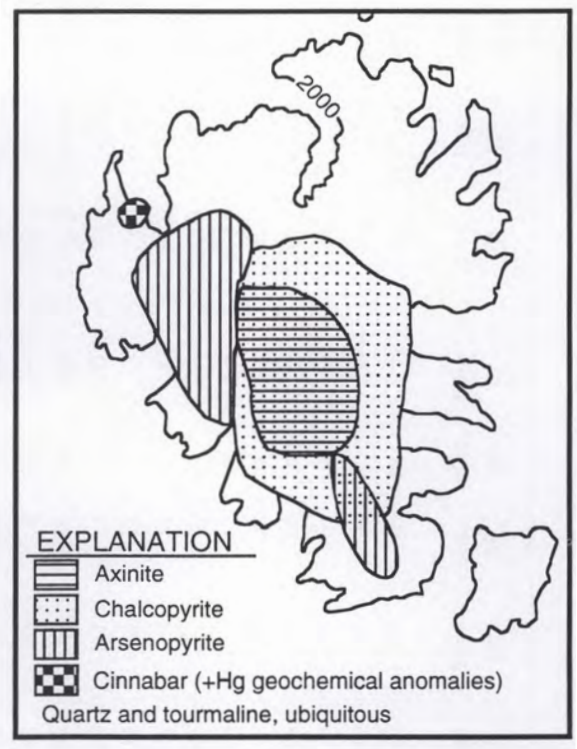

Figure 4. *Vein mineral zoning in the Beaver Mountains. Area is the same as that shown in figure 1. The Beaver Mountains are outlined by the 2,000-foot contour line. The axinite zone includes veining with axinite, or axinite + chalcopyrite. Other minerals, such as sphalerite and galena, may form zones beyond those shown, but there are not enough data to determine these zones.*

SOUTH QUARTZ ZONE PROSPECT

The most significant lode prospects in the Beaver Mountains are in an area informally named the South Quartz zone. The South Quartz zone encompasses approximately 12 km^2 on the southern edge of the Beaver Mountains (fig. 1) and includes the Cirque deposit (Bundtzen and Laird, 1982) and several previously unknown prospects. Mineralization appears to be controlled by at least four discrete structural zones with northeasterly trends that approximately parallel the Iditarod-Nixon Fork fault. Quartz veining has been traced for 1.2 and 2.4 km along the strike of two of these zones.

As in the rest of the Beaver Mountains, veins in the South Quartz zone weather easily and usually have a negative topographic expression. Quartz-bearing structures include zones of silicification, microveinlets, and veins to about a meter wide. Several veins in outcrop trend N. 30° E. with vertical dips. Mineralized float distribution suggests that mineralization may be more than 180 m wide, with discrete veins as wide as 3 m.

Table 2. *Trace-element determinations from mineralized samples in the Beaver Mountains*

Map no.	Sample[a] no.	Sample type	Au ppb	Ag ppm	Cu ppm	Pb ppm	Zn ppm	Mo ppm	As ppm	Sb ppm	Hg ppb	Sn ppm
1	BM-PC1	Heavy-mineral concentrate	400	na	na	na	na	na	na	na	na	na
2	BM-PC2	Heavy-mineral concentrate	385	na	na	na	na	na	na	na	na	na
3	BM-PC3	Heavy-mineral concentrate	880	na	na	na	na	na	na	na	na	na
4	BM-PC4	Heavy-mineral concentrate	215	na	na	na	na	na	na	na	na	na
5	BM-PC5	Heavy-mineral concentrate	220	na	na	na	na	na	na	na	na	na
6	90Z9547	Quartz veinlets in fault zone	757	26.8	38	1,598	711	4	>2,000	913.0	537	19
7	90R9967	Quartz-veined breccia with iron oxides	879	39.4	1147	229	150	9	288.0	111.3	7,875	16
8	90Z9539	Quartz float	<5	<0.2	15	7	32	2	45	<5.0	>50,000	<5
8	90Z9540	Silicified breccia with cinnabar and iron oxides	<5	<0.2	14	7	38	1	30.5	6.1	>50,000	<5
8	90Z9541	Smoky-quartz float with iron oxides	696	<0.2	4	3	7	5	10.3	10.0	12,792	<5
8	90Z9542	Iron-oxide stained chalcedonic quartz	1,266	3.5	22	25	25	28	305.1	1,549.1	>50,000	28
8	90R9938	2 in.-wide quartz vein	1,960	3.9	12	13	8	13	191.3	1,896.4	22,025	37
8	90R9943	Cinnabar-rich sinter	39	0.3	59	14	94	3	896.8	26.0	>50,000	<5
8	90R9944	Amethyst vein with 2 in. long crystals	1,721	0.3	5	9	6	1	5.2	7.1	11,011	<5
8	90R9945	Quartz float	8	<0.2	10	20	30	2	48.6	7.3	>50,000	7
9	90Z9543	Quartz-vein float	<5	<0.2	49	8	103	3	71.1	25.1	>50,000	<5
10	90R9979	Massive arsenopyrite with pyrite, minor quartz	9,613	100.5	927	4,372	4,251	11	1,911.6	214.8	1,293	<5
10	90R9981	Quartz vein with pyrite, galena, & arsenopyrite	2,185	18.1	341	2,517	761	32	228.1	85.0	1,070	<5
10	90R9983	Silicified andesite with arsenopyriterite and iron oxides	12,994	317.8	1,423	9,835	4,394	23	>2,000	621.2	3,849	9
10	90R9984	Massive milky quartz and arsenopyrite vein	11,623	58.6	685	8,937	1,915	29	>2,000	336.2	2,733	13
11	90R9988	Massive arsenopyrite and galena float	722	86.1	3,129	12,400	8,547	9	>2,000	201.1	1,986	10
12	90R9825	Massive sulfide float	458	32.8	1,636	2,888	611	3	>2,000	120.0	314	9
12	90Z9682	Massive sulfide float	927	29.8	719	5,894	426	3	>2,000	400.4	6,146	81
13	90Z9594	Quartz-tourmaline-pyrite veined intrusive	151	58.3	139	4,453	2,975	22	>2,000	108.5	3,690	53
13	90Z9596	Quartz-tourmaline-pyrite veined intrusive	11	4.0	15	688	244	8	480.7	45.6	190	26
13	90Z9598	Quartz-tourmaline-arsenopyrite-galena veins	1,137	86.1	657	20,300	1,085	6	>2,000	773.0	3,166	49
13	90Z9601	Tourmaline-quartz-iron oxides-arsenopyrite veined syenite	285	10.7	130	1,763	262	7	>2,000	125.3	684	34
14	90Z9633	10 ft zone quartz-tourmaline-chalcopyrite veinlets	43	60.0	10,359	108	247	3	94.9	11.1	338	73
15	90Z9588	Quartz-tourmaline-chalcopyrite-iron oxides veined intrusive	28	37.5	6,906	21	21	4	937.7	12.5	625	35
16	90Z9638	Tourmaline-quartz-sulfide-iron oxides veinlets	91	129.9	4,879	17,100	17,855	14	>2,000	103.1	1,086	<5
17	90Z9578	Axinite-quartz-tourmaline veined andesite	<5	0.4	24	28	47	<1	21.5	84.7	<10	19
18	90R9894	Crystalline quartz vein	52	71.0	1,624	481	213	3	157.6	18.6	10,106	53
18	90R9889	10-ft-wide quartz veins, breccia, stockwork	10,697	5.7	57	97	38	6	76.0	12.7	368	57

18	90Z9692	Quartz-tourmaline vein	391	>50	2,879	983	140	4	380.8	368.2	4,206	90
19	90R9927	5-in.-wide quartz vein	228	10.1	249	1,231	196	5	714.8	507.9	94	<5
20	90R9913	0.5-ft-iron oxides-quartz-arsenopyrite massive vein	1,730	78.2	589	3,619	328	4	>2,000	467.1	650	9
21	90R9915	Iron-oxides stained andesite with arsenopyrite	601	12.8	489	910	2,527	5	>2,000	115.6	201	7
21	90R9917	0.5-ft-wide iron oxide-quartz-sulfide vein	835	87.1	761	16,100	6,232	7	>2,000	319.3	712	14
22	90Z8481	Iron-oxide stained soil and rock chips	418	1.1	78	15	65	3	1,594.0	38.4	3,266	<5
23	90Z8494	Iron-oxide stained tourmaline-quartz vein	143	185.1	3,346	9,408	2,712	29	>2,000	56.6	2,709	94
23	90Z8495	Iron-oxide stained silicified and quartz vein	435	78.9	1,348	18,100	10,565	11	1,687.8	509.4	2,083	38
24	90Z8496	Quartz veined volcanic with gossan	309	100.8	706	25,400	2,278	8	>2,000	280.5	2,929	40
25	90Z8453	Quartz-tourmaline-axinite-sulfide vein	23	52.5	3,212	15,300	3,725	9	121.6	79.1	2,811	na
26	90R9923	30-ft-wide quartz-arsenopyrite veined syenite	322	22.4	166	1,215	763	4	>2,000	86.3	75	<5
26	90R9925	Quartz vein	220	2.3	11	558	645	3	>2,000	43.5	42	9
27	90R9823	Gossany quartz veins with arsenopyrite and chalcopyrite	941	>50	1,180	>10,000	1,173	130	>2,000	904.6	>50,000	68
27	90R9474	Gossany quartz vein with arsenopyrite and chalcopyrite	879	88.5	1,028	31,600	1,784	75	>2,000	646.6	3,482	na
27	90R9475	Porphyritic syenite	<5	0.4	52	10	60	3	26.7	5.4	<10	na
28	90Z9505	Gossaneous quartz-sulfide vein	266	43.4	1,001	16,400	14,756	25	>2,000	228.0	805	42
29	90Z9510	Quartz vein	81	89.8	52,000	189	178	8	214.1	147.0	454	22
32	90Z9677	Quartz-chalcopyrite-pyrite breccia	236	12.0	261	259	44	<1	1,313.8	120.8	2,267	9
32	90Z9679	Quartz-chalcopyrite-pyrite breccia	67	31.2	2,228	199	182	<1	641.7	171.2	2,866	8
32	90Z9741	40-ft-wide silicified breccia with iron oxide staining	3,958	41.1	na	na	na	na	na	na	na	<5
3290Z9742Quartz veins and breccia with sphalerite and malachite			100	0.8	na	na	na	na	na	na	na	23
3290Z974340-ft-wide silicified breccia with iron oxide staining			164	2.9	na	na	na	na	na	na	na	15
3390J8209Quartz-tourmaline-chalcopyrite veined lapilli tuff			1,569	194.0	2,715	5,449	304	12	122.8	22.3	462	na
34	90J8223	Quartz stockworks with iron oxide	287	6.2	52	1,175	1,910	3	758.2	11.8	1,259	7
35	90Z6613	Quartz vein	204	1.6	7	na	na	na	na	na	na	na
36	90Z6614	Scorodite-stained quartz vein in argillized volcanic	935	<5	na	na	na	na	na	na	na	na
89	90Z9561	Pegmatite dike	<5	<0.2	4	10	12	1	<5.0	<5.0	40	10
78	90Z8432	Altered porphyritic monzonite 1	<5	<0.2	7	12	47	<1	<5.0	<5.0	<10	na
78	90Z8433	Equigranular monozonite 1	<5	<0.2	21	13	36	<1	7.9	5.5	29	na
90	90Z9644	Monzodiorite porphyry	<5	<0.2	15	<2	17	<1	22.6	<5.0	46	<5

[a]Samples were analyzed by Bondar-Clegg & Co. Ltd., Vancouver, B.C., Canada. Au analyzed by fire assay AA; Ag, Cu, Pb, Zn, Mo, As, and Sb by induced coupled plasma (ICP); Hg by cold vapor AA; and Sn by XRF. The lower detection limits are Au-5 ppb, Ag-0.2 ppm, Cu-1 ppm, Pb-2 ppm, Zn-1 ppm, Mo-1 ppm, As-5.0 ppm, Sb-5.0 ppm, Hg-10 ppb, and Sn-5 ppm. Values above 50 ppm Ag, 20,000 ppm Cu, 10,000 ppm Pb, and 10,000 ppm Zn analyzed by atomic absorption.Values above 10,000 ppb Au analyzed by fire assay.
na = Not analyzed.

Mineralization at the Cirque deposit consists of tourmaline-axinite-fluorite[2] breccia zones with chalcopyrite, minor galena, and sphalerite; and massive sulfide zones containing greater than 30 percent sulfides cut by quartz-tourmaline-axinite veinlets (Bundtzen and Laird, 1982). Bundtzen (oral commun., 1991) reported that chalcopyrite and bornite are present in topographically lower exposures of the Cirque deposit

The South Quartz zone prospect contains several rock units (fig. 2), the most extensive are porphyritic basaltic andesite and monzonite-2 porphyry. All igneous rock units within the prospect area are propylitically altered. Volcanic rocks possess a chloritized groundmass and slight to moderate sericitic replacement of plagioclase phenocrysts. Plutonic rocks have sericitic alteration of plagioclase and potassium feldspar phenocrysts and partial alteration of clinopyroxene and biotite to a mixture of amphibole, chlorite, epidote, and iron oxides. Propylitized basaltic andesite contains up to 0.5 percent fine-grained disseminated pyrite.

The nature of the host rock controls the character of quartz veining. Quartz-vein mineralization in the more massive volcanic units varies from thin stringers and veinlets of waxy green quartz (vein assemblage of chlorite-calcite-epidote-quartz) to 1.5-m-wide massive to drusy quartz veins. Some of the larger veins have chlorite-epidote alteration halos up to 30 cm wide. Veining in the porphyritic andesite consists of sparse to dense quartz stockworks.

Veins in the South Quartz zone change character across the width of the mineralized zone from vuggy quartz to vuggy quartz veins with silicified wall rocks to vuggy quartz with galena (or supergene pyromorphite) to vuggy quartz with chlorite. Small patches of silicified breccia are also present in the South Quartz zone. The best exposed breccia is adjacent to a propylitized trachytic dike. The highest grade and most mineralized breccia is commonly iron oxide and jarosite stained, with very fine-grained, disseminated pyrite and minor galena (sample 9526, table 2).

Most elements considered as pathfinder (characteristic of hydrothermal gold deposits) are present in elevated concentrations for most vein samples collected in the South Quartz zone prospect. Results from 180 rock samples collected in the South Quartz zone averaged 248 ppb Au (unpub. data, 1991 Battle Mountain Exploration Co. report). Pathfinder element concentrations from channel or representative grab samples from the most mineralized areas range up to 19 ppm Au, 1,106 ppm Ag, 21.05 percent Cu, 12,150 ppm As, 13,344 ppm Sb, 10.45 percent Pb, 2,000 ppm Bi, and 100 ppm Sn. Individual sample results and brief descriptions are listed in table 2.

In several other parts of the Beaver Mountains (for example, sample 90R9889, fig. 1, table 2) thick quartz veins are present along contacts between andesite and monzonite. Contacts between plutonic rocks and any other rock type contain the most alteration and some of the highest grade mineralization. Vein abundance is greatest in the contact areas and generally decreases systematically away from the contact. The volcanic rocks in these areas may act as a cap to the hydrothermal fluids, a conclusion also reached by Bundtzen and Gilbert (1983) for the Cirque and Tolstoi deposits. However, in most places in the Beaver Mountains, veins are just as common in volcanic rocks as in surrounding plutonic rocks. The capping could be due to a number of factors that differ between the andesite and the monzonite, including differences in fracturing (pattern and intensity) and composition.

DISCUSSION

Similar to other volcano-plutonic complexes in the Kuskokwim region, field relationships, rare-earth element patterns, and radiometric dating suggest that volcanic and plutonic rocks in the Beaver Mountains are comagmatic (Moll and others, 1981; Bundtzen and Laird, 1982; Bundtzen and Laird, 1991; Szumigala, 1993). The porphyritic texture of the stocks and absence of xenoliths suggest that intrusions were emplaced at shallow depths with minimal wallrock interaction. Regional structures may have controlled emplacement of the Beaver Mountain stocks. Similar controls have been suggested to explain localization of stocks near Flat in the southwestern Iditarod Quadrangle (Bundtzen and others, 1992). Miller and Bundtzen (1992) propose that the Yankee-Ganes Creek fault projects beneath the Beaver Mountains, and this fault could have influenced emplacement of the volcano-plutonic complex.

Hydrothermal tourmaline breccias in the Beaver Mountains are similar to Chilean deposits described by Sillitoe and Sawkins (1971), Boyle (1979), and Colley and others (1989). The Chilean deposits in cross section are shaped like inverted cones. This type of breccia has been interpreted to represent the explosive release of volatiles during transition from magmatic to hydrothermal stages of evolution of a pluton (Jackson, 1979).

Axinite occurrences in plutonic rocks in the Russian Mountains south of the Beaver Mountains have been interpreted by other workers to be primary (Hietanen and Erd, 1978; Bundtzen and Laird, 1991). Axinite and tourmaline in igneous rocks in the Beaver Mountains are of replacement origin. In either case, the presence of axinite and ubiquitous tourmaline imply that the hydrothermal system in the Beaver Mountains, and possibly the magma, was boron-rich.

[2]Fluorite identified by Bundtzen and Laird, 1982, but not identified in samples collected during this study.

VEIN-MINERAL ZONING

Most mineralization in the Beaver Mountains is the result of one large hydrothermal system. This relationship is indicated by the distinct zoned distribution of vein minerals (fig. 4). The gross mineral zoning in veins represents two superimposed zoning patterns, one for boron-bearing silicates and one for sulfides. The first zoning pattern is the change from axinite-dominant veins with minor tourmaline to tourmaline-rich veins and breccias without axinite in outlying areas.

The change from axinite[3] to tourmaline[4] reflects the intensity of boron metasomatism. The basic difference between axinite and tourmaline is that axinite (B:Al:Si = 3:2:3) has twice as much B for a given Al or Si than tourmaline (B:Al:Si = 3:7:6). This difference in B content also accounts for axinite being paragenetically later than tourmaline. The addition of more BO_3 to a tourmaline-rich rock results in the replacement of tourmaline by axinite.

Vein mineral zoning is the key evidence that mineralization in the Beaver Mountains (or at least the southern half of the Beaver Mountains) is related to one large hydrothermal system. The sulfide zoning pattern can be understood in the Cu-Fe-As-S system in terms of a continuous variation in activity of arsenic (a_{As}) or fugasity of sulfur (f_{S_2}). The phase equilibria diagram of Gustafson (1963) for the Cu-Fe-As-S system is shown in figure 5. In the Beaver Mountains veins in the central zone are dominantly chalcopyrite, with minor amounts of pyrite. There is an overlap of the chalcopyrite and arsenopyrite zones, outside of which arsenopyrite is present without chalcopyrite. This progression is represented in figure 5 by the solid arrows in three parts of the Cu-Fe-As-S system. The mineral changes can occur at constant log f_{S_2}, with a progressive increase in log f_{AS2}. The presence of bornite at the Cirque deposit may indicate that the middle phase diagram is most appropriate. Figure 5 also indicates that tennantite may be a stable mineral in parts of the arsenopyrite zone, and it is present in at least one vein in the southern Beaver Mountains.

Metal zoning, such as that described in this study, has been documented in a number of mining districts, such as Butte, Montana (Meyer and others, 1968), Cornwall, England (Davidson, 1927; Hosking, 1964: and Jackson, 1979), and Bingham, Utah (Moore and Nash, 1974; John, 1978; Tooker, 1990). A generalized sequence of ore mineral zoning for hydrothermal deposits by Barnes (1975) is based largely on these classic ore deposits. In this sequence, zoning proceeds from earliest (most central) outward as: molybdenite-arsenopyrite-pyrrhotite-pentlandite-stannite-chalcopyrite-sphalerite-tetrahedrite-galena-acanthite-gold tellurides-stibnite-cinnabar. This is a composite sequence and no single deposit presents the entire idealized sequence.

The Cornwall district has often been cited as the classic example of metal zoning at both local and district scales. At Cornwall, the zoning pattern from deepest to shallowest (perpendicular to paleoisothermal surfaces) is tin, copper, lead-zinc, and iron (Mn, Sb) sulfosalt; and extends from the intrusion to beyond the metamorphic aureole (Davidson, 1927; Hosking, 1951). Mineralization at Cornwall (Jackson, 1979), as well as in many other mining districts is recognized as polyphase, rather than a simple, single metallogenic event.

At Cornwall, joint systems within granitic intrusions control the orientation and distribution of fissure veins (Jackson, 1979). Most fractures that host mineralization are steeply dipping and oriented parallel to the axis of the Cornubian batholith; the emplacement of the batholith was controlled by the regional stress field (Jackson, 1979). Similar evidence from the Beaver Mountains also suggests a regional stress control on emplacement of the stocks and orientation of the veins.

GOLD DEPOSITS

Gold deposits exist at many different structural levels within igneous systems. The South Quartz zone occurs in and above the uppermost part of the Beaver Mountains plutonic system. Much of the central Beaver Mountains volcanic edifice was eroded during glaciation. Mineralization from areas similar to the South Quartz zone may be the source of much or all of the placer gold in the Innoko mining district. The best chance for development of economic lode gold deposits in the Beaver Mountains area would be around, at, or near the plutonic-volcanic contact, such as in the South Quartz zone. The contacts could serve as loci for mineralizing fluids.

Other possible lode gold occurrences could be hidden beneath volcanic rocks or the extensive till surrounding the Beaver Mountains. The volcanic rocks may cover coeval plutonic rocks and possible associated mineralization.

Ore deposits in the Kuskokwim region are exposed at several erosional levels of vertically zoned hydrothermal systems. Bundtzen and Miller (1989, 1992) have suggested that metal zonation in Kuskokwim igneous complexes progresses from Hg-Au-Sb near the surface to As-W-Au-Sb at mid levels to Sn-U-Bi-B-Zn in the deepest structural zones within igneous complexes. A Kuskokwim region ore deposit model proposed by Szumigala (1993) generally agrees with the model by Bundtzen and Miller (1989, 1992). If the above models are correct, then the occurrence

[3] $(Ca, Fe, Mn, Mg)_3Al_2(BO_3)(SiO_4)3(OH)$

[4] $(Na, K, Ca)(Mg, Fe, Mn, Li, Al)_3(Al, Fe, Cr, V)_6(BO_3)_3Si_6O_{18}(OH)_4$

of cinnabar mineralization and chalcedonic quartz veins with moderate gold concentrations at the Syenite Porphyry prospect may overlie additional gold resources.

COMPARISON OF BEAVER MOUNTAINS MINERALIZATION WITH OTHER PLUTON-HOSTED MINERALIZATION

Mineralization in the Beaver Mountains is similar to other pluton-hosted occurrences in the Kuskokwim region, including the Russian Mountains (Bundtzen and Laird, 1991), the Golden Horn Mine and associated prospects at Flat (Bundtzen and others, 1992), and the Nixon Fork mines (Herreid, 1966). The Beaver Mountains mineralization is most similar to occurrences in the Russian Mountains, northeastern Russian Mission Quadrangle, Alaska, described by Bundtzen and Laird (1991). Mineralization in the Russian Mountains is hosted by intrusive rocks, and consists of quartz-tourmaline-axinite-sulfide veins with significant concentrations of gold and arsenic and anomalous amounts of antimony, tin, zinc, bismuth, lead, tungsten, uranium, and cobalt (Bundtzen and Laird, 1991). Descriptions of vein mineralogies, morphologies, and parageneses by Bundtzen and Laird (1991) are almost identical to veins examined in the Beaver Mountains.

Many of the characteristics observed at prospects in the Beaver Mountains are also present in disseminated and stockwork gold-silver deposits in intrusive rocks. Boyle (1979, p. 295-301) briefly described several examples of pluton-hosted precious metal deposits that contain tourmaline associated with quartz stringers, veins, or breccias (examples include the Abitibi region of Quebec, Canada, Chilean breccia pipes, and the Klychi gold deposit in the eastern Transbaikal region of the former USSR). Ore minerals in each of these examples are dominated by pyrite and chalcopyrite and in most cases are associated with arsenopyrite and native gold.

Veins at the Broken Shovel prospect (Moore Creek) are similar in terms of mineralogy, structural style, and metal content to the Beaver Mountains veins. Results from fluid inclusion studies of the Broken Shovel veins may help establish some constraints on conditions for the formation of the Beaver Mountain veins. Homogenization temperatures of quartz fluid inclusions from the Broken Shovel prospect range from 254° to 380°C and average 297°C (n = 14) (Bundtzen and others, 1988). These homogenization temperatures are lower than those measured in many porphyry copper deposits (Roedder, 1984), but within the range of temperatures for veins peripheral to the porphyry deposits.

Alaska has three distinct porphyry copper provinces: the Yukon-Koyukuk plutonic belt (previously called the Hogatza plutonic belt), the Continental margin belt, and the Interior belt. The Beaver Mountains are located about halfway between the Yukon-Koyukuk plutonic belt and the Continental margin belt (Hollister, 1978, figure 27).

Porphyry copper deposits in the Yukon-Koyukuk Plutonic belt are associated with porphyritic, multiphase intrusives radiometrically dated at about 80-82 Ma (Miller and others, 1966; Miller, 1972). Ore is closely related spatially and temporally to a quartz-bearing monzonite phase (Hollister, 1978). Usually mineralized intrusions are oval, apparently forcefully injected, and epizonal. The mineralized intrusions are restricted to the youngest period of plutonic activity, whereas older, silica undersaturated plutons with alkalic affinities tend to be unmineralized (Miller and others, 1966). Hornblende is present in each mineralized pluton. Argillic, phyllic, and propylitic alteration assemblages appear in all deposits, but no potassic zone has been identified in any deposit within the Hogatza Plutonic belt. These alteration zones follow Lowell and Guilbert's (1970) model fairly closely (Hollister, 1978). Pyrite forms halos at all deposits, with an associated distinct color anomaly. Mineralization is dominantly copper with associated molybdenum (Hollister, 1978). Some deposits have zoned peripheral zinc, lead, silver, and gold veins on their margins. Tourmaline may be present as an alteration product such as rosettes replacing magmatic ferromagnesian silicates in igneous rocks, as vein fillings with other silicate and sulfide minerals, as a constituent cementing breccia fragments, or as an apparent magmatic mineral in aplite dikes (Miller and Ferrians, 1968).

Plutonic rocks in the Beaver Mountains have many characteristics similar to plutons in the Yukon-Koyukuk plutonic belt, such as multiphase intrusions, porphyritic textures, dominantly quartz monzonite compositions, and tourmaline as an alteration product. One obvious difference is the lack of hornblende in the Beaver Mountains plutonic rocks. The Beaver Mountains plutonic rocks also have lower oxidation states than typical porphyry plutonic rocks (Szumigala, 1993).

Other evidence suggests that mineralization in the Beaver Mountains is not similar to porphyry copper systems. Porphyry style mineralization and zoned alteration patterns have not been recognized in the Beaver Mountains. Preliminary qualitative studies of fluid inclusions in quartz from Beaver Mountains veins indicate that fluid inclusions are usually small, liquid-rich inclusions with no to slight amounts of vapor and no daughter crystals. Samples from the Syenite Porphyry prospect (associated with the mercury anomalies) have extremely abundant, planarly arranged fluid inclusions that are mostly liquid with little vapor. These types of fluid inclusions are similar to liquid-rich, moderate salinity inclusions that are associated with peripheral vein mineralization from some porphyry copper deposits (Nash, 1976; Spooner, 1981),

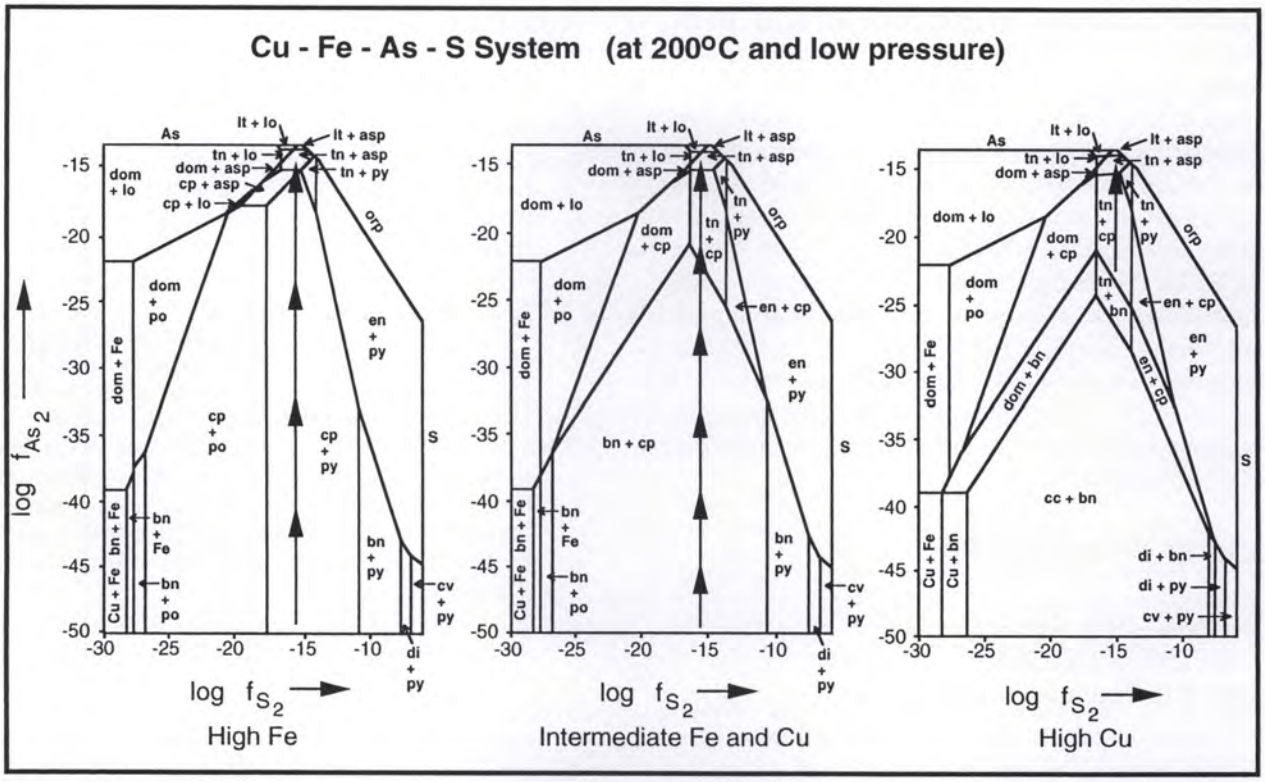

Figure 5. *Phase equilibria for the Cu-Fe-As-S system. From left to right the diagrams are the high-iron, intermediate-iron and copper, and high-copper portions of the system at 200°C and low pressure. Vertical arrows show suggested paths that could have been taken by hydrothermal fluids from the Beaver Mountains system. Abbreviations of the phases are: As = arsenic, Cu = copper, Fe = iron, S = sulfur, dom = domeykite, lo = loellingite, po = pyrrhotite, bn = bornite, cp = chalcopyrite, lt = lautite, tn = tennanite, asp = arsenopyrite, py = pyrite, orp = orpiment, en = enargite, di = digenite, cv = covellite, and cc = chalcocite. (Modified from Gustafson, 1963.)*

but these types of fluid inclusions are common in a wide range of environments. Fluid inclusions from peripheral veins are very different from inclusions from within the porphyry deposits. Fluid inclusions in most porphyry copper deposits are remarkably uniform with respect to high maximum temperatures, high salinities, and evidence of "boiling" (Roedder, 1984, p. 446), and usually contain daughter crystals (Spooner, 1981). No high-salinity fluid inclusions appear in Beaver Mountains samples, so a key aspect of porphyry-related mineralization is missing.

SUMMARY

The Beaver Mountains are a volcano-plutonic complex consisting of dominantly andesitic volcanic rocks and quartz monzonitic plutonic rocks. The plutonic rocks have contact metamorphosed nearby volcanic rocks and Kuskokwim Group sedimentary rocks. All igneous rock units have been ubiquitously altered by late hydrothermal fluids. It is possible that the Beaver Mountains may be the source of a significant portion of the placer gold in the Innoko mining district. The Beaver Mountains contain many areas with mineralized veins, stockworks, and breccias that have anomalously high Au, Ag, Cu, Pb, and As values.

Mineralization appears to be related to a large hydrothermal system. Sulfide mineral occurrences in the Beaver Mountains are zoned. The zoning is consistent with increasing activity of arsenic at constant temperature proceeding outward from the system center. Distinctive Hg-rich mineralization on the northwest side of the Beaver Mountains is most likely due to a separate and younger hydrothermal event.

Vein mineralization, vein character, and fluid inclusions from veins in the Beaver Mountains are similar to peripheral veins associated with some porphyry copper deposits. This study reveals that there may be other magmatic-hydrothermal systems in the Kuskokwim Mountains and that these systems may contain significant gold mineralization.

ACKNOWLEDGMENTS

This work is part of a doctoral dissertation completed at the UCLA Department of Earth and Space Sciences.

Doctoral committee members, especially Mark Barton, improved this paper by their review of earlier versions. I thank Don DePaolo for providing office and laboratory space at the Berkeley Center For Isotope Geochemistry. Discussions with Marti Miller (U.S. Geological Survey, Anchorage) and Tom Bundtzen (Alaska Division of Geological & Geophysical Surveys) added considerably to my understanding of the Kuskokwim region. Reviews by Rainer Newberry and Mark Robinson were greatly appreciated and improved this paper. Mapping and geochemical sampling by the author and Paul Racenet, with contributions by Joan Vallie Ruh, were conducted as part of an exploration program by Battle Mountain Exploration Company (BMEC) during three months of the 1990 field season.

REFERENCES CITED

Barnes, H.L, 1975, Zoning of ore deposits: Types and causes: Transactions of the Royal Society of Edinburgh, v. 69, p. 295-311.

Boyle, R.W., 1979, The geochemistry of gold and its deposits: [together with a chapter on geochemical prospecting for the element], Geological Survey of Canada Bulletin 280, 584 p.

Bundtzen, T.K., 1981, Multiple glaciation in the Beaver Mountains, western interior Alaska, *in* Short notes on Alaskan geology - 1979-80: Alaska Division of Geological & Geophysical Surveys Geologic Report 63, p. 11-18.

Bundtzen, T.K., Cox, B.C., and Veach, N.C., 1987, Heavy mineral provenance studies in the Iditarod and Innoko Districts, western Alaska, *in* Vassiloo, A.H., Hausen, D.M., and Carson, D.J., eds., Process Mineralogy VII: Warrendale, Pennsylvania, The Metallurgical Society, p. 221-245.

Bundtzen, T.K., and Gilbert, W.G., 1983, Outline of geology and mineral resources of upper Kuskokwim region, Alaska *in* Proceedings of the 1982 symposium on western Alaska geology and resource potential: Journal of Alaska Geological Society, v. 3, p. 101-117.

Bundtzen, T.K., and Laird, G.M., 1982, Geologic map of the Iditarod D-2 and eastern D-3 Quadrangles, Alaska: Alaska Division of Geological & Geophysical Surveys Geologic Report 72, 1 sheet, scale 1:63,360, 14 p.

_____1991, Geology and mineral resources of the Russian Mountain C-1 Quadrangle, southwest Alaska: Alaska Division of Geological & Geophysical Surveys Professional Report 109, 24 p. 2 sheets, scale 1:63,360.

Bundtzen, T.K., Laird, G.L., and Lockwood, M.L., 1988, Geologic map of the Iditarod C-3 quadrangle, Alaska: Alaska Division of Geological & Geophysical Surveys Professional Report 96, 16 p., 1 sheet, scale 1:63,360.

Bundtzen, T.K., and Miller, M.L., 1992, Petrology and metallogeny of Late Cretaceous-early Tertiary igneous rocks, Kuskokwim Mountains, Southwest Alaska: Geological Society of America Abstracts with Program, v. 24, no. 5, p. 11.

Bundtzen, T.K., and Miller, M.L., 1989, Geology and metallogeny of Cretaceous-early Tertiary volcanic and plutonic rocks of western Alaska: Circum Pacific Council on Energy and Mineral Resources Meeting, Kharbarovsk, USSR, 1989, 8 p.

Bundtzen, T.K., Miller, M.L., and Kline, J.T., 1985, Geology of heavy mineral placer deposits of the Iditarod and Innoko Precincts, western Alaska: *in* Proceedings of the 7th Annual Conference on Alaskan Placer Mining, Madonna, J.A., ed., Alaska Prospecting Co., Fairbanks, p. 35-41.

Bundtzen, T.K., Miller, M.L., Laird, G.M., and Bull, K.F., 1992, Geology and mineral resources of Iditarod mining district, Iditarod B-4 and eastern B-5 Quadrangles, southwestern Alaska: Alaska Division of Geological & Geophysical Surveys Professional Report 97, 46 p., 2 sheets, scale 1:63,360.

Colley, H., Treloar, P.J., and Diaz, F., 1989, Gold-silver mineralization in the El Salvador region, northern Chile, *in* Keays, R.R., Ramsay, W.R.H., and Groves, D.I., eds., The Geology of Gold Deposits: The Perspective in 1988: Economic Geology Monograph 6, New Haven, Economic Geology, p. 208-217,

Davidson, E.H., 1927, Recent evidence confirming the zonal arrangement of minerals in the Cornish lodes: Economic Geology, v. 22, p. 475-479.

Guilbert, J.M., and Park, C.F., Jr., 1986, The geology of ore deposits: New York, W.H. Freeman and Co., 985 p.

Gustafson, L.B, 1963, Phase equilibria in the system Cu-Fe-As-S: Economic Geology, v. 58, p. 667-701.

Herreid, Gordon, 1966, Geology and geochemistry of the Nixon Fork area, Medfra Quadrangle: Alaska Division of Geological & Geophysical Surveys Geologic Report. 22, 29 p.

Hietanen, A., and Erd, R.C., 1978, Ferroaxinites from the Feather River area, northern California, and from the McGrath and Russian Mission quadrangles, Alaska: U.S. Geological Survey Journal of Research, v. 6, p. 603-610.

Hollister, V.F., 1978, Geology of the porphyry copper deposits of the Western Hemisphere: New York, Society of Mining Engineers, 219 p.

Hopkins, D.M., Gray, J.E., and Slaughter, K.E., 1991, Low-level gold determinations by use of flow injection analysis-atomic absorption spectrophotometry an application to precious-metal-resource assessment in the Iditarod 1° X 3° quadrangle, southwestern Alaska: Annual McKelvey Forum in mineral and energy resources: U.S. Geological Survey Circular 1062, p. 39.

Hosking, K.F.G., 1951, Primary ore deposition in Transactions of the Royal Society of Cornwall, v. 18, p 309-356.

_____1964, Permo-Carboniferous and later primary mineralization of Cornwall and southwest Devon, *in*, Hosking, K.F.G., and Shrimpton, G.J., eds., Present Views of Some Aspects of the Geology of Cornwall and Devon: Penzance, Royal Geological Society of Cornwall, p. 201-245.

Hudson, T., 1979, Calc-alkaline plutonism along the Pacific rim of southern Alaska: U.S. Geological Survey Open-File Report 79-953, 31 p.

Jackson, N.J., 1979, Geology of the Cornubian tin field—A review, *in* Yeap, C.H., ed., Geology of Tin Deposits: Kuala Lumpur: Bulletin of the Geological Society Malaysia, v. 11, p. 209238.

John, E.C., 1978, Mineral zones in the Utah Copper ore body: Economic Geology, v. 73, p. 1250-1259.

Leveille, R.A., Newberry, R.J., and Bull, K.F., 1988, An oxidation state-alkalinity diagram for discriminating some gold-favorable plutons: An empirical and phenomenological approach: Geological Society of America Abstracts with Programs, v. 20, p. A142.

Lowell, J.D., and Guilbert, J.M., 1970, Lateral and vertical alteration and mineralization zoning in porphyry ore deposits: Economic Geology, v. 65, p. 373-408.

Meyer, C., Shea, E.P., Goddard, C.C., Jr., and staff, 1968, Ore deposits at Butte, Montana, *in* Ridge, J.D., ed., Ore Deposits of the United States 1933/1967, Graton-Sales Volumes: New York, American Institute of Mining, Metallurgical, and Petroleum Engineering, Inc., p. 1373-1416 p.

Miller, M.L., and Bundtzen, T.K., 1988, Right-lateral offset solution for the Iditarod-Nixon Fork fault, western Alaska: *in* J.P. Galloway and T.D. Hamilton, eds., Geological Studies in Alaska by the U.S. Geological Survey during 1987: U.S. Geological Survey Circular 1016, p. 99-103.

_____1992, Geologic history of the post-accretionary rocks, Iditarod quadrangle, west-central Alaska: Geological Society of America Abstracts with Program, v. 24, no. 5, p. 71.

_____1994, Generalized geologic map of the Iditarod quadrangle, Alaska, showing potassium-argon, major-oxide, trace-element, fossil, paleocurrent, and archaeological sample localities: U.S. Geological Survey Miscellaneous Field Studies Map MF-2219A, 48 p., 2 sheets, scale 1:250,000.

Miller, T.P., and Ferrians, O.J., Jr., 1968, Suggested areas for prospecting in the central Koyukuk River region, Alaska: U.S. Geological Survey Circular 570, 12 p.

Miller, T.P., 1972, Potassium-rich alkaline intrusive rocks of west-central Alaska: Geological Society of America Bulletin, v. 83, p. 2111-2128.

Miller, T.P., Patton, W.W., Jr., and Lanphere, M.A., 1966, Preliminary report on a plutonic belt in west-central Alaska: U.S. Geological Survey Professional Paper 550-D, D158-162.

Moll, E.J., Silberman, M.L., and Patton, W.W., Jr., 1981, Chemistry, mineralogy, and K-Ar ages of igneous and metamorphic rocks of the Medfra quadrangle, Alaska: U.S. Geological Survey Open-File Report 80-811C, 24 p.

Moll-Stalcup, E.J., 1990, Latest Cretaceous and Cenozoic magmatism in mainland Alaska: U.S. Geological Survey Open-File Report 90-84, 82 p.

Moore, W.J., and Nash, J.T., 1974, Alteration and fluid inclusion studies of the porphyry copper ore body at Bingham, Utah: Economic Geology, v. 69, p. 631-645.

Mutschler, F.E., Griffin, M.E., Stevens, D.S., and Shannon, Jr., S.S., 1985, Precious metal deposits related to alkaline rocks in the North American Cordillera - an interpretive review: Transactions of the Geological Society of South Africa, v. 88, p. 355-377.

Nash, J.T., 1976, Fluid-inclusion petrology—data from porphyry copper deposits and applications to exploration: U.S. Geological Survey Professional Paper 907D, D1–D16.

Newberry, R.J., Burns, L.E., Solie, D.N., and Clautice, K.H., 1988, A revised geologic model for the North Star Gold belt, interior Alaska: Progress report: Alaska Division of Geological & Geophysical Surveys Public-Data File 88-23, 20 p.

Nokleberg, W.J., Bundtzen, T.K., Berg, H.C., Brew, D.A., Grybeck, D., Robinson, M.S., Smith, T.E., and Yeend, W., 1987, Significant metalliferous lode deposits and placer deposits of Alaska: U.S. Geological Survey Bulletin 1786, 104 p., 2 plates.

Roedder, E., 1984, Fluid Inclusions: Reviews in Mineralogy, v. 12, 644 p.

Sillitoe, R.H., and Sawkins, F.J., 1971, Geologic, mineralogic, and fluid inclusion studies relating to the origin of copper-bearing tourmaline breccia pipes, Chile: Economic Geology, v. 66, p. 1028-1041.

Spooner, E.T.C., 1981, Fluid inclusion studies of hydrothermal ore deposits, *in* Hollister, L.S., and Crawford, M.L, eds., Fluid Inclusions: Applications to Petrology: Mineralogical Association of Canada Short Course Handbook, v. 6, p. 209-240.

Streckeisen, A.B., and LeMaitre, R.W.L., 1979, A chemical approximation to the modal QAPF classification of the igneous rocks: Neues Jahrbuch für, Mineralogic Abhandlungen., v. 136, p. 169-206.

Szumigala, D.J., 1993, Gold mineralization related to Cretaceous-Tertiary magmatism in the Kuskokwim Mountains of west-central and southwestern Alaska: University of California, Los Angeles, Ph.D. dissertation, 301 p.

Tooker, E.W., 1990, Gold in the Bingham District, Utah, *in* Shawe, D.R., and Ashley, R.P., eds., Gold in porphyry copper systems (Chapter E of Geology and Resources of Gold in the United States): U.S. Geological Survey Bulletin 1857-E, p. E1-E16.

Wallace, W.K., and Engebretson, D.C., 1984, Relationships between plate motions and Late Cretaceous to Paleocene magmatism in southwestern Alaska: Tectonics, v. 3, p. 295-315; publishers correction: Tectonics, v. 3, p. 497-498.

POSSIBLE THRUST WINDOWS ON THE CENTRAL SEWARD PENINSULA, ALASKA

by
Lorne E Young[1]

ABSTRACT

The Seward Peninsula is areally dominated by the Nome Group, a metacarbonate- to metaclastic-dominated assemblage of Late Proterozoic to Devonian age. Four domains on the central Seward Peninsula constitute the No Mans assemblage.These domains are dominated by Ordovician to Devonian carbonate rocks, calc-schist, and mica-schist. Early Ordovician and older rocks of the lower Nome Group overthrust and imbricated the No Mans assemblage, which is exposed in structurally-modified windows and partially unroofed horses or thrust slices. Variably tectonized siliciclastics are spatially associated with proposed thrust faults. Thrust faulting on the Seward Peninsula may be an expression of Late Jurassic to Early Cretaceous thrust faulting in the hinterlands of the western Brooks Range fold and thrust belt.

INTRODUCTION

Contemporary geologic mapping and faunal studies of the Seward Peninsula (Till and others, 1986) have led to a better understanding of the stratigraphy of this region. Cominco Alaska Exploration has conducted mineral-related geologic studies on the Seward Peninsula in the 1975–1978, and 1989–1994 periods. Figure 1 shows the geographic and geologic locales discussed in this paper. Geologic data on figures 1–6 include information from Cominco (unpub. data, 1975–94), Smith (1910), Sainsbury (1972, 1974), Sainsbury, Hudson, and others (1972), Sainsbury, Hummel, and others (1972), Miller and others (1972), Sainsbury (1975), and Till and others (1986). This paper discusses the possible significance of four domains of Ordovician to Devonian or younger rocks in the central Seward Peninsula (figs. 1–6). The rocks in these areas are here informally termed the No Mans assemblage, and for the purposes of discussion, the domains are referred to as windows, recognizing that at least one domain (figs. 3 and 4) may constitute a partially unroofed horse or thrust slice.

Exclusive of the Kigluaik–Bendeleben Mountains, bedrock exposure on the central Seward Peninsula is generally poor, and critical geological relationships are seldom exposed. Geologic relationships in better-exposed areas, such as No Mans Creek, must be used to explain relationships from rubble crop in poorly exposed areas. The subject of regional-scale thrust faulting of the Nome Group is controversial. Structural relationships are not unequivocally resolved, and this paper presents evidence and tentative interpretations that will be useful for more detailed studies by future workers.

[1]Cominco Alaska Exploration, 5660 B Street, Anchorage, Alaska 99518.

GEOLOGY

The Nome Group and Kigluaik Group constitute the older and oldest parts of the Seward terrane (Till and Dumoulin, 1994). For this study, the Nome Group is divided into five mappable units (fig. 2) based largely on the hierarchy of Till and others (1986). Stratigraphically these units are, from lowest to highest: C unit, Mixed unit, Casadepaga Schist unit, Oim unit, and DSl unit. For purposes of description, all units below the DSl unit are described as lower Nome Group. The Nome Group underwent deep burial and blueschist metamorphism in Middle Jurassic through Early Cretaceous time followed by decompression and overprinting to greenschist facies (Armstrong and others, 1986; Patrick and Lieberman, 1988). North-vergent deformation during blueschist metamorphism created and subsequently rotated fold hinges at outcrop scale (Patrick and Lieberman, 1988) into a north–south to N. 20° W. orientation, parallel with stretching lineation. The rotation of fold hinges is not universal, as demonstrated by the regional presence of subordinate outcrop-scale isoclinal and chevron folds, rods, and lineations that strike N. 20°–75° E. and N. 40° W. to west. In the Kougarok Mountain area, Puchner (1986) describes early planar fabric and east-west trending recumbent isoclinal folds that are refolded about north–south trending axes. Regional-scale north- to northwest-trending folds on the central Seward Peninsula (fig. 2) are developed in the Nome Group and No Mans assemblage and might constitute evidence for a discrete event of east–west compression.

A Barrovian thermal overprint is most strongly recorded in the Kigluaik Group. It began after peak blueschist metamorphism at 100 Ma or earlier (Patrick and Lieberman, 1988). Uranium-lead zircon geochronology indicates mafic magmatism at post-120 Ma with partial melting and felsic magmatism by 105 Ma. Granulite-

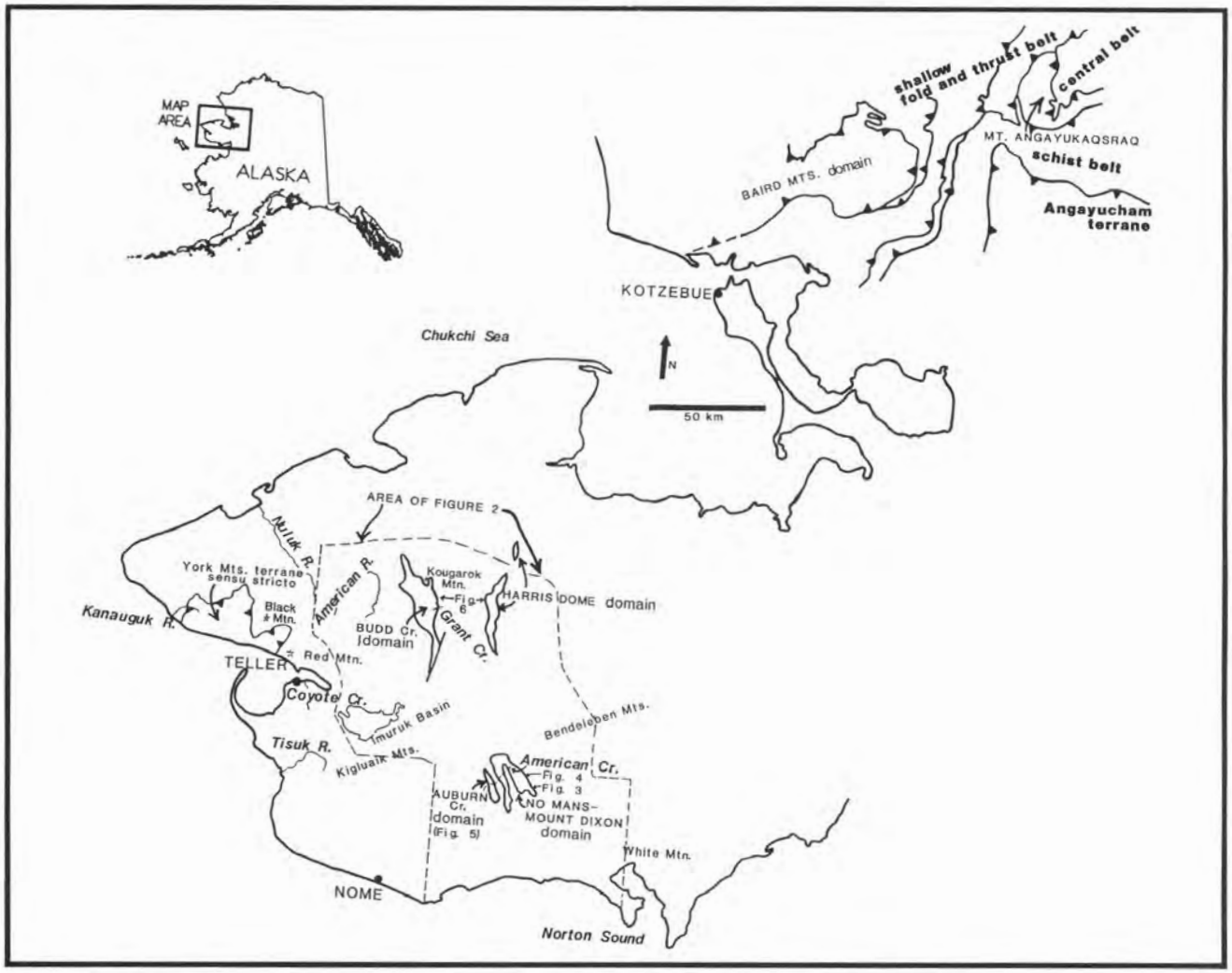

Figure 1. *Regional location map showing geographic and geologic locales referenced in the text.*

facies metamorphism began by 105 Ma and continued to 92 Ma, contemporaneous with uplift of the Kigluaik Group via a combination of extension, tectonic or erosional thinning, and diapirism (Amato and others, 1991, 1992, 1994; Miller, Amato, and others, 1992; Miller, Calvert and Little, 1992). The Kigluaik and Bendeleben Mountains constitute east–west trending antiforms that developed along the axis of this uplift; the antiforms are modified by flanking easterly trending normal faults that are still active (Kaufman, 1985; Thurston, 1985; Amato and others, 1994). Lower intercepts of 124 ± 6 and 117 ± 7 Ma for zircons from orthogneiss in the Nome Group, are ascribed to exhumation and greenschist-facies overprinting (Patrick and McClelland, 1993). Miller and others (1992a) suggest that the latest metamorphism of the Nome Group occurred at post-120–115 Ma. White mica from a metamorphogenic gold vein in the Nome Group 76 km east of Nome yields a $^{40}Ar/^{39}Ar$ age of 109 Ma (Ford and Snee, 1993) and may locally date the change from ductile to brittle deformation. This change is physically expressed by regional northwest-, northeast-, and east-trending block faults and subvertical veinlet sets, which cut across all ductile features.

KIGLUAIK GROUP

KIG UNIT

This unit essentially constitutes the Kigluaik Group, is distributed in the Kigluaik Mountains and possibly the Bendeleben Mountains (fig. 1), and is designated as *Kig* in figure 2. More detailed subdivisions of the Kig unit of this paper have been made by Till (1983) and Till and others (1986). The Kig unit includes quartzitic and quartzofeldspathic schist and gneiss, marble, and metaintrusive and intrusive bodies of several ages. Much of the Kig unit has a sedimentary protolith (Till, 1983). An orthogneiss body intruded near the top of the Kig unit has a U-Pb zircon crys-

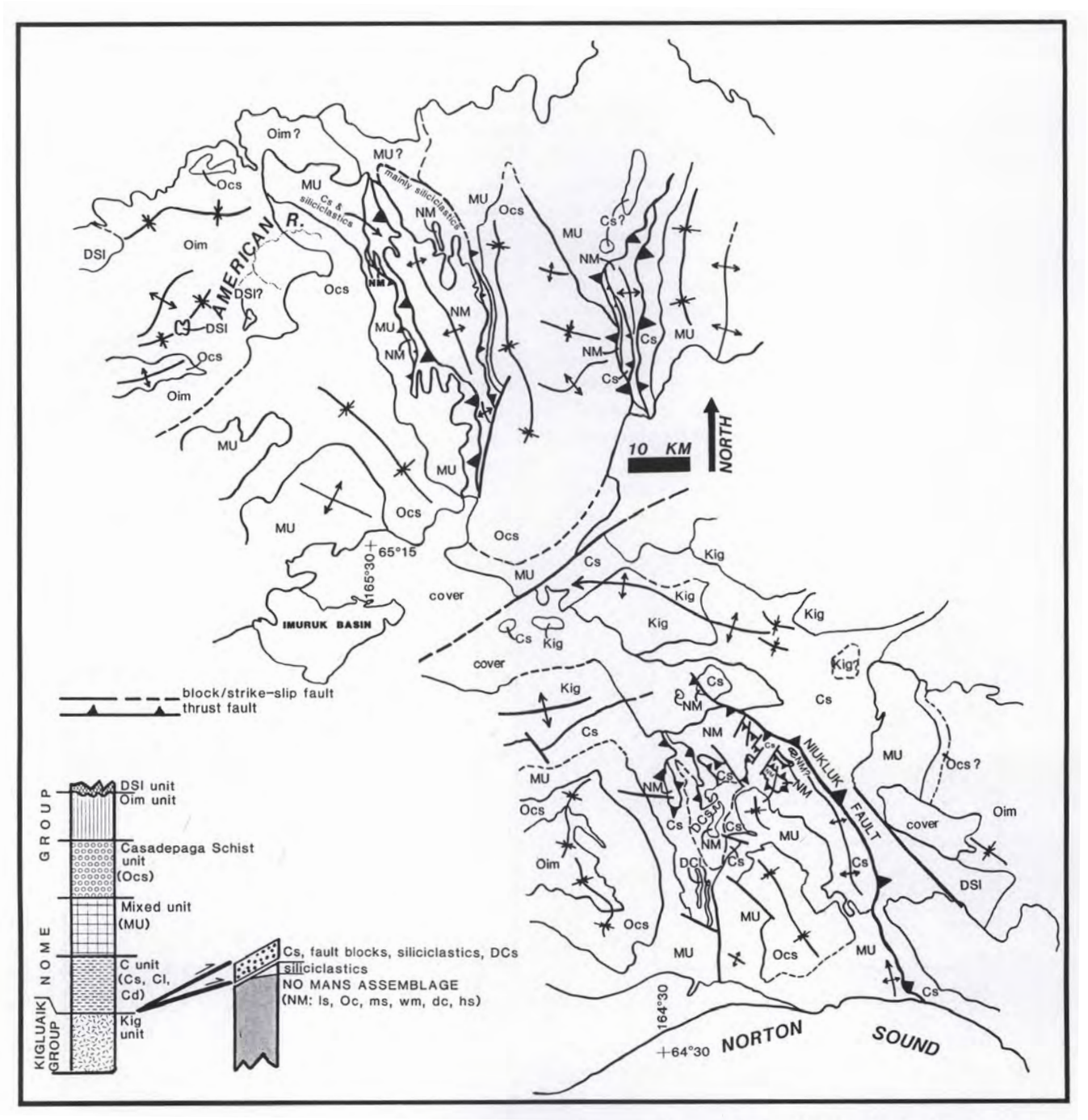

Figure 2. *Generalized geologic map and stratigraphic columns for the central Seward Peninsula. Listed units described in text.*

tallization age of 555 ± 25 Ma (Amato and others, 1991); gneiss of the Kig unit has a Rb/Sr isochron age of 735 Ma (Bunker and others, 1979). Patrick and Lieberman (1988) report Rb-Sr ages of Late Precambrian or Early Paleozoic for granulite-facies migmatite in the Kigluaik Group. Although a Cambrian age is possible for part of the Kig unit, evidence from the overlying Nome Group supports an entirely Proterozoic age. Thermally upgraded rocks of the lower Nome Group have possibly been included with the Kig unit in the Bendeleben Mountains.

NOME GROUP

C UNIT

The C unit is an abbreviation for the CpCs unit of Till and others (1986), who describe pelitic quartz-rich

schist, and subordinate calc-schist and marble; schist is composed of quartz, muscovite, chlorite, chloritoid, graphite, glaucophane, and garnet. Schist-, marble-, and dolostone-dominant subunits are designated Cs, Cl, and Cd respectively on figures 2–6. Rock types here noted in areas mapped as CpCs by Till and others (1986) or by Cominco (unpub. data, 1975–94) include, in decreasing order of abundance: (1) variegated greenish chlorite-muscovite (biotite)-quartz schist with abundant fine-grained sucrosic white quartz layers and coarsely-textured bull quartz segregations; (2) light-colored chlorite or biotite metaquartzite to metasiltite; (3) black carbonaceous metasiltite and silty phyllite: (4) muscovite-chlorite ± chloritoid-quartz schist: (5) marble, micaceous calc-schist and impure micaceous marble: (6) chlorite-albite ± garnet schist and dense mafic schist: (7) light-colored silicified dolostone: and (8) chloritoid -muscovite-quartz schist.

At outcrop scale, the C unit preserves evidence of ductile shearing. Chlorite-muscovite schist of the C unit commonly contains light-colored sucrosic quartz (metaclastic?) and bull-quartz segregations that parallel early foliation. These quartz layers are commonly isoclinally folded, and axial planes have been rotated into parallelism with stretching lineation with development of boudinage structure. Some folded quartz layers have remained intact, while adjacent former layers have failed brittlely and are now represented by trains of rootless isoclinal clasts and angular clasts. In several areas, an early subvertical ductile to locally brittle fabric is cut by a later ductile fabric, which dips gently southwest to southeast. As an example, north of No Mans creek (fig. 3), chlorite-muscovite schist of the C unit contains subvertical trains of angular quartz clasts alternating with intact isoclinally folded sucrosic quartz layers, all of which are slightly deflected by gently southwest-dipping foliation. It has not been determined whether both fabrics were developed under blueschist metamorphic conditions.

The stratigraphically higher Mixed and Oim units (described in the following sections) of the Nome Group

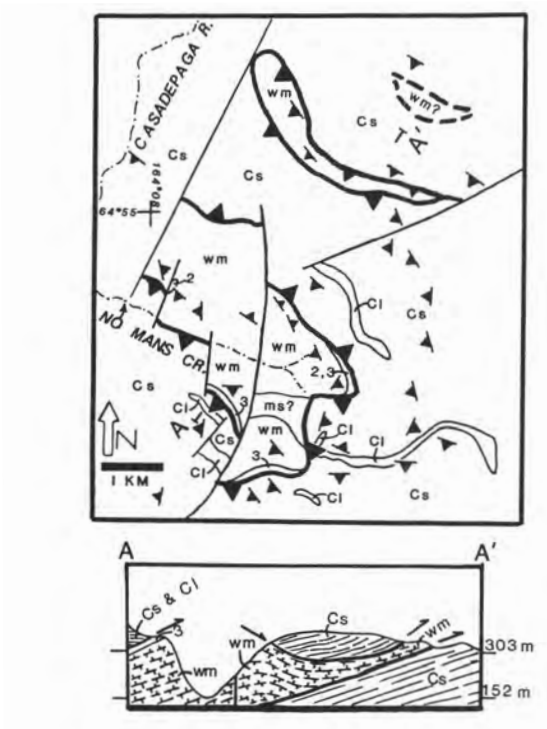

Figure 3. *Geologic map and cross section of the southern portion of the No Mans–Mount Dixon window. Horizontal scale is the same for the map and cross section. Listed units are described in the text. Some units are stippled to depict observed and projected angles of late schistosity in the plane of section. Thrust fault arrows are not intended to show vergence.*

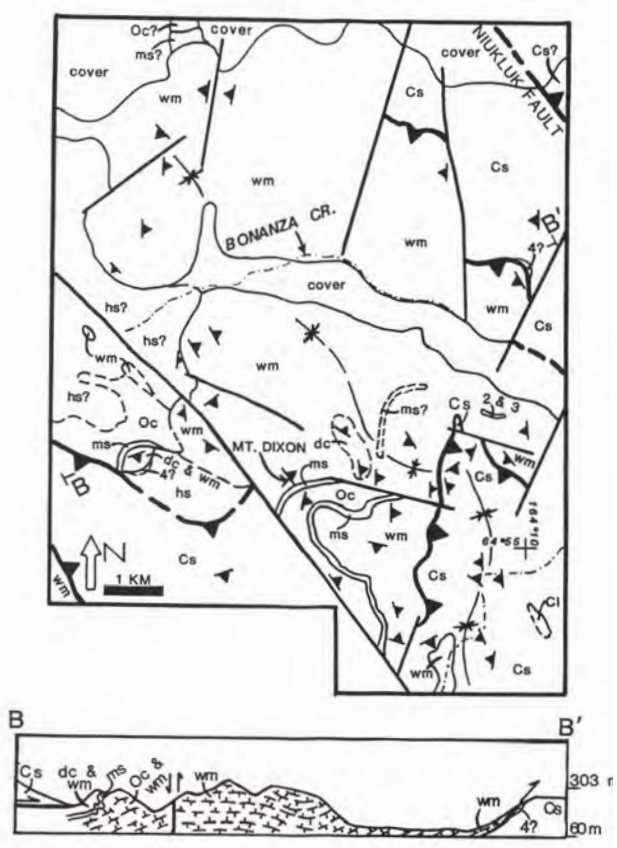

Figure 4. *Geologic map and cross section of the northern portion of the No Mans–Mount Dixon window. Horizontal scale is the same for the map and cross section. Some units are stippled to show measured angles of foliation. Thrust fault arrows are not intended to show vergence. Listed units are described in the text.*

yield Ordovician, Early Ordovician, and Early through Middle Ordovician conodonts (T. Carr, Anaconda Minerals unpub. report, 1984; Till and others, 1986), providing a minimum age for the C unit. An Early to early Middle Cambrian microfossil was recovered from a dolostone subunit (Till and others, 1986) that lies near the fault-defined base of the C unit west of the Auburn Creek window (Cd, fig. 5). Samples of orthogneiss that intrude the C unit in the Nome region yield Rb/Sr whole-rock ages in the 488-470 Ma and 636-628 Ma range (Armstrong and others, 1986); these results only demonstrate an Early Paleozoic or older age. Patrick and McClelland (1993) and McClelland and Patrick (1994) report U-Pb zircon ages of 676 ± 15 Ma and 681 ± 3 Ma respectively for altered tonalite(?) which intrudes lower Nome Group east of Nome, and metadiorite and metadacite in the Mixed unit north of Nome.

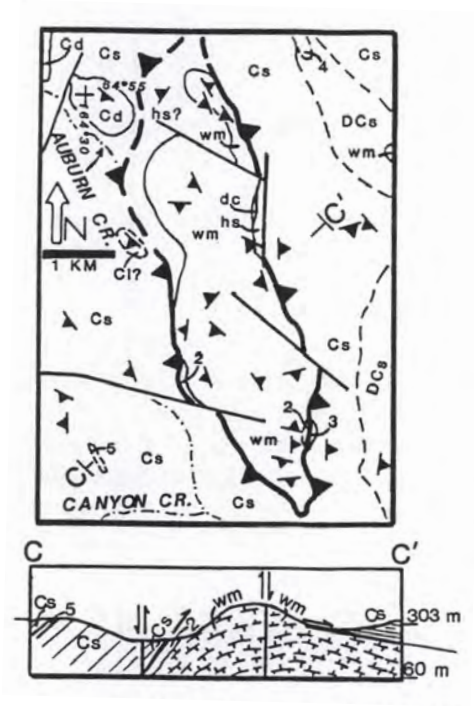

Figure 5. *Geologic map and cross section of the Auburn Creek window. Horizontal scale is the same for the map and cross section. Some units are stippled to show measured angles of foliation. Thrust fault arrows are not intended to show vergence. Listed units are described in the text.*

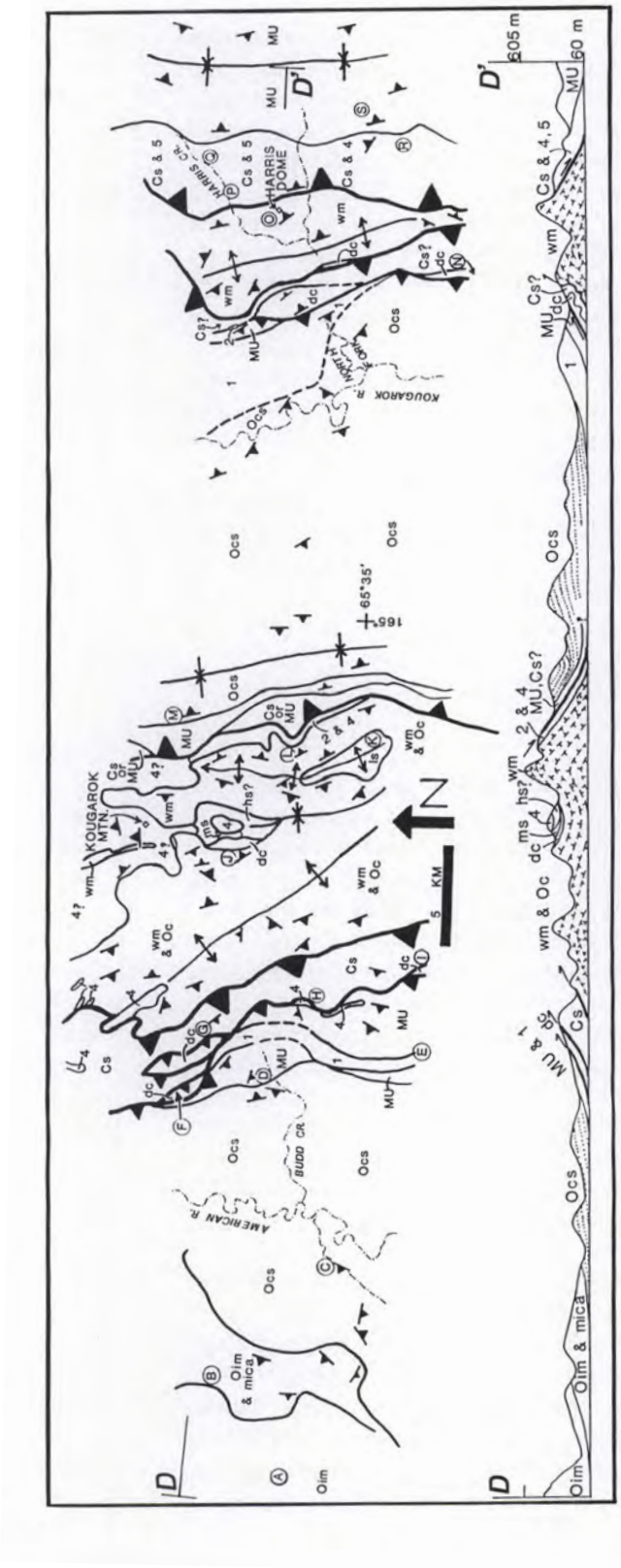

Figure 6. *Geologic transect and diagrammatic cross section of the Budd Creek and Harris Dome windows. Horizontal scale is the same for the map and cross section. Some units are stippled to show the approximate surface dip of foliation; downward dip of foliation is speculative. Geologic observation points (stops) are circled and labeled A to S. The stops are described in the text. Thrust fault arrows are not intended to show vergence.*

In summary, the C unit is proposed to span part of Late Proterozoic and part of Cambrian time. The contact between the Kig unit and overlying C unit is typically faulted; examples are the Tumit Creek fault of Thurston (1985) and the Crater Creek and Kigluaik faults of Kaufman (1985). In the westernmost Kigluaik Mountains, the transition from the Kig unit to the C unit is not clearly fault defined, although the attenuated metamorphic gradient in this area (for example, Miller, Calvert, and Little, 1992) and postulated stratigraphic attenuation make interpretations difficult. Patrick and Lieberman (1988) found no petrographic evidence for a structural discontinuity between the Kigluaik and Nome Groups. The contact between the C unit and Kig unit in the Bendeleben Mountains is very speculatively designated on figure 2, and is probably not everywhere faulted.

Several large areas of chlorite-muscovite schist with locally abundant quartz segregations in the American Creek to No Mans Creek region are shown as *CpCs* unit by Till and others (1986). Also present in this region is brown-weathering quartz-mica schist, calc-schist, and impure micaceous marble that overlie and grade to the white marble unit or dark carbonate subunit of the No Mans assemblage. Accordingly, areas where assignment to the C unit is uncertain are depicted as *DCs* on figures 2 and 5.

MIXED UNIT

The Mixed unit (after Till and others, 1986) conformably overlies the C unit (fig. 2) and is depicted as *MU* on figures 2 and 6. Till and others (1986) describe interlayered pure and impure marble, quartz-graphite schist, pelite, calc-schist, and mafic schist. The Mixed unit contains several mappable subunits, including two major and several minor marble subunits, calc-schist and muscovite-chlorite schist subunits, and one or two subunits of black carbonaceous metasiltite. Chlorite-feldspar schist, garnet metabasite, and amphibolite are a subordinate component of the Mixed unit. Foliation-parallel quartz segregations are only locally as abundant as in the C unit, and generally restricted to mica-dominant schist subunits. Two samples of Till and others (1986, 84ADn75 and 82ATi197) from the Mixed unit contain nonspecific Ordovician conodonts. The Dorothy Creek orthogneiss(?), which lies in the Mixed unit north of Nome, has been dated as Late Proterozoic via U-Pb zircon (Patrick and McClelland, 1993; McClelland and Patrick, 1994). However, geological relationships at the dated locale are ambiguous: a broad but relatively thin zone contains quartz-rich metasediments closely interlayered with metadiorite, and metadacite or metavolcaniclastic(?) containing zircon and rutile. Thus, although the lower Mixed unit could be as old as Late Proterozoic, the previously-cited evidence of a Cambrian age for part of the underlying C unit, makes a Cambrian to Ordovician age more likely for the Mixed unit. As no fossils have been recovered from the Mixed unit depicted immediately east or west of the Budd Creek window (figs. 2 and 6), the assignments there are based purely on lithology and stratigraphic position.

CASADEPAGA SCHIST UNIT

The Mixed unit is conformably overlain by the Casadepaga Schist unit and designated as *Ocs* on figures 2 and 6. Till and others (1986) describe chlorite-albite schist, mafic schist, chlorite-albite-epidote-white mica schist, chloritoid-glaucophane metapelite, calc-schist, and metabasite. The metabasite generally contains glaucophane, actinolite, chlorite, epidote, garnet, albite, white mica, and sphene.

The Casadepaga Schist unit contains mappable subunits of chlorite-albite schist, chloritic metasandstone, chlorite-muscovite schist, dense garnet metabasite, and impure marble. A transitional subunit that includes black carbonaceous metasiltite and carbonaceous muscovite-quartz schist defines the uppermost portions of the Casadepaga Schist unit. Major-oxide analyses and limited petrography suggest that the Casadepaga Schist unit includes protoliths of graywacke, intermediate volcanics(?), basalt, gabbro, and carbonaceous silty shale to siltstone. The presence of Ordovician microfossils in the underlying Mixed unit and microfossils as old as Early Ordovician in the overlying Oim unit (T. Carr, Anaconda Minerals unpub. report, 1984; Till and others, 1986), indicates that the Casadepaga Schist unit is of probable Early Ordovician age.

The Tisuk River to Teller area northwest of the Kigluaik Mountains, and the Black Mountain and Kanauguk River areas in the York Mountains region (fig. 1) are proposed to be underlain by less-recrystallized Casadepaga Schist unit. The less metamorphosed locales are included in the York terrane by Till and Dumoulin (1994), but are here correlated with the Nome Group. Ordovician or younger conodont fragments are reported from the Coyote Creek area south of Teller (T. Carr, Anaconda Minerals unpub. report, 1984); middle Early through Late Ordovician conodonts are reported for graywacke-type rocks (Till and Dumoulin, 1994) west of the York Mountains. The areas of Casadepaga Schist unit shown east and west of the Budd Creek window in figures 2 and 6 are identified solely by lithology and interpreted stratigraphic position; no fossils have been recovered from the proposed Casadepaga Schist unit in this area.

OIM UNIT

The Casadepaga Schist unit grades upsection through the transitional subunit to the Oim unit of Till and others (1986) who describe impure marble containing

chlorite and albite, with local pods of metabasite. This unit is designated as *Oim* in figures 2 and 6. A distinctive orangish-weathering light-colored flaggy cleaving micaceous marble that constitutes a portion of the Oim unit can generally be distinguished from other gray- and white-weathering more-pure carbonate units and subunits of the Nome Group and No Mans assemblage. A large area of mixed gray and orangish brown weathering marble and basal micaceous marble to calc-schist north and northeast of the York Mountains proper mapped as York terrane by Till and Dumoulin (1994) is here included with the Oim unit of the Nome Group. Assignment of rocks north and northeast of the York Mountains to the Nome Group is based on age of conodonts, local presence of flaggy orangish-weathering marble, and uncomplicated gradation to the east with underlying calc-schist, chloritic schist, black carbonaceous metasiltite, and meta-mafic rocks assigned to the Casadepaga Schist unit. Till and others (1986) report Early through Middle Ordovician conodonts from the Oim unit west of the Auburn Creek window; earliest Ordovician and Early to Middle Ordovician conodonts are reported from rocks here correlated with the Oim unit in the upper American River, and at Red Mountain (T. Carr, Anaconda Minerals unpub. report, 1984). The Oim unit is therefore regarded as Early or Early to Middle Ordovician in age.

DSL UNIT

Certain areas of Siluro-Devonian carbonates on the central Seward Peninsula are assigned to the Nome Group and designated as *DSl* on figure 2. This includes the Ddm unit at White Mountain, which Till and others (1986) include with the Nome Group; however, Siluro-Devonian units of the northeastern York terrane of Till and Dumoulin (1994) are here also included with the DSl unit of the Nome Group. The DSl unit at White Mountain lies in uncertain relationship with the Oim unit but overlies rocks here assigned to the Oim unit in three synforms along the Nuluk River and east of the American River (fig. 1). In the Nuluk River area the DSl unit includes massive-weathering grayish-brown micritic limestone, and very dark-gray bedded micritic limestone or dolostone. Conodonts from rocks herein assigned to the DSl unit in the Nuluk River area are of middle Middle Silurian age; corals are Late Silurian to early Late Devonian aspect (Till and Dumoulin, 1994). In the Nuluk River area the contact zone between the Oim and DSl units is recessively weathering. However, the decreased recrystallization of carbonate of the DSl unit relative to the underlying Oim unit, the apparently abrupt lithologic change upsection to the DSl unit, the lack of identified Late Ordovician and Early Silurian fossils, and lateral variation in the DSl unit might indicate an unconformable or disconformable contact with the underlying Oim unit. Dark shallow-water dolostone and marble at White Mountain yields microfossils and megafossils of combined middle Early Devonian to earliest Late Devonian age (Till and others, 1986).

NO MANS ASSEMBLAGE

The No Mans assemblage is exposed in four domains, here designated as structural *windows* for purposes of discussion: No Mans-Mount Dixon, Auburn Creek, Harris Dome, and Budd Creek (fig. 1). Lower Nome Group units constitute the structurally highest element and lie in the upper plate outside of the Auburn Creek, Harris Dome, and Budd Creek window margins. In the more deeply eroded No Mans–Mount Dixon window, the lower Nome Group is proposed to both structurally overlie and underlie the No Mans assemblage. Strongly to weakly recrystallized light-colored pure marble of the No Mans assemblage is the dominant lithology in the structural windows.

Figure 2 shows the simplest possible scenario for the No Mans assemblage and related geologic elements; revised interpretations could significantly alter the position of the depicted thrust faults and unit designations. The No Mans assemblage includes most of the Pzm, Od, and Ddm units of Till and others (1986) in the region of No Mans Creek to Harris Dome. The assignment of these units to the No Mans assemblage is based principally on interpreted structural position beneath the lower Nome Group and not on demonstrated lithological differences with time-equivalent units of the Nome Group. Carbonate units comparable to those of the No Mans assemblage are present on the easternmost Seward Peninsula and described by Till and others (1986). Although there are several definable units in the No Mans assemblage, these units do not constitute a continuously mappable section in any single area. From lowest to highest, the No Mans assemblage is proposed to contain unquantified mica schist and calc-schist; light-colored Ordovician marble and dolostone; minor mica schist and calc-schist; major light-colored and subordinate dark-colored Siluro-Devonian marble and local dolostone; and unquantified siliciclastics, mica schist, very impure marble, and calc-schist.

Certain types of siliciclastics, defined later in the section titled Siliciclastics on page 105, are shown to occur in a variety of geologic settings. However, color-banded siliciclastics and lineated or rodded siliciclastics are most common in the No Mans assemblage within the windows, and in the immediate footwall to known or postulated thrust faults between the Nome Group and No Mans assemblage.

On average, carbonate units here assigned to the No Mans assemblage contain less mica than do the carbonate units of the Nome Group. Although carbonate units of the Nome Group and No Mans assemblage are deformed in the same manner, evidence that the No Mans assemblage

is locally less recrystallized is provided by preserved megafossils in marble units of the No Mans assemblage in three of the four windows. In the No Mans–Mount Dixon and Auburn Creek windows, conodonts have color alteration indexes of 4, 5, 5.5, and 5 to 6; conodonts from Nome Group in this region have color alteration indexes of 5.5 to 6, 6, and 7 (Till and others, 1986). These color indexes indicate that the Nome Group has been locally subjected to higher temperatures than the structurally lower No Mans assemblage, suggesting that thermal maturation preceded thrust faulting. However, conodont color alteration indexes in the Harris Dome to Budd Creek region do not demonstrate a similar relationship; here, unrecognized thermal events have produced locally higher color-alteration indexes in both the No Mans assemblage and the Nome Group (Till and others, 1986; A. Till, written commun., 1994).

LOWEST SCHIST UNIT

This unit is included in areas labeled *NM* on figure 2, and designated as *ls* on figure 6. The oldest or structurally lowest exposed rocks in the Budd Creek window consist of pencil-cleaved chlorite-calcite-quartz schist exposed in an anticline in the east central Budd Creek window (stop K, fig. 6). This exposure is equivalent to part of the Kougarok schist of Puchner (1986) and lies gradationally downsection of pure to impure foliated marble here assigned to the No Mans assemblage. Along American Creek (figs. 1 and 2) between the Auburn Creek and No Mans-Mount Dixon windows is planar-foliated and homogenous-textured, chlorite-muscovite-quartz (calcite) schist and subordinate variegated gray sparry marble. The sparry marble grades upsection to light-colored marble and subordinate dolostone of the Ordovician carbonate unit, which contains a conodont of middle Early Ordovician to earliest Middle Ordovician age (Till and others, 1986).

ORDOVICIAN CARBONATE UNIT

This unit is partly equivalent to the Od and Pzm units depicted on the central Seward Peninsula by Till and others (1986) here designated as *Oc* in figures 4 and 6. Along the west side of the No Mans-Mount Dixon window is white, light-gray, and grayish-brown silicic or quartzose, very fine-grained to fine-grained tan to salmon-weathering dolostone, and mottled white, light-gray, and gray fine- to medium-grained dolostone to marble. Conodonts from this unit indicate a middle Early Ordovician and Early through Middle Ordovician age (Till and others, 1986). The assignment of these carbonate rocks to the No Mans assemblage is based on (1) their apparent stratigraphic relationship with the white marble unit on the west flank of Mount Dixon, which is described in the next paragraph, and (2) their interpreted structural position beneath the older C unit of the Nome Group. The Ordovician carbonate unit and white marble unit are not differentiated in the Budd Creek window (fig. 6).

MEDIAN SCHIST UNIT

As noted by Smith (1910), there is a thin but distinctive band of schist that crosses the west flank of Mount Dixon. This band of schist is here called the median schist unit, designated as *ms* on figures 3, 4, and 6. It consists of variably carbonaceous light- to dark-colored chlorite-muscovite-quartz schist. The schist contains varying proportions of granular quartz with a few discrete layers of fine-grained muscovite-metaquartzite. On the west flank of Mount Dixon the median schist unit overlies the Ordovician carbonate unit, and underlies fine- to medium-grained light-gray to white massive marble of the white marble unit described in the following section. Two and one-half km west of Mount Dixon (fig. 4), a possibly correlative unit of light-colored muscovite-quartz-calcite schist overlies the Ordovician carbonate unit and underlies color-banded dark-gray and white marble and dolostone of Late Silurian through Devonian age (Till and others, 1986). A possibly correlative section is preserved 5 km south of Kougarok Mountain in the Budd Creek window (stop J, fig. 6). Here, fine- to medium-grained light-colored and foliated, weakly dolomitized marble is overlain by mixed foliated marble and chlorite-quartz-calcite schist. Upsection, foliation is less developed, and weakly-foliated chlorite-quartz-calcite schist and chloritic metasandstone grade upsection to dark and light color-laminated dolostone of Siluro-Devonian lithotype.

WHITE MARBLE UNIT

This unit is equivalent to some areas of the Pzm unit of Till and others (1986) on the central Seward Peninsula. The white marble unit is designated as *wm* on figures 3–6. Rocks here assigned to the white marble unit are common to dominant in the No Mans assemblage. The most diagnostic rock type is thickly bedded to massive and blocky cleaving, relatively nonmicaceous micritic to sparry white to locally gray to black marble. However, in many areas the white marble unit contains small to moderate amounts of white mica, and exhibits closely spaced foliation and flaggy to platy cleavage. In part, conspicuously foliated marble represents more deformed and/or impure zones in the white marble unit, or alternately unrecognized Ordovician carbonate unit. Tan- to salmon-weathering zones of siliceous to quartz-veined dolostone are locally developed in the white marble unit. Two zones of light-colored schistose to massive marble and carbonate breccia that lie south of the Auburn Creek window and lack faunal

and stratigraphic control are shown as *DCl* on figure 2; however, these zones may lie in the lower Nome Group.

Conodont and coral collections reported by Till and others (1986) from the white marble unit or zones of dolostone within the white marble unit indicate Middle Silurian through Early Devonian and Middle Devonian age. Microfossils have not been identified in the white marble unit of the Budd Creek window; however, corals from this window include Devonian forms (Puchner, 1986).

DARK CARBONATE SUBUNIT

This subunit is equivalent to some areas of the Ddm unit of Till and others (1986) on the central Seward Peninsula and was included in some of the previous descriptions. This subunit is designated as *dc* on figures 4–6, and includes variably carbonaceous very fine- to medium-grained dark or dark-light banded micritic to sparry marble and dolostone, strongly calcareous dark phyllite, and light-colored marble. Color-banding is characteristic and accentuated by the presence of white calcitic laminations in dark dolostone. Planar-laminated foliation or cleavage is common, however, corals are recognized only in less closely-foliated samples from the dark carbonate subunit.

The dark carbonate subunit locally interfingers with and is largely a carbonaceous variant of the white marble unit, but possibly includes the youngest carbonate rocks of the No Mans assemblage. Coral-bearing examples of the dark carbonate unit most commonly occur as float cobbles in streams draining the structural margins of the Budd Creek, Harris Dome, and northern No Mans–Mount Dixon windows. In the Harris Dome area the cobbles are possibly sourced from exotic fault blocks in the lower Nome Group.

Samples here correlated with the dark carbonate unit have yielded Silurian, Late Silurian through Early Devonian and Middle Devonian through earliest Mississippian conodonts (Till and others, 1986; A. Till, written commun., 1994), Late Ordovician through Middle Devonian corals, and Silurian through Devonian corals. Tan- to salmon-weathering siliceous dolostone is locally developed in the dark carbonate subunit. Highly oxidized and vuggy carmine and yellow dolostone breccia is present on the margins of the central portion of the Harris Dome window and in the northern Budd Creek window near proposed thrust faults. This type of dolostone is in part developed in the dark carbonate subunit.

HIGHEST SCHIST UNIT

In several areas the white marble unit or dark carbonate subunit grades upsection to brown-weathering muscovitic calc-schist to very impure muscovite marble, carbonaceous calc-schist, brown-weathering silvery muscovite (quartz-calcite) schist, and ferruginous dark chlorite-muscovite (carbon) schist. These areas are designated as *hs* on figures 4–6. The highest schist unit contains rocks similar to those that would generally be assigned to the C unit of the Nome Group, except that they grade downsection to carbonate rocks assigned to the No Mans assemblage and contain fewer or no metamorphic quartz segregations. Areas where assignment to the C unit versus the No Mans assemblage is uncertain are shown as *DCs* on figures 2 and 5.

FAULT BLOCKS

The C unit of the Nome Group commonly contains clasts of white sucrosic to bull quartz. These clasts principally represent boudins, rods, and truncated intrafolial folds formed during ductile shearing; all such clasts are considered native and are not considered tectonic melange. In contrast, as described later in the section titled Geology of the Windows on page 107, there are several areas where carbonate units of known or inferred post-Ordovician age are underlain and overlain by Ordovician and older units tentatively assigned to the lower Nome Group. In these cases the younger carbonate units are here assigned to the No Mans assemblage, and possibly constitute horses or thrust slices developed in ductile shear zones during thrust faulting.

SILICICLASTICS

Siliciclastics, as used here, include rocks of clastic protolith, and rocks which may represent silicified calcareous siltstone, silty carbonate, and calc-schist. Siliciclastics occur in the Nome Group and No Mans assemblage. All discussed siliciclastic rock types are interpreted to have been metamorphosed and deformed, although some display little or no recrystallization. The origin of certain types of siliciclastics is equivocal and not fully resolved, for example, Puchner (1987) and Sainsbury (1987).

CLASSIFICATION

Five types of quartz-dominant siliciclastic rocks are relevant to this paper; these are depicted by numbers 1–5 on figures 3–6.

Type 1

The most common type of siliciclastic, previously mentioned in the section titled Nome Group on page 99, forms several subunits in the lower Nome Group and includes platy to locally blocky dark-gray to black carbonaceous to graphitic metasiltite with traces of fine-grained muscovite on parting planes. Petrographic studies and regional stratigraphic context designate type 1 siliciclastics

as a sedimentary unit, with a siltstone to siliceous silty-shale protolith.

Type 2

Very fine-grained cream-colored sucrosic quartz layers are locally common in carbonate subunits of the C unit, Mixed Unit, and the white marble unit of the No Mans assemblage. These quartz layers are host to copper carbonate occurrences and contain only traces of primary sulfide in surface samples. Petrographic and field studies demonstrate a lack of heavy resistate minerals; however, a (silty) clastic quartz component is present in this rock type. Field relations suggest zones of type-2 siliciclastics are discontinuous or variable in thickness along strike to poddy or irregular. The protolith may be silty carbonate that has been silicified during metamorphism and layer-parallel or thrust faulting. This conclusion is based on the interpreted lack of heavy resistate minerals, the direct association with carbonate layers near interpreted thrust faults or layer-parallel faults, and the occurrence of this rock type in both the Nome Group and No Mans assemblage. Sainsbury (1975) relates silicification to thrust faulting, although on a more regional scale and not necessarily in the same study areas as those of this paper.

Type 3

Color-laminated white, light-gray, gray, bluish-gray, dark-gray, and brown very fine-grained to cherty quartz layers are a subordinate component of carbonate units of the No Mans assemblage and are most common near interpreted thrust faults. Color-laminated fine- to medium-grained siliciclastics that lack cherty layers are presumed to be more thoroughly recrystallized and are included with type-4 siliciclastics, described in the following section. Type-3 siliciclastics are commonly encrusted with dark lichens, occur as bands within upper portions of the white marble unit and directly upon the white marble unit, and locally contain relict centimeter-scale layers and pod-shaped inclusions of marble. Petrographic studies suggest a cherty protolith with some clastic (silty) layers that are lacking in heavy resistate minerals. Type-3 siliciclastics may represent silty and carbonaceous carbonate of the No Mans assemblage that has been silicified near faults. The evidence for this conclusion is the direct association with marble units near proposed thrust faults, very fine grain size, presence of carbonate inclusions, lack of heavy resistate minerals, and local association with type-2 siliciclastics. The overall darker colors of type-3 siliciclastics possibly reflect a higher original carbon content of the parent rock. As an example, in the Auburn Creek window, dark color-banded cherty siliciclastics occur along strike from color-banded carbonaceous marble of the dark carbonate subunit.

Type 4

These siliciclastics include a variably tectonized bluish-gray to dark bluish-gray moderately carbonaceous end member, and a white, light-gray, and gray end member. Both end members include coarsely-textured lineated quartz-rich schist composed of variably rodded and broken folia of mixed chalk-colored quartz (with sericite inclusions) and vitreous translucent to semi-translucent quartz, with light greenish-gray to silvery fine- to coarse-grained muscovite or chlorite partings. Lichen encrustations create a conspicuous dark-weathering aspect to these rock types. As petrographically determined, type-4 siliciclastics are composed mainly of quartz and muscovite, with variable amounts of carbon. Calcite is a local accessory. Type-4 siliciclastics commonly contain randomly distributed flecks of iron oxide and local copper carbonate occurrences on late brittle fractures. Locally, type-4 siliciclastics visually resemble feldspathic schist, but as demonstrated by high SiO_2 (+81-92 percent), low to very low total alkali content, and petrography, the resemblance is superficial. Type-4 siliciclastics correlate with a portion of the Kougarok schist and micaceous–carbonaceous quartzite of Puchner (1986), and are tentatively interpreted to be widely distributed around Kougarok Mountain near or at the top of the white marble unit (fig. 6). On the east side of the Harris Dome window and south from American Creek, type-4 siliciclastics may lie near the structural boundary between lower Nome Group and No Mans assemblage, and not exclusively in association with carbonate units. Petrographic studies demonstrate a proportion of formerly rounded clastic quartz grains, local traces of heavy resistate minerals, and local very minor feldspar. Type-4 siliciclastics are interpreted to represent both tectonized type-3 siliciclastics and rocks with a greater original (silty or sandy) clastic component.

Type 5

Type-5 siliciclastics have been studied throughout the Seward Peninsula, and this discussion includes observations east of the area shown in figure 2. Fine- to medium-grained light-colored vitreous and granular quartz layers that contain significant unoxidized iron and base metal sulfides in surface samples are restricted to the lower Nome Group. This type of siliciclastic displays distinctive tan- to bronze- weathering muscovitic parting planes and occurs as layers or zones in mica schist with no associated carbonate, or alternately, adjacent to subunits of variably silicified and brecciated ferroan dolostone. Petrographic studies indicate a silty to cherty protolith, none to abundant heavy resistate minerals, and variable feldspar or clay (after feldspar) content. Type-5 siliciclastics are considered to represent a variety of protoliths, including silicified silty dolomitic carbonate, calcareous quartz-rich siltstone and shale, and quartz-rich feldspathic siltstone.

GEOLOGY OF THE WINDOWS

NO MANS-MOUNT DIXON WINDOW: SOUTHERN PORTION

The southern portion of the No Mans–Mount Dixon window is here described separately as the No Mans window. Rocks in the No Mans window (figs. 3 and 7) consist primarily of massive and blocky cleaving to tightly foliated and flaggy to platy cleaving white marble and subordinate dolostone of the white marble unit. A stromatoporoid of possible Silurian or Devonian age was collected from the white marble unit (73APa79; Till and others, 1986). Dip of the dominant foliation within and outside the window is uniformly moderate, between 16° and 33°. The window is cored by a gently southeast plunging antiform, which is possibly truncated on the west by a steeply-dipping northeast-striking fault. The C unit structurally and topographically overlies the white marble unit, primarily exhibits gently southwest-dipping (late) foliation, and consists of chlorite-muscovite schist with abundant sucrosic quartz interlayers and bull quartz segregations. Type-2 and type-3 siliciclastics are interlayered with and/or directly overlie the white marble unit in several areas north and south of No Mans Creek (fig. 3). On the south side of the window is local well-indurated breccia that contains angular clasts of type-2 and type-3 siliciclastics in a matrix of light brown cherty quartz. This breccia is possibly related to latest block faulting; however in one stream-worn boulder, breccia clasts define isoclinal folds. A northwest-trending slab of dominantly micritic to fine-grained white marble that lies within the lower Nome Group 1.6 km northeast of the No Mans window is assigned to the No Mans assemblage and considered to represent a culmination. This interpretation suggests that the white marble unit in the No Mans window proper is the upper surface of a horse or thrust slice in the Nome Group that roughly conforms to gentle southerly-dipping late fabrics (fig. 3). A smaller block or slab of flaggy to platy cleaving gray and white mottled to color-banded marble and salmon-weathering siliceous gray dolostone 3 km northwest of the No Mans window might constitute a second and structurally lower horse or thrust slice.

NO MANS-MOUNT DIXON WINDOW: NORTHERN PORTION

The more deeply eroded northern portion of the No Mans-Mount Dixon window (fig. 4) is similarly interpreted to be a large southwesterly dipping horse or thrust slice of the No Mans assemblage. Ordovician and Siluro-Devonian microfossil collections from the Mount Dixon area were described in the section titled No Mans Assemblage on page 103. Massive blocky-cleaving to strongly-foliated flaggy white marble is the dominant rock type; however zones of siliceous to quartz veined tan- and salmon-weathering dolostone locally grading to type-2 siliciclastics are developed in all carbonate units. Dips of the dominant foliation fabric are gentle throughout the map area (fig. 4), between 14° and 35°. The horse or thrust slice is considerably modified by block faults and preserves a broad internal synform locally cored by dark-gray fine- to medium-grained carbonaceous marble, here assigned to the dark carbonate unit that contains highly recrystallized corals, including Late Ordovician to Middle Devonian Favosites. A former northwest-trending antiform along the west side of the horse or thrust slice has been truncated by a northwest-trending block fault. The informally

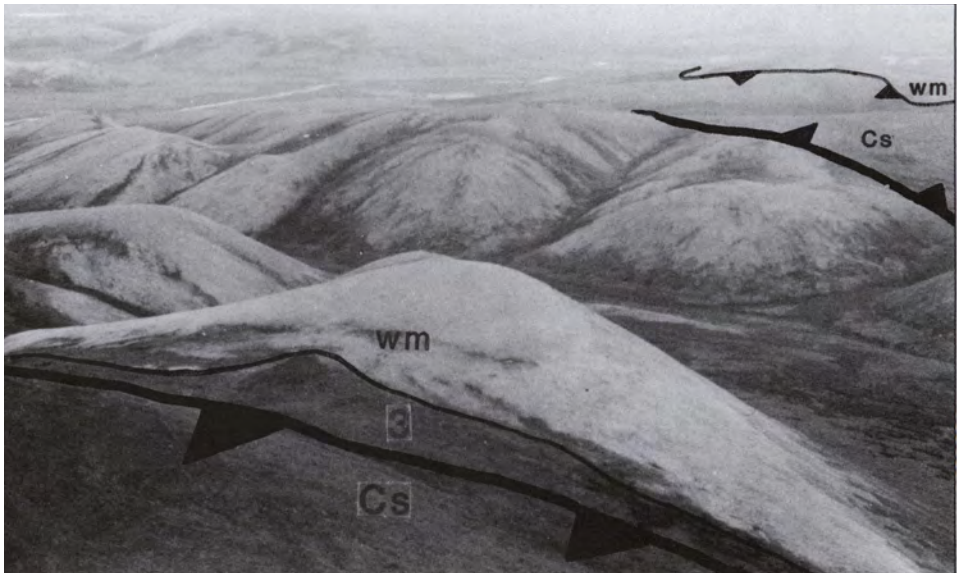

Figure 7. *View northeast across No Mans Creek at the southern portion of the No Mans–Mount Dixon window. Note the dark lichen-encrusted zone of type-3 siliciclastics (3). The proposed culmination of the white marble unit (wm) is depicted at the upper right, in the far background. Cs = schist of the C unit.*

named Niukluk fault defines a structural boundary along the northeast corner of figure 4. This northwest-striking regional fault (fig. 2) is interpreted to be a folded thrust and is locally marked by inactive hot springs and undeformed basalt flows. The relationship between the Niukluk fault and other thrust faults described in this paper is unknown.

AUBURN CREEK WINDOW

This window constitutes a tight antiformal structure (figs. 5 and 8), possibly locally overturned to the east. Mica schist of the C unit and local marble and dolostone, which contains an Early through possible early Middle Cambrian microfossil (Till and others, 1986), structurally overlies the window on all sides. Dips of foliation in the window and vicinity are highly variable between 15° and 70°, possibly as a consequence of drag folds developed during latest block faulting. Massive and blocky to strongly-foliated and flaggy white marble is dominant within the window. Patches of dolostone in the white marble unit of the window are common and have yielded a Middle Silurian through Early Devonian conodont (Till and others, 1986). Although the cross section, plan view, and age relationships define a structural window, the No Mans assemblage could be rootless and constitute a folded and partially unroofed horse or thrust slice within the lower Nome Group.

BUDD CREEK AND HARRIS DOME WINDOWS (STOPS A-S)

The geology of these windows is presented as a transect (fig. 6), oriented to show the major known and unresolved structural and stratigraphic relationships. In addition to previous published and unpublished data, the author has conducted more than 90 ground traverses and outcrop stops in this region. From this, 19 geologic observation points ("stops"), labeled A through S and circled on figure 6, have been selected for detailed description.

At stop A, an earliest Ordovician conodont has been reported (T. Carr, Anaconda Minerals unpub. report, 1984). Rocks east from the microfossil site consist of light orange- to tan-weathering, laminated planar-cleaving, variegated gray fine-grained siliceous marble. These rocks are here assigned to the Oim unit of the Nome Group. The Oim unit displays increasing white mica content downsection and at stop B consists of planar- to flaggy-cleaving, variegated gray and black, weakly micaceous fine-grained siliceous marble.

Southeast from stop B the micaceous marble grades downsection through a narrow zone of chloritic green marble and chloritic schist with calcite boudins to rocks here assigned to the Casadepaga Schist unit. Till and Dumoulin (1994) depict a structural boundary between their York and Seward terranes that would pass northward through stop B; although the precise contact is completely covered, the author tentatively interprets this to be a gradational boundary. Black metasiltite is common in stream float at stop C, and considered to originate from the transitional subunit that regionally lies near the top of the Casadepaga Schist unit. The Casadepaga Schist unit near stop C includes light-colored muscovite-chlorite-quartz schist and chloritic metaquartzite, marble, and darker-colored chlorite-albite schist, mafic schist, and medium- to coarse-grained metagabbro.

Stop D records the character of the contact between rocks here assigned to the Casadepaga Schist unit and underlying rocks here assigned to the Mixed unit. At this stop, chlorite-muscovite schist and brown-weathering chloritic schist of mafic or intermediate composition is interlayered downsection with white to gray fine-grained sparry marble assigned to the upper Mixed unit. At stop E, a black carbonaceous metasiltite subunit grades downsection through planar laminated-cleaving light-gray fine-grained sparry marble with minor black metasiltite and associated dark-gray to black sparry marble, to rocks here assigned to the lower part of the Mixed unit. The lower Mixed unit consists of a thick sequence of flaggy to platy cleaving, light-gray to gray, fine- to medium-grained sparry marble.

Stops F-I are located along a structurally complex zone, which includes Siluro-Devonian carbonate to calc-schist of the No Mans assemblage and type-4 siliciclastics, collectively bracketed by marble or type-1 siliciclastics of the Mixed unit on the west, and strongly deformed quartz boudin-rich schist here assigned to the C unit on the east; the latter unit correlates with portions of the Kougarok schist of Puchner (1986). If the lower Nome Group does in fact bracket younger carbonate rocks at stops F through I, then these carbonate rocks constitute west-dipping fault blocks, possibly horses. At stop F, Late Silurian through Devonian conodonts with a color alteration index of 5 to 5.5 were collected[2] (A. Till, written commun., 1994) from an assemblage of platy gray to black fine-grained dolostone or marble, and orangish-brown weathering light-gray to white muscovite marble and calc-schist. This assemblage is here assigned to the dark carbonate subunit of the No Mans assemblage. Eastward, across a recessive zone of lustrous muscovite schist with bull quartz segregations (C unit?) is a second zone here assigned to the dark carbonate subunit. This second zone, immediately west from stop G includes planar-cleaving dark gray marble, zebra dolostone, and carmine and yellow dolostone breccia. At stop H are sharply fault-bounded blocks of impure micaceous marble and calc-schist, carbonaceous gray type-4 siliciclastics,

[2]U.S. Geological Survey collection number 11231-SD, collected by J. Dumoulin, identified by A. Harris.

and light-gray metaquartzite(?). At stop I, late Llandoverian through Ludlovian (Silurian) conodonts with a color alteration index of 6 to 7 are reported[3] (A. Till, written commun., 1994) from an assemblage of flaggy- to platy-cleaving, color banded white, dark-gray, and black fine-grained carbonaceous marble and dolostone. This assemblage is assigned to the dark carbonate subunit. Recessive weathering mica schist with quartz segregations lies east from the dark carbonate subunit and is tentatively assigned to the C unit.

Stop J has been partly described above. East of this stop is light and dark color-laminated dolostone and minor carmine and yellow dolostone breccia, impure flaggy marble and calc-schist, micaceous schist, and carbonaceous type-4 siliciclastics preserved upon the white marble or Ordovician carbonate unit in a synform. Stream float in a small west-flowing creek, which cuts the dark carbonate subunit here, includes cobbles of dark marble with fasciculate rugose corals; a Devonian coral is reported (Puchner 1986) 5 km north of stop J, and Collier and others (1908) report Silurian corals to the west. The white marble unit in the region west from stop J includes massive and blocky to strongly foliated and platy- to flaggy-cleaving white to gray marble. Some of the foliated gray marble in this region, here assigned to the No Mans assemblage on the basis of structural position, is lithologically undistinguishable from marble of the Mixed unit. At stop K, strongly rodded chloritic calc-schist assigned to the lowest schist unit, is exposed in the core of an antiform.

At stop L, a siliciclastic zone lies east and above foliated marble (fig. 9) of the white marble or Ordovician carbonate unit. The uppermost marble layers contain 10 percent clastic quartz grains and local type-2 siliciclastic layers, followed upward by a major zone of type-4 siliciclastics, which extends along the east side of the Budd Creek window from Grant Creek, 11 km north-northwest to Kougarok Mountain and beyond. This zone includes massive fine-grained gray siliciclastic rock that resembles quartzite, locally flooded with two generations of quartz veins, and color-laminated white, light-gray, and brownish variably tectonized siliciclastics with muscovite partings. A portion of the "micaceous and carbonaceous quartzite of the micaceous marble unit" and some northern exposures of Kougarok schist (Puchner, 1986) probably correlate with the strike extensions of the rocks at stop L. A petrographic examination of color-banded recrystallized siliciclastic rock at stop L shows it has a probable clastic component, containing 80 percent

Figure 8. *View northwest at the Auburn Creek window. Note the distinctive light-weathering colors of the white marble unit in the window, compared with lower Nome Group units beyond the window.*

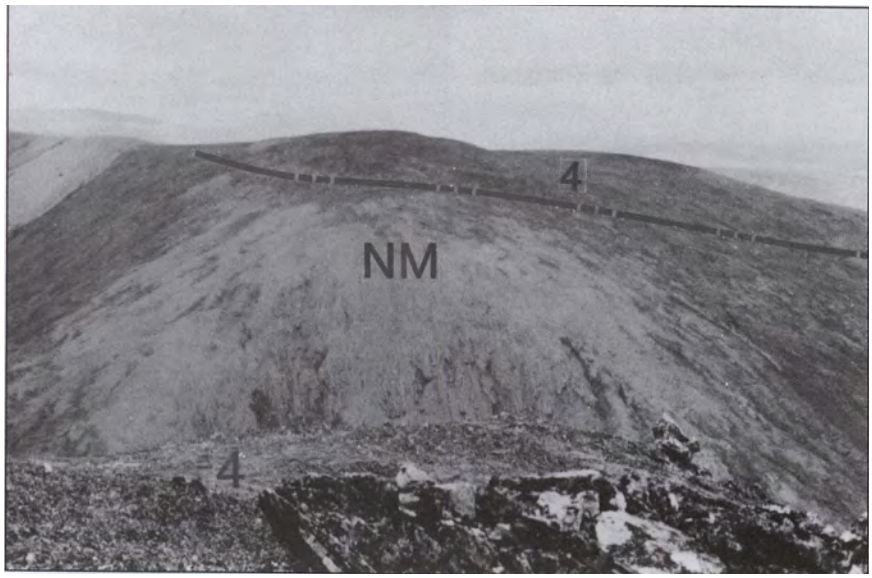

Figure 9. *View north along the east side of the Budd Creek window. Dark lichen-encrusted type-4 siliciclastics (4) overlie undifferentiated marble of the No Mans assemblage(NM).*

[3]U.S. Geological Survey collection number 11399-SD, collected by J. Dumoulin, identified by A. Harris.

quartz, with the remainder being muscovite, with traces of orthoclase, apatite, and zircon. Tectonized siliciclastics at this stop include quartz schist with domains of rodded milky white and semi-translucent quartz. Petrographically this rock type contains quartz and subordinate muscovite, iron oxides, rutile, and pyrite; copper carbonates locally occupy late fractures. The siliciclastic zone is here proposed to follow an east-dipping thrust fault, along which a former sandy calc-schist to marble unit of uncertain age and assignment has been silicified. Muscovite-chlorite schist and calc-schist here assigned to the Nome Group lie east and above the siliciclastic zone.

At stop M a subunit of planar cleaving light-gray to gray micritic to fine-grained sparry marble contains clastic quartz grains. This subunit is assigned to the upper Mixed unit, as it grades eastward and upsection to a large area of chloritic marble, chloritic calc-schist, chlorite-albite-quartz schist, chlorite-muscovite schist, mafic schist, and metagabbro assigned to the Casadepaga Schist unit by the author and Till and others (1986).

Stop N defines the southernmost of at least two zones of the dark carbonate subunit that lie west of the Harris Dome window, in a geologically similar fashion to the west side of the Budd Creek window. At this stop is white, light-gray, grayish-brown, and subordinate dark-gray to black carbonaceous fine-grained marble. Colonial and possible rugose corals are preserved in dark marble; conodonts from this stop indicate a Middle Devonian through earliest Mississippian age (Till and others, 1986). The dark carbonate subunit at stop N is bracketed on the west by the Casadepaga Schist unit, and on the east by light-colored muscovite-chlorite schist with abundant sucrosic and bull quartz segregations, here assigned to the C unit.

In the vicinity of stop O is massive and blocky cleaving white and light-gray to gray dominantly fine-grained marble of the white marble unit. A stromatoporoid and conodont collected near stop O, together indicate a Middle Devonian age (Till and others, 1986).

Outcrops at stop P consist of ductilely-deformed dark and dense chlorite-rich schist with variable muscovite and sericite, and subordinate laminated interlayers of white sucrosic quartz. Petrographic examination shows that the dark chloritic schist at Harris Creek contains pennine, muscovite, sericite, and quartz, with an inferred protolith of finely laminated sediment composed of reworked mafic volcanic detritus. Early severe isoclinal folds defined by foliation of pennine and sericite are cut at right angles by later foliation defined by muscovite, pennine, and rhombic domains of quartz. In this report the mafic schist is interpreted to correlate with the C unit and to lie in thrust relationship upon the white marble unit of stop O. In addition to chlorite schist, float cobbles in Harris Creek at stop P include color-laminated white, gray, and dark bluish-gray micritic to sparry marble, and black micritic marble with recrystallized tabulate corals of possible Siluro-Devonian morphotype; these may be derived from an unexposed fault block of the dark carbonate unit not far upstream. Sainsbury (1974) indicated a thrust melange zone east from the Harris Dome window, which would include the rocks at stop P. At stop Q, the above-described dark mafic schist contains cobble- to boulder-sized isoclinally folded native clasts of type-5 siliciclastic rock, composed of white to brownish laminar- to thinly-foliated sucrosic to vitreous quartz and chlorite, which represent truncated intrafolial folds. Other isoclinally folded clasts include variable amounts of iron carbonate interlayered with quartz. Many folded clasts contain layers of pyrite, pyrrhotite, and chalcopyrite; granoblastic textures and plastic flowage of sulfides suggest the mineralization is predeformation or prefolding or both.

At stop R, stream float derived from the west includes rodded light-colored coarsely-textured type-4 siliciclastics. Petrographically this rock is composed of quartz, with subordinate muscovite, pennine, minor untwinned plagioclase crystalloblasts, and rutile. Petrography, major oxide composition, and geologic setting provide evidence that the protolith is possibly a quartz-rich clastic sediment, or silicified sandy carbonate.

East of the Harris Dome window, the C unit grades upsection to a broadly-exposed assemblage of orangish- to gray-weathering flaggy light-gray, gray, and dark-gray fine- to medium-grained muscovitic marble and subordinate calc-schist and dolostone. This is assigned to the Mixed unit by Till and others (1986). Stop S has yielded a conodont fragment of probable Ordovician age (Till and others, 1986).

SUMMARY

The geology of the windows indicates that Cambrian, Early Ordovician, and Ordovician units here assigned to the lower Nome Group on the basis of age, lithology, and stratigraphic relations may overlie Ordovician, Silurian, and Devonian units of the No Mans assemblage, along zones locally characterized by fault blocks and/or siliciclastic rocks. Evidence for structural superposition in part consists of measured foliation attitudes; these are not a confident measure of original sedimentary bedding. However, the defined stratigraphy of the Nome Group supports a structurally-lower position for the No Mans assemblage, that is, progressively (stratigraphically) lower units and subunits of the Nome Group occur in a regional transect towards the windows. In addition, at No Mans Creek, topographic relations show the white marble unit to physically underlie rocks assigned to the C unit of the Nome Group.

DISCUSSION

The following overview of the geology of the western Brooks Range fold and thrust belt is presented for purposes of comparison. The western Brooks Range preserves a former Proterozoic to Mesozoic passive continental margin and outboard oceanic assemblage. During the Middle Jurassic to Early Cretaceous periods of the Brookian orogeny, these assemblages were initially telescoped as a result of south-directed subduction and closure of a marginal ocean basin, and then thrust relatively northward. Southward subduction of portions of the continental margin and related crustal thickening led to development of high-pressure blueschist metamorphic facies (Till and others, 1988).

The western Brooks Range can be subdivided into four domains (Till and others, 1988; Moore and others, 1992): (1) *Angayucham terrane*. This terrane consists of Late Paleozoic to Mesozoic marginal sedimentary and igneous (including ophiolitic) rocks. It is preserved as regionally-extensive thrust sheets and melange blocks in a root zone along the south side of the Brooks Range and as outlying klippen to the north, which represent the structurally highest allochthons in the northwestern Brooks Range (Moore and others, 1992). (2) *Schist belt*. This east-west trending belt occupies the southern Brooks Range and includes Late Paleozoic pelitic schist and metavolcanics that were metamorphosed under blueschist conditions at or before 149 Ma (Till 1992). The schist belt has undergone some north-south shortening and has been thrust northward (Armstrong and others, 1986; Till and others, 1988). (3) *Central belt*. This east-west belt occupies the central axis of the western Brooks Range and encompasses Proterozoic through Mississippian rocks, including metacarbonate, pelitic schist, metaplutonic, and metavolcanic rocks. The central belt was metamorphosed and deformed under blueschist facies conditions, but at lower pressures than the schist belt, with conditions intermediate between deep ductile (schist belt) and (shallow brittle) fold and thrust-belt-style deformation. A white mica $^{40}Ar/^{39}Ar$ plateau age of 120 Ma may establish the age of blueschist metamorphism of the central belt (Till 1992). The central belt contains hinterland duplexes, for example, Mount Angayukaqsraq (Karl and others, 1989) (fig. 1), with thrust faults that involve rocks as old as Proterozoic and as young as Early Mississippian. Recorded thrust vergence is both north and south (Till and others, 1988). (4) *Endicott allochthon*. The Endicott allochthon is included in the area shown as *shallow fold and thrust belt* in figure 1. This allochthon and other clastic and carbonate- to igneous-dominated (Angayucham) allochthons occupy the northern half of the western Brooks Range. The minimum ages of thrust-involved formations indicate that north-vergent thrusting occurred from Late Jurassic through Early Cretaceous (Moore and others, 1992). An east- to northeast-vergent Albian (Early Cretaceous) or older fold and thrust belt is also expressed in northwestern Alaska, the offshore Herald arch and onshore Tigara uplift of Moore and others (1992). In the northwesternmost Brooks Range, east- to northeast-vergent brittle structures (Tigara uplift) are shown locally to post-date north- to northwest-vergent thrusts and related folds (Young, 1992). In addition, regional extension in central and northern Alaska is proposed at 130-90 Ma (Miller and Hudson, 1991); however, the scope of this extensional event is questioned by Till and others (1993).

The Nome Group blueschist event is dated as Middle Jurassic to Early Cretaceous (Armstrong and others, 1986; Patrick, 1988; Patrick and Lieberman, 1988). This event is partly contemporaneous with low-pressure 171–163 Ma metamorphism at the sole of thrusted ophiolitic assemblages in the Brooks Range fold-and-thrust belt (Moore and others, 1992) and is fully contemporaneous with blueschist metamorphism of the schist belt. The central belt records a younger and lower-pressure blueschist metamorphic episode than the Nome Group. However, the central belt is geologically more similar to the combined Nome and Kigluaik Groups than the schist belt.

Regionally, metamorphic grade decreases to the northwest on the western Seward Peninsula. This decrease is shown by decreasing thermal maturity indexes (Johnsson and others, 1993) and by the transition to the less-recrystallized Casadepaga Schist unit in the northwestern Seward Peninsula. In addition, evidence indicates that an allochthon structurally higher than the Nome group (Sainsbury, 1972; and the SOl unit of Till and Dumoulin, 1994) exists in the northwestern Seward Peninsula. This allochthon is shown as *York Mountains terrane sensu stricto* on figure 1. An allochthon with stratigraphy comparable to the York Mountains terrane sensu stricto is identified in the Baird Mountains domain (fig. 1) (Till and Dumoulin, 1994). The northwestward decrease in metamorphic grade and thermal maturity and appearance of structurally higher allochthons is comparable to the changes along a north or northwesterly transect across the central belt of the western Brooks Range and through the Baird Mountains domain.

CONCLUSIONS

Collectively, the Seward Peninsula is proposed to correlate with the hinterlands of the western Brooks Range fold and thrust belt, being geologically comparable to western portions of the central belt (Till and others, 1988) and the carbonate-dominant allochthon(s) of the Baird Mountains domain, while noting that the Nome Group records blueschist metamorphism temporally and mineralogically more similar to the schist belt. Thrust faulting was active in the Brooks Range thrust and fold belt, including the hinterlands, from Late Jurassic to Early Cretaceous time. The favored hypothesis is that the

Seward Peninsula is within the hinterlands of the Brooks Range fold and thrust belt, and has been subjected to north- and south-vergent thrust faulting temporally and physically comparable with the central belt. However, not yet established is the contribution of Albian or older east- to northeast-vergent compression during the Tigara uplift (Moore and others, 1992) and regional 130–90 Ma extension (Miller and Hudson, 1991) with regard to the present north to northwest geometric bias of the No Mans assemblage and similarly-oriented regional antiforms and synforms in the Nome Group and No Mans assemblage. In addition, the scale of horizontal translation during thrusting has not been determined.

The No Mans assemblage is areally dominated by Ordovician and Siluro-Devonian carbonate, with three or more zones of schist and calc-schist. As shown by the accompanying geologic maps and transects, the No Mans assemblage both structurally underlies and is imbricated with older rocks of the lower Nome Group. There are no lithofacies in the No Mans assemblage that do not have probable regional correlatives in the Nome Group; thus at present the distinction between the Nome Group and No Mans assemblage is one of solely structural placement. The paucity or absence of certain Nome Group lithotypes such as type-1 siliciclastics, chlorite-albite schist, or metabasite in the No Mans assemblage may merely reflect the lack of exposure of older rocks of the latter assemblage. Areas of mica schist with abundant quartz segregations that have been assigned here to the C unit, especially those areas along the west sides of the Budd Creek and Harris Dome windows, could actually represent ductilely-deformed schist of the No Mans assemblage. This problem remains unresolved.

Type 2, 3, and 4 siliciclastics are commonly associated with the margins of the structural windows. In part, these rock types are proposed to originate via silicification of carbonate, silty carbonate, and calcareous siltstone during metamorphism and thrusting. Certain of the siliciclastic rocks, especially type-4, may represent protoliths of siltstone, although Puchner (1987) favored quartzite.

Thrust faulting on the Seward Peninsula possibly postdates peak metamorphism, if, as here proposed, higher-grade units of the Nome group structurally overlie less recrystallized or less thermally-affected units of the No Mans assemblage. The widespread presence of ductile fabrics in the Nome Group and No Mans assemblage, and the general lack of widespread brittle deformation near the traces of proposed thrust faults indicate that thrust faulting occurred mainly under ductile conditions. The approximate conformity of a horse or thrust slice of the white marble unit to late gently-dipping ductile fabrics north of the No Mans window shows a possible relationship between the late fabric and thrust faulting. Although outcrop-scale brittle failure is suggested by trains of angular quartz in the C unit, regional brittle deformation postdates thrusting, as evidenced by steep block faults, which displace the structural window margins of the No Mans Creek–Mount Dixon and Auburn Creek windows. The indicated 109 Ma age for metamorphogenic gold mineralization in the Nome Group provides a minimum age for the transition from regional ductile to regional brittle deformation. Assuming thrust faulting (1) is later than peak metamorphism, (2) occurred primarily under ductile conditions, and (3) precedes regional brittle deformation, thrust faulting on the Seward Peninsula is constrained to the Middle Jurassic to Early Cretaceous interval.

ACKNOWLEDGMENTS

The author would like to thank Alison Till and Gil Mull for reviewing the manuscript and Bruce Bouley of Cominco Alaska Exploration for permission to publish this paper. Additional thanks go to geologists John Robinson and Chris Gierymski for their contributions to the Seward Peninsula field programs.

REFERENCES CITED

Amato, J.M., Gans, P.B., Hannula, K., Calvert, A.T., and Miller, E.L., 1991, Pre-, syn-, and post-tectonic mafic to silicic magmatism in the Kigluaik Mountains gneiss dome, Seward Peninsula, Alaska: Geological Society of America, Abstracts with Programs, v. 23, no. 2, p. 2.

Amato, J.M., Wright, J.E., and Gans, P.B., 1992, The nature and age of Cretaceous magmatism and metamorphism on the Seward Peninsula, Alaska: Geological Society of America, Abstracts with Programs, v. 24, no. 5, p. 2.

Amato, J.M., Wright, J.E., Gans, P.B., and Miller, E.L., 1994, Magmatically induced metamorphism and deformation in the Kigluaik gneiss dome, Seward Peninsula, Alaska: Tectonics, v. 13, no. 2, p. 515-527.

Armstrong, R.L., Harakal, J.E., Forbes, R.B., Evans, B.W., and Thurston, S.P., 1986, Rb-Sr and K-Ar study of metamorphic rocks of the Seward Peninsula and southern Brooks Range, Alaska: Geological Society of America Memoir 164, p. 185-203.

Bunker, C.M., Hedge, C.E., and Sainsbury, C.L., 1979, Radioelement concentrations and preliminary radiometric ages of rocks of the Kigluaik Mountains, Seward Peninsula, Alaska: U.S. Geological Survey Professional Paper 1129-C, 12 p.

Collier, A.J., Hess, F.H., Smith, P.S., and Brooks, A., 1908, The gold placers of parts of Seward Peninsula, Alaska: U.S. Geological Survey Bulletin 328, 343 p.

Ford, R.C., and Snee, L.W., 1993, $^{40}Ar/^{39}Ar$ thermochronology of white mica from the Bluff area—The first ages for lode sources of placer gold deposits in the Seward Peninsula: Geological Society of America, Abstracts with Programs, v. 25, no. 6, p. A-469.

Johnsson, M.J., Howell, D.G., and Bird, K.J., 1993, Thermal maturity patterns in Alaska—Implications for tectonic evolution and hydrocarbon potential: American Association of Petroleum Geologists Bulletin, v. 77, p. 1874-1903.

Karl, S.M., Dumoulin, J.A., Ellersieck, I., Harris, A.G., and Schmidt, J.M., 1989, Preliminary geologic map of the Baird Mountains and part of the Selawik quadrangles, Alaska: U.S. Geological Survey Open-File Report 89-551, 65 p., scale 1:250,000.

Kaufman, D.S., 1985, Windy Creek and Crater Creek faults, Seward Peninsula, *in* Bartsch-Winkler, Susan, and Reed, K.M., The United States Geological Survey in Alaska, Accomplishments during 1983: U.S. Geological Survey Circular 945, p. 22-24.

McClelland, W.C., and Patrick, B.E., 1994, U-Pb evidence for a Barentian origin of Northern Alaska: Geological Society of America, Abstracts with Programs, v. 27, no. 7, p. A-383.

Miller, E.L., Amato, J., Calvert, A., Dumitru, T., Gans, P., Hannula, K., Lee, J., Little, T., and Rubin, C., 1992a, Structural evolution of the Seward Peninsula, Alaska—A progress report: Geological Society of America, Abstracts with Programs, v. 24, no. 5, p. 70.

Miller, E.L., Calvert, A.T., and Little, T.A., 1992b, Strain-collapsed metamorphic isograds in a sillimanite gneiss dome, Seward Peninsula, Alaska: Geology, v. 20, p. 487-490.

Miller, E.L., and Hudson, T.L., 1991, Mid-Cretaceous extensional fragmentation of a Jurassic-Early Cretaceous compressional orogen, Alaska: Tectonics, v. 10, no. 4, p. 781-796.

Miller, T.P., Grybeck, D.J., Elliott, R.L., and Hudson, T.L., 1972, Preliminary geologic map of the eastern Solomon and southeastern Bendeleben quadrangles, eastern Seward Peninsula, Alaska: U.S. Geological Survey Open-File Report 72-256, 11 p., scale 1:250,000.

Moore, T.E., Wallace, W.K., Bird, K.J., Karl, S.M., Mull, C.G., and Dillon, J.T., 1992, Stratigraphy, structure, and geologic synthesis of northern Alaska: U.S. Geological Survey Open-File Report 92-330, 183 p., scale 1:2,500,000.

Patrick, B.E., 1988, Synmetamorphic structural evolution of the Seward Peninsula blueschist terrane, Alaska: Journal of Structural Geology, v. 10, p. 555-565.

Patrick, B.E., and Lieberman, J.E., 1988, Thermal overprint on blueschists of the Seward Peninsula—the Lepontine in Alaska: Geology, v. 16, p. 1100-1103.

Patrick, B.E., and McClelland, W.C., 1993, Proterozoic magmatism on the Seward Peninsula, Alaska: EOS, Transactions, American Geophysical Union, v. 74, no. 43, p. 659.

Puchner, C.C., 1986, Geology, alteration, and mineralization of the Kougarok Sn deposit, Seward Peninsula, Alaska: Economic Geology, v. 81, p. 1775-1794.

_____1987, Geology, alteration, and mineralization of the Kougarok Sn deposit, Seward Peninsula, Alaska—A reply: Economic Geology, v. 82, p. 2201-2204.

Sainsbury, C.L., 1972, Geologic map of the Teller quadrangle, western Seward Peninsula, Alaska: U.S. Geological Survey Map I-685, 4 p., scale 1:250,000.

_____1974, Geologic map of the Bendeleben quadrangle, Seward Peninsula, Alaska: Anchorage, The Mapmakers, 29 p., scale 1:250,000.

_____1975, Geology, ore deposits, and mineral potential of the Seward Peninsula, Alaska: U.S. Bureau of Mines Open-File 73-75, 108 p., scale 1:250,000.

_____1987, Geology, alteration, and mineralization of the Kougarok Sn deposit, Seward Peninsula, Alaska—A discussion: Economic Geology, v. 82, p. 2199-2200.

Sainsbury, C.L., Hudson, T., Ewing, R., and Marsh, W.R., 1972, Reconnaissance geologic map of the west half of the Solomon quadrangle, Alaska: U.S. Geological Survey Open-File Report 72-324, 10 p., scale 1:250,000.

Sainsbury, C.L., Hummel, C.H., and Hudson, T., 1972, Reconnaissance geologic map of the Nome quadrangle, Seward Peninsula, Alaska: U.S. Geological Survey Open-File Report 72-326, 28 p., scale 1:250,000.

Smith, P.S., 1910, Geology and mineral resources of the Solomon and Casadepaga quadrangles, Seward Peninsula, Alaska: U.S. Geological Survey Bulletin 433, 234 p., scale 1:62,500.

Thurston, S.P., 1985, Structure, petrology, and metamorphic history of the Nome Group blueschist terrane, Salmon Lake area, Seward Peninsula, Alaska: Geological Society of America Bulletin, v. 96, p. 600-617.

Till, A.B., 1983, Granulite, peridotite, and blueschist-Precambrian to Mesozoic history of Seward Peninsula: Journal of the Alaska Geological Society, 1982 symposium proceedings v. 3, p. 59-66.

_____1992, Detrital blueschist-facies metamorphic mineral assemblages in Early Cretaceous sediments of the foreland basin of the Brooks Range, Alaska, and implications for orogenic evolution: Tectonics, v. 11, no. 6, p. 1207-1223.

Till, A.B., and Dumoulin, J.A., 1994, Geology of Seward Peninsula and Saint Lawrence Island: *in* Plafker, G., and Berg, H.C., eds., Geology of Alaska: Boulder, Geological Society of America v. G-1, p. 141-152.

Till, A.B., Dumoulin, J.A., Gamble, B.M., Kaufman, D.S., and Carroll, P.I., 1986, Preliminary geologic map and fossil data, Solomon, Bendeleben, and southern Kotzebue quadrangles, Seward Peninsula, Alaska: U.S. Geological Survey Open-File Report 86-276, 71 p., scale 1:250,000.

Till, A.B., Schmidt, J.M., and Nelson, S.W., 1988, Thrust involvement of metamorphic rocks, southwestern Brooks Range, Alaska: Geology, v. 16, p. 930-933.

Till, A.B., Box, S.E., Roeske, S.M., and Patton, W.W. Jr., 1993, Comment on "Mid-Cretaceous extensional fragmentation of a Jurassic-Early Cretaceous compressional orogen, Alaska" by Miller, E.L., and Hudson, T.L.: Tectonics, v. 12, no. 4, p. 1076-1081.

Young, L.E., 1992, The Wolverine Creek sequence—Evidence for an allochthon below the Brooks Range allochthon, western Brooks Range, Alaska: Alaska Division of Geological & Geophysical Surveys, Report of Investigations 92-4, 19 p.

PREVIOUS EDITIONS OF *SHORT NOTES ON ALASKA GEOLOGY*

Short Notes on Alaskan Geology 1976: **DGGS Geologic Report 51 (out of stock, $3.50 photocopied)**

Reconnaissance geology along the Variegated Glacier, Saint Elias Mountains
Evidence for early Cenozoic orogeny in central Alaska Range
The Shumagin-Kodiak batholith: A Paleocene magmatic arc?
Speculative tectonic evolution of the Cenozoic Shelikof Trough, south-central Alaska
Discovery of blueschists on Kodiak Island
Large kaolinite crystals in the Chignik Formation (Upper Cretaceous), Herendeen Bay
Occurrence of sodic amphibole-bearing rocks in the Valdez C-2 Quadrangle
High-quality coal near Point Hope, northwestern Alaska

Short Notes on Alaskan Geology 1977**: DGGS Geologic Report 55 (out of stock, $5.00 photocopied)**

A Givetian (Late Middle Devonian) fauna from Healy B-4 Quadrangle, central Alaska Range
Probable karst topography near Jade Mountains, southwestern Brooks Range
Tectonic significance of the Knik River schist terrane, south-central Alaska
Geochronology of southern Prince of Wales Island Katmai caldera: Glacier growth, lake rise, and geothermal activity
Geology and K-Ar age of mineralized intrusive rocks from the Chulitna mining district, central Alaska
The Richardson lineament: A structural control for gold deposits in the Richardson mining district, interior Alaska
Boulder Creek tin lode deposits
Comparison of mercury-antimony-tungsten mineralization of Alaska with strata-bound cinnabar-stibnite-scheelite deposits of the Circum-Pacific and Mediterranean regions
Earthquake recurrence and location in the western Gulf of Alaska

Short Notes on Alaskan Geology 1978**: DGGS Geologic Report 61 ($2.00)**

Holocene displacements measured by trenching the Castle Mountain fault near Houston
Bluff Point landslide, a massive ancient rock failure near Homer
Recurrent late Quaternary faulting near Healy
Glaciation of Indian Mountain, west-central Alaska
The Cantwell ash bed, a Holocene tephra in the central Alaska Range
Geochronology of metamorphic and igneous rocks in the Kantishna Hills, Mount McKinley Quadrangle
The Chilikadrotna Greenstone, an Upper Silurian metavolcanic sequence in the central Lake Clark Quadrangle
Tectonic and economic significance of Late Devonian and late Proterozoic U-Pb zircon ages from the Brooks Range

Short Notes on Alaskan Geology 1979-80**: DGGS Geologic Report 63 ($1.00)**

Lead isotope ratios from the Red Dog and Drenchwater Creek lead-zinc deposits, De Long Mountains, Brooks Range
^{40}K-^{40}Ar ages from rhyolite of Sugar Loaf Mountain, central Alaska Range: Implications for offset along the Hines Creek strand of the Denali fault system
Multiple glaciation in the Beaver Mountains, western interior Alaska
Fossil algae in Lower Devonian limestones, east-central Alaska
Tertiary tillites(?) on the northeast flank of Granite Mountain, central Alaska Range
Evidence for suprapermafrost ground-water blockage, Prudhoe Bay oil field

Short Notes on Alaskan Geology 1981: **DGGS Geologic Report 73 ($3.00)**

Alkaline igneous rocks in the eastern Alaska Range
Shear moduli and sampling ratios for the Bootlegger Cove Formation as determined by resonant-column testing
Clinoptilolite and mordenite deposits of possible economic value at Iliamna Lake, Alaska
The Keete Inlet thrust fault, Prince of Wales Island
Two Holocene maars in the central Alaska Range
Radiometric-age determinations from Kiska Island, Aleutian Islands, Alaska
Geochemical signature of the Goon Dip Greenstone on Chicagof Island, southeastern Alaska
Uranium mineralization in the Nenana Coal Field, Alaska
Reconnaissance of rare-metal occurrences associated with the Old Crow batholith, eastern Alaska - north-western Canada
A recent earthquake on the Denali fault in the southeast Alaska Range
Triassic paleomagnetic data and paleolatitudes for Wangellia, Alaska

Short Notes on Alaskan Geology 1982-83**: DGGS Professional Report 86 ($2.50)**

An unconformity with associated conglomeratic sediments in the Berners Bay area of southeast Alaska
An iron-rich lava flow from the Nenana coal field, central Alaska
Results of shallow seismic survey for ground water at McGrath
Evaluation of a shallow sand-and-gravel aquifer at Eagle River
Correlation of geophysical well logs for a water development in south Anchorage
Garnet compositional estimates as indicators of progressive regional metamorphism in polymetamorphic rocks, Kantishna Hills
Geology of the Miss Molly molybdenum prospect, Tyonek C-6 Quadrangle
Glacial geology of the Mt. Prindle area, Yukon-Tanana Upland

***Short Notes on Alaskan Geology 1991*: DGGS Professional Report 111 ($8.00)**

Tin placers associated with the downcutting of fissure basalts, Ray River drainage, Alaska

Geology and geochemistry of the Gagaryah barite deposit, western Alaska Range, Alaska

Geology and geochemistry of Tatlawiksuk Hot Springs, a newly discovered geothermal area in western Alaska

Geology and geochemistry of the Sleitat Mountain tin deposit, southwestern Alaska

Native mercurian-silver, silver, and gold nuggets from Hunter Creek, Alaska

Late Pleistocene volcanic deposits near the Valley of Ten Thousand Smokes, Katmai National Park, Alaska

Deglaciation of the Allison-Sawmill Creeks area, southern shore of Port Valdez, Alaska

Dating Holocene moraines of Canwell Glacier, Delta River valley, central Alaska Range

Gilead sandstone, northeastern Brooks Range, Alaska: An Albian to Cenomanian marine clastic succession

Kikiktat Mountain klippe: A link between the Copter Peak and Nuka Ridge allochthons, northcentral Brooks Range, Alaska

Sample media useful for a systematic geochemical survey of upper Valdez Creek, Alaska

***Short Notes on Alaskan Geology 1993*: DGGS Professional Report 113 ($6.00)**

Mississippian terrigenous clastic and volcaniclastic rocks of the Ellesmerian sequence, upper Sheenjek River area, eastern Brooks Range, Alaska

The penultimate great earthquake in southcentral Alaska: evidence from a buried forest near Girdwood

Geology, alteration, and mineralization of the Vinasale Mountain gold deposit, west-central Alaska

Fumarolic gas chemistry (1982) and thermal spring water chemistry (1985), Crater Peak, Mount Spurr, Alaska

Organic-rich shale and bentonite in the Arctic Creek unit, Arctic National Wildlife Refuge: implications for stratigraphic and structural interpretations

Dating Holocene moraines of Black Rapids Glacier, Delta River valley, central Alaska Range

Paleomagnetism of the Fairbanks basalts, interior Alaska

The Hayes Glacier fault, southern Alaska Range: evidence for post-Paleocene movement

Detachment folds and a passive-roof duplex: examples from the northeastern Brooks Range, Alaska

EDITORIAL POLICY

Short Notes on Alaska Geology is a collection of brief scientific papers describing recent geological investigations of limited scope. This publication is widely distributed to a state, national, and international audience that represents industry, academia, government agencies, and the general public. Manuscripts are accepted for consideration with the understanding that they have not been previously published and are not being submitted for publication elsewhere, that all persons listed as authors have given their approval for submission of the paper, and that any person cited as a source of personal communication has approved such a citation. Authors are encouraged to suggest appropriate reviewers and provide reviewers telephone numbers.

SUBMISSION OF MANUSCRIPTS

Authors should submit three paper copies of their draft manuscripts to Short Notes Editor, Alaska Division of Geological & Geophysical Surveys, 794 University Avenue, Suite 200, Fairbanks, Alaska 99709-3645. Contributors should retain one copy of all materials submitted. DGGS is not responsible for materials lost in the mail. In general, articles are limited to about 10 manuscript pages (approximately 2,000 words of text), including references, figures, and tables.

All draft manuscripts will be examined and approved by the DGGS editor and at least two reviewers. After technical reviews are completed, copies of review forms and reviewed manuscript pages will be returned to the author for revision (if required) and resubmittal. Conflicts between reviewers and authors must be resolved to the satisfaction of the DGGS editor before final acceptance of manuscripts. Final submittals must be provided as double-spaced paper copy and on high-density PC diskette (Microsoft Word or Word Perfect). Questions should be directed to the DGGS editor 907-451-5015. Major changes by the author—whether scientific or editorial—are not permitted after the manuscript is in galley form.

TEXT PREPARATION

Manuscripts should be double spaced with 1-inch margins on all sides. The title page should include the title of the article and the name(s) and affiliation(s) of the author(s). Because of the brevity of *Short Notes* articles, table of contents, lists of illustrations, and abstracts are not required. Words to be printed in italics should be typed in italics.

Specific guidelines for units of measure, abbreviations, and references are provided in *Suggestions to Authors of Reports of the United States Geological Survey* (7th edition) or *Government Printing Office Style Manual 1973*. Potential authors are also encouraged to consult the latest issue of *Short Notes* for information.

PREPARATION OF ILLUSTRATIONS

All figures should be provided in camera-ready form. Computer-generated illustrations are acceptable. Line figures are generally published in black and white, but color art may be accepted with the understanding that the author will pay additional costs (color separation and printing) for colored figures. Current page-cost information can be obtained from the DGGS editor. Maximum size for figures is 6.5 by 8.5 inches.

View of Kemik Sandstone looking east up Ignek Valley on the south side of the Sadlerochit Mountains in the Arctic National Wildlife Refuge (ANWR). Kemik Sandstone, repeated by out-of-syncline thrust faulting, forms low ridges in the left foreground and in the valley to east, and it is overlain by red-weathering tuff in Hue Shale (see the paper by R.R. Reifenstuhl). Triassic to Permian Sadlerochit Group (Ivishak and Echooka Formations) forms prominent dipslopes on the south side of the Sadlerochit Mountains, and overlies light-gray Lisburne Group limestone that forms the mountain crest. Photograph by C.G. Mull.